Synthesis and electrochemical behavior of shape-controlled Pt nanoparticles synthesized using water in oil microemulsion in acid aqueous phase for ammonia oxidation

Roberto Alexis Martínez Rodríguez

Doctoral Thesis Submitted in Partial Fulfillment of the Requirements

for the Degree of Doctor in Philosophy

with international joint custody between the University of Alicante, Spain and the

University of Puerto Rico, Rio Piedras Campus

Electrochemistry, Science and Technology

Chemistry

Advisors:

Dr. Juan Miguel Feliu Martinez

Professor from the Physical Chemistry Department

University of Alicante

Dr. Francisco José Vidal Iglesias

Technician at the Institute of Electrochemistry

University of Alicante

Dr. Carlos Raúl Cabrera Martínez

Professor from the Chemistry Department

University of Puerto Rico, Rio Piedras Campus

Doctoral Program from the University of Alicante, Spain

Doctoral Program from the University of Puerto Rico, Rio Piedras Campus

July, 2019

Accepted by the Institute of Electrochemistry from the University of Alicante, in Partial Fulfillment of Requirement to obtain the degree of Doctor in Philosophy

_____

Dr. Vicente Montiel Leguey

Institute of Electrochemistry Chair

_____ _____

Dr. Juan Miguel Feliu Martínez

Advisor

Dr. Francisco José Vidal Iglesias

Advisor

July, 2019

Accepted by the Faculty of Natural Sciences from University of Puerto Rico in Partial Fulfillment of Requirement to obtain the degree of Doctor in Philosophy

_____

Dr. Liz M. Díaz Vázquez

Department Chair

_____

Dr. Carlos R. Cabrera Martínez

Advisor

July, 2019

Acknowledgments

First of all, I want to thank all my family, in special to my dad Mr. Roberto Martínez Ayala and my mom, Mrs. Ana Rosa Rodríguez Morales for all the help and the support provided during my whole life and their guidance that helps me to take decisions about my career and future projects. Also, I would like to thanks my sisters Brenda Ivette Martínez Rodríguez and Rosa Isela Martínez Rodríguez for always providing me support in this stage of my life.

A special appreciation needs to be addressed to my thesis advisors, Dr. Carlos Raúl Cabrera Martínez, Dr. Juan Miguel Feliu Martinez and Dr. Francisco Vidal Iglesias which provided me all the necessary advice, guidance and all the help during all of these years. I would like to thank Dr. Carlos Raul Cabrera Martínez, his trust and the given opportunity to being part of his lab as an undergraduate student when I thought that the idea of having a Ph.D. was very difficult to reach. Thank you for believing in this life project. I thank Dr. Juan Miguel Feliu Martínez for opportunity to be part of his research lab from the first time when I visited the lab only to learn more about electrochemical methods and finally help me to become one more of his research lab crew to enroll into the doctorate program of the University of Alicante. I want to address my special appreciation to Dr. Francisco Vidal Iglesias who has been helping me during all of these years with all the things related to the research and their trust who have made him feel like a big brother. In the same way, I would like to appreciate Dr. Jose Solla Gullón who also helped me during these years as providing me advice and the tools necessary to run my research project. I really appreciate all your mentoring and guidance during these years.

I would like to offer my appreciation to Dr. Javier Figueroa and Dr. Ana Rita Mayol which they gave me the opportunity to be part of the Puerto Rico Louis Stokes Alliance for Minority Participation (PR-LSAMP) program and the “Bridge to Doctorate” fellowships, which impulse me to starts collaborations with Dr. Juan Miguel Feliu Martinez and his research group at the Institute of Electrochemistry from the University of Alicante in Spain.

A special thanks to Dr. Enrique Herrero Rodríguez who helped with all the things involved to enroll and achieve all the requirements necessary for the doctorate program of the University of Alicante, as well as for helping me to submit the Santiago Grisolía fellowship from the “Generalitat Valenciana” to afford this work.

Furthermore, I would like to recognize the financial support for this research project including NASA-URC Center of Advanced Nanoscale Materials (CANM), PR-LSAMP, Research Initiative for Scientific Enhancement (RISE), Sloan Research Fellowship and the NASA Puerto Rico SPACE GRANT Consortium (PRSGC).

Finally, I would like to thank my friends and all my labmates in special to Dr. Nestor E. Mendieta, Fabian Quesada Plata, Jose A. Quintero Ruiz, Dr. Myreisa Morales and Nadja E. Solis for being part of this beautiful experience and their help in several things. I am sure that the friendship forged with all of you will last for many years.

to my beloved family

Table of Contents

Abbreviation List

Abbreviation	Name
BP	British Pretoleum
H_2	Hydrogen
NH_3	Ammonia
CO_2	Carbon dioxide
HB	Haber-Bosh
N_2	Nitrogen
DAFC	Direct Alkaline Fuel Cells
SOFC	Solid Oxide Fuel Cell
Pt	Platinum
N_{ads}	Adsorbed monoatomic nitrogen
N_2	Nitrogen
OH^-	Hydroxide ion
Ir	Iridium
Ru	Ruthenium
Rh	Rhodium
Pd	Palladium
Cu	Cooper
Ag	Silver
Au	Gold

Ni	Nickel
fcc	Face-centered cubic
V	Voltage
A	Amperes
cm^2	Square centimeters
E	Potential
RHE	Reversible Hydrogen Electrode
w/o	water in oil
Me	Metal
$NaBH_4$	Sodium borohydride
M	Molar concentration
HCl	Hydrochloric acid
H_2SO_4	Sulfuric acid
HBr	Hydrobromic acid
HI	Hydriodic acid
H_3PO_4	Phosphoric acid
$HClO_4$	Perchloric acid
w/w	weight/weight
K_2PtCl_4	Potassium tetrachloroplatinate (II)
CV	Cyclic Voltammetry
RE	Reference Electrode
WE	Working Electrode
CE	Counter Electrode
Ar	Argon

O_2	oxygen
GC	Glassy Carbon
Cl^-	Chloride
Ge	Germanium
NP’s	Nanoparticles
I^-	Iodide
NaOH	Sodium hidroxyde
TEM	Transmision Electron Microscopy
EDX	Electron Dispersive X-rays
TGA	Thermogravimetric analysis
ISS	International Space Station

Resumen

La nanotecnología es la rama de la ciencia que estudia la materia a la escala de una mil millonésima parte de metro. Para tener una idea de la escala a la que se logra manipular la materia con la nanotecnología, podemos decir que es aproximadamente mil veces menor que una célula humana. La manipulación de la materia a esta escala ha logrado grandes avances. Dentro de las tecnologías que más se han desarrollado se encuentran: la electrónica, producción y almacenamiento de energía, óptica, medicina, computación, entre otras. Cabe destacar que la producción y almacenamiento de energía es una de las áreas más estudiadas en los últimos años. Esto se debe al incremento en la demanda energética, consecuente al aumento de la población, con un crecimiento aproximado del 1.2-2.0 % por año y al desarrollo de nuevas tecnologías que requieren energía para su funcionamiento. Se estima que para el año 2100 la demanda energética podría alcanzar hasta un consumo de 1,300,000,000 de barriles de petróleo por día. Este nivel de consumo no puede ser suministrado por la actual fuente principal de energía, que son los combustibles fósiles. Además, es evidente que la producción energética, partiendo de esta fuente, produce contaminación que posteriormente genera problemas ambientales como el incremento en la temperatura global, consecuente del efecto invernadero. Es por esta razón que el desarrollo conducente a la producción y almacenamiento de energía cada vez es más importante en nuestra sociedad.

Para la producción de energía se han investigado distintas fuentes renovables. Una de ella es la producción de energía utilizando hidrógeno (H_2) como combustible, la cual ofrece una alternativa limpia y renovable con la cual se logran evitar productos de combustión con base de carbón, que son los que suelen ser causantes de problemas ambientales. Sin embargo, la baja densidad energética por volumen junto con el problema asociado a su almacenaje y transporte, son algunas de las

desventajas que se han encontrado al promover la utilización de este combustible como fuente de energía. Una de las alternativas estudiadas para la utilización de H_2 es el almacenaje por medio de compuestos que contengan hidrógeno en su estructura molecular. El amoniaco (NH_3) es uno de los candidatos más prominentes, no solo por su gran capacidad de aportar hidrógeno, sino también por la habilidad para ser utilizado como una fuente alternativa para la producción de energía.

La utilización del NH_3 es atractiva por razones como las de ser un compuesto libre de carbono, lo cual disminuiría considerablemente la huella de carbono, producto de las emisiones de dióxido de carbono, y consecuentemente causantes del calentamiento global. Otro factor de interés es su abundancia y su fácil producción, lo que lo hacen un candidato viable en términos económicos. En lo que respecta al transporte y almacenaje, el NH_3 puede ser transportado con cuidados similares a los que transporta y almacenan los combustibles actuales, con lo cual, la infraestructura no se afectaría como en el caso de la implantación del H_2 como combustible. Por último, está la densidad energética que proporciona el NH_3 en comparación con el H_2, la cual es aproximadamente catorce veces superior, con lo que se confirma nuevamente la posibilidad de utilizar NH_3 como combustible alternativo.

Una de las formas más destacadas para la utilización del NH_3 como fuente de energía, son las pilas de combustible, las cuales son un dispositivo que genera electricidad a partir de reacciones electroquímicas. Para el caso particular de las pilas de combustible de NH_3, este pasa a través de un electrodo, conocido como el ánodo de la pila, donde un catalizador facilita la reacción de oxidación del combustible y genera una corriente que pasa a un circuito externo. Consecutivamente este flujo de electrones pasa al otro electrodo conocido como el cátodo, donde ocurre una reacción

de reducción. Finalmente, los iones producidos en esa reacción viajan a través de una membrana. El interés en estos dispositivos viene en la alta eficiencia energética que poseen, ya que las posibles pérdidas por calor pueden aprovecharse en cogeneración, no como en los motores de combustión interna y particularmente por la versatilidad de construcción que va desde pequeños dispositivos que pueden ser transportados fácilmente hasta grandes plantas de producción de energía.

Las aplicaciones más comunes incluyen tecnologías basadas en transporte (vehículos, autobuses, camiones, trenes, barcos, entre otros), tecnología militar (generadores portátiles de energía), productos portátiles (antorchas, cargadores de baterías, productos electrónicos personales) y fuentes de energía estacionarias. También se incluyen aquellas tecnologías dedicadas a la eliminación electroquímica del NH_3 de aguas residuales con los que se logra reutilizar agua y a su vez generar electricidad de este proceso. Este caso particular se ha estudiado para el desarrollo de tecnología espacial que pueda ser utilizada en transbordadores o estaciones espaciales, e incluyendo la posibilidad de utilizarla en la exploración humana de otros planetas, donde la carencia de recursos hace que se tenga que aprovechar todo desperdicio generando, para su reutilización y probablemente también, para producción de energía.

La reacción de oxidación de NH_3 ha sido ampliamente estudiada utilizando platino (Pt) como catalizador. Se ha comprobado que es una reacción extremadamente sensible a la estructura superficial de Pt, llevándose a cabo casi exclusivamente en los sitios con geometría (100). Teniendo en cuenta que un cubo idealmente tiene una estructura de seis caras con planos de simetrías (100), se ha estudiado la actividad catalítica para la oxidación de amoniaco en nanopartículas

cúbicas de Pt, las cuales han demostrado actividad catalítica superior a las nanopartículas sin ningún tipo de orientación preferencial superficial o, como se conocen comúnmente, poliorientadas.

Las nanopartículas de Pt con formas preferenciales han demostrado una alta actividad catalítica en un gran número de reacciones, por lo cual han sido ampliamente estudiadas en el desarrollo de tecnología conducente a catalizadores para pilas de combustible. Una de las razones por las cuales las nanopartículas han triunfado en el ámbito de catálisis es gracias a la gran cantidad de área superficial que poseen, haciendo posible la disponibilidad de más sitios activos para que las reacciones se puedan llevar a cabo. Sin embargo, muchas de estas reacciones son sensibles a la estructura superficial, lo que implica que la actividad catalítica depende la selectividad que tienen las moléculas a poder adsorberse adecuadamente en un determinado tipo de sitio. Por esta razón, la búsqueda de métodos para sintetizar nanopartículas con formas controladas y que incluya características como la facilidad de preparación, un corto tiempo de producción y, a su vez, que puedan realizarse a gran escala, se ha convertido en un reto actual.

Una de las síntesis más estudiadas para la preparación de nanopartículas de Pt con formas preferenciales son las síntesis coloidales. Sin embargo, estos métodos cuentan con la desventaja de que son difícilmente escalables, lo que hace imposible la tarea de producir en gran cantidad nanopartículas con orden superficial con estas metodologías. Actualmente se han estudiado métodos que pueden ser fácilmente escalables para la producción de nanopartículas de Pt, como es el método de microemulsión agua en aceite. Este es un método que comprende la interacción de una fase orgánica y una pequeña fracción de fase acuosa en presencia de un

surfactante, con el fin de formar nano-cápsulas en donde el precursor del metal se encuentra confinado, y consecutivamente reaccionar con el agente reductor, para obtener finalmente las nanopartículas. Sin embargo, este método carece de la capacidad para controlar la estructura superficial de las nanoestructuras obtenidas convirtiéndose en la principal desventaja del sistema.

En base a lo previamente discutido, es necesario la búsqueda de nuevos métodos capaces de obtener nanopartículas de una manera fácil, rápida, escalable y en la que se pueda lograr controlar la estructura superficial de las nanopartículas obtenidas. Por lo tanto, la presente Tesis Doctoral ha propuesto optimizar el método de microemulsión agua en aceite con el propósito de obtener nanopartículas de Pt con formas preferenciales y que cumpla con los requisitos necesarios para que pueda ser utilizada en la producción a gran escala de estos materiales. Esta Tesis Doctoral se presenta como un compendio de publicaciones y está organizada con una estructura que cuenta con un total de 9 capítulos de los cuales el primer capítulo es una introducción que relata con detalle lo que se ha discutido previamente en este resumen.

En el segundo capítulo de esta Tesis se encuentran los objetivos que se han logrado alcanzar en esta investigación. Estos se pueden resumir en tres objetivos específicos, siendo el primero la síntesis, caracterización y determinación del comportamiento electroquímico de nanopartículas preferencialmente cúbicas de platino sintetizadas utilizando el método de microemulsión agua en aceite, empleando la adición de ácidos en la fase acuosa como agentes modificadores de la forma estructural. El segundo objetivo de la tesis es la síntesis, caracterización y comportamiento electroquímico de nanopartículas bimetálicas con base de Pt (Pt/Me

con Me = Pd, Rh, Ir y Ru). Finalmente, el tercer objetivo de esta Tesis Doctoral comprende la evaluación del comportamiento electroquímico de monocristales de platino bajo la influencia de distintos ácidos, los cuales actuaron como agentes modificadores de superficie en la síntesis de nanopartículas de platino con formas preferenciales.

El tercer capítulo explica el método experimental para la preparación de las nanopartículas sintetizadas en esta investigación y describe las técnicas experimentales utilizadas. Dentro de estas técnicas resaltan los métodos electroquímicos, que han sido una herramienta de gran utilidad en el desarrollo de este proyecto de investigación. Una de las técnicas más utilizadas ha sido la voltametría cíclica, con la cual se ha caracterizado el material de manera cualitativa al comparar la presencia o ausencia de ciertas contribuciones en los perfiles voltamétricos característicos. También destaca el análisis cuantitativo, que se obtiene de la adsorción irreversible de germanio (Ge), con el que hemos logrado cuantificar la cantidad de sitios activos Pt (100) en las nanopartículas y podido comparar la síntesis de cara a obtener mayor control en la estructura superficial. Hemos conseguido medir el rendimiento catalítico de las partículas comparando la intensidad de los picos de oxidación para la reacción de interés, al igual que en algunos de los casos pudimos evaluar la estabilidad del catalizador utilizando técnicas como la cronoamperometría.

En este capítulo también se discuten técnicas de análisis de superficie con las que se pudo confirmar la estructura superficial de las nanopartículas, como la microscopía de transmisión de electrones (TEM) y también la composición para las nanopartículas bimetálicas con la técnica de dispersión de rayos X (EDX). Otra

técnica discutida comprende el análisis termogravimétrico (TGA) realizado a muestras soportadas que se realizaron para la colaboración con otros proyectos de investigación llevados a cabo en la Universidad de Puerto Rico, recinto de Río Piedras, de los cuales se destaca, la participación en el proyecto de Micro-G, para la preparación y evaluación de actividad catalítica de las nanopartículas de Pt preferencialmente cúbicas para la oxidación de NH_3 en una pila de combustible, bajo los efectos de la efectos de la ingravidez en un avión ZERO-G de la Agencia Nacional de Aeronáutica y Administración Espacial (NASA). Así mismo, un segundo proyecto con Micro-G relacionado a la oxidación electroquímica de NH_3, utilizando nanopartículas preferencialmente cúbicas, se llevará a cabo en la estación espacial internacional (ISS) para estudiar su comportamiento en condiciones de cero gravedad.

Por último, un proyecto con el logramos colaborar con el trabajo de investigación realizado por la Ph. D. Myreisa Morales acerca del depósito de las nanopartículas de Pt, sintetizadas con nuestro método, para la preparación de cepillos de fibra de carbono con el objetivo de medir su actividad catalítica frente la oxidación de amoniaco. La visión de este proyecto se basa en realizar los primeros estudios en la fabricación de un reactor con bacterias tipo *P. vulgaris,* las cuales son capaces de oxidar la urea, proveniente de orina, en amoniaco y consecutivamente, oxidar el amoniaco producido con las nanopartículas de platino para obtener energía de este proceso y la reutilización de aguas residuales.

En el cuarto, quinto y sexto capítulo, se exponen los resultados de los trabajos publicados en revistas científicas con alto índice de impacto. En el cuarto capítulo podemos encontrar la **primera publicación**, donde por primera vez, se publica una

síntesis de nanopartículas de Pt preferencialmente cúbicas utilizando el método de microemulsión agua en aceite en donde el ácido clorhídrico (HCl) se utilizó como un agente modificador de superficie. La microemulsión agua en aceite que se escogió para la realización de este trabajo está constituida por 80.5 % de la fase orgánica (N-heptano), 16.5 % del surfactante (Brij® 30) y 3% de la fase acuosa. En este trabajo se realizó una comparación de las formas preferenciales que obtenían las nanopartículas de platino a medida que cambiaba la concentración de HCl en la fase acuosa donde se encuentra el precursor de Pt, que en este caso fue ácido hexacloroplatínico (IV) hidratado (H_2PtCl_6 x H_2O). Para obtener las nanopartículas el precursor de Pt fue reducido añadiendo borohidruro de sodio ($NaBH_4$) en polvo, directamente en la microemulsión. Una vez se obtuvieron las nanopartículas, estas fueron limpiadas con acetona y agua ultra pura para ser analizadas.

En este trabajo, se estudiaron varias concentraciones de HCl en la fase acuosa de la microemulsión, entre ellas 5, 10, 15, 20, 25 y 37% w/w, que es la mayor concentración a la que se puede obtener el ácido comercialmente. Para tener una idea de la estructura superficial obtenida en las nanopartículas sintetizadas, se realizó principalmente un estudio electroquímico utilizando voltametría cíclica. El estudio de los perfiles voltamétricos en 0.5 M ácido sulfúrico confirmó la mayor presencia de nanopartículas de platino preferencialmente cúbicas como resultado de la síntesis que se preparó a una concentración entre el 15-25 % HCl. En los perfiles voltamétricos de las nanopartículas preparadas bajo estas condiciones, resaltaron dos contribuciones cerca de 0.26 V y 0.38 V, correspondientes a la presencia de dominios pequeños (100) y a las terrazas anchas con simetría (100), respectivamente. Estas nanopartículas suministran mayor densidad de corriente en comparación con las otras nanopartículas preparadas bajo distintas concentraciones de HCl. También se notó

que, para ciertas concentraciones de HCl, una reducción significativa en el pico correspondiente a los sitios (110), que está centrado aproximadamente en 0.12 V y así mismo una reducción en la contribución en 0.55 V correspondiente a los sitios (111). Este comportamiento electroquímico confirmó la presencia de cubos en las nanoestructuras obtenidas, ya que como se ha mencionado anteriormente, los cubos están constituidos por seis planos (100). Sin embargo, cuando se aumentó la concentración al máximo (37% HCl) el perfil voltamétrico obtenido mostró menos densidad de corriente en los picos correspondientes al plano Pt (100), lo que indicó la corrosión de la estructura preferencial que genera la presencia de defectos en la superficie de las caras.

La presencia de estructuras preferencialmente cúbicas fue confirmada en este trabajo con un análisis TEM, en donde pudimos ver la evolución de la estructura forma con las nanopartículas preparadas a diferentes concentraciones. A medida que aumentaba la concentración de HCl, hasta el valor de 25%, las nanopartículas adquirieron cada vez una mayor estructura preferencialmente cúbica con menor cantidad de defectos en la superficie. En este caso nos referimos con defectos presentes en las nanopartículas a otros sitios con geometrías no conducentes a un cubo, o a estructuras geométricas similares a cubos pero que posean algún defecto en alguno de sus lados, como se ha observado en las imágenes TEM de las nanopartículas sintetizadas.

Cuando la concentración alcanzó el máximo, 37%, las nanoestructuras reportadas tenían particularmente la forma de cubos truncados, lo que responde a la disminución en la concentración de los sitios (100) en las nanopartículas sintetizadas. Este resultado explica la razón por la cual el perfil voltamétrico de estas partículas

muestra una reducción en la densidad de corriente para los picos relacionados con la presencia de sitios (100) en las nanopartículas sintetizadas. La realización de un histograma del tamaño de las nanopartículas sintetizadas a partir de las imágenes TEM, dio como resultado un valor aproximado al tamaño promedio de las nanopartículas de 14 nm.

Para cuantificar la cantidad de sitios (100) en las nanopartículas de platino preferencialmente cúbicas, se realizó el estudio electroquímico de adsorción irreversible de Ge. Este estudio confirmó nuevamente el aumento de la cantidad de los sitios (100) en las nanopartículas de platino hasta llegar a un máximo (alrededor de un 44%) para las nanopartículas sintetizadas con un 25% de HCl y consecutivamente una disminución cuando la concentración de HCl seguía aumentando.

Las nanopartículas sintetizadas fueron evaluadas finalmente en la determinación de la actividad catalítica frente a la oxidación de NH_3 en medio alcalino. Esta reacción es particularmente sensible a los sitios (100) y nuevamente confirma que las nanopartículas sintetizadas poseen una estructura preferencialmente cúbica, ya que se logra obtener una densidad de corriente superior a la obtenida con nanopartículas de platino poliorientadas. Una comparación entre las nanopartículas sintetizadas determinó que las nanopartículas sintetizadas con 25% HCl son las que mayor densidad de corriente lograron obtener sobre la oxidación de NH_3. En conclusión, en este estudio se logró sintetizar nanopartículas preferencialmente cúbicas utilizando la microemulsión agua en aceite en donde se añadió HCl como agente modificador y se observó que las nanopartículas preparadas con

concentración entre 20-25% de HCl obtuvieron una estructura preferencialmente cúbica con la menor cantidad de defectos en la estructura superficial.

En el quinto capítulo de esta tesis doctoral se encuentra la **segunda publicación** que está dirigida a la síntesis de nanopartículas preferencialmente cúbicas utilizando ácido sulfúrico (H_2SO_4). En este trabajo, de manera análoga a la primera publicación, se logra obtener nanopartículas preferencialmente cúbicas utilizando H_2SO_4 como agente modificador de superficie utilizando una microemulsión agua en aceite. Al igual que en nuestro primer trabajo, el ácido es añadido en la solución acuosa en la que se prepara el precursor de Pt. Una vez es añadido en la microemulsión se reduce con borohidruro de sodio en forma de polvo, que es añadido directamente a la microemulsión. Finalmente, las nanopartículas sintetizadas fueron lavadas con varios enjuagues de acetona y agua ultra-pura hasta que finalmente se dejan suspendidas en agua para su estudio.

En este trabajo, se lograron sintetizar nanopartículas con distintos porcentajes de H_2SO_4 (6.25, 12.5 y 25%). En los perfiles voltamétricos correspondientes a la caracterización electroquímica de las nanopartículas sintetizadas, se observó un aumento de la densidad de corriente en los picos correspondientes a la presencia de nanopartículas preferencialmente cúbicas tal y como fue observado con las nanopartículas sintetizadas con HCl. Este patrón fue observado en todos los perfiles voltamétricos siendo el de las nanopartículas sintetizadas al 25% H_2SO_4, el perfil con los picos de mayor intensidad. Las imágenes TEM confirman nuevamente la presencia de nanoestructuras preferencialmente cúbicas, especialmente para aquellas que fueron sintetizadas al 25% H_2SO_4 cuyas imágenes TEM mostraron la menor cantidad de defectos estructurales. En términos de tamaño, el histograma

determinó que el valor promedio estaba cercano a los 9 nm, que, en comparación con las muestras sintetizadas con HCl, son relativamente más pequeñas, lo que es muy importante desde un punto de vista aplicado.

La determinación cuantitativa de los planos de sitios con geometría (100) en las nanopartículas preferencialmente cúbicas se realizó por dos métodos distintos para comparar los resultados obtenidos. Primero se realizó una deconvolución del perfil voltamétrico de cada muestra y se pudo determinar concretamente la cantidad de sitios superficiales (100) de las nanopartículas sintetizadas. En el caso de las nanopartículas sintetizadas con un 25 % H_2SO_4, se obtuvo un valor cercano al 50% de sitios (100). Para la determinación específica de los dominios o terrazas anchas, el método de adsorción de Ge fue utilizado y se pudo determinar un valor aproximado de 35% para las nanopartículas sintetizadas con 25 % H_2SO_4.

La oxidación de monóxido de carbono (CO) fue estudiada para ver el comportamiento electroquímico sobre esta reacción y se pudo concluir que los perfiles voltamétricos contaban con dos contribuciones, una a 0.70 V y la otra en 0.75 V. Estos picos característicos mostraron una evolución clara que consistía en una disminución de la intensidad del primer pico y un aumento de la intensidad del segundo pico conforme al aumento de la concentración de H_2SO_4 utilizado para sintetizar las nanopartículas de Pt. Este comportamiento nuevamente confirmó la presencia de estructuras preferencialmente cúbicas para las nanopartículas sintetizadas con la mayor cantidad de H_2SO_4. Las nanopartículas también fueron evaluadas frente a la oxidación de NH_3 y se encontró que las nanopartículas de Pt que mayor actividad tenían alcanzaron una densidad de corriente hasta tres veces mayor que la obtenida con las nanopartículas poliorientadas.

En resumen, se lograron sintetizar nanopartículas preferencialmente cúbicas utilizando H_2SO_4 como agente modificador de superficie y logramos ver la evolución en la estructura superficial a medida que cambiaba la concentración de H_2SO_4 que se utilizaba para sintetizar las nanopartículas de Pt. Se pudo observar también una evolución del comportamiento sobre la oxidación de CO y también de NH_3 que, como se ha mencionado anteriormente, son reacciones altamente sensibles a la estructura superficial de Pt. En comparación con las nanopartículas sintetizadas en la primera publicación podemos decir que HCl sigue siendo un mejor agente modificador de superficie, ya que la concentración a la que se estudió el H_2SO_4, el HCl pudo facilitar nanopartículas preferencialmente cúbicas con mejores rendimientos sobre la oxidación de NH_3. Sin embargo, las nanopartículas preparadas mediante H_2SO_4 mostraron un tamaño medio significativamente menor a las preparadas con HCl.

En el sexto capítulo se encuentra la **tercera publicación** que hace un estudio comparativo de todos los casos estudiados en la síntesis de nanopartículas con formas controladas utilizando el método de microemulsión agua en aceite bajo la presencia de distintos ácidos. Dentro de los ácidos estudiados se encuentra nuevamente el H_2SO_4 a concentraciones mayores de las estudiadas previamente, ácidos halogenados como el ácido bromhídrico (HBr) y el ácido yodhídrico (HI). También el estudio se realizó con un ácido poliprótico, el ácido fosfórico (H_3PO_4) y finalmente con ácidos orgánicos, de los cuales se estudiaron el ácido ascórbico, el ácido cítrico y el ácido oxálico. Los resultados obtenidos partiendo de los perfiles voltamétricos de cada una de las nanopartículas sintetizadas, demostró que los ácidos tales como el HBr y el H_3PO_4 sirvieron también como agentes modificadores de superficie en la síntesis de nanopartículas de Pt.

Para el caso donde se utilizó HBr, se observó que con hasta un 25% se lograba obtener una mayor cantidad de nanopartículas preferencialmente cúbicas, observándose claramente en el perfil voltamétrico, donde las nanopartículas obtenían altas densidades de corriente en los picos correspondientes a los sitios con geometrías (100), en comparación con las muestras sintetizadas con otras concentraciones. En este caso cabe destacar que se prepararon nanopartículas con la concentración más alta disponible comercialmente (48% w/w), sin embargo, como se ha visto con el caso de HCl, una concentración muy alta, produce otro tipo de estructura superficial en donde se degradan los sitios o terrazas (100) en las nanopartículas sintetizadas. En cuanto a la oxidación de CO para estas muestras, nuevamente se pudo confirmar un patrón en donde la presencia de los picos en esta reacción sensible a la estructura denota la presencia de pequeños dominios y terrazas (100) en las nanopartículas sintetizadas. La presencia de los dominios o terrazas (100) fue confirmado con la adsorción irreversible de Ge, en donde la muestra preparada con el 25% HBr destacó sobre las demás obteniendo un 44.9% de dominios, con esta geometría.

Las muestras que fueron sintetizadas con H_3PO_4 lograron obtener cierto grado de control sobre la superficie, pero no tan marcado como en los casos anteriores. Esto se pudo evaluar al comparar las densidades de corriente de los picos obtenidos en los perfiles voltamétricos en donde los picos correspondientes a los pequeños dominios y terrazas (100) no alcanzaron la intensidad de los casos anteriores con HCl o HBr. En este caso es importante mencionar que se lograron sintetizar nanopartículas de Pt con hasta un 85% de H_3PO_4 siendo estas las que mayor presencia de sitios (100) obtuvieron empleando este modificador. Esto se pudo

confirmar nuevamente con la adsorción irreversible de Ge con la que se obtuvo solo un 29.2% de dominios y terrazas (100) para esta muestra en particular.

En cuanto a las muestras que se sintetizaron con HI, no se logró ver un cambio importante en el perfil voltamétrico, comparando los mismos con el perfil voltamétrico de las nanopartículas de Pt poliorientadas. En este caso se logró estudiar hasta un máximo de 10% de HI, ya que, a concentraciones más altas, el Pt no lograba reducirse y consecuentemente no se podían obtener nanopartículas. Un comportamiento similar ocurrió cuando se emplearon ácidos orgánicos. Las bajas concentraciones a las que se estudiaron no lograron ningún tipo de influencia en la estructura superficial de las nanopartículas de Pt, a pesar de que estas concentraciones habían sido empleadas en otras metodologías de síntesis para producir estructuras preferenciales.

Otro parámetro que se evaluó en este trabajo fue el cambio del agente precursor de Pt. En este caso particular pudimos observar el efecto en el cambio del H_2PtCl_6 comúnmente utilizado por el tetracloroplatinato de potasio (K_2PtCl_4), utilizando HCl y H_2SO_4 como agentes modificadores de superficie. Con este nuevo precursor, y en el caso particular de la adición de HCl, se observó un perfil voltamétrico mucho más definido en cuanto a la presencia de sitios y terrazas (100) para el caso de las nanopartículas que se sintetizaron al 15% HCl. Este comportamiento fue confirmado con la adsorción irreversible de Ge en donde alcanzó un valor aproximado de 46.7% de dominios o terrazas (100). La síntesis de las nanopartículas de Pt se realizó con hasta el 20% HCl, ya que, a concentraciones mayores la sal de Pt era insoluble. Para el caso donde se utilizaron distintas concentraciones de H_2SO_4 como agente modificador en la síntesis de nanopartículas

de Pt, se observó que la concentración optima a la que se ve una mayor cantidad de sitios y terrazas (100) en las nanopartículas fue de 50% H_2SO_4 empleando K_2PtCl_4 como precursor.

Finalmente, se estudió la oxidación de NH_3 para las nanopartículas que mostraron una mayor contribución de sitios y terrazas (100) en la caracterización en H_2SO_4. De esta comparación cabe destacar que las nanopartículas preferencialmente cúbicas sintetizadas con el precursor K_2PtCl_4 en presencia de un 15% HCl obtuvieron la mayor densidad de corriente. Las segundas más activas fueron las nanopartículas estudiadas en la primera publicación de esta investigación y en tercer lugar las nanopartículas que fueron sintetizadas con un 47% H_2SO_4 como agente modificador de la superficie. Las otras muestras estudiadas dieron valores menores a las antes mencionadas. Sin embargo, cabe destacar que todas fueron por encima del valor obtenido para las nanopartículas poliorientadas, que son las que menor rendimiento catalítico tienen frente a la oxidación de NH_3 en dicho estudio.

El séptimo y octavo capítulo exponen más resultados, pero de trabajos que están en proceso de publicación. En el **séptimo capítulo** presentamos la síntesis, caracterización y determinación de la actividad catalítica sobre etanol y amoniaco para nanopartículas bimetálicas platino-rodio con formas preferenciales. Esas nanopartículas fueron sintetizadas utilizando el método de microemulsión agua en aceite previamente discutido y evaluando el efecto de ácidos (HCl, HBr y H_2SO_4) a las mismas concentraciones que se estudiaron en las publicaciones previamente discutidas. También se estudió el efecto en el cambio del precursor de Pt en la preparación de nanomateriales bimetálicos. La comparación de los precursores fue

entre el H_2PtCl_6 y el K_2PtCl_4 manteniendo el cloruro de rodio ($RhCl_3$), precursor de Rh, constante.

Las nanopartículas de Pt/Rh que se sintetizaron con el H_2PtCl_6 y el $RhCl_3$ en presencia de 20% HCl se prepararon a varias composiciones Pt/Rh que incluyen 0/100, 25/75, 50/50, 75/25, 90/10 y 100/0, siendo 0/100 y 100/0 las nanopartículas puras de Rh y Pt, respectivamente. Una comparación entre los perfiles voltamétricos de Pt y Rh puros con los perfiles voltamétricos de las nanopartículas sintetizadas que están a distintas composiciones de Pt/Rh, denota la transición entre ambos perfiles en donde las contribuciones presentes dependen estrictamente del metal que tenga el mayor grado de composición atómica. Un caso interesante son las nanopartículas Pt_{75}/Rh_{25} en donde las contribuciones más importantes son prácticamente los mismos picos característicos de los dominios y terrazas del Pt (100). La aportación más grande del Rh la vemos con la presencia de un pico centrado en 0.12 V. Esos picos van cambiando sucesivamente de acuerdo a la concentración del Pt/Rh en cada una de las muestras, de manera tal que los perfiles voltamétricos obtuvieron similaridades en los perfiles voltamétricos a los de las nanopartículas puras. En la oxidación de CO vimos también un patrón similar, donde los perfiles de las nanopartículas Pt/Rh muestran un comportamiento intermedio al de los dos metales puros. También se observa un comportamiento similar al cambiar de precursor, al K_2PtCl_4 junto con $RhCl_3$, en presencia de 15% HCl.

Con respecto a la forma preferencial obtenida, los análisis confirmaron la presencia de nanoestructuras bimetálicas con formas preferenciales. Para esto las partículas se analizaron mediante TEM y EDX. Concretamente, las partículas analizadas fueron los cuatro tipos de nanopartículas Pt_{75}/Rh_{25} sintetizadas tres agentes modificadores y los dos precursores. Para el caso de las nanopartículas que

fueron sintetizadas utilizando H_2PtCl_6 como precursor y 20% HCl como agente modificador, se obtuvo que la composición era prácticamente la nominal (75.81% Pt y 24.19% Rh). Por el contrario, las otras muestras preparadas mostraron tener alrededor de un 80% Pt y un 20% Rh que son valores aceptables, pero que difieren de los valores teóricos con los que se sintetizaron las nanopartículas. En cuanto a la forma de las nanopartículas es evidente la presencia de nanoestructuras tipo cúbicas tanto en aquéllas que fueron sintetizadas con H_2PtCl_6 como precursor y 50% H_2SO_4 como agente modificador, como con el precursor K_2PtCl_4 en presencia de 15% HCl como agente modificador. Sin embargo, en aquellas en las que se utilizó el precursor de H_2PtCl_6 en presencia de 25% HBr como agente modificador, se observó otro tipo de estructura con lados bastante definidos.

La determinación de la actividad catalítica de las nanopartículas sintetizadas fue determinada para la oxidación de NH_3 y etanol en medio alcalino respectivamente. En cuanto a la oxidación de NH_3, los resultados obtenidos al evaluar las nanopartículas que fueron sintetizadas con H_2PtCl_6 y $RhCl_3$ al 20% HCl muestran claramente que la oxidación del amoniaco comienza a un potencial menos positivo para las muestras Pt_{75}/Rh_{25} y Pt_{90}/Rh_{10}, en comparación con los perfiles de los dos metales puros. Sin embargo, las nanopartículas puras de Pt son las que mayor densidad de corriente obtuvieron. Además, la tendencia es muy clara al observar que a medida que aumenta el porcentaje de Rh disminuye la corriente de pico, llegando a valores muy bajos para el caso de Rh puro, confirmando que las nanopartículas de Rh no poseen prácticamente actividad catalítica sobre la oxidación de NH_3. Sin embargo, el estudio cronoamperométrico realizado a 0.55 V confirmó que las muestras Pt_{90}/Rh_{10} y Pt_{75}/Rh_{25} poseen una mayor densidad de corriente a este potencial en comparación con las nanopartículas de Pt puro. Este desplazamiento del

potencial de arranque hacia valores menos positivos es importante ya que significa que el Rh en cierta manera favorece el proceso.

Un caso similar al evaluado anteriormente es observado con las muestras sintetizadas con K_2PtCl_4 y $RhCl_3$ preparadas al 15% HCl donde vemos nuevamente la tendencia de una disminución de la densidad de corriente en el pico a medida que disminuimos la concentración de Pt en las muestras y aumentamos la del Rh. En cuanto a los perfiles de las cronoamperometrías, se observa que a 0.55 V la muestra Pt_{90}/Rh_{10} obtuvo una densidad de corriente levemente mayor que la muestra de Pt puro y seguido por la muestra Pt_{75}/Rh_{25}.

La tercera serie de nanopartículas de Pt/Rh sintetizadas, que se prepararon con el precursor H_2PtCl_6 en 25% HBr, muestra una tendencia similar a las otras muestras sintetizadas. La actividad catalítica para la oxidación de amoniaco presentó una disminución de la densidad de corriente tanto como para las muestras bimetálicas, en comparación con las muestras de las nanopartículas puras de Pt y además, la sucesiva disminución de la actividad catalítica al aumentar el porcentaje de Rh en las muestras. La baja actividad catalítica para toda la serie, se le atribuyó a la posibilidad de una estructura superficial de las nanopartículas con menor proporción de dominios (100).

Al igual que en los casos anteriores, las muestras que se sintetizaron con los precursores H_2PtCl_6 y $RhCl_3$ en presencia de 50% H_2SO_4 como agente modificador, mostraron una tendencia similar, que también se observa para la oxidación de NH_3.

Otro estudio que se realizó, para confirmar el efecto en la formación de dominios con orientaciones preferenciales fruto de la adición del agente modificador, fue la comparación de los perfiles voltamétricos entre nanopartículas con la misma

composición Pt_{75}/Rh_{25} pero comparando las muestras que se prepararon con y sin agente modificador. Las nanopartículas a las que no se no se les añadió ningún tipo de modificador, no poseen una formación preferencial para un tipo de facetas, siendo por lo tanto poliorientadas. Cuando comparamos los perfiles voltamétricos, vemos leves diferencias en los tres picos característicos que se han descrito anteriormente. El efecto de la forma preferencial se confirma por la reactividad electroquímica en la oxidación de NH_3, donde el perfil voltamétrico de las nanopartículas en las que se utilizó el agente modificador obtuvo un aumento significativo de la densidad de corriente en comparación con aquellas nanopartículas que fueron sintetizadas sin la presencia de ningún agente modificador. De la misma manera, podemos ver el mismo patrón en la cronoamperometría, con mayores densidades de corriente obtenidas por las nanopartículas bimetálicas con formas preferenciales.

En cuanto a la oxidación de etanol, esta fue escogida para el estudio de la actividad catalítica en las nanopartículas bimetálicas sintetizadas debido a que es también, una reacción sensible a la estructura superficial. Estudios previos han demostrado que los nanocubos de Pt presentan una alta actividad catalítica sobre la reacción de oxidación de etanol. Nuestro experimento se basó en la comparación de la actividad catalítica de las distintas composiciones de las nanopartículas Pt/Rh preparadas, incluyendo las nanopartículas de Pt y Rh puras que fueron sintetizadas en la serie. En estos experimentos se pudo comprobar la excelente actividad catalítica de las nanopartículas cúbicas de Pt en comparación con las nanopartículas de Rh. Sin embargo, una pequeña adición de Rh en las nanopartículas de Pt logra mejorar la actividad catalítica de las mismas. En el caso de las nanopartículas sintetizadas con H_2PtCl_6 al 20% HCl, las nanopartículas Pt_{75}/Rh_{25}, muestran menores potenciales de inicio para la reacción y una densidad de corriente considerablemente más alta en

comparación con las nanopartículas de Pt. Un caso similar se observa para las nanopartículas sintetizadas con K_2PtCl_4 donde las nanopartículas Pt_{90}/Rh_{10}, fueron las mejores en términos de densidad de corriente. Sin embargo, el potencial de inicio de la oxidación estuvo más desplazado hacia potenciales más positivos que para las nanopartículas Pt_{75}/Rh_{25}.

Para concluir la clasificación de las muestras que evidenciaron la mejor actividad catalítica sobre la oxidación de etanol, se realizó una comparación de las distintas curvas obtenidas de las nanopartículas Pt_{75}/Rh_{25}, que se sintetizaron con los distintos precursores y modificadores. De este estudio se llegó a la conclusión que las nanopartículas sintetizadas con K_2PtCl_4 al 15% HCl presentaron un mejor rendimiento, con picos de mayor densidad de corriente para la oxidación de etanol. Sin embargo, aquellas que fueron sintetizadas con H_2PtCl_6 al 20% HCl demostraron un desplazamiento del pico a potenciales menos positivos con lo cual, podemos concluir que ambas demostraron una actividad catalítica similar.

En conclusión, se pudieron sintetizar nanopartículas bimetálicas Pt/Rh con formas preferenciales y se observó que las muestras con ciertas concentraciones de Rh lograron mejorar el rendimiento en la oxidación de etanol y favorecer el desplazamiento del potencial de inicio de la reacción a potenciales menos positivos en la oxidación de NH_3.

El **octavo capítulo** presenta los resultados obtenidos de un estudio fundamental con monocristales de platino en la búsqueda de información que sustente la capacidad de los ácidos a elevadas concentraciones a convertirse en un agente modificador de la superficie. Hemos realizado una serie de experimentos en donde hemos logrado ver el comportamiento electroquímico de los monocristales de

Pt con los tres planos de bases de Pt que son Pt (100), Pt (111) y Pt (110), y compararlos con el electrodo que reúne todos los planos, conocido como Pt poliorientado [Pt(poli)].

El primer estudio fue la realización de voltametrías cíclicas en distintas concentraciones de ácido clorhídrico (HCl). Se escogieron las concentraciones (5, 10, 15, 20, 25, 35% m/v) similares a las que se habían empleado para realizar la síntesis de las nanopartículas de Pt en la primera publicación de esta tesis doctoral. La evaluación del comportamiento electroquímico frente a las distintas concentraciones dio como resultado una serie de curvas características con unos desplazamientos progresivos de los picos voltamétricos a medida que aumentaba la concentración de HCl. También se observó la sensibilidad a la estructura superficial, obteniendo un comportamiento característico para cada uno de los planos de bases estudiados. Otro comportamiento observado fue obtenido por el electrodo Pt(poli) donde pudimos ver que en el perfil voltamétrico se suman todas las contribuciones prominentes de cada uno de los planos de base de Pt. Por último, realizamos un tratamiento matemático con el que pudimos hallar una relación lineal entre el potencial de los picos obtenidos en cada uno de los monocristales de Pt estudiados en función del logaritmo de la actividad [Log (a)] del ácido empleado como electrolito soporte.

El mismo estudio fue realizado también para distintas concentraciones de H_2SO_4. Aunque el análisis de los monocristales de Pt en este electrolito soporte ha sido ampliamente estudiado, no se había publicado el comportamiento electroquímico a concentraciones tan altas. A diferencia del comportamiento electroquímico que se observó en HCl, con este electrolito solo se presenció el desplazamiento del perfil voltamétrico a potenciales menos positivos a medida que aumentaba la concentración

de H_2SO_4. Para cada uno de los planos de base, se observó un comportamiento electroquímico característico y también pudimos hallar una relación lineal entre el potencial del máximo del pico en función del Log a.

En este capítulo, también se muestra la caracterización electroquímica en 0.5 M HCl de los monocristales de Pt utilizados y de nanopartículas con formas preferenciales de las cuales destacan cubos, octaedros y esferas. Haciendo una comparación de los perfiles voltamétricos de los monocristales de Pt y las nanopartículas, pudimos ver que cada estructura superficial responde a un comportamiento característico y esperado según su estructura superficial. Por lo tanto, al igual que el H_2SO_4, el HCl funciona como electrolito soporte con el que podemos determinar electroquímicamente la estructura preferencial de las nanopartículas de Pt.

Finalmente, el último capítulo de este trabajo se basa en las conclusiones generales de la presente Tesis Doctoral, destacando una vez más algunos de los sectores que se han beneficiado gracias al desarrollo de esta investigación. Se han dejado puertas abiertas a profundizar sobre este proyecto de investigación por lo cual nos queda un camino largo para continuar el trabajo futuro. Cabe destacar que este trabajo ha sido parte de un proyecto de investigación para el desarrollo de pilas de combustible de NH_3 en el espacio y pudimos colaborar con el grupo de investigación de la Universidad de Puerto Rico conocido como *Micro-G*, con el cual pudimos realizar una publicación estudiando la oxidación de NH_3 bajo los efectos de la microgravedad. Como proyecto futuro, estamos desarrollando junto a Micro-G un sistema con el que podamos evaluar la oxidación de amoniaco con nanopartículas cúbicas de Pt en la estación espacial internacional (ISS). En este último proyecto hemos sido parte fundamental en el desarrollo del tratamiento experimental que se realizará en

condiciones de ingravidez. Este es un ejemplo de las aplicaciones más interesantes que ha tenido este proyecto de investigación. En resumen, podemos decir que esta Tesis Doctoral junto con el proyecto de investigación que se llevó a cabo, ha aportado una pieza clave para el desarrollo de nuevas tecnologías que, a día de hoy, necesitan de más investigación para que puedan ser accesibles en un futuro.

Chapter 1.

Introduction

1. Introduction

1.1. Aims for ammonia oxidation study

Worldwide energy consumption is reaching alarming levels. The energy demand is increasing at an exponential rate due to a combination of factors, including the growth of population, which increases at a rate of 1.2-2.0% per year.[1] A rise in the demand for new technologies and services for the population, claims an energy demand that we currently cannot afford. At present, fossil fuels are the primary source for power generation. The most used non-renewable resources include crude oil, coal and natural gas. About two-thirds of the world's oils are consumed in the transportation industry.[2]

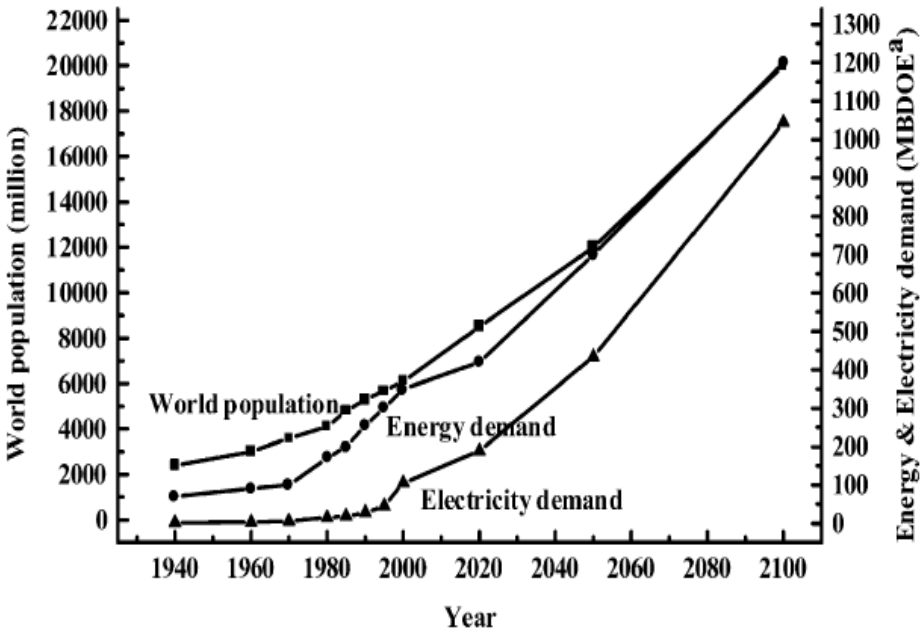

Figure 1-1. Graphic illustration of the estimated world global energy and electricity demand ([a] Millions of barrels per day of oil equivalent). Reproduced from E. Traversa and A. Boudghene Stambouli (2002).[1]

According to the BP statistical review of the world energy and with the current dependence on fossil fuels, crude oil reserves will last about 50 years approximately.[3] In addition, the contamination resulting mainly from the combustion products from fossil fuels leads us and the new generations to live in a world with several environmental problems. The most evident one is the climate change caused by the increase of global temperatures, as a consequence of the emission of greenhouse gases.

In relation to this problem, researchers are currently studying different renewable energy resources. The most studied is hydrogen (H_2), which offers clean and renewable energy over combustion, avoiding the emission of harmful pollutants.[4-6] However, low volumetric energy density together with storage and transportation issues have been considered as drawbacks when taken into consideration as an alternative fuel. In addition, several hydrogen carriers and substitutes have been considered to improve the energy density and decrease the risk of its usage.

Ammonia (NH_3) is considered one of the most promising candidates, not only for its H_2 carrier capacity but also for its ability to be used as an alternative fuel. The use of NH_3 is very attractive for several reasons especially that is it a ‘’carbon free’’ molecule. This means that the incorporation of NH_3 to the fuel industry could considerably decrease the carbon footprint which mostly corresponds to carbon dioxide (CO_2) emissions produced by using carbon-based materials and which cause global warming.

Another important advantage to consider NH_3 as an alternative fuel is its abundance and its profitable production, which could improve the fuel economy. Approximately 130 million tons of NH_3 is produced per year, that as shown in figure 1-

2. This amount obtained for the year 2009 and 2010, is distributed among NH_3 producers around the world.[7] The production of significant quantities of NH_3 are intended mostly for the industrial feedstock as fertilizer.[8]

World Ammonia Production and Reserves:

	Plant production		Reserves
	2009	2010	
United States	7,700	8,300	Available atmospheric nitrogen and sources of natural gas for production of ammonia are considered adequate for all listed countries.
Australia	1,200	1,200	
Bangladesh	1,300	1,300	
Canada	4,000	4,000	
China	42,300	42,000	
Egypt	2,000	2,300	
Germany	2,360	2,500	
India	11,200	11,700	
Indonesia	4,600	4,600	
Iran	2,000	2,000	
Japan	1,100	1,000	
Netherlands	1,800	1,800	
Pakistan	2,300	2,300	
Poland	1,990	1,900	
Qatar	1,800	1,800	
Romania	1,300	1,300	
Russia	10,400	10,400	
Saudi Arabia	2,600	2,600	
Trinidad and Tobago	5,100	5,500	
Ukraine	4,200	3,300	
Uzbekistan	1,000	1,000	
Venezuela	1,160	1,160	
Other countries	17,000	17,000	
World total (rounded)	130,000	131,000	

World Resources: The availability of nitrogen from the atmosphere for fixed nitrogen production is unlimited. Mineralized occurrences of sodium and potassium nitrates, found in the Atacama Desert of Chile, contribute minimally to global nitrogen supply.

Substitutes: Nitrogen is an essential plant nutrient that has no substitute. Also, there are no known practical substitutes for nitrogen explosives and blasting agents.

Figure 1-2. World NH_3 production and reserves in thousands metric tons obtained from the U.S. Geological Survey, Mineral Commodity Summaries (2011).[7]

There are currently several methods for the industrial production of NH_3. The main industrial method today for this purpose is the Haber-Bosh (HB) process, which consists basically into artificial nitrogen fixation. This process, in summary, takes H_2 extracted mostly from steam reforming of natural gas and it is combined with atmospheric nitrogen (N_2) gas under controlled high pressures (15-25 MPa) and high temperatures (400-500 °C) in the presence of a catalyst.[9] However, biomass is the

main renewable source for the H_2 used in this process. This means that HB process favors, indirectly, the CO_2 emissions which put this process in a disadvantage in environmental terms. However, statistically, only 3-5 percent of the world's natural gas production is consumed in the HB process which implies a low rate compared to other procedures that are more polluting.

Licht's method is another NH_3 production process which provides an alternative to the HB process due to the improvement in both energy efficiency and carbon footprint.[10] This process combines natural resources as air, water and sunlight to produce NH_3. In summary, water electrolysis is used to obtain H_2 by a procedure in which bubbles of wet air pass through a nanoscale suspension of Fe_2O_3 and molten salts. Finally, generated H_2 interacts directly with air producing NH_3. Licht's ammonia production process claims only 77% of the energy necessary to obtain NH_3 from the HB process. In addition, there is no CO_2 generated as a byproduct during the process.

Currently, the most ''green'' method to obtain NH_3 is to recover it from wastewater, mainly from agriculture, due to the use of NH_3 as fertilizer, as mentioned above. This environmental application could be used for water recycling systems, which is a current important topic due to the lack of drinkable water[11] and to reduce the nitrogen discharged into the oceans which strongly affects ecosystems. Furthermore, for aerospace technology applications, the recycling of waste-waters with NH_3 has been an important topic with the aim of developing electrochemical reactors which could generate electrical energy from the NH_3 oxidation and drinkable water from this process.[12-15]

Another technique involved in NH_3 generation is the electrochemical induce conversion. The most recent work was performed by F. Lu and G. G. Botte[16] and

consisted in the electrochemical conversion of urea into NH_3 using a graphene-coated nickel electrode. A relevant issue of this work is the use of urea, the main component of human urine, as a source of NH_3. This topic has been considered by other research groups in terms of the sustainable use of wastewater for the recovery of NH_3 and other nutrients.[12,17-20] As previously stated, the methods are shown here to produce NH_3 show the possibility to make it abundant and, in turn, very attractive to be an alternative fuel.

Energy density is another important parameter to be evaluated when considering alternatives fuels. In comparison with hydrogen, NH_3 has approximately three times more energy density (15.6 MJ L^{-1}) than compressed H_2 (5.6 MJ L^{-1}).[6,21] In addition, from a storage point of view, NH_3 is easy to liquefy in comparison with H_2, which requires much lower temperatures (about -253 °C).[21] Also, NH_3 transportation and supply can be handled with similar cares to that taken with current fuels, so that possibility to adapt the current infrastructure seems feasible.[21]

In summary, NH_3 is one of the most prominent candidates to be used as an alternative fuel due to advantages shown in comparison with other proposed fuels including carbon-free emissions, abundance, costs, high energy density and ease of storage and transportation. Taking consideration of all the mentioned benefits, the next section describes one of the most efficient ways to obtain energy from NH_3.

1.2. Direct Ammonia Alkaline Fuel Cells

NH_3 has been proposed as a fuel for fuel cells, as it is considered a clean source of energy production. A fuel cell is an electrochemical device that produces an electron

flow by the interaction of a fuel and an oxidant with two different electrodes attached across an ion-conducting electrolyte.[6,22,23] Figure 1-3 shows the typical structure of a fuel cell. As seen in the image, the electrochemical device consists of two electrodes, the anode which interacts with the fuel and where the oxidation reaction takes place and the cathode, where reduction reaction occurs. The resulting ions from the reduction reaction migrate across the electrolyte, which can be a liquid or selective ions membrane. The electrochemical reactions occurring in the electrodes generate the electron flow that is used as energy for an external appliance.

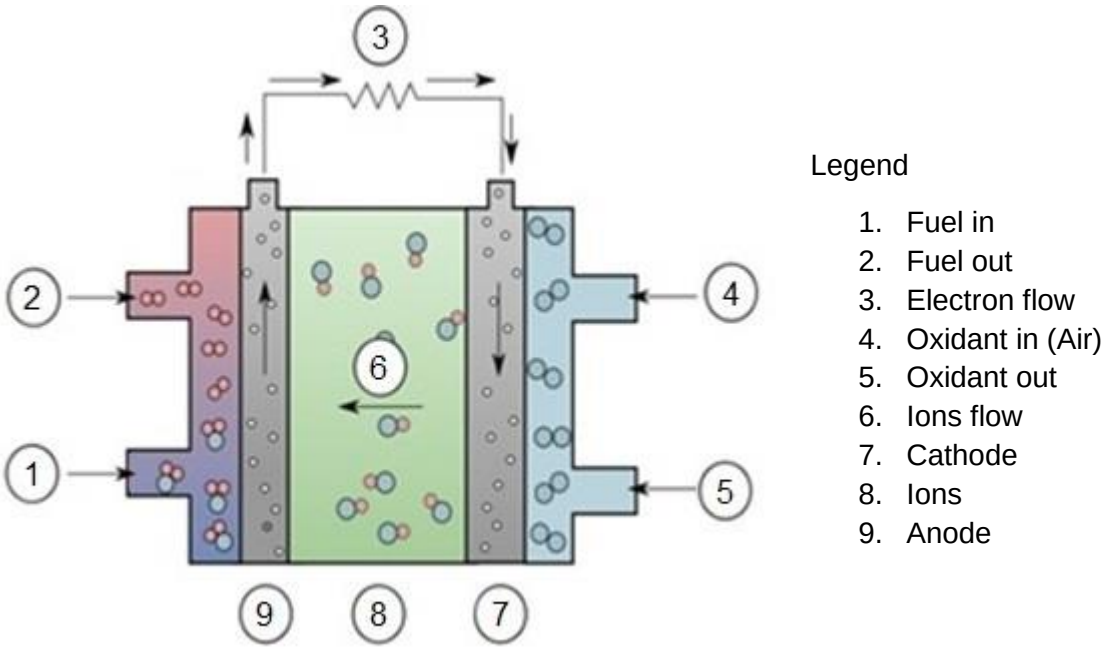

Figure 1-3. Schematic representation of a fuel cell device.

Direct Ammonia Fuel Cells (DAFC) are electrochemical devices that generate electricity directly from NH_3. Researchers have been testing different kinds of fuel cells in this operational mode. As an example, one of them is the Solid Oxide Fuel Cell (SOFC), which consists in a system with a solid ceramic electrolyte and with

operational temperatures of about 800° C to 1000° C.[24] First studies of ammonia SOFC were developed by C. G. Vayenas and R. D. Farr early in 1980.[25] High efficiency makes this device the best choice for direct ammonia fuel cell. However, the high temperatures required, the frailness of ceramic components and the slow startup makes this kind of fuel cells difficult to be commercialized at domestic level and for the transportation industry.

Alkaline membrane fuel cells have recently attracted the attention to the fuel cell society due to the possible use of inexpensive non-precious catalysts and of easily to handle organic membranes. [26-31] These systems also have versatility in construction between small compact systems and large power plants. This makes these devices interesting for the development of technology dedicated to space, vehicles, domestic use and energy storage applications.[31] However, in comparison with other fuel cells, this one shows low peak power densities which can be mostly related to the catalyst performance. Researchers hope to develop this technology and are compromised to enhance the performance of this kind of devices with the goal to commercialize it. To make it possible, it is important to further explore possible reactions such as NH_3 oxidation.

1.3. Electrocatalysts for ammonia oxidation in alkaline media

The electrochemical oxidation of NH_3 has been studied since 1963 and different mechanisms have been proposed over platinized platinum (Pt). This noble metal has shown to be the most catalytic for a variety of electrocatalytic reactions including the ammonia oxidation. Oswin and Salomon [32] were the pioneers to propose a mechanism for NH_3 oxidation in alkaline medium. This mechanism involved NH_3 dehydrogenation

on the Pt surface and the recombination of the adsorbed monoatomic nitrogen (N_{ads}) for the nitrogen (N_2) molecules formation. Later, Gerisher and Mauerer [33] proposed a mechanism whereby oxidation of ammonia occurs as shown below:

$$OH_{aq}^{-} \rightarrow OH_{ad}^{(\delta-)} + (1-\delta)e^{-}$$

$$NH_{3_{aq}} \rightarrow NH_{3,ad} \qquad 1$$

$$NH_{3\,ad} + OH_{ad}^{-} \rightarrow NH_{2\,ad} + H_2O + \delta e^{-} \qquad 2$$

$$NH_{2\,ad} + OH^{-} \rightarrow NH_{ad} + H_2O + \delta e^{-} \qquad 3$$

$$NH_{2\,ad} + NH_{ad} \rightarrow N_2H_{3\,ad} \qquad 3'$$

$$NH_{2\,ad} + NH_{2\,ad} \rightarrow N_2H_{4\,ad} \qquad 3''$$

$$NH_{ad} + OH^{-} \rightarrow N_{ad} + H_2O + \delta e^{-} \qquad 4$$

$$NH_{ad} + NH_{ad} \rightarrow N_2H_{2\,ad} \qquad 4'$$

$$NH_{ad} + NH_{2ad} \rightarrow N_2H_{3\,ad} \qquad 4''$$

$$NH_{ad} + NH_{3ad} \rightarrow N_2H_{4\,ad} \qquad 4'''$$

$$N_2H_{x+y\,ad} + (x+y)OH_{ad}^{(\delta-)} \rightarrow N_{2\,ad} + (x+y)H_2O + (x+y)\delta e^{-} \qquad 5$$

$$with\ x, y = 1\ or\ 2, \qquad 0 < \delta < 1$$

As shown above, the mechanism starts with the simultaneous adsorption of NH_3 and hydroxide radicals (OH^-) onto the Pt surface. Then, authors suggest various steps in which adsorbed NH_3 ($NH_{3\ ad}$) reacts with adsorbed OH (OH_{ad}) and the obtained active intermediate can also react with OH_{ad}, thus having $NH_{2\ ad}$ and NH_{ads} which recombine to form several $N_2H_{x+y\ ad}$ (with x,y = 1 or 2) species. Finally, these species are oxidized to N_2 and released from the surface with water as a byproduct in step 5. In this mechanism, steps 3 and 4 have many prime steps which start with the same intermediate. Step 3'' was determined as the rate-limiting step.

Authors have suggested that N_{ad}, NH_{ad} and NH_{2ad} intermediates are the most susceptible to be irreversibly adsorbed on the Pt surface, turning into poison for the electrode. Years later, Gerischer's mechanism and hypothesis about the poisonous species were supported using Differential Electrochemical Mass Spectrometry (DEMS).[34,35]

In addition, N_{ad} adsorption was also studied with noble metals different from Pt, including Ir, Ru, Rh, Pd, Cu, Ag and Au.[36] Using the Density Functional Theory (DFT) calculations, researchers determined that adsorption energy of N_{ad} varies with the metal in the following order: Ru >Rh > Pd > Ir > Pt >>Au, Ag, Cu. The results demonstrate that Au, Ag and Cu show the highest catalytic activity for NH_3 oxidation but only when the metal surface is oxidized. However, authors concluded that Pt was still the most electrocatalytic pure metal for NH_3 oxidation.

1.3.1. Ammonia oxidation on Pt single crystal electrodes

In order to study the possible effect of the platinum surface orientation, NH_3 oxidation was studied on different Pt single crystal electrodes. This type of electrodes have a controlled surface in which atoms are ordered with a specific symmetry for a determined plane. In the case of face-centered cubic (fcc) metals, such as Pt, the atom orientation is represented by three integers *h*, *k* and *l* commonly known in crystallography as *Miller indices*.[37] The lower Miller indices obtained in a fcc crystalline structure *(h,k,l)* are three: (100), (110) and (111) and correspond to the arrange of the surface atoms with a single type of symmetry.[38] These *low-index planes* or commonly known as *basal planes*, are represented by atomically flat surface of square (100), rectangular (110) and hexagonal (111) arrangement as shown in figure 1-4 for the particular case of fcc metals. This is the case of Pt for which the three basal planes electrodes [Pt (100), Pt (110) and Pt (111)] have been studied carefully to evaluate the interaction with different adsorbed species.

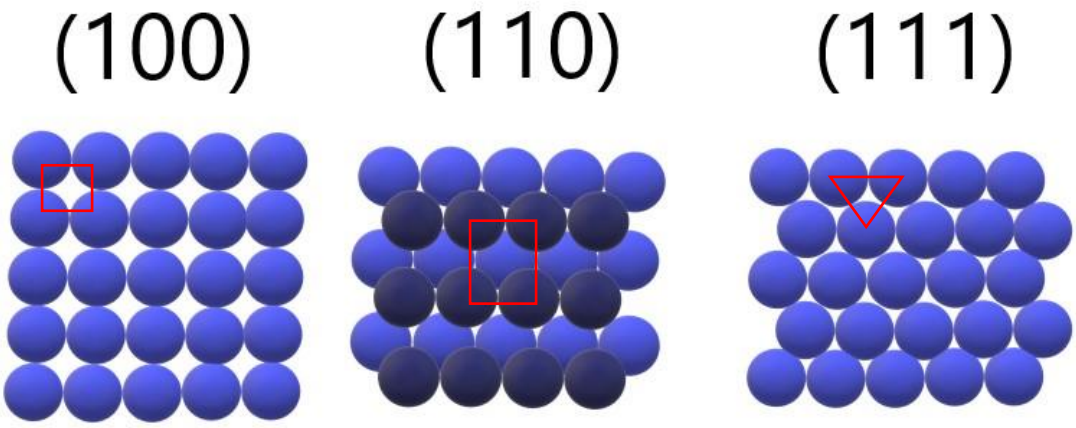

Figure 1-4. Hard sphere model for the basal planes in an fcc metal.

For an adsorbed species on each surface arrangement, different energies are obtained in terms of differences in electronic local density. Therefore, species 'choose' where to be adsorbed, thus resulting in structure-sensitive reactions. Vidal Iglesias et al.[39] were the first who studied NH_3 oxidation on Pt single crystal electrodes and concluded that NH_3 oxidation is a structure-sensitive process that occurs preferentially, in fact almost exclusively, on Pt (100) sites.

Figure 1-5 shows the selectivity of NH_3 oxidation towards Pt (100) sites with a comparison of the corresponding voltammograms of the three Pt basal planes and polyoriented Pt single crystal. In these profiles, Pt (100) obtained the highest current density with a well-remarked peak at 0.55 V.

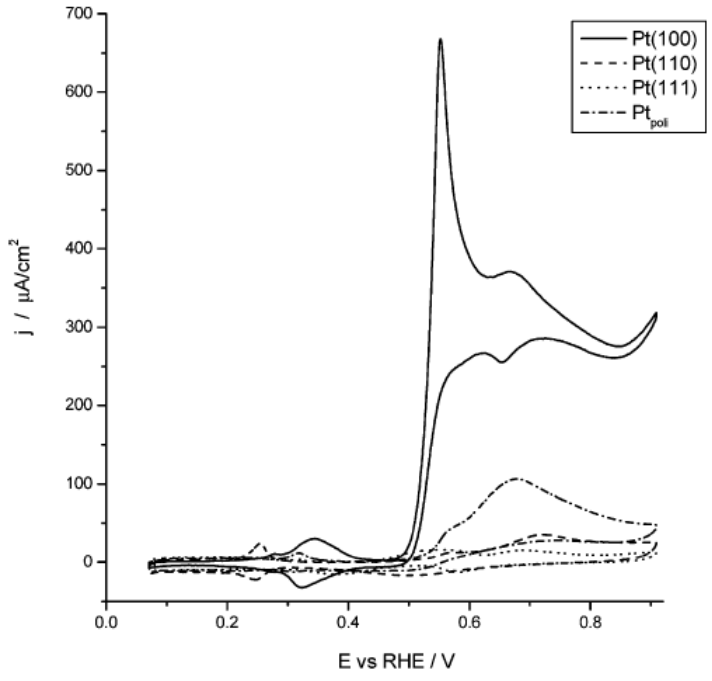

Figure 1-5. Voltammetric profile for NH_3 oxidation on Pt (100), Pt (110), Pt (111), and polyoriented Pt single crystal in 0.1 M NaOH + 10^{-3} M NH_3. Scan rate 10 mVs^{-1}. Reproduced from F. J. Vidal-Iglesias (2005). [39]

A subsequent study performed by the same research group confirmed Pt (100) behavior for NH_3 oxidation and determined a strong sensitivity to the width of (100) terraces.[40] Moreover, a future study reported DEMS analysis of the three Pt basal planes to determine the product distribution resulting from the NH_3 oxidation.[41] This research showed again the high activity and selectivity for oxidation of NH_3 to N_2 on Pt (100) single crystal electrode. Nitrous oxide (N_2O) and nitric oxide (NO) were also formed, being the three products yielded to a lower extent on Pt (111) and Pt (110) single crystal electrodes. Also, this study confirmed the formation of poisonous intermediates which irreversibly adsorb on Pt surface and inhibit the formation of N_2. Another research group evaluated the ammonia oxidation on Pt (100) electrodes using in-situ mass spectrometry and confirmed once more that production of N_2 takes place preferentially on Pt (100) surface sites.[42]

Other techniques such as chronoamperometry and In-situ Fourier Transform Reflection Absorption Infrared Spectroscopy (FTIRRAS) were employed by V. Rosca and M.T. M Koper [43] to identify the initial stages of the electrochemical oxidation of NH_3 on Pt (100) and Pt (111) single crystal electrodes. Authors concluded that the higher catalytic activity of Pt (100) is due to the ability of this surface to stabilize the NH_2 adsorbate. In addition, they proposed a new mechanism in which two adsorbed NH_2 are combined to form surface-bonded hydrazine which is rapidly dehydrogenated to form N_2.

1.3.2. Ammonia oxidation on Pt nanoparticles

From a practical point of view, Pt nanoparticles bring the possibility to scale-up new technology based on the NH_3 oxidation, either for energy such as DAFC, NH_3

sensors or waste-water recycling systems. This is due to the much higher surface to volume ratio in comparison with bulk electrodes. In addition, the reactivity of nanoparticles for a particular reaction can be modulated by controlling the size, shape and composition. Shape tunability of the nanoparticles has become trendy in the search of new materials with better catalytic performance. This is due, in part, because dependency on their shape, polyhedral nanocrystals can be analogically organized in a stereographic triangle equivalent to that for single crystals, as shown in figure 1-6 where each vertex is characterized by a nanocrystal with geometrical figures including cubes enclosed by (100), octahedron by (111) and rhombic dodecahedron by (110) basal facets.[44] This highlights the importance of the search of methods to obtain shape control and tunability in the synthesis of nanoparticles.

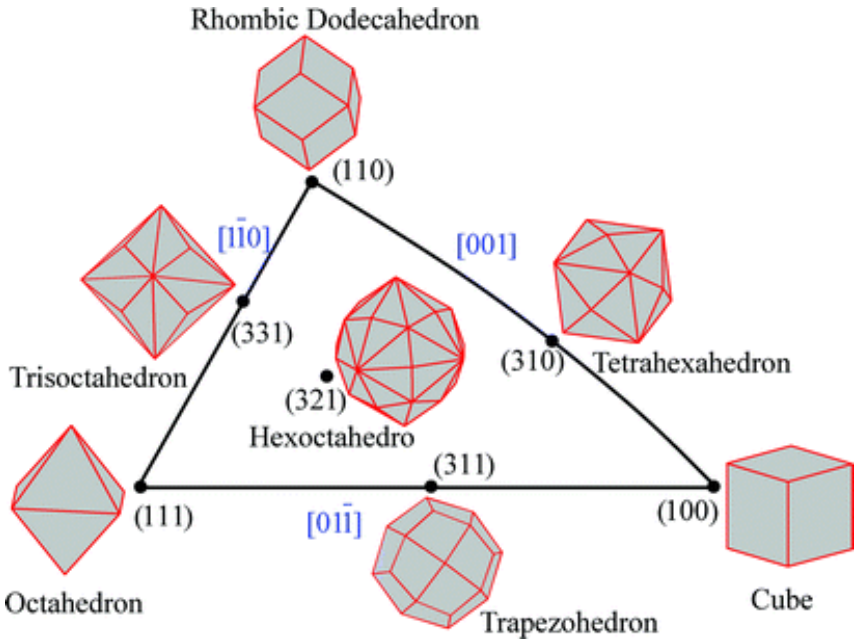

Figure 1-6. Unit stereographic triangle of polyhedral nanocrystal bounded by different crystal planes. Reproduced by Zhou et al. (2008). [44]

For NH_3 oxidation, the use of Pt nanoparticles with controlled shape was firstly reported by Vidal-Iglesias et al.[45] Their study confirmed the preferential oxidation on cubic Pt nanoparticles which are ideally enclosed by six Pt (100) facets. Their catalytic activity was found to be over four to six times higher (Figure 1-7) than that reported for poly-oriented Pt nanoparticles. In summary, this work confirmed the structure-sensitive process of ammonia oxidation over Pt (100) surface sites in nanoparticles and the importance to control the surface/shape to get the best electrocatalytic performance.

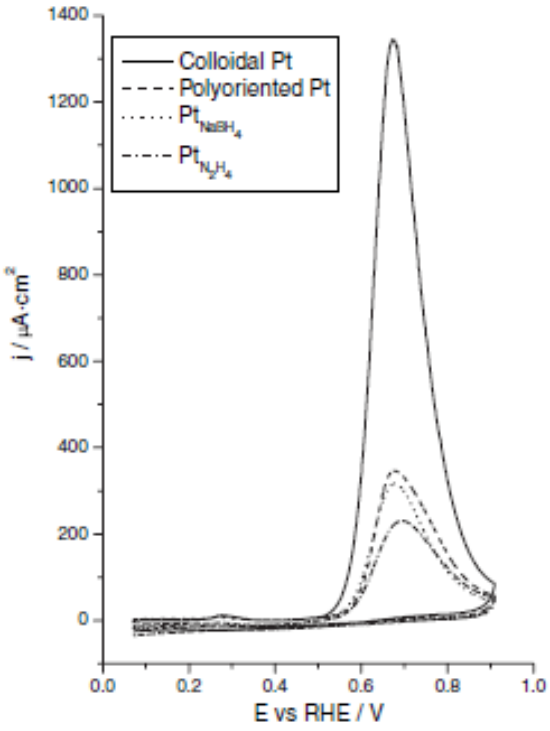

Figure 1-7. Ammonia oxidation on cubic nanoparticles (Colloidal Pt), polyoriented Pt electrodes and polyoriented Pt nanoparticles synthesized by using $NaBH_4$ (Pt_{NaBH4}) and N_2H_4 (Pt_{N2H4}) as reducing agents in w/o microemulsion. Reproduced from Vidal-Iglesias et al. (2004).[45]

Other studies have focused on the different reactivity of nanoparticles when changing their composition. For example, the synthesis of bimetallic nanostructures with the aim of improving the catalytic properties of Pt for NH_3 oxidation. K. Endo et al. [46,47] showed the electrochemical behavior of bulk Pt/Me (Me: Ir, Cu, Ru, Ni) alloyed surfaces reporting that only Ru and Ir enhance the electrocatalytic activity of pure Pt due to a kind of cooperation with both metals at the surface. With this research work as reference, Vidal-Iglesias et al.[48] performed a study of dispersed Pt/Me (Me: Ir, Rh Pd, Ru) nanoparticles. The selected metals to use, together with Pt, were chosen due to their ability already showed in previous publications to dehydrogenate NH_3 in order to ease the formation of NH_x. However, their results reported a significant decrease of the NH_3 oxidation current density in comparison with pure Pt nanoparticles. Nevertheless, bimetallic nanostructures of Pt/Ir and Pt/Rh both with 75/25 molar ratio, respectively, showed a decrease in the onset potential for the NH_3 oxidation thus showing an enhancement on the oxidation current density at lower potentials.

Other bimetallic nanostructures have been prepared, using Pt group metals to determine the long-term stability for NH_3 oxidation in fuel cells. For example, palladium (Pd) and metal oxides, such as SnO_x, have been compared with Ir and have confirmed their comparable activity and stability.[49] In addition, authors have also concluded that metal oxides can improve the electrocatalyst longevity.

Finally, carbon supported Pt-Ru nanoparticles have recently received attention as catalysts for NH_3 oxidation.[50] Researchers reported the improvement in the catalytic activity with the addition of 10 % atomic percentage of Ru to Pt. Authors assumed that the increase in performance was due to the increment in the abundance of OH_{ads} species on the surface, these playing a key role in the ammonia oxidation reaction.

In summary, these studies have demonstrated the possibility of improving the catalytic activity of nanoparticles with the modification of the chemical composition. Furthermore, cubic Pt nanoparticles still showed the best catalytic performance for ammonia oxidation. Interestingly, for this reaction, the use of Pt-based bimetallic structures with controlled-shapes has not been reported yet. In addition, Pt has demonstrated to be the best pure catalytic metal towards the oxidation of NH_3 in alkaline media. This means that the development of an easy, fast and scalable synthesis method to prepare Pt nanoparticles could be interesting from an applied point of view due to the potential of this reaction in many fields and is also one of the aims of this thesis. For this reason, it is very important to deepen into the understanding of the most relevant methods to synthesize this type of materials.

1.4. Methods to synthesize Pt nanoparticles

The development of reliable methods to synthesize shape-controlled Pt nanoparticles has advanced remarkably over the last decade. The most recent studies have been focused on the search for strategies to synthesize of Pt nanoparticles with desirable size and shape due to the influence of these parameters to control both the reactivity and selectivity of the nanostructures. For Pt nanoparticles, the most common syntheses involve techniques such as: hydrothermal[51-53], solvothermal[52-54], sol-gel[55,56], sputtering[57-59], electron-beam deposition[60], laser ablation[61,62], electrochemical deposition[63,64], electroless deposition[65,66], colloidal[67-70] and microemulsions[71-81]. In the following we describe those used in the present work.

1.4.1. Colloidal methods

Colloidal methods have demonstrated for the last 25 years the potential to obtain nanoscale materials from a broad range of inorganic compounds exhibiting remarkable narrow size distribution, interesting morphological and compositional tunability, well-controlled surface chemistry and stoichiometric composition variation.[69,70] Colloidal synthesis could be considered as the mainstay of the wet chemical synthetic strategies due to the easy way in which the products are obtained. In most cases, the method implies the combination of different ions under controlled temperature and pressure to finally obtain nanoparticles in the form of an insoluble precipitate. The presence of a capping or stabilizing agent in the colloidal synthesis is the key to prevent the agglomeration and to improve the chemical stability that controls the morphology tunability, in several cases.

The formation of metal nanocrystals using colloidal synthesis is governed principally by thermodynamics which is controlled by several parameters including temperature, reduction potentials, solubility and the concentration of the reactants. Also, kinetics plays an important role in terms of the reactant diffusion and reaction rate. The mechanism for the formation of monodispersed colloids was first studied by LaMer and co-workers in the early ’50s.[82] The proposed mechanism can be divided into three stages: nucleation, seed formation and nanocrystal growth. Figure 1-8 shows the schematic representation of the different steps for the metal nanocrystal growth.

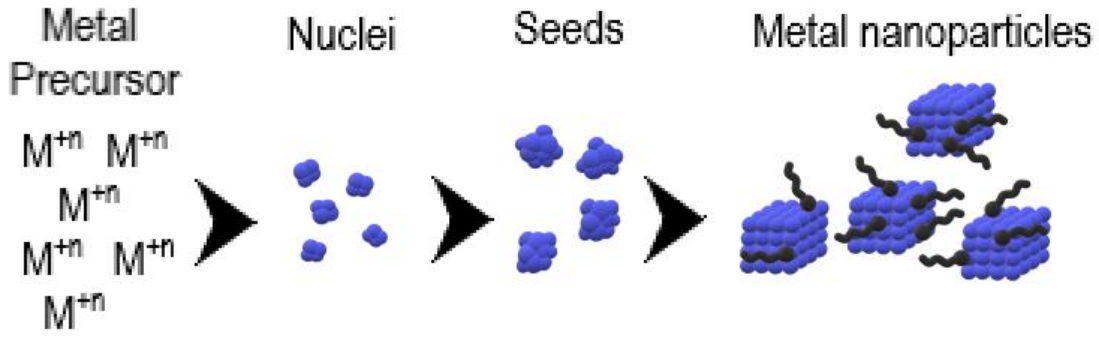

Figure 1-8. Schematic representation of the stages in the synthesis of metal nanoparticles.

In the first stage, the precursor compound is reduced to generate zero-valent atoms which constitute the starting material for the formation of the nanocrystal. During the process, the concentration of metallic atoms increases steadily with time as the precursor is decomposed. Also, the concentration of metallic atoms reaches the supersaturation and then, they start to aggregate into smalls clusters known as nuclei. Once formed, nuclei grow rapidly as a consequence of the faster depletion of the reactants. The first stage then finalizes when nucleation stops after the reactant concentration is kept below the level of minimum supersaturation.

The second stage is initiated with the formation of seeds that could be defined as particles bigger than nuclei with relatively stable crystallinity and well-defined crystallographic facets exposed on their surface. In this stage capping agents play an important role due to their effect associated with the control over the shape, which relates to the binding energy between the seed and the capping agent.[83,84] This means that the final shape is, in part, determined by the internal structure of the nanocrystal.

The final stage is the subsequent growth of the seeds into nanocrystals. This process is controlled by the so-called Ostwald ripening process, consisting in the competition between a decrease in bulk energy, which favors the growth and the increase in surface energy which favors the equilibrium displacement to the products. Interestingly, the overgrowth process can be modulated by both the capping and the reducing agent. In this stage, capping agents can act as shape-directing promotes inducing the final shape by adsorbing strongly on a specific facet which will endure through the synthesis process.

For the preparation of Pt nanoparticles with controlled shape, a variety of shape-directing agents have been studied including: citrate ion[85-88], amines[89,90], formic acid[84], polyvinylpyrrolidone (PVP)[92-94] and metal carbonyls[95]. J. Michel et al.[96] studied the use of common anions and small molecules such as amino acids and polycarboxylate species in the synthesis of shaped Pt nanoparticles. In addition, this work showed the effects of several common anions such as $CF_3SO_3^-$, ClO_4^-, NO_3^-, CO_3^{-2}, PO_4^{-2}, SO_4^{-2}, Cl^-, Br^-, and I^-. Authors highlighted the use of small molecules including: glycine, sarcosine, dimethylglycine, betaine and β-alanine to obtain preferentially cubic shaped Pt nanoparticles. Moreover, in this work, it was also evaluated the strength of the reducing agent for which an important role during the nanocrystal formation process was assigned. Also, the role of the pH was evaluated when predominantly Pt nanocubes (Figure 1-9) was synthesized only by reducing of $K_2[Pt(OH)_6]$ with H_2 at controlled pH = 9.7. Finally, it was concluded that by using stronger reducing agents such as hydrazine or borohydride, the formation of Pt nanoparticles was accelerated in comparison with the use of H_2, but led to a lowered shape selectivity.

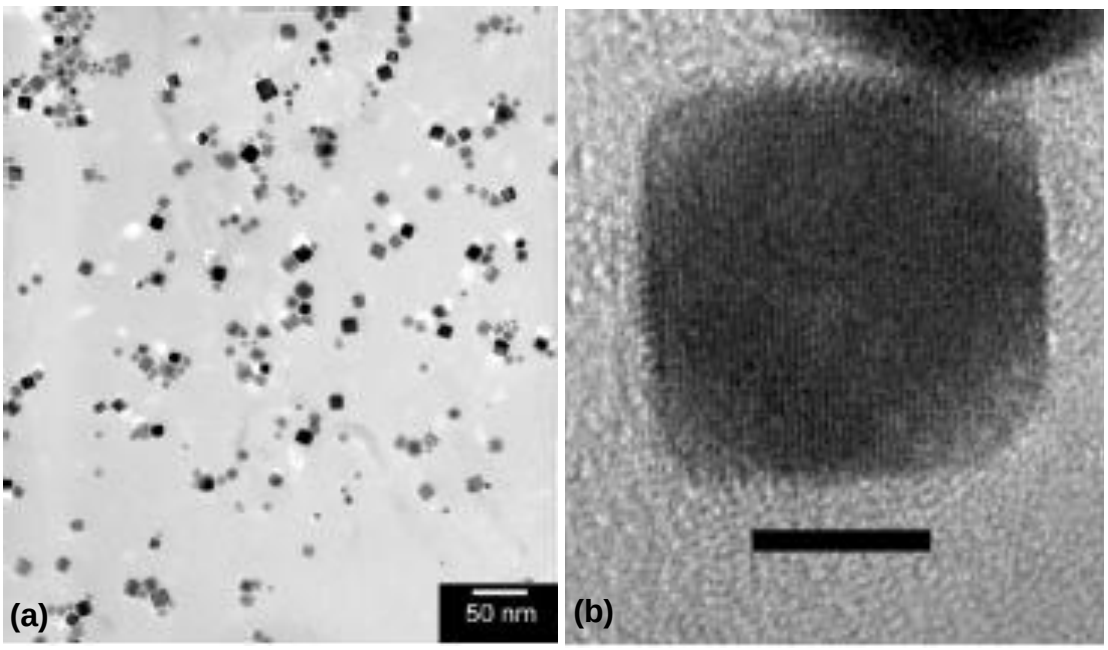

Figure 1-9. (a)Transmission electron microscopy (TEM) image and (b) high-resolution TEM (HR-TEM) images of the Pt nanocubes synthesized by reduction of K_2 [Pt $(OH)_6$] with H_2 at pH =9.7. Scale bar = 5 nm. Image reproduced from Michel et al. (2015)[96].

In summary, the formation process to obtain shape-controlled Pt nanoparticles is slow and requires strict selection of several parameters including: concentrations, temperatures and pH range. In the search of practical ways to obtain Pt nanocubes with narrow size distribution, Ahmadi et al. [97] were the pioneers in achieving it by using a colloidal synthesis. Pt nanocubes were prepared by adding polyacrylic acid sodium salt (PAA) as shape-directing agent and H_2 as a reducing agent. Years later, Yamada et al. [98] used a similar method for the synthesis of Pt cubes, but this time, using sodium iodide (NaI) as shape-directing agent. In this latter work, the influence of other experimental parameters such as temperature and the concentration of the Pt precursor was studied. Authors concluded that iodide (I^-) anion acts as a good controller for the growth of Pt (100) facets.

From all the information it is concluded that colloidal methods are one of the best choices for the synthesis of shape-controlled Pt nanoparticles. However, these processes also show complex steps which difficult the possibility to scale-up the production of Pt nanoparticles and consequently is unattractive from an applied point of view.

1.4.2. Microemulsion methods

Microemulsion methods are one of the best-known chemical synthetic tools used for the synthesis of nanoparticles. A microemulsion can be defined as a thermodynamically stable, isotropic, transparent colloidal solution of low viscosity which consists of, at least, three components: a surfactant, a polar solvent, and a non-polar solvent.[70-71] This method involves the exchange of the solution content into the globular droplets on perpetual fusion and fission between them.[72] Microemulsions can be classified depending on the nature of the bulk solvent, having two different types: oil-in-water (o/w) and water-in-oil (w/o) microemulsions. Figure 1-10 shows a hypothetical phase diagram of a microemulsion system published by M. J. Lawrence and G.D. Rees[73] in which each vertex of the triangle represents each pure component of the microemulsion and each edge a mixture between the two components of the corresponding apexes. In this phase diagram each field section of the triangle is formed with different phases in equilibrium such as conventional micelles, reverse micelles, w/o and o/w microemulsions and a lamellar phase observed at very high concentrations of the surfactant. In addition, there are three different sections which are classified according to their droplet to volume fraction (Φ). In this phase diagram, not all the combinations of components produce microemulsions. The extent where

microemulsions take place is localized principally at each border of the center section of the phase diagram. This means that microemulsions can exist in equilibrium with excess of water or oil.

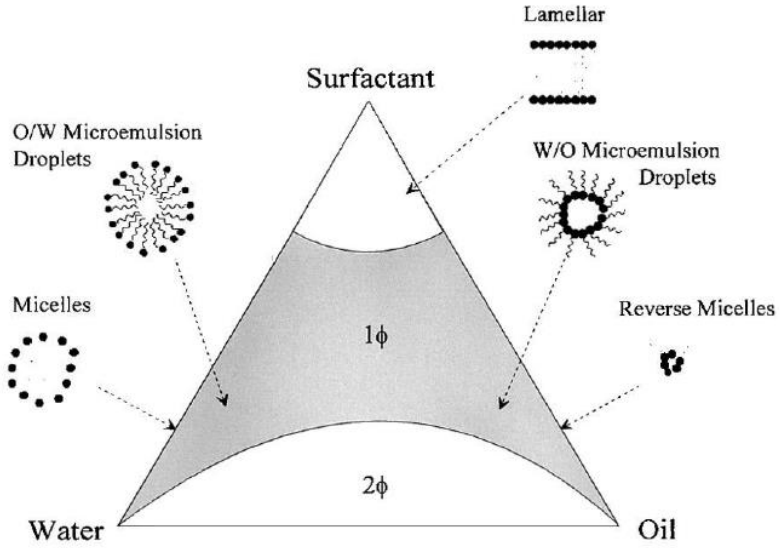

Figure 1-10. Schematic representation of different structures presented in a pseudo-ternary phase diagram of an oil/surfactant/water microemulsion system. Image reproduced from Lawrence M.J. Rees G.D. (2000) [73].

Interestingly, reverse micelles produced in the w/o microemulsion can be used as nanoreactors for the synthesis of nanoparticles with a low polydispersity. [74-80] This type of micelles (Figure 1-11) are made of a small aqueous core surrounded by the polar head group of the surfactant molecules, which also come with a hydrocarbon tail that interacts directed with the oil phase. Depending on the nature of the amphiphilic head, the surfactant can be classified as ionic (cationic or anionic) or non-ionic. The surfactant is one of the main components in charge of the microemulsion dynamics. This suggests that the nature of the chemical interaction between the amphiphilic

structure with the other microemulsion components, has an impact on the size structure of the nanoreactors and consequently onto the nanoparticle's size. The size of the produced nanodroplets is estimated to range from 5-50 nm and strongly depends on the 'R' factor, which can be calculated by dividing the concentration of the water divided by the concentration of the surfactant (R= [H_2O] / [surfactant]).

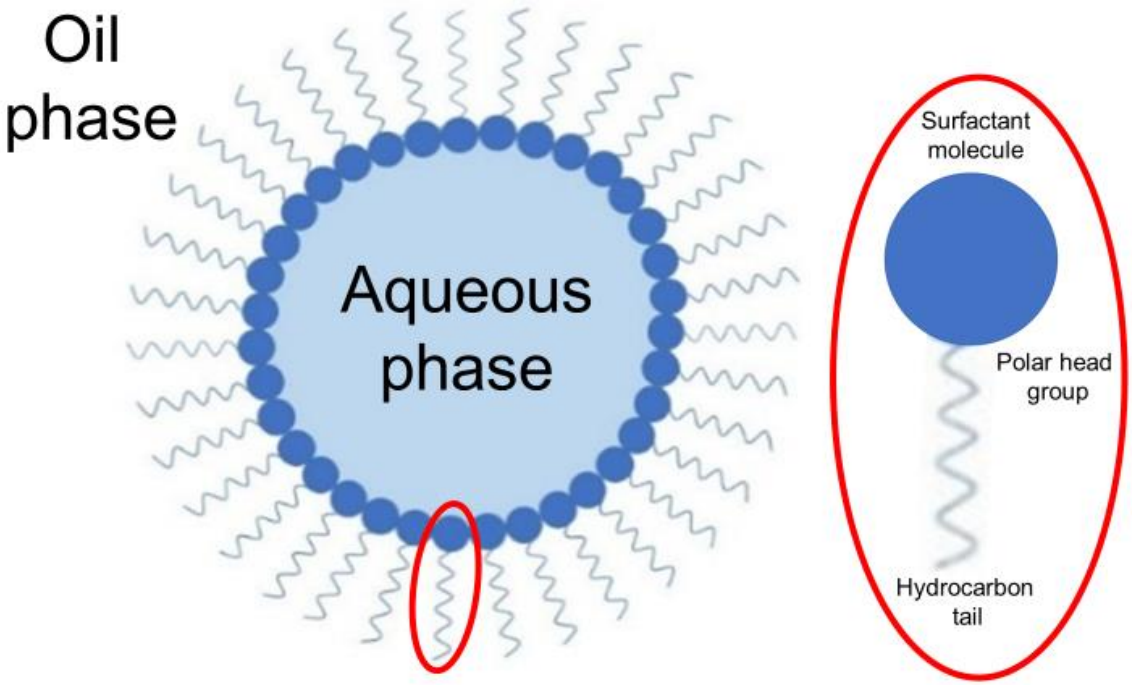

Figure 1-11. Schematic representation of a typical structure of the reverse micelle and a zoom image of a surfactant molecule.

The chemical process to prepare nanoparticles from w/o microemulsion involves the interaction of reverse micelles containing the metal precursor with reverse micelles containing a reducing agent. The mixture of both microemulsions produces a dynamic exchange of the material inside of the reverse micelles at a high rate of 10^6-

10^7 mol s^{-1}. After the exchange process takes place, the nucleation and growth steps occur in a single micelle, which controls the size of the nanoparticle. Figure 1-12 shows the mechanism steps for the formation of metal nanoparticles in which two micelles containing the metallic precursor and the reducing agent respectively, collide and interchange the reactants. Then, the nucleation reaction takes place inside the droplet and the collisions promote the growth of the nanoparticle with the size imposed by the size of the nanoreactors.

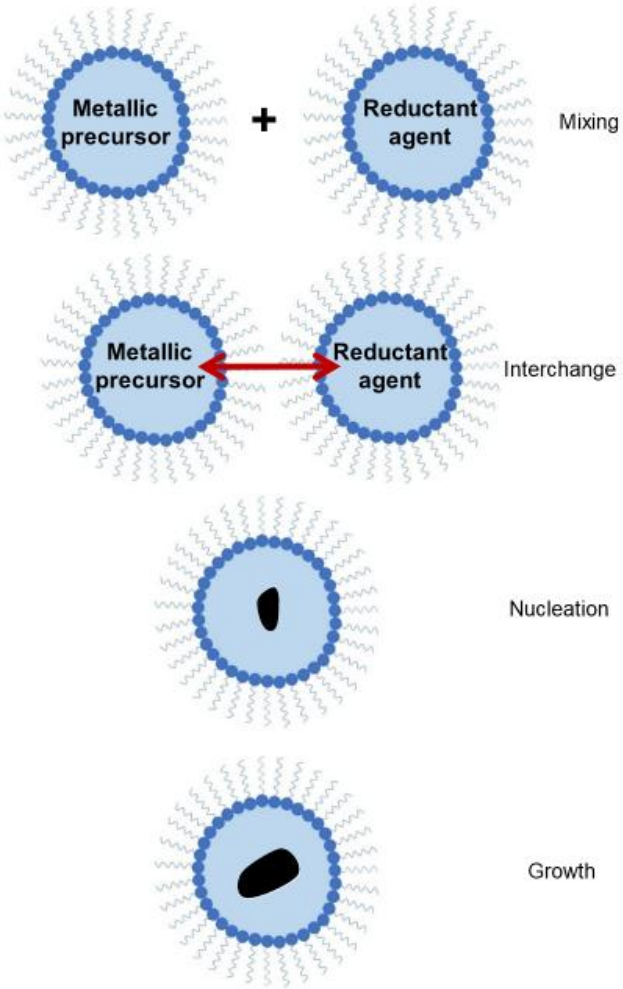

Figure 1-12. Schematic representation of the mechanism for the formation of nanoparticles in w/o microemulsion.

The synthesis of metal nanoparticles using the w/o microemulsion method has been studied since 1970 by many research groups in different research areas. One of the pioneer works was published by M. Boutonnet et al.[79] who reported the synthesis of uniform size and shape Pt, Rh and Pd nanoparticles using reverse micelles. In the particular case of Pt, authors used H_2PtCl_6 as a metal precursor dissolved in CTAB/water/octanol microemulsion followed by the reduction of the Pt salt by hydrazine.

Also, the synthesis of Pt nanoparticles has been reported using different non-ionic surfactants such as polyethylene sorbitane tristearate (Tween® 65) and pentaethylene glycol (ethylene oxide) dodecylether (PEGDE).[99] This research paper compares the catalytic activity of Pt nanoparticles synthesized using both ionic and non-ionic surfactants towards catalytic hydrogenation of butene. Authors concluded that ionic surfactants could hinder the accessibility of the reactant to the catalyst surface and thus, a decrease in activity was shown. Years later, the same authors also performed a similar research about the catalytic hydrogenolysis and isomerization of hydrocarbons using Pt nanoparticles synthesized using a w/o microemulsion with a non-ionic surfactant (pentaethyleneglycoldodecylether, $C_{12}E_5$), n-hexadecane and water. [100] In this work, the authors prepared Pt nanoparticles with a small size, 2 nm approximately, and reported a good reactivity towards the studied reactions.

Another remarkable work in this field was carried out by M. Arturo Lopez-Quintela and Jose Rivas[81], in which proposed microemulsion to synthesize ultrafine particles of various materials which developed single metallic particles, bimetallic alloys, magnetic oxides and high temperature superconducting oxides.

From a different approach, an interesting study about the electrochemical behavior of Pt nanoparticles synthesized using w/o microemulsion was published by J. Solla-Gullón et al. [101] In this work, a simple way to clean the nanoparticles surface from the surfactant molecules was reported for the first time. In this way, the characteristic voltammetric profile of the clean nanoparticles, which is related to the surface structure could be obtained. Results showed that the Pt nanoparticles processed with the decontamination procedure showed a reproducible electrochemical behavior, thus, minimizing the surface contamination that could affect the reactivity and consequently the structure sensitivity for the reactions under study. Reactivity of decontaminated pure Pt and bimetallic (Pt/Ir, Pt/Rh, Pt/Pd, Pt/Ru) nanoparticles synthesized using w/o microemulsions was evaluated for the oxidation of NH_3 [48], carbon monoxide (CO)[102] and organic compounds including methanol[103,104] and formic acid.[105] In the particular case of CO oxidation, authors reported the capacity to use this electrochemical process as decontamination tool of the Pt nanoparticle's surface due to the capacity of CO to displace the unwanted adsorbed species from the surface.

As previously stated, by using w/o microemulsions small Pt nanoparticles with an average size from 2 to 5 nm can be produced. These accurate values result from the microemulsion dynamics and the interaction of the surfactant with other components of the microemulsion. Although the surfactant molecules provide the capacity to control the growth process of the nanocrystals, their presence affects the electrochemical reactivity of the nanostructure since it also covers their surface, thus causing a lower catalytic activity. However, only by applying a decontamination process and having clean surfaces, the real electrochemical behavior of the synthesized nanoparticles can be obtained.

Taking all the previous information concerning microemulsions into consideration, it could be thought as an alternative to consider for the mass production of Pt nanoparticles. Especially, this methodology is quite easy and short time-consuming. However, before the present Ph D. thesis was carried out, research lacked the control over the surface structure of the nanostructures in this process, which meant that the search for new alternatives in the scale up production of shape-controlled Pt nanoparticles needed to be performed. In the next chapter, a description of the statement of the problem of this Ph. D. thesis is introduced, in order to know about the aims and goals of this investigation.

1.5. References

1. Traversa, E. & Boudghene Stambouli, A. *Renew. Sust. Energ. Rev.* **2002**, 6, 297-306.
2. Krane, J. *MRS Energ. & Sustan. A Review Journal*. **2017**,4, 1-12.
3. BP statistical Review of World Energy. **2017** Editor: BP Statistical Review of World Energy BP p.l.c.1 St James's Square London, SW1Y 4PD UK.
4. Acar, C.; Dincer, I. *Int. J. Hydrogen Energy* **2016**, 41,19, 7950-7959.
5. Maclean, H.L., Lave, L.B., Environ. Sci. Technol. **2003**, 37, 5445-5452.
6. Boggs, B. & Botte, G. *J. Power Sour.* **2009,** 192 (2009) 573-581.
7. U.S. Geological Survey, Mineral Commodity Summaries, 2011.
8. Klerke, A.; Christensen C.H.; Nørskov, J.K.; Vegge, T. *J. Mat. Chem*. **2008**, 18, 2304-2310.
9. Jenning, J. R. Ed. Catalytic Ammonia Synthesis: Fundamentals and practice. *Springer Science & Business Media*, New York, 1991.
10. Licht, S.; Cui, B.; Wang, B.; Li, F-F.; Lau, J. & Liu, S. *Science* **2014**, 345, 637-640.
11. Sidiqui, O.; Dincer, I. *Thermal. Sci. Eng. Prog*. **2018**, 5, 568-578.
12. Nicolau, E.; Fonseca, J. J.; Rodríguez-Martínez, J.A.; Richardson, T.M.J.; Flynn, M.; Griebenow, K.; Cabrera, C. R.; *ACS Sustain. Chem*. **2014**, 2, 749-754.
13. Cabrera, C. R. & Miranda, F. A. (eds): Advanced Nanomaterials for Aerospace Applications, Chapter 1. Pan Stanford Publishing Pte. Ltd., Singapore (2014).
14. Acevedo, R.; Puventud-Estrada, C.M.; Morales-Navas, C.; Martínez-Rodríguez, R.A,; Ortíz-Quiles, E.; Vidal-Iglesias, F.J.; Solla-Gullón, J.; Nicolau,

E.; Feliu, J. M.; Echegoyen, L.; Cabrera, C. R. *Microgravity Sci. Technol.* **2017**, 29, 253-261.

15. Puventud-Estrada, C. M.; Acevedo, R.; Morales, C.; Betancourt, L.; Díaz, D. C.; Rodríguez, M. A.; Larios, E.; Yacamán, M.J.; Nicolau, E.; Flynn, M.; Cabrera, C. R. *Microgravity Sci. Technol*. **2017**, 29, 381-389.
16. Lu, F.; Botte, G. G. *Coatings* **2017**,7, 72.
17. Zamora, P.; Georgieva, T.; Hekjine, A. T.; Sleutels, T.H.J.A.; Jeremiasse, A. W.; Saakes, M.; Buisman, C.; J.N.; Kuntke, P. *J. Power Sources* **2017**, 356, 491-499.
18. Li, Y.; Styczynski, J.; Huang, Y.; Xu, Z.; McCutcheon, J. *J. Power Sources*, **2017**, 356, 529-538.
19. Cunci, L., Velez, C. A., Perez, I., Suleiman, A., Larios, E., José-Yacamán, M.; Watkins, J. J.; Cabrera, C. R. ACS Appl. Mater. Interfaces, **2014**, *6, 2137–2145.*
20. Kapalka, A.; Katsaounis, A.; Michel, N-L.; Leonidova, A.; Souentie, S.; Comninellis, C.; Udert, K.M. *Electrochem. Comm*. **2010**, 12, 1203-1205.
21. Valera-Medina, A., Xiao, H., Owen-Jones, M., David, W. I. F., & Bowen, P. J. *Progress in Energy and Combustion Science* **2008***,* 69*, 63–102*.
22. Mench, M. Fuel Cell Engines; John Wiley & Sons, **2008**. 14-20.
23. Kordesh, K. V. & Simader, G. R. Environmental Impact of Fuel Cell Tehnology. *Chem. Rev*. **1995**, 95, 191-207.
24. Mathew, Melvin & Thaker, Amar. (2015). A Review of Ammonia Fuel Cells. 10.13140/RG.2.1.1700.7129.
25. Vayenas, C. G. Farr R. D. *Science* **1980**, 208, 593-594.
26. Lan, R. & Tao, S. Electrochem. *Sol. State Lett*. **2010**, 13, B83-B86.

27. Varcoe, J. R.; Slade, C. T.; Yee, E. L.; Ooynton, S. D.; Driscoll, D.; J. Apperley, D. C. *Chem Mater.* **2007**, 19, 2686.

28. Scott K.; Yu E.; Vlachogiannopoulos, G.; Shivare, M.; Duteanu. N. *J. Power Sources*, **2008**, 175, 452.

29. Park, J.-S.; Park, S.-H.; Yim, S.-D. Yoon, Y.-G.; Lee, W.-Y.; Kim, C. S. *J. Power Sources*, **2008**, 178,620.

30. Ewing, S.; Lan, X.; Xu, X.; Tao, S. W. *Fuel Cells* **2010**, 10,72.

31. Gulzow, E. *J. Power Sources* **1996**, 61, 99-104

32. Oswin, H. G.; Salomon, M. Canad *J. Chem*. **1963** 41, 1686.

33. Greisher, H.; Mauerer, A. *J. Electroanal. Chem*. **1970**, 25, 421.

34. Gootzen, J.F.E; Wonders, A.H.; Visscher, W.; van Santen, R.A.; Van Venn, J.A.R. *Electrochim. Acta*, **1998**, 43, 1851.

35. Wasmus, S.; Vasini, E. J.; Krausa, M.; Mishima, H.T.; Vielstich, W.; *Electrochim Acta*, **1994**, 39, 23.

36. de Vooys, A.C.A.; Koper, M.T.M.; van Santen, R.A.; van Veen, J.A.R. *J. Electroanal. Chem.* **2001**, 506, 127.

37. Ashcroft, N. W. and Mermin, D. Solid State Physics (Harcourt: New York) 1976.

38. Masel, R. I., *Principles of Adsorption and Reaction on Solid Surfaces*. John Wiley & Sons Inc.: New York, 1996.

39. Vidal-Iglesias, F. J.; García-Aráez, N.; Montiel, V.; Feliu, J.M.; Aldaz, A. *Electrochem. Comm.* **2003**,5, 22-26.

40. Vidal-Iglesias, F.J.; Montiel, V.; Feliu, J.M.; Aldaz, A.; *J. Phys. Chem*. **2005**, 109, 12914-12919.

41. Vidal-Iglesias, F. J.; Solla-Gullón, J.; N.; Feliu, J.M.; Baltrushchat, B.; Aldaz, A. *J. Electroanal. Chem.* **2006**, 588, 331-338.

42. Gao, Y.; Kita, H.; Hattori, H. *Chem. lett.* **1994**, 11, 2093-2096.

43. Rosca, V.; Koper, M.T.M. *Phys. Chem. Chem. Phys*. **2006**, 8, 2513-2524.

44. Zhou, Z.; Tian, Na.; Huang, Z.Z.; Chen, D.J. and Sun, S.G. *Faraday Discuss.,* **2008**, 140, 81-92.

45. Vidal-Iglesias, F. J.; Solla-Gullón, J.; Rodríguez, P.; Herrero, E.; Montiel, V.; Feliu, J.M.; Aldaz, A. *Electrochem. Comm.* **2004**, 1080-1084.

46. Endo, K.; Katayama, Y.; Miura, T.; *Electrochimica Acta*. **2004**, 49, 1635.

47. Endo, K.; Nakamura, K.; Katayama, Y.; Miura, T.; Electrochimica Acta. **2004**, 49, 2503

48. Vidal-Iglesias, F.J.; Solla-Gullón, J.; Montiel, V.; Feliu, J.M.; Aldaz, A. *J. Power Sources,* **2007**, 171, 448-456.

49. Lomocso, T.; Baranove, E*. Electrochimica Acta*, **2011**, 56, 8551-8558.

50. Silva, J.C.; Ntais, S.; Teixera-Neto, E.; Spincae, E.V.; Cui, X.; Neto, A. O.; Baranove, E. *Int. J. Hyd. Energy* **2017**, 42, 193-201.

51. Krehula, S. & Music, S. *Croat. Chem. Acta*, **2011**,4, 465-468.

52. Feng, S.H. & Li, G.H. *Modern Inorganic Chem 2nd Edition*. Chapter 4. 2017, 73-104.

53. Rao., H.G. Mukherjee, D.; Reddy, B.M. Nanostructures for Novel Therapy. Synthesis, Characterization and Application A volume in Micro and Nano Technologies. Chapter 1, **2017**, 1-36.

54. Gumeci, C.; Marathe, A.; Behrens, R.; Chaudhurri, J,; Krozeniewski, C. *J. Phys. Chem. Soc.* **2014**, 118(26), 14433-14440.

55. Sakka, S. Handbook of Advanced Ceramics (2nd Edition) Materials, Appplications, Processing and Properties. Academic Press, 2013, 883-910.

56. Ingale, S.V.; Wagh, P.B.; Bandyopadhyay D.; Singh I.K.; Tewari R.; Gupta S.C. *IOP Conf. Series: Mater. Sci. Eng*. **2015**, 73, 012076.

57. Alvisi, M.; Galtieri, G.; Giorgi, L.; Giorgi, R.; Serra, E.; Signore, M. A. *Surf. Coat. Tech.* **2005**, 200, 1325-1329.

58. O'Hayre, R.; Lee, S.J.; Cha, S.W.; Prinz F.B. *J. Power Sources*, **2002**, 109, 483-493.

59. Biro, F.; Radnóczi, G.; Takacs, M.; Baji, Z.; Dűcsó, C.; Bársony, I. *Procedia Eng.* **2016**, 168, 1148-1151.

60. Raso, M.A.; Carillo, I.; Mora, E.; Leo, T.J. *Int. J. Hyd. Energy* **2014**, 39, 5301-5308.

61. Cueto, M.; Sanz, M.; Oujja, M.; Gámez, F.; Martínez-Haya, B.; Castillejo, M. *J. Phys. Chem. C*. **2011**, 115, 22217-22224.

62. Mafune, F.; Kohno, J.; Takeda, Y.; Kondow, T. *J. Phys. Chem. B.* **2003,** 107, 4218-4223.

63. Zhang, D.; Cheng-Chang, W.; Okajima, T.; Ohsaka, T. *Langmuir*, **2011**, 27, 14662-14668.

64. Lin, Z.; Ji, L.; Zhang, X. *Mat. Lett*. **2009**, 63, 2115-2118.

65. Zhang, D.; Okajima, T.; Lu, D.; Ohsaka, T. *Langmuir*, **2013**, 29(38), 11931-11940.

66. Pernstich, K. P.; Schenker, M.; Weibel, F.; Rossi, A.; Caseri, W. *ACS Appl. Mater. Interfaces*, **2010**, 2, 639-643.

67. Islam, A.; Kabir, Bhuiya, A.; Saidul, Islam M. *Asia Pacific J Energy Environ.* **2014**, 1, 107-121.

68. Schelly Z.A. *Current Opinion in Colloid & Interface Science*. **1997**, 2, 37-41.

69. Ghosh S.; Manna L. *Chem. Rev*. **2018**, 118, 7804-7864.

70. Kovalenko M.; Manna L.; Cabot A.; Henz Z.; Talapin D.; Kagan C.; Klimov V.; Rogach A.; Reiss P.; Milliron D.; Guyot-Sionnnest P.; Konstantatos G.; Parak W. J.; Hyeon T.; Korgel B. A.; Murray C. B.; Heiss W. *ACS NANO* **2015**, 2, 1012-1057.

71. Friderg, SE.; Bothorel, P. (Eds): *Microemulsion: Structure and Dynamics*. Boca Ratón: CRC Press (1998).

72. Ethayaraja, M.; Dutta K.; Muthukumaran, D.; Bandyopadhyaya, R. *Langmuir*, **2007**, 23, 3418-3423.

73. Lawrence, M.J. Rees, G.D. *Advanced Drug Delivery Rev*. **2000**, 45, 89-121.

74. Destree, C.; Debuigne, F; George, S.; Champagne B.; Guillaume, M.; Ghijsen, J.; Nagy, J.B.; *Colloid. Polym. Sci*. **2008**, 286, 1463-1470.

75. Julian, E.; Martín, J.; Hollamby, L.H.; *Adv. Colloid. Interf. Sci.* **2006**, 128, 5-15.

76. Wanzhong, Z.; Xueliang, Q.; Jianguo, C. *Chem. Phys*. **2006**, 330, 495-500.

77. Zhong-Min, O.; Hiroshi, Y.; Keisaku, K.. *J. Photochem,* **2007**, 189, 7-14.

78. Ahmad Malik, M.; Younus Wani, M.; Ali-Hashim, M.; *Arabian. J. Chem*. **2012**, 5, 397-417.

79. Boutonnet, M.; Kizling, J.; Stenius, P. *Colloids and Surface*, **1982**, 5, 209-225.

80. Sjöblom, J.; Lindberg, L.; Friberg, S. E*. Adv. Colloids Int. Sci.* **1996**, 65, 125-287.

81. Quintela-Lopez, M.A.; Rivas, J.; *J Colloids Interface Sci.* **1993**, 158,446-451.

82. LaMer, V. K.; Dinegar, R, H*. J. Am. Chem. Soc.* **1950**, 72, 4847-4854.

83. Tao, A. R.; Habas, S.; Yang, p.; *Small,* **2008**, 4,310-325.

84. Murphy, C. J.; Sau, T. K.; Gole, A. M.; Orendorff, C. J.; Gao, J.; Gou, J.; Hunyadi, S. E.; Li, T.*; J. Phys. Chem. B.,* **2005**, 109, 13857-13870.

85. Attard, G. A.; Ye, J. Y.; Jenkins, P.; Vidal-Iglesias, F. J.; Herrero, E.; Sun, S. G., *J. Electroanal. Chem.* **2013**, 688, 249-256.

86. Zeng, J.; *Mater. Chem*. **2012**, 22, 3170-3176.

87. El Sayed, M. A.; Yoo, J. W. *ChemCatChem.* **2010**, 2, 268-271.

88. Chen, D.; Ye, J.Y.; Xu, C.; Li, Xun J. T.; Zhen, C.H.; Tian, N.; Zhou, Z. Y.; Sun, S.G. *Sci. China Chem.* **2012**, 55, 2353-2358.

89. Lacroix, L. M.; Gatel, C.; Arenal, R.; Garcia, C.; Lachaize, S.; Blon, T.; Waron-Fonrose, B.; Snoeck, E.; Chaudret, B.; Viau, G. *Angew. Chem Int. Ed*. **2012**, 51, 4690-4694.

90. Kim, C.; Kim, S. S. Yang, S.; Han, J. W. Lee, H.; *Chem. Commun.* **2012**, 48, 6396-6398.

91. Sattayasamitsathit, S.; Gu. Y.; Kaufmann, K.; Jia, W.; Xiao, X.; Rodriguez, M.; Minteer, S.; Cha, J.; Burckel, D. B.; Wang, C. *J. Mater. Chem. A,* **2013**, 1, 1639-1645.

92. Alayoglu, S.; Alaiga, C.; Sprung, C.; Somorjai, A. *Catal. Lett.* **2011**, 141, 914-924.

93. Long, N. V.; Thi, C. M.; Nogami, M.; Ohtaki, M. *New J. Chem.,* **2012**, 36, 1320-1334.

94. Yang, Y.; Huang, Z.; Li D.; Nogami, M. *Proc. SPIE*, **2010**, 7658, 76580 H.

95. Kang, Y.; Pyo, J. B.; Ye, X.; Diaz, R. E.; Gordon, T. R.; Stach, E. A.; Murray, C. B. *ACS Nano*, **2013**, 7, 645-653.

96. Michel, J. A.; Morris, III W. H.; Lukehart, C. M. *J. Mater. Chem. A*. **2015**, 3, 2012-2018.

97. Ahmadi, T. S.; Wang, Z. L.; Green, T. C.; Henglein, A.; El-Sayed, M. A. *Science* **1996**, 272, 1924-1925.

98. Yamada, M., Kon, S., Miyake*, M. Chemistry Letters*, **2005**, 7, 1050–1051.

99. Boutonnet, M. A.; Kizling, J.; Touroude, R.; Maire, G.; Stenius, P. *Applied Catal.* **1986**, 20, 163-177.

100. Boutonnet, M. A.; Kizling, J.; Touroude, R.; Maire G.; Stenius, P. *Catal. Let*. **1991**, 9, 347-354.

101. Solla-Gullón, J.; Montiel, V.; Aldaz, A.; Clavilier, J. *J. Electroanal. Chem.* **2000**, 491, 69-77.

102. Solla-Gullón, J.; Vidal-Iglesias, F. J.; Herrero, E.; Feliu, J. M.; Aldaz, A. *Electrochem. Comm.* **2006**, 8, 189-194.

103. Waszczuk, P.; Solla-Gullón, J.; Kim, S.; Tong, Y. Y.; Montiel, V.; Aldaz, A.; Wieckowski, A. *J. Catal.* **2001**, 203, 1-6.

104. Solla-Gullón, J.; Vidal-Iglesias, F. J.; Montiel, V.; Aldaz, A. *Electrochimica Acta* **2004**, 5079-5088.

105. Solla-Gullón, J.; Vidal-Iglesias, F. J.; López-Cudero, A.; Garnier, E.; Feliu, J.M.; Aldaz, A. *Phys. Chem. Chem. Phys.* **2008**, 10, 3689-3698.

Chapter 2.

Significance and statement of the problem

2. Significance and statement of the problem

Many reactions are structure-sensitive. That is to say, depending on the arrangement of the atoms at the surface, their reactivity can be remarkably improved.[1-8] Therefore, the search for new methods to synthesize shape-controlled nanoparticles in a fast and easily way and that could be scaled-up, has currently become a challenge. Thus, the research of this Ph. D thesis aims to contribute in the development of specific syntheses of nanostructures which could be possible scalable and consequently, be a step key in the adoption of new technologies.

Technology based on the production of energy, such as fuel cells, is one of the most attractive fields which could benefit with the development of such methods to prepare shape-controlled nanoparticles. Furthermore, many sectors of the industry who needs technology based on the search of new energy sources could benefit with the improvement of knowledge including: transportation (buses, trucks, rail vehicles, fuel cell electric vehicles, boats, etc.), military (portable soldier-borne power, skid-mounted generators), portable products (torches, battery chargers and small personal electronics) and stationary units as power source.[9]

For the particular case of technology based on NH_3 oxidation, the development of methods for its electrochemical elimination of wastewater, as well as the production of electrochemical sensors for the analysis of air/water quality is an important environmental aspect that could also be considered.[10] Incidentally, today attractive proposals have become from the aerospace engineering to perform technology based on the production of energy for space exploration as well as recycling waste-water for the astronauts.[11-14] Interestingly, NH_3 oxidation is extremely sensitive to the surface structure, as previously seen in chapter 1 of this research thesis, taking place almost

exclusively on Pt (100) sites.[15,16] In this respect, it must be taken to accent that a cube is ideally enclosed by 6 (100) faces, highlighting the performance of controlling the nanoparticles shape.

On this basis, we have been working in collaboration with the Microgravity research group (Micro-G) from the University of Puerto Rico, Rio Piedras Campus, in the development and preliminary evaluation of the catalysts for this kind of technology which were tested under the influence of non-gravity today simulated by the Zero-G aircraft by NASA (See Annexes I and II).[14] Certainly, this topic requires today more exploration and develop new studies that aid to build the basis for the advancement of this technology.

In order to contribute for the aforementioned objective, one of the starting steps required to the development of new technologies by supplying the scalable production of high-performance catalysts, this research is focused on the synthesis of shape-controlled Pt nanoparticles by using a similar methodology to that previously reported consisting in w/o microemulsion.[17,18] The main difference is the addition of acids as shape directing agents in the aqueous phase. The presence of acids such as HCl (Figure 2-1), H_2SO_4, HBr, HI, H_3PO_4, $HClO_4$, and some organic acids is evaluated in this Ph D. thesis. Also, in this research work, we evaluate the effect of the concentration of the above-mentioned modifiers to study its influence on the corresponding obtained structure.

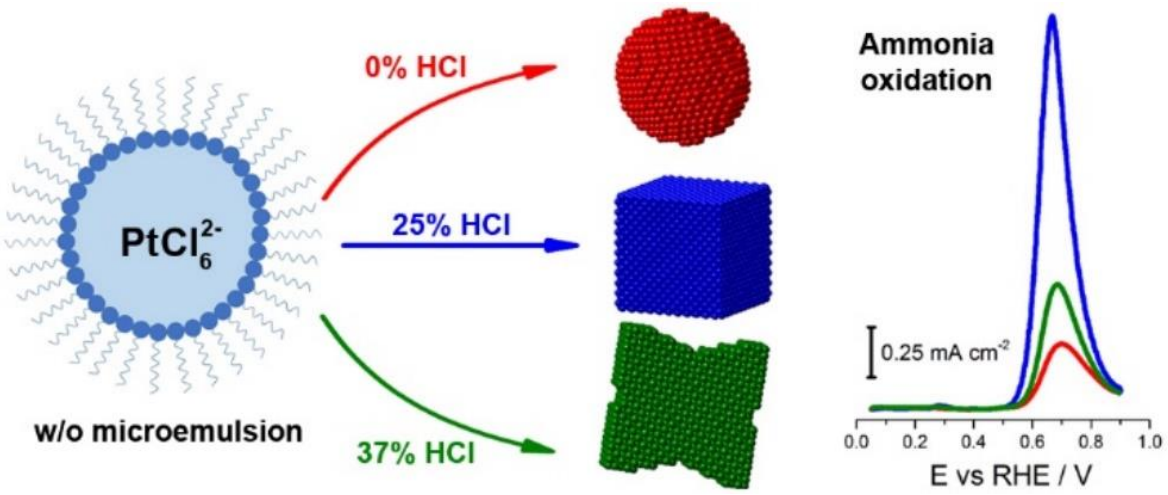

Figure 2-1. Schematic representation of surface-structure change reported by the addition of different concentration of HCl into the aqueous phase of w/o microemulsion and the voltammetric profiles of NH_3 oxidation for the corresponding nanoparticles synthesized.

Another explored parameter was the Pt precursor in the studied syntheses. In this regard, the effect of the oxidation state of the Pt precursor is analyzed. The study was performed by using hexachloroplatinic acid (H_2PtCl_6) and potassium tetrachloroplatinate (K_2PtCl_4). In order to compare the structure modifications, the electrochemical behavior of the synthesized Pt nanoparticles has been evaluated using several structure-sensitive reactions such as NH_3 oxidation, which also, could help us to determine the best-synthesized electrocatalyst for this reaction, which is extremely sensitive to (100) sites[19,20], taking place almost exclusively on those sites which are predominant in cubic nanoparticles.[21]

The study has also been extended to the synthesis of Pt-based shape-controlled bimetallic nanostructures, using the most significant shape directing agents

in the case of pure Pt. The preparation of Pt-based bimetallic nanoparticles (Pt/Me with Me: Ir, Ru, Rh, Pd) using w/o microemulsion methods was previously published by J. Solla-Gullón et. al [22-27] but in this work a step further has been considered with the addition of different acids into the aqueous phase, as proposed in the preparation of shape-controlled pure Pt nanoparticles. This research aims to explore the possibility to synthesize shape-controlled bimetallic nanostructures and evaluate their reactivity and their catalytic performance on structure-sensitive reactions. Pt-based bimetallic nanoparticles have been prepared with different atomic composition ratios and the reactivity of each Pt/Me series has been evaluated.

Finally, a fundamental study using single crystal electrodes was carried out to reach a better understanding of the proposed synthesis method. This fundamental study has been done using the three main basal planes of Pt, that is to say, Pt (100), Pt (111), Pt (110) single crystal electrodes, under the influence of different concentrations of some of the acids used as shape directing agents in the synthesis of the shape-controlled Pt and Pt/Me nanoparticles.

2.1. Hypothesis

This research involves the synthesis, characterization and catalytic performance evaluation of the prepared shape-controlled Pt and the Pt/Me nanoparticles using a modified w/o microemulsion method and evaluate the addition of different acids into the aqueous phase in this process.

The hypothesis of this research is the successful synthesis of shape-controlled Pt nanoparticles for which the surface structure and shape strongly depend on the

acid, and its concentration added into the aqueous phase of the w/o microemulsion. The use of different acids may provide the possibility to obtain cubic shaped Pt nanoparticles, which reflects the possible growth of Pt (100) surface sites on the nanoparticles surface, as shape and surface structure are interlinked on Pt because no reconstruction is expected. In consequence, they would show higher catalytic activity for some reactions due to the fact that this domain is the most active for some structure-sensitive reactions, such as NH_3 oxidation. Finally, the addition of acids into the aqueous phase could also direct the shape of the nanoparticles and therefore, change the surface structure of Pt-based bimetallic nanostructures thus, modifying their resulting catalytic properties.

2.2. Research goals and specific aims

The main goal of this Ph. D dissertation research project is to contribute with a new scalable and fast methodology to synthesize shape-controlled Pt nanoparticles and Pt-based bimetallic nanoparticles which could improve the efficiency towards the electrocatalytic oxidation of NH_3. On this basis, the proposed materials could help also, to study many other structure-sensitive processes that could be evaluated in the near future. To achieve this goal, we divided this research work into three specific aims.

2.2.1. Specific Aims

- Synthesis, characterization and electrochemical behavior of the shape-controlled Pt nanoparticles

- Synthesis, characterization and electrochemical behavior of Pt based bimetallic nanoparticles (Pt/Me, Me = Pd, Rh, Ir and Ru)

- Evaluation of the electrochemical behavior of Pt single crystal electrodes in the presence of different concentrations of surface modifiers used in the synthesis of shape-controlled nanoparticles.

2.2.2. Techniques

The techniques used in this research project to characterize the synthesized materials include surface analysis techniques such as Transmission Electron Microscopy (TEM), Energy Dispersive X-Ray Spectroscopy (EDS) or Thermal Gravimetric Analysis (TGA). Also, shape-controlled nanoparticles were characterized by using cyclic voltammetry (CV) which is a very common, yet powerful, electrochemical technique used for both the characterization of nanoparticles and single crystals.[28-34] Also, CV and chronoamperometry (CA) were used to evaluate the catalytic performance of the nanoparticles towards NH_3 oxidation. In the next chapter, a precise description of all these applied experimental techniques mentioned above is introduced.

2.3. References

1. Aliofkhazraei, M. (ed) Handbook of nanoparticles. Springer International Publishing, Switzerland, 2016; Chapter 42, pp1101-1019.
2. Franco, A. A. (ed.) Polymer electrolyte fuel cells: Applications and Challenges. Pan Stanford Publishing Pte. Ltd., Boca Ratón Fl, 2013; Chapter 3, pp 93-135.
3. Wieckowski, A., Savinova, E. R., and Vayenas, C. G. *Catalysis and Electrocatalysis at Nanoparticle Surfaces.* Marcel Dekker, New York. 2003.
4. Vielstich, W., Lamm, A., and Gasteiger, H.*Handbook of Fuel Cells: Fundamentals*, *Technology and Applications.* John Wiley & Sons Ltd., Chichester, UK. 2003.
5. Zhang, J. *PEM Fuel Cell Catalysts and Catalyst Layers -Fundamentals and Applications.* Springer-Verlag London Ltd., London, UK. 2008.
6. Zhang, J., and Liu, H. (2009). *Electrocatalysis of Direct Methanol Fuel Cells*, (Wiley-VCH Verlag GmbH & Co. KGaA, Weinheim, Germany).
7. Koper, M. T. M. (2009). *Fuel Cell Catalysis: A Surface Science Approach*. John Wiley & Sons, Inc., Hoboken, EEUU. 2009.
8. Figueiredo, M. C.; Solla-Gullón, J.; Vidal-Iglesias, F. J.; Nisula, M.; Feliu, J. M. & Kallio, T. (2015). *Electrochem. Comm.,* **2015**, 55, 47–50.
9. The Fuel Cell Industry Review 2017, www.FuelCellIndustryReview.com**. (accessed: Jan. 7,2019).**
10. Aslam M.; Chaudhary V.A.; Mulla I.S.; Sainkar, S.R.; Mandale, A.B.; Belhekar A.A.; and Vijayamohanan, K. Sensors and Actuators A: Physical,**1999**, 75 (2), 162-167.

11. Nicolau, E.; Fonseca, J. J.; Rodríguez-Martínez, J.A.; Richardson, T.M.J.; Flynn, M.; Griebenow, K.; Cabrera, C. R.; *ACS Sustain. Chem*. **2014**, 2, 749-754.
12. Cabrera, C. R. & Miranda, F. A. (eds): Advanced Nanomaterials for Aerospace Applications, Chapter 1. Pan Stanford Publishing Pte. Ltd., Singapore (2014).
13. Puventud-Estrada, C. M.; Acevedo, R.; Morales, C.; Betancourt, L.; Díaz, D. C.; Rodríguez, M. A.; Larios, E.; Yacamán, M.J.; Nicolau, E.; Flynn, M.; Cabrera, C. R. *Microgravity Sci. Technol*. **2017**, 29, 381-389.
14. Acevedo, R.; Puventud-Estrada, C.M.; Morales-Navas, C.; Martínez-Rodríguez, R.A.; Ortíz-Quiles, E.; Vidal-Iglesias, F.J.; Solla-Gullón, J.; Nicolau, E.; Feliu, J. M.; Echegoyen, L.; Cabrera, C. R. *Microgravity Sci. Technol.* **2017**, 29, 253-261.
15. Vidal-Iglesias, F. J.; García-Aráez, N.; Montiel, V.; Feliu, J.M.; Aldaz, A. *Electrochem. Comm.* **2003**, 5, 22-26.
16. Vidal-Iglesias, F.J.; Montiel, V.; Feliu, J.M.; Aldaz, A.; *J. Phys. Chem*. **2005**, 109, 12914-12919.
17. Solla-Gullón, J.; Montiel, V.; Aldaz, A.; Clavilier, J. *J. Electroanal. Chem.* **2000** 491 (1-2), 69-77.
18. Solla-Gullón, J.; Vidal-Iglesias, F. J.; Sánchez-Sánchez, C.M.; Expósito, E., Montiel, V.; Aldaz, A.; *Trends in Electrochemistry and Corrosion at the Beginning of the 21st,* **2004**, 20, 103-112.
19. Vidal-Iglesias, F. J.; García-Aráez, N.; Montiel, V.; Feliu, J.M.; Aldaz, A. *Electrochem. Comm.* **2003**, 5, 22-26.
20. Vidal-Iglesias, F.J.; Montiel, V.; Feliu, J.M.; Aldaz, A.; *J. Phys. Chem*. **2005**, 109, 12914-12919.

21. Vidal-Iglesias, F. J.; Solla-Gullón, J.; Rodríguez, P.; Herrero, E.; Montiel V.; Feliu J.M.; Aldaz A. *Electrochem. Comm.* **2004**, 1080-1084.
22. Solla-Gullón, J.; Montiel, V.; Aldaz, A.; Clavilier, J. *Electrochem. Comm*, **2002**, 4 (9), 716-721.
23. Solla-Gullón, J.; Montiel, V.; Aldaz, A.; Clavilier, J.; *J. Electrochem. Soc.* **2003**, 150 (2), E104-E109.
24. Solla-Gullón, J.; Rodes, A.; Montiel, V.; Aldaz, A.; Clavilier, J. J. Electroanal. Chem. **2003**, 554, 273-284.
25. Solla-Gullón, J.;Vidal-Iglesias, F. J.; Montiel, V.; Aldaz, A. *Electrochimica Acta* **2004**, 49 (28), 5079-5088.
26. Waszczuk, P.; Solla-Gullón, J.; Kim, H-S.; Tong, Y.Y.; Montiel, V.; Aldaz, A.; Wieckowski, A. *J. Catal*. **2001**, 203 (1), 1-6.
27. Vidal-Iglesias, F. J.; Solla-Gullón, J., Montiel, V.; Feliu, J.M.; Aldaz, A. *J. Power Sources*, **2007**, 171 (2), 448-456.
28. Bard, A. J.; Faulkner, L. R. "Electrochemical Methods: Fundamentals and Applications", John Wiley and Sons, New York, 2nd ed. 2000.
29. Brett, C. M. A.; Oliviera-Brett, A. M., "Electrochemistry: Principles, Methods and Applications" Oxford University Press, Oxford, 1993.
30. Gosser, D. K. "Cyclic Voltammetry: Simulation and Analysis of Reaction Mechanism" VCH Publisher, New York, 1993
31. Hamann, C. H.; Hamnett, A.; Vielstich, W. "Electrochemistry" Wiley, 1998.
32. Clavilier, J. In Interfacial Electrochem. Ed. Marcel Dekker, Inc.: New York, **1999**, 231-248.
33. Rodes, A.; Elachi, K.; Zamakhchari, M. A.; Clavilier, J.; *J. Electroanal. Chem*. **1990**, 284, 245-253.

34. Clavilier, J.; Elachi, K.; Rodes, A.*Chem. Phys.* **1990**, 141, 1-14.

Chapter 3.

Experimental

3. Experimental

In this chapter, the experimental procedures employed in the development of this research thesis are described, including the general procedures used to synthesize both polyoriented and shaped Pt nanoparticles as well as and the characterization techniques used to determine their shape, size, composition, surface structure, and their catalytic performance.

3.1. Preparation of the Pt and Pt/Me nanoparticles

The preparation of the Pt nanoparticles was done by using the water-in-oil (w/o) microemulsion method and cleaning protocol proposed by J. Solla-Gullón et al.[1] in his Ph. D. thesis research. This methodology has been demonstrated to be an easy way to obtain both monometallic[1,2] and bimetallic nanoparticles[2-5], which can be easily cleaned in order to be used for electrochemical studies, which require clean surfaces to be properly analyzed. This is, in part, feasible to be carried out due to the use of the surfactant known as Brij L4 ®. The absence, in this surfactant, of a functional group which could be strongly adsorbed results in a weak metal-surfactant interaction and consequently, it can be easily removed, thus cleaning the nanostructures. This is done by using organic solvents such as acetone.

3.1.1. Synthesis of polyoriented Pt nanoparticles

The general procedure to obtain the polyfacetted Pt nanoparticles is shown in figure 3-1. This methodology is divided into four simple steps. The first step (step # 1) consists in the preparation of a w/o microemulsion mixture of 80.46%, in volume, of n-

heptane, which corresponds to the organic phase of the microemulsion, 16.54% of the surfactant, and 3% of the aqueous phase. The water phase is the one in which the metal precursor is dissolved at a concentration of 0.1 M. The solution is then sonicated and stirred until it shows homogeneity, which corresponds to the translucent property for this kind of microemulsions.

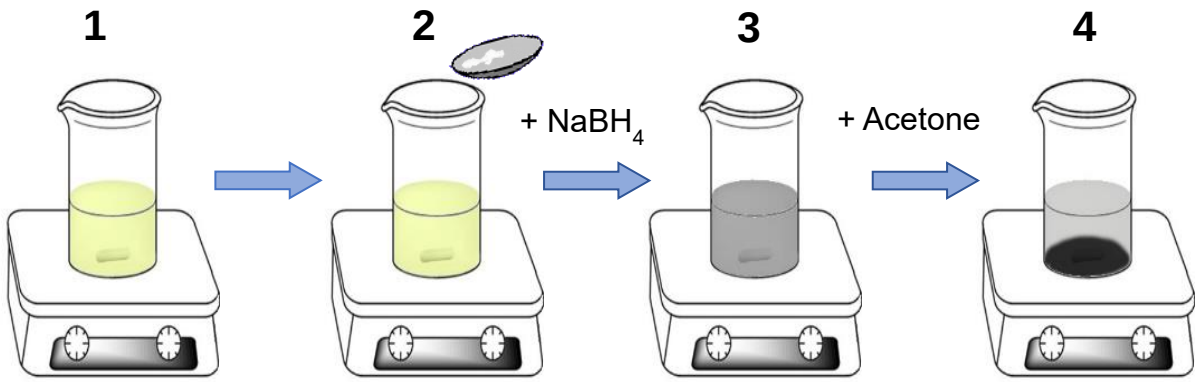

Figure 3-1. Illustrative representation for the preparation of Pt nanoparticles using w/o microemulsion using $NaBH_4$ as a reducing agent and acetone for phase separation.

For this research work, sodium borohydride ($NaBH_4$) has been chosen as the reducing agent. This compound was added to the w/o microemulsion (step # 2) as fine powder at excess with a concentration of approximately 1 M. The solution was stirred during the addition of the reducing agent. After a few seconds, the solution turned black, which is indicative of the metal reduction and the growth of the nanocrystals (step # 3). Finally, the last step (step #4) consisted in the addition of acetone to the w/o microemulsion, which promotes phase separation. When the nanoparticles were supported on carbon Vulcan XC-72R, the required amount was added as a solution

prepared with n-heptane at a concentration of 5 mg/mL, before the last step and sonication was performed until it was well dispersed.

3.1.2. Synthesis of shaped Pt nanoparticles

The synthesis of shaped Pt nanoparticles was performed by using a similar methodology to that previously used for Pt polyoriented nanoparticles, but in this case, the water phase solution of the w/o microemulsion was prepared to contain a certain percentage of the studied acids. In particular, the acids evaluated were HCl, H_2SO_4, HBr, HI, H_3PO_4, $HClO_4$ and their concentrations in the aqueous phase varied depending on the percentage in weight/weight (w/w) of the commercial solution and the stability of the precursor (H_2PtCl_6 or K_2PtCl_4) solution as well as that of the w/o microemulsion.

The evaluation of the stability of the precursor solution was done by visually analyzing the dissolution turbidity at the solubility of the precursor into the acid aqueous solution. In many cases, particularly at high acidic concentrations, sonication was used during the preparation. When the solution was properly prepared it was ready to be added into the w/o microemulsion. Also, and especially for some high acid concentration, once the water phase was added, the transparency of the microemulsion disappeared. However, this property was once again regained after sonication. When the w/o microemulsion became homogenous and translucent it was placed under magnetic stirring and then, the steps corresponding to reduction and phase separation were performed in a similar way to that used during the synthesized of Pt polyoriented nanoparticles, which was previously discussed in the preceding section.

3.1.3. Synthesis of shaped Pt-based bimetallic nanoparticles (Pt/Me with Me: Pd, Rh, Ir, Ru)

Pt/Me nanoparticles were also synthesized with a similar method to that used for the synthesis of the shaped Pt nanoparticles but with the addition of two different aqueous solutions corresponding to the two metal precursors in the w/o microemulsion. The preparation of the aqueous solution of the metal precursor was prepared with an acid concentration at which the surface modifying effect was observed for the synthesis of shaped Pt nanoparticles. By using H_2PtCl_6 as Pt precursor, HCl, HBr and H_2SO_4 were studied at concentrations of 20, 25 and 50 (% w/w) respectively. The use of K_2PtCl_4 as Pt precursor was also evaluated by using 15% HCl.

Once the Pt precursors were prepared, Pd, Rh, and Ir salt solutions were prepared with K_2PdCl_4, $RhCl_3$, and $IrCl_4$ precursors, respectively, in the presence of the same acid concentration at which the Pt precursor was prepared. Different Pt/Me volume ratios were tested in order to evaluate their catalytic performance. The studied ratios of Pt/Me evaluated were 100/0, 90/10, 75/25, 50/50, 25/75 and 0/100, for which 0/100 and 100/0 are pure Pt and Me nanoparticles, respectively. Once both precursor solutions were added into the w/o microemulsion, the stability of the mixture was promoted by using sonication and magnetic stirring. Finally, reduction and phase separation processes were also done as previously described. During the preparation of each ‘Me’ precursor solution, we noticed that only the Rh metal solution, achieved stability to successfully synthesize bimetallic Pt/Rh nanoparticles. For this reason, Chapter 7 of this research thesis will be focused on the synthesis, characterization and electrochemical behavior of Pt/Rh nanoparticles.

3.1.4. Cleaning protocol

The removal of the surfactant or capping agent from the nanoparticle's surface is an important step during the preparation of the nanoparticles, as electrochemical measurements require clean surfaces to be studied.[6] Figure 3-2 shows an illustrative representation of the differences of the voltammetric profiles obtained by shaped Pt nanoparticles covered with capping agents versus the same Pt nanoparticles with a clean structure. This example highlights the importance of having clean surfaces from capping agents. Without a proper cleaning step, the nanoparticle's surface is partially blocked and the electrochemical characterization results are not those of clean nanoparticles, also making them less reproducible as they also depend on the degree of surface contamination.

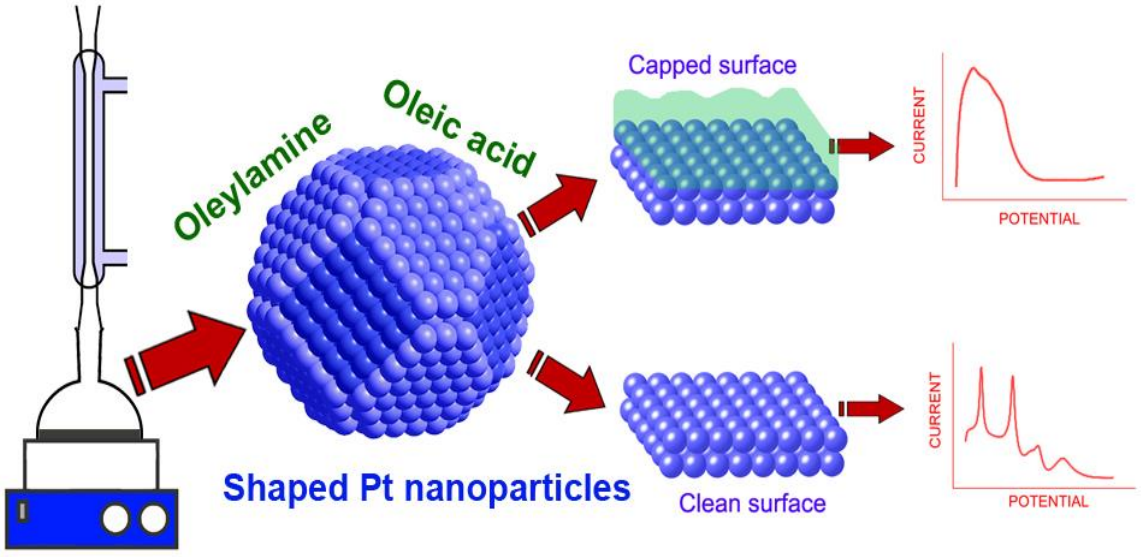

Figure 3-2. Illustrative representation of shaped Pt nanoparticles synthesized by using oleylamine and oleic acid as a capping agent and the corresponding voltammetric profile with and without impurities. Image reproduced from Arán-Ais R. M. et al. (2015).[6]

The most common methods considered in the bibliography to remove impurities from the surface of the nanoparticles include solvent cleaning[7], Ultra-Violet (UV) radiation[8,9], thermal annealing[10], acetic acid washing[11,12], and plasma treatment[13]. Also, electrochemical treatments have been explored such as cycling the applied potential to ranges of oxidation/reduction of the material under study[14] as well as the electrochemical imposition of a constant high voltage.[2] Most of these methods usually induce compositional and structural modifications. This is the case of the cleaning treatment of shaped controlled Pt nanoparticles by using UV/ozone treatment, which evidences atomic surface disordering.[15] Figure 3-3 shows the electrochemical measurements of the three Pt single crystal electrodes before and after the exposure of UV/ozone at different times. For each Pt single crystal electrode, the exposure to UV/ozone induces severe structural modifications, which can be noticed by the change of the electrochemical response of the electrodes. Also, it is observed that as exposure time increases, the structural modification increased by comparing the profiles obtained in the same electrode. Furthermore, the Pt facet with the most significant structure modification is the Pt (111).

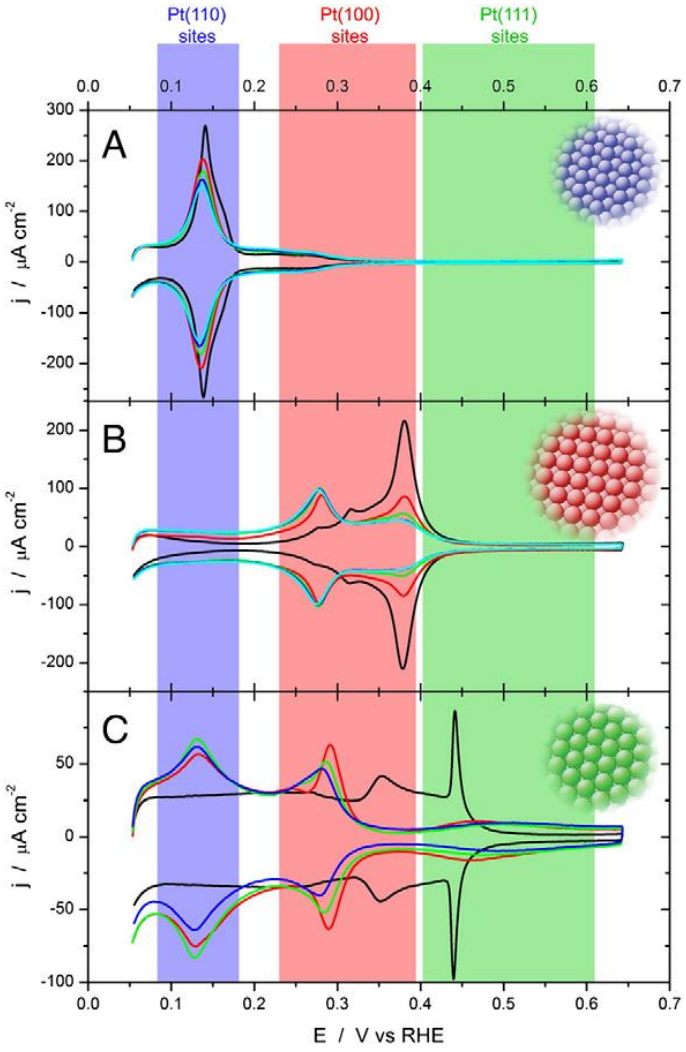

Figure 3-3. Voltammetric profiles of (A) Pt (110), (B) Pt (100) and (C) Pt (111) before (black) and after 5 (red), 15 (green), 35 (blue) and 65 (cyan) minutes of UV/ozone exposure. Test solution: 0.5 M H_2SO_4. Sweep rate 50 mV s^{-1}. Reproduced from Vidal Iglesias et al. (2011). [15]

During the experimental work of this Ph.D. thesis, and in order to keep the surface without any modification, the cleaning protocol chosen was the solvent cleaning, which implies several washes of acetone and water. This step was done by adding acetone into the w/o microemulsion solution and by shaking the vial manually. Then, the solution was allowed to rest until the nanoparticles precipitated by gravity to

the bottom. This procedure was done at least 3-4 times, followed then by the same process with ultra-pure water (resistivity of 18.2 MΩ*cm) to remove the acetone. After a successful cleaning process done, nanoparticles are ready to be electrochemically analyzed.

3.2. Electrochemical analysis

The electrochemical experiments performed with nanoparticles in this research have had an important role, not only for the purpose of surface characterization, but also as a tool to successfully determine the catalytic performance of the studied materials. The electrochemical analysis implies a deep study of the structure of the whole material in contrast with other surface analyses such as Transmission Electron Microscopy (TEM). In addition, it is a powerful technique which can give important information about the surface structure of the material under study. This type of analyses neither was performed with conventional TEM. A good example of this is provided by the induced modification of the structure by using the UV/ozone cleaning treatment previously discussed. In this case, octahedral Pt nanoparticles were subjected to this cleaning treatment and TEM images obtained before and after, from the nanoparticles did not allow to see any changes in their shape.[15] However, an electrochemical analysis of the octahedral Pt nanoparticles confirmed a strongly induced structure modification. Figure 3-4 illustrates the limitation mentioned for TEM, unable to track the changes on the nanoparticles surface after being subjected to UV/ozone cleaning). In the next sections of this chapter, the main two electrochemical techniques used in this research thesis are explained

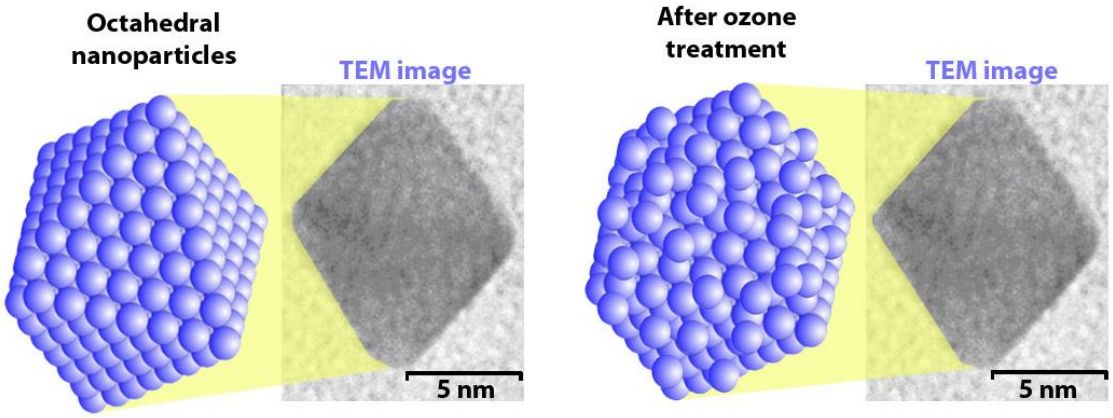

Figure 3-4. Illustrative representation and TEM images of octahedral Pt nanoparticles before and after the induced modification of the structure by using the UV/Ozone treatment. Reproduced from Vidal Iglesias et al. (2011). [15]

3.2.1. Cyclic Voltammetry (CV)

CV has been one of the most employed techniques in this research thesis due to its capacity for providing a lot of information. This technique facilitates information about two important aspects in the material characterization, including the surface structure and cleanliness of the electrode, as well as the catalytic properties towards the reaction under study. In addition, this technique has been also used to measure the electroactive surface area of the catalyst. During a CV, a linear potential sweep is applied to the studied material at a controlled rate while recording the changing in the current.[16-19] As a result of this, a graphic representation, commonly known as cyclic voltammogram, is obtained in which the intensity correlates with the applied potentials (E) and the process taking place within the potential range explored.

CV experiments require the use of a potentiostat instrument to apply the required potential and to collect the intensity of the working electrode (WE). This

electrode is where the electrochemical reaction of interest occurs. The potential of this electrode is known by using a reference electrode (RE), which in these experiments was a reversible hydrogen electrode (RHE), connected with the electrochemical cell through a Luggin capillary. This electrode consists of a platinized Pt wire submerged in the same working solution and saturated by H_2, which is continuously bubbled. Finally, a counter electrode (CE), closes the circuit in which the electron flow is in the opposite direction to that of the WE. For the experiments prepared in this research thesis, a Pt wire was used as CE.

Experiments were carried out in a three-electrode electrochemical cell. Figure 3-5 (A) shows an image of the electrochemical cell used for experiments in this work. This cell also contains a gas nozzle that is used mostly for bubbling Argon (Ar) into the working solution in order to remove the oxygen (O_2) dissolved in the solution. Also, in order to keep the solution without O_2, measurements were performed under Ar blanket atmosphere. In addition, in the case of the experiments that were carried out to compare the catalytic performance of many samples, a multiple WE electrochemical cell was used. This one consisted of an arrangement of multiple WE (up to 8) with a single CE and a single RE. For these measurements, a multi-channel potentiostat VMP3 Bio-logic was used. Figure 3-5 (B) shows an image of the multiple WE cell used in this research thesis. This later arrangement allowed to compare the catalytic performance up to 8 samples under the same experimental conditions such as concentration and temperature, which facilitated the analysis and gave more reliable results.

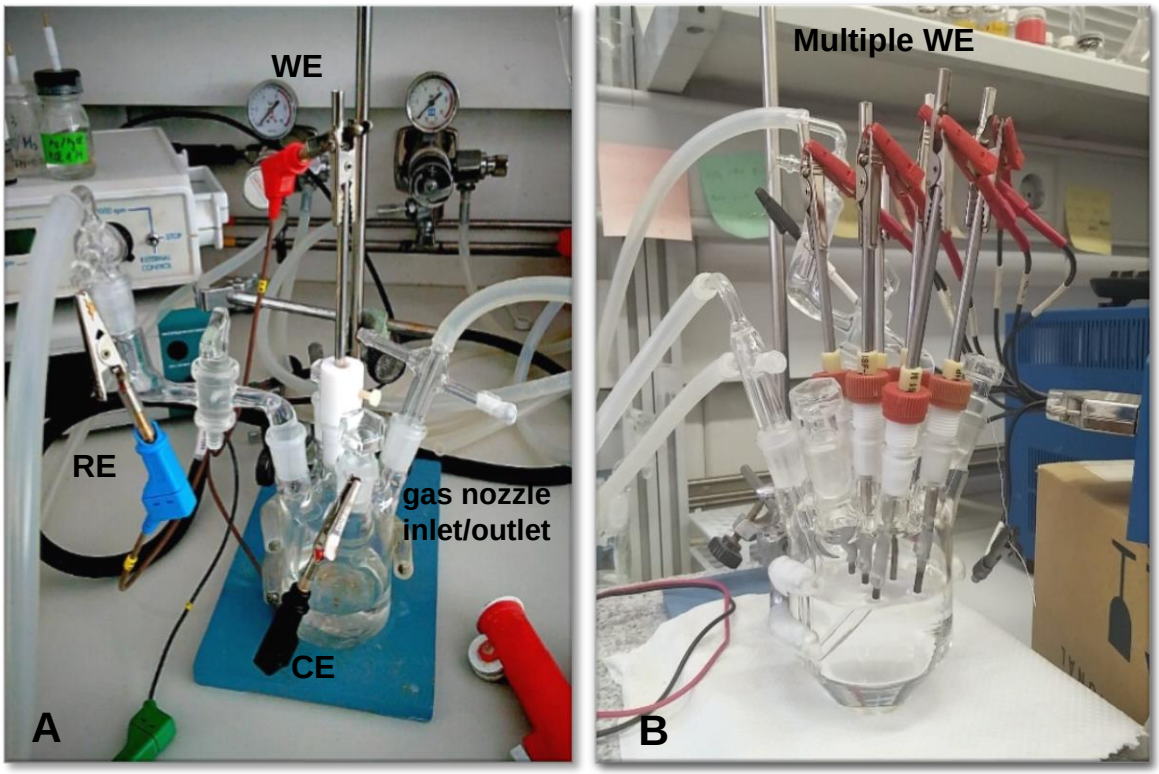

Figure 3-5. (A) Picture of the three-electrode and (B) multiple WE electrochemical cells used for experiments in this research thesis.

For the electrochemical analysis of the nanoparticles, a gold (Au) disk of about 5mm of diameter was chosen as the WE. Figure 3-6 shows an image of the Au electrode used in this research thesis.

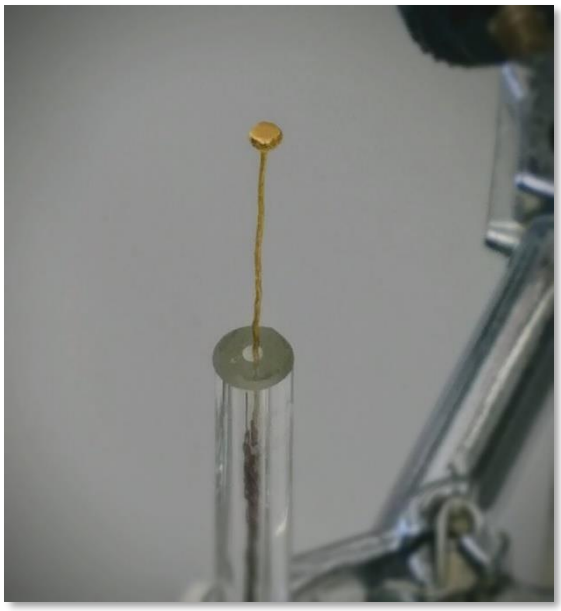

Figure 3-6. Illustrative picture of Au electrode commonly used in this research thesis.

Au metal was chosen as support due to its inert electrochemical behavior in a wide potential region in which the electrochemical properties of the nanoparticles were evaluated. It was previously polished with alumina, sonicated with ultra-pure water and finally cleaned by flame annealing treatment. This treatment consisted of heating the WE with a butane flame until the metal reached an incandescent color and then cool it down in air and finally protected with ultra-pure water. After the cleaning process, a CV was recorded in order to confirm the surface cleanliness. Thus, CV's were performed in 0.5M H_2SO_4 prepared with ultra-pure Milli-Q® water and analytical grade electrolyte every time an experiment was carried out. Figure 3-7 shows the cyclic voltammogram of the characteristic clean Au disk electrode used as WE. In this image, it is noticeable the wide range of potentials of the double layer region in which no other contribution takes place (0 - 1.3 V vs RHE) and also, the characteristic peaks produced

by the oxidation of the Au surface at higher potentials, which clearly identifies the metal and its corresponding reduction.

In the experiments performed with the multiple WE electrochemical cell, glassy carbon (GC) rods were used instead of Au electrodes. In this case, these supports were cleaned with alumina and sonicated with ultra-pure water.

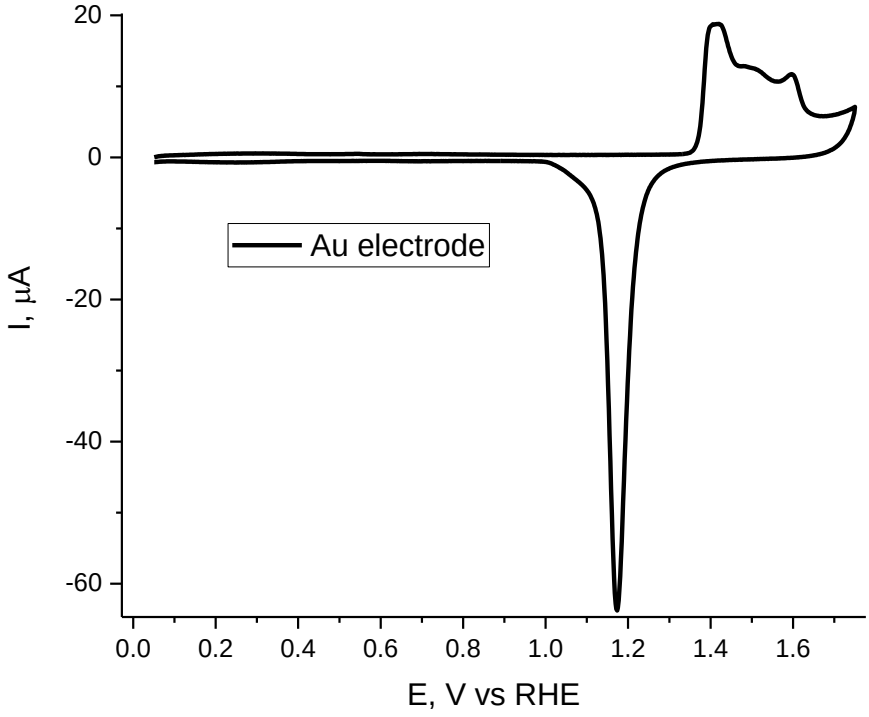

Figure 3-7. Voltammetric profile of the gold electrode. Test solution 0.5 M H_2SO_4, scan rate 50 mVs^{-1}.

As soon as the WE was evaluated to confirm the surface cleanliness, a drop of about 2-5 µL of the sonicated solution of the clean nanoparticles suspended in ultra-pure water was deposited on the Ar-dried Au disk. This drop was dried by placing the

electrode under Ar atmosphere for a few minutes and finally transferred to the electrochemical cell to be characterized.

The electrochemical analysis of Pt in H_2SO_4 provides qualitative information about the different sites present on the surface of any Pt surface, including those present in the case of nanoparticles. Previous research has correlated the characteristic behavior represented in voltammograms as peaks with contributions of the bi-dimensional ordered sites, terrace and stepped surfaces.[20,21] Figure 3-8 shows a voltammetric profile in 0.5 M H_2SO_4 of polyoriented Pt nanoparticles with their respective contributions assigned depending on the potential at which the signal takes place. For each contribution, a surface domain is assigned which will be discussed later in section 3.2.3. The main voltammetric features of the polyoriented nanoparticles are the peaks at 0.125 V, which is related to (110) sites, the peak at 0.27 V corresponding to the small (100) ordered domains, the shoulder at 0.37 V related to wide (100) terraces and finally, the broad contribution at 0.50 V is related to bi-dimensionally ordered (111) terraces. The nanoparticles prepared in this work were qualitatively analyzed by comparing the voltammetric profiles obtained for each sample.

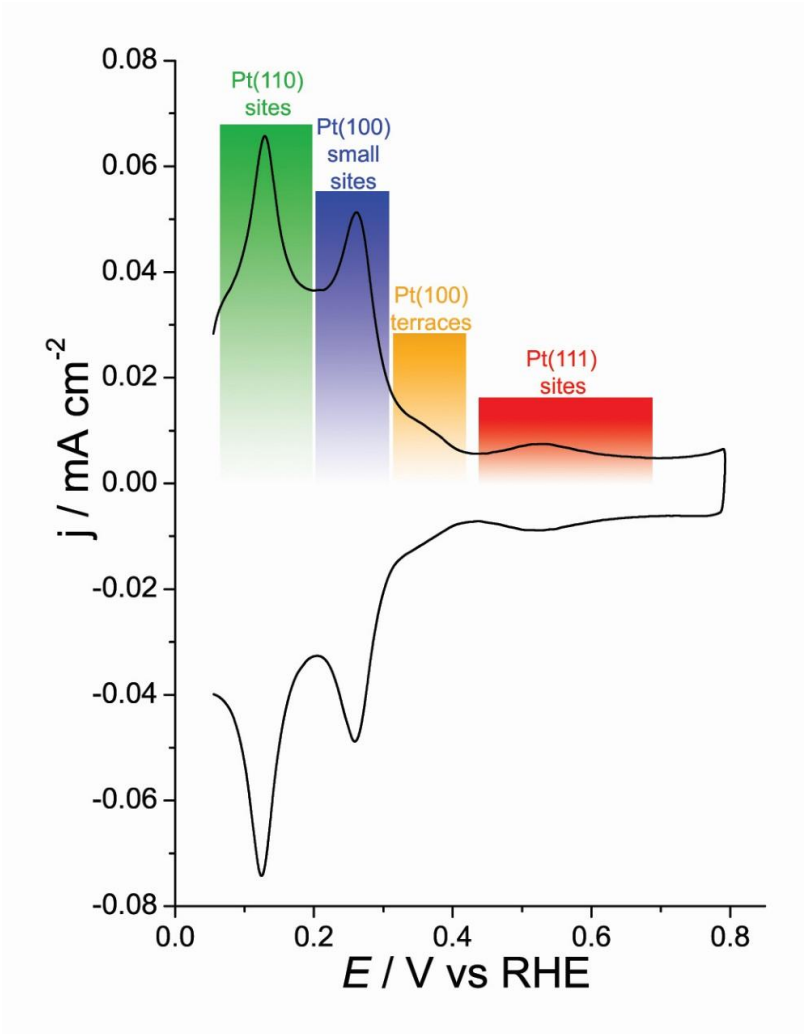

Figure 3-8. Voltammetric profile of quasi-spherical nanoparticles and their respective contributions separate by the corresponding signals at determined potentials. Reproduced from J. Solla-Gullón et al. (2011).[20]

3.2.1.1. Carbon monoxide (CO) monolayer oxidation

Once the CV of the deposited nanoparticles was recorded, CO was adsorbed at constant potential on the nanoparticles surface and subsequently, electrochemically oxidized. The obtained CV allows for gaining additional qualitative information about the surface structure of the samples under study. For Pt surfaces, CO adsorption/oxidation process have been widely studied in electrocatalysis. Also, it has

been demonstrated that adsorbed CO oxidation is an extremely structure-sensitive reaction useful to establish correlations with the surface structure of platinum.[22-29] This means that the CO monolayer oxidation can be a powerful method to be used for surface structure characterization.[30,31] However, in this research, CO monolayer oxidation has been mainly used for deep cleaning the surface of the Pt nanoparticles by removing other species such as surfactants or capping agents due to its high adsorption energy.

Figure 3-9 shows some characteristic CO monolayer oxidation voltammetric profiles corresponding to different Pt nanoparticles, synthesized with different methodologies, and having different surface structures.[31] These profiles confirm the sensitivity of this reaction to the presence of bi-dimensional ordered domains on Pt nanostructures. For polyoriented Pt nanoparticles, a voltammetric profile similar to that shown in figure 3-9 (A) and (B) is obtained. These profiles are different from each other due to the different surface structure presented. In figure 3-9 (B) two main peaks at ≈ 0.72 V and ≈ 0.77 V, the latter denoting that these Pt nanoparticles have a higher fraction of (100) and (111) domains than the polyoriented Pt nanoparticles from figure 3-9. In the case of cubic Pt nanoparticles, authors observed the presence of two contributions at approximately 0.73 V and 0.78 V (figure 3-9 (C)) whereas for the octahedral Pt nanoparticles [figure 3-9 (D)], contributions at ≈ 0.68 V, which includes a shoulder at 0.70 V, and at ≈ 0.75 V are reported. In both profiles, cubic and octahedral Pt nanoparticles, show that the second contribution is represented by a sharp peak with a higher current density in comparison with the wider peak of the first contribution.

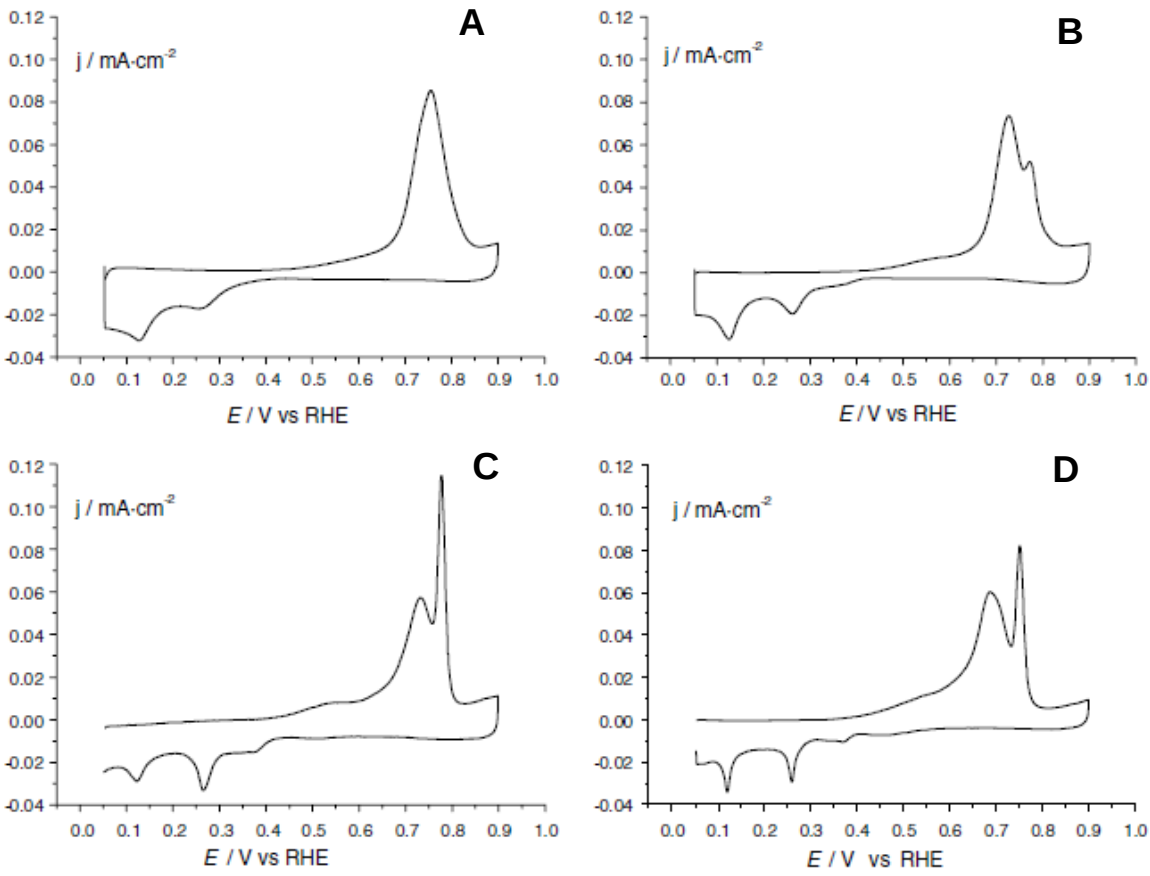

Figure 3-9. CO stripping corresponding of Pt nanoparticles synthesized by using w/o microemulsion with (A) hydrazine and (B) sodium borohydride as reducing agents and (C) cubic and (D) octahedral Pt nanoparticles. Test solution 0.5 M H_2SO_4 and scan rate 50 mVs^{-1}. Reproduced from J. Solla-Gullón et al. (2006). [31]

The procedure to clean the nanoparticles by using CO adsorption / oxidation starts by bubbling CO inside the electrochemical cell for a couple of minutes with a controlled potential in the WE of 0.05 V vs RHE. After a voltammetric test from 0.05-0.30 vs RHE that could confirm the surface blockage, Ar bubbling is allowed in the working solution for approximately 15 minutes, in order to remove all of the CO dissolved and remaining inside the electrochemical cell. The blocked surface indicates that CO has effectively displaced other molecules from the nanoparticle's surface, particularly the surfactant or capping agents. Then CO oxidation is run with a CV from

0.05 to 0.90 V and a voltammetric profile similar to those shown in figure 3-9 is collected.

Afterward, now having the clean surface, a voltammetric profile of the real sample is obtained and the electrochemically active surface area (cm^2) can be determined. The active surface area of the Pt nanoparticles was calculated by the charge involved in the so-called hydrogen UPD region (between 0.06 V and 0.6 V) after the subtraction of the double layer charging contribution and assuming, the CV rate (mVs^{-1}) and the calibration ratio as 210 $\mu C*cm^{-2}$. [32] In the case of shape-controlled Pt nanoparticles it has been reported that when working in H_2SO_4, a value of 230 $\mu C*cm^{-2}$ is more accurate.[33]

For bimetallic nanoparticles, the calibration ratio was obtained from the value of hydrogen UPD charge density for the pure metals, and the ratio of both metals assuming that the percentage of both metals at the surface is the same as that of the nominal composition.

3.2.1.2. Irreversibly adsorption of germanium (Ge)

In order to carry out the quantification of the (100) surface active sites on Pt, irreversible adsorption of Ge was performed. Previous studies have shown that irreversibly adsorbed Ge on Pt sites with a (100) surface orientation shows a well-defined peak at around 0.55 V. The interesting fact about this process is that other sites symmetries do not show any contribution close to that potential. This electrochemical tool has been successfully applied to quantify the amount of (100) sites by integrating the voltammetric peak observed at the aforementioned potential.[21,34,35]

This process was experimentally carried out by placing the clean WE with deposited Pt nanoparticles, in a 10^{-2} M solution of germanium oxide (GeO_2) + 1 M NaOH. The WE covered with a droplet attached was immersed in the electrochemical cell at a controlled potential of 0.1 V vs RHE to keep Ge adsorbed. Then, 10 cycles were performed in order to obtain the best profile of the Ge oxidation and used for the (100)-site quantification. From the area of the peak in the positive sweep scan, the charge of the Ge (q_{ge}) desorption was calculated. The quantification of the (100) domains of the Pt nanostructures was determined by using the normalization factor (Equation 3-1) obtained in calibration plots previously reported.[35] Consequently, the charge of the (100) terrace sites can be obtained with a simple mathematical treatment.

Equation 3-1. $q_{Ge} = 0.56\ q^{t}_{(100)}$

Finally, the percentage of (100) terrace sites can be obtained by dividing the $q^{t}_{(100)}$ to the current density value of 209 μCcm^{-2} which is the assigned charge density value for a Pt(100) (100% (100) sites).

3.2.2. Chronoamperometry

This electrochemical technique consists in recording the intensity as a function of time at a controlled potential. This type of study allowed to get information related to the stability of different electrocatalyst in more applied conditions. This technique generates currents, which decay readily with time.[16] Figure 3-10 shows an illustrative

example of a typical chronoamperometric measurement performed in this case for two different samples of shaped Pt-Rh nanoparticles and compared with the shaped and polyoriented Pt nanoparticles for NH_3 oxidation at 0.55 V vs RHE.

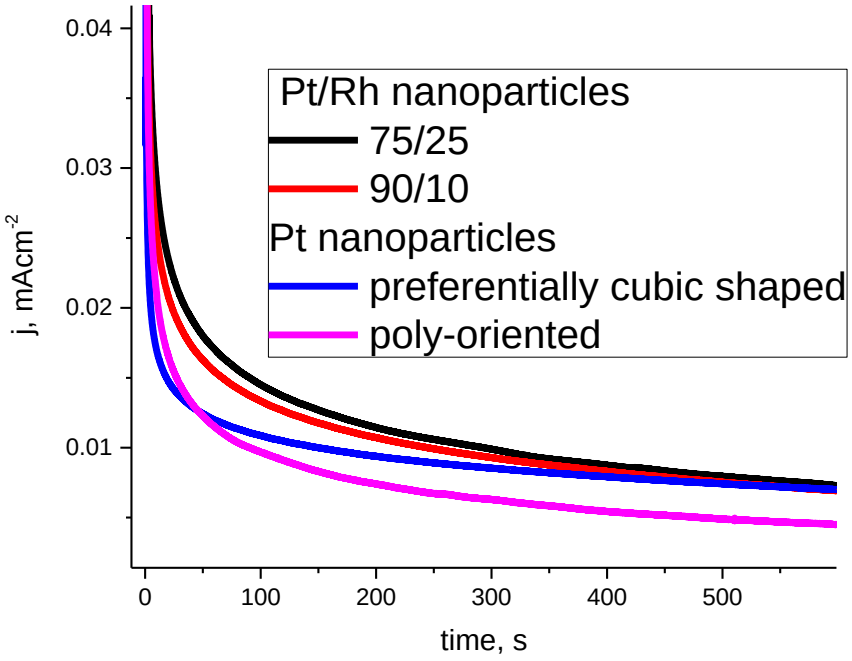

Figure 3-10. Chronoamperometric measurement of NH_3 oxidation at 0.55 V vs RHE for shaped Pt/Rh nanoparticles versus shaped and polyoriented Pt nanoparticles. Test solution NH_3 0.1 M + NaOH 0.2 M.

During this research thesis, we used this technique to evaluate the electrocatalytic activity for the NH_3 oxidation reaction for relatively long-term experiments at controlled potentials that ranged from 0.5-0.6 V vs RHE.

3.2.3. Pt single crystal electrodes preparation and treatment

Pt single crystal electrodes can be obtained by cutting, orienting and polishing Pt spherical crystals using the methodology developed performed by Clavilier.[36] In this research thesis the three Pt low index or basal plane electrodes, Pt (100), Pt (111) and Pt (110), have been used. These basal planes represent the apexes of the stereographic triangle (Figure 3-11) of a face-centered cubic metal, which is an analogous three-component phase diagram.[20]

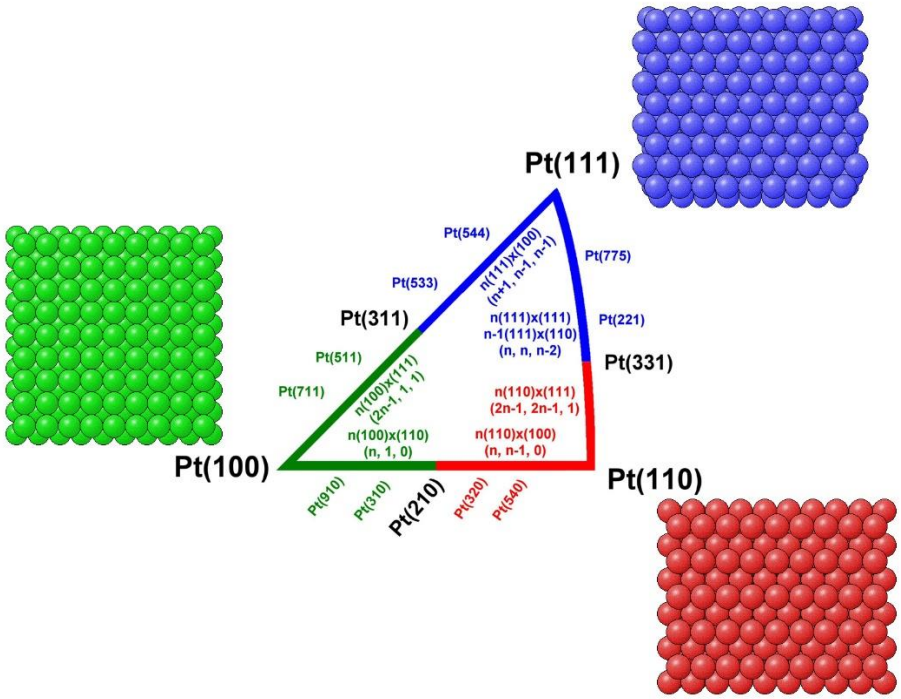

Figure 3-11. Stereographic triangle for the Pt crystalline structure system. Reproduced from J. Solla-Gullón et al. (2013).[20]

A typical single crystal electrode is shown in figure 3-12. The use of this kind of electrodes for electrochemical experiments requires strictly clean and handling conditions including several washes of the electrochemical cell where the study will be carried out. A cleaning thermal methodology was performed by Clavilier et al.[37-39] to

remove any adsorbed impurities from the surface of the Pt single crystal electrodes. Furthermore, this treatment can be used to reorganize the surface structure of the single crystal electrode. For the experiments performed in this research thesis using Pt single crystal electrodes, the thermal treatment was used before each time the electrode was electrochemically tested. This thermal treatment consisted of flame annealing the Pt single crystal electrodes using a butane flame. Once the Pt single crystal electrode reached an incandescent color, it was allowed to cool down under a H_2 + Ar atmosphere at a gas volume ratio of 1:3 respectively. For Pt (100) and Pt (110) single crystal electrodes, this process is crucial, due to the influence of oxygen in the final structure, which generates defects in the crystal arrangement at an atomic level.[40-42] After the cooldown process takes place, the Pt single crystal electrode is submerged in ultra-pure water in equilibrium with the aforementioned gas mixture and finally is ready to be transferred in the electrochemical cell and analyzed.

Figure 3-12. Image of Pt (111) single crystal electrode as a reference model for the electrodes used in this research thesis.

Once the electrode is clean, the surface of the Pt single crystal electrode can be electrochemically studied by using CV. The experiments were performed in the so-called meniscus configuration in order to that only the surface plane of the single crystal electrode interacts with the electrolyte solution.[43,44] Once the electrode is correctly placed in the electrochemical cell the analysis is carried out. Figure 3-13 shows the characteristic voltammograms of the three basal planes of Pt and the polyoriented Pt electrode, all of them tested in 0.5 M H_2SO_4. These voltammetric profiles can be taken as fingerprints of the crystalline surface structure of each

electrode [20], as the reported signals represent the characteristic behavior of each surface domain.

A comparison between the voltammograms of the basal plane electrodes and that of the polyoriented surface electrode shows that most of the peaks or contributions of the Pt single crystal electrodes also appear for the poly-oriented surface. In conclusion, the voltammetric features of the polyoriented surface can be assigned to each of the basal plane. The first signal peak at 0.125 V is related to (110)-type sites, and the peak at 0.27 V results from two different contributions, one coming from the (100) step sites on (111) domains and the other one arising from the sites on a (100) ordered domain close to a step or a defect. In addition, the shoulder-like shape at 0.37 V is ascribed to wide (100) terraces and finally, the small peak at 0.45 V to the presence of bi-dimensionally ordered (111) terraces.

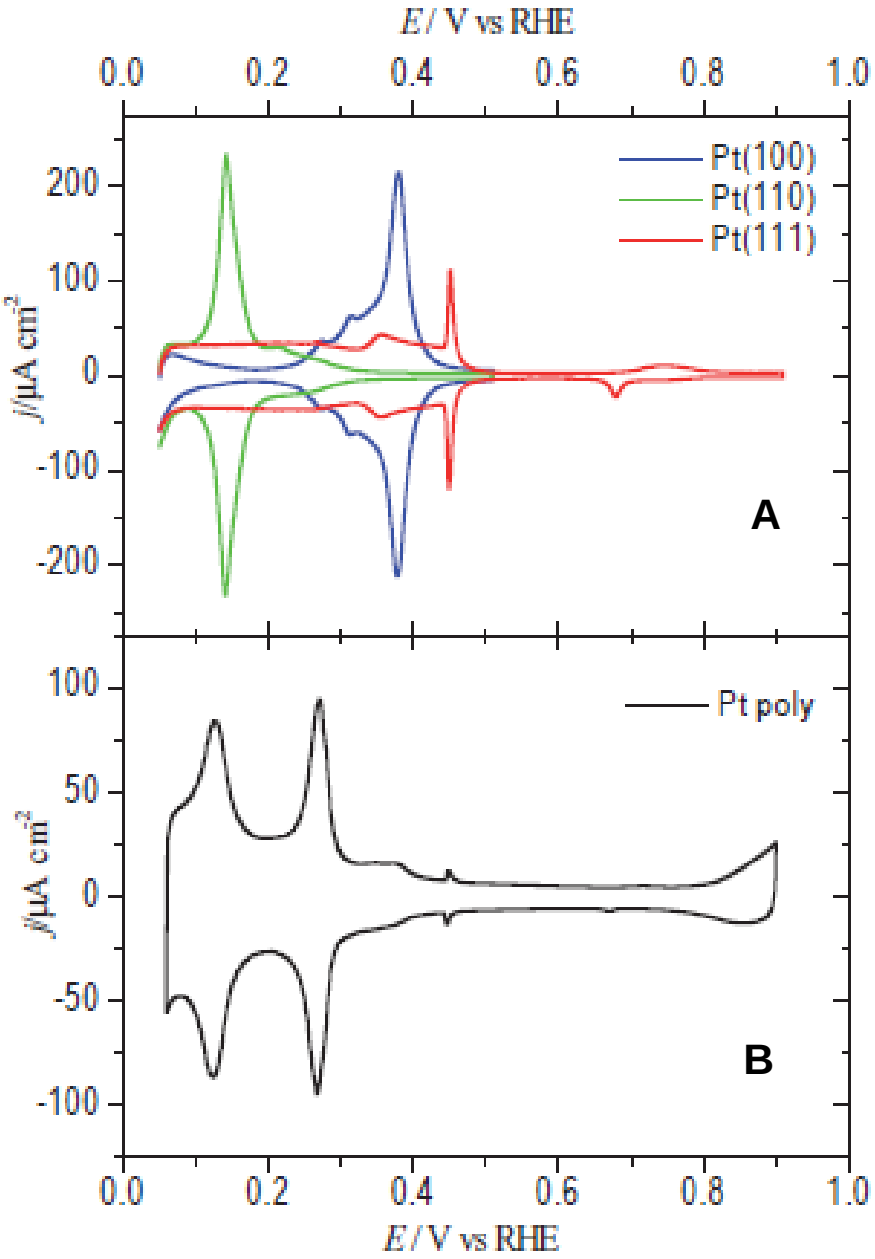

Figure 3-13. Voltammetric profiles of (A) the three Pt basal planes and (B) a polyoriented Pt electrode in 0.5 M H_2SO_4. Scan rate: 50 $mV*s^{-1}$. Reproduced from Solla-Gullón et al. (2013).[20]

3.3. Surface characterization

In this section, the techniques used to physically characterize the materials prepared in this research thesis are introduced. Each of these techniques is a powerful tool to provide important information about the nanoparticles that have been prepared in this work.

3.3.1. Transmission Electron Microscopy (TEM)

Transmission electron microscopy (TEM) is a very well-known technique which provides an image of the studied material at the nanoscale range and is based in the interaction of an electron beam impacting the sample. This electron beam is focused by using a complex system of electromagnetic fields acting as lenses and focusing the beam in the area of interest. The interaction of the incident electron beam with the sample and its transformation into an image brings some physical properties of the studied material, including size, agglomeration level, and shape of the material.[45] For this research, TEM microscopes used to obtain the images of the nanostructures were the model JEOL JEM-2010 and the JEOL JEM-1400 plus from the research technical services from the University of Alicante in Spain.

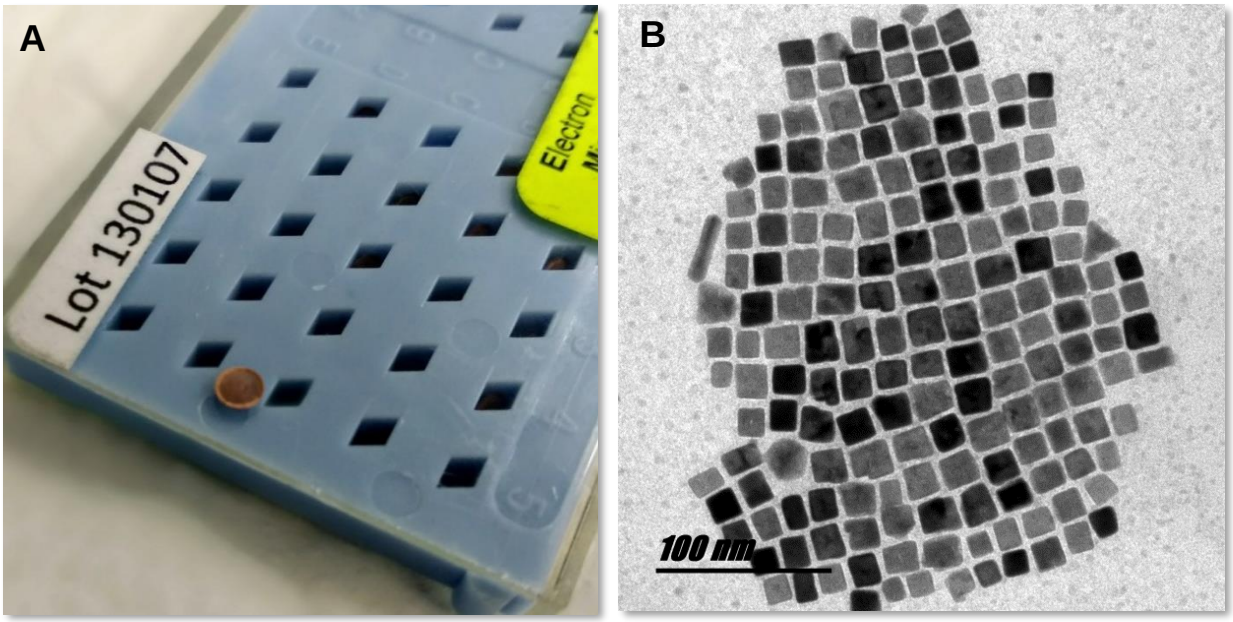

Figure 3-14. (A) TEM grid commonly used for sample testing and (B) TEM image of preferential cube Pt nanoparticles.

The sample preparation consists into deposition of a small drop of the sample, in this case, a drop of about 20-40µL of the w/o microemulsion with the suspended nanoparticles onto a TEM grid (Figure 3-14 A). The sample is then allowed to dry and then it is finally analyzed obtaining an image like to that shown in figure 3-14 B.

3.3.2. Electron Dispersive X-ray (EDX)

TEM instruments can also perform microanalysis of EDX which represents an invaluable tool to simultaneously obtain imaging and quantitative composition data at the atomic scale for bimetallic and multimetallic structures.[46] This technique is based on the interaction that occurs when a high-speed electron beam collides with the

sample, resulting in the X-Ray flourescence emission. The radiation emitted is analyzed and assigned for the corresponding element presented in the sample. Finally, a distribution of the elements, as well as elemental mapping, can be obtained. In this work, we have been using EDX analysis to determine the atomic composition as well as the element distribution of the bimetallic nanostructures synthesized. Figure 3-15 shows a typical EDX analysis of Pt-Rh nanoparticles prepared with 75:25 mass ratio respectively and the TEM image of the chosen place analyzed by using this EDX. In this analysis, the presence of different peaks from the elements presented in the sample and the atomic percentage are showed. EDX analysis was performed with an X-ray detector OXFORD model INCA Energy TEM 100.

Quantitation method : Cliff Lorimer thin ratio section.
Processing option : All elements analyzed
Number of iterations = 1

Standardless

Element	Peak Area	Area Sigma	k factor	Abs Corrn.	Weight%	Weight% Sigma	Atomic%
Rh L	971	126	1.706	1.000	14.40	1.67	24.19
Pt L	3797	148	2.592	1.000	85.60	1.67	75.81
Totals					100.00		

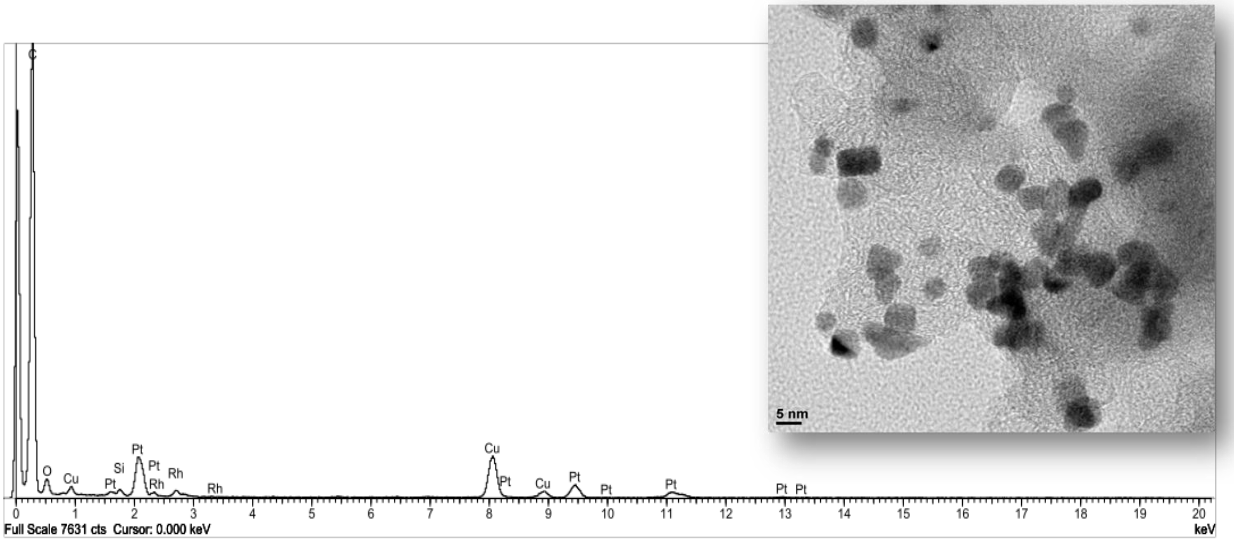

Figure 3-15. EDX analysis and TEM image of shaped controlled Pt/Rh 75/25 atomic ratio.

3.4. Other techniques

3.4.1. Thermogravimetric Analysis (TGA)

The thermogravimetric analysis (TGA) technique involves the heating of a sample to evaluate its weight loss and provides information about the sample composition, thermal stability, material purity, and humidity. Through this research, TGA has been employed to obtain the Pt loading (% in weight) of the prepared carbon-supported Pt nanoparticles. (See Annexes I and II) In the analysis performed in this thesis, the methodology involves the heating of a known mass of the sample in a temperature ramp that goes from 25 to 850 °C at a heating rate of 10 °C*min^{-1} under N_2: O_2 (4:1) atmosphere. The difference in weight due to the loss of carbon sublimated from the sample allows the Pt loading to be calculated. TGA analysis was done by using the Mettler-Toledo, TGA/SDTA851. Figure 3-16 shows a typical TGA analysis for the determination of the Pt of Pt nanoparticles supported with Vulcan (Pt/V). TGA measurements were performed in a TGA Mettler-Toledo model SDTA851 thermobalance.

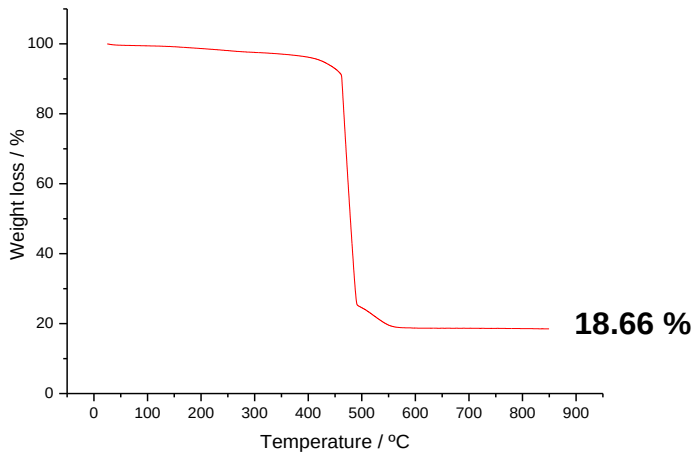

Figure 3-16. TGA of Pt/ V nanoparticles and the Pt loading value.

3.5. Chemicals

All the reagents used in this research work were performed with high purity chemicals. Table 2-1 summarizes the reagents used for this Ph. D. thesis.

Table 2-1. List of reagents employed

Reagent	***Formula***	***Grade***	***Company***
Chloroplatinic acid hydrate	H_2PtCl_6-x H_2O	40 %	Acros Organics
Potassium teracloroplatinate (II)	K_2PtCl_4	99%	Acros Organics
Hydrochloric acid	HCl	37%	Panreac
Sulphuric acid	H_2SO_4	95-97 %	Merck
Hydrobromic acid	HBr	48%	Acros Organics
Phosphoric acid	H_3PO_4	85%	Merck
Perchloric acid	$HClO_4$	suprapur®	Merck
Rhodium Chloride	$RhCl_3$	38-40%	Sigma-Aldrich
Sodium hydroxide	NaOH	suprapur®	Merck
Ethanol	C_2H_5OH	p.a.	Merck
Ammonium sulphate	$(NH4)_2SO_4$	p.a.	Merck
hydroquinone	C_6H_4-1,4,-$(OH)_2$	99%	Sigma-Aldrich
Germanium (IV) oxide	GeO_2	99.999%	Sigma-Aldrich
Citric acid	$C_6H_8O_7$	99.7%	Prolabo
Glycol dodecyl ether (Brij® L4)	$C_{12}H_{25}(OCH_2CH_2)_4OH$	p.a.	Sigma-Aldrich
n-heptane	C_7H_{16}	99.86%	Acros organics
Sodium borohydride	$NaBH_4$	99%	Sigma-Aldrich
Iodhydric acid	HI	57%	Sigma-Aldrich
Ascorbic acid	$C_6H_8O_6$	p.a.	Sigma-Aldrich
Oxalic acid	$(COOH)_2$ x $2H_2O$	99.5%	Merck
Vulcan XC-72 R	Carbon black	p.a.	

3.6. References

1. Solla-Gullón, J., Tesis Doctoral, Universidad de Alicante (2003).
2. Solla-Gullón, J.; Montiel, V.; Aldaz, A.; Clavilier, J. *J. Electroanal. Chem.* **2000**, 491, 69-77.
3. Solla-Gullón, J.; Rodes, A.; Montiel, V.; Aldaz, A.; & Clavilier, J. *J. Electroanal. Chem.* **2003**, 554-555, 273-278.
4. Solla-Gullón, J.; Montiel, V.; Aldaz, A. & Clavilier, J. *J. Electrochem. Soc.* **2003**, 150, E104-E109.
5. Vidal-Iglesias, F.J.; Solla-Gullón, J.; Montiel, V.; Feliu, J.M.; Aldaz, A. *J. Power Sources,* **2007**, 171, 448-456.
6. Arán-Ais, R.M.; Vidal-Iglesias, F. J.; Solla-Gullón, J.; Herrero, E. & Feliu, J. M. *Electroanalysis,* **2015**, 27, 945-956.
7. Krier, J.M.; Michalak, W. D.; Baker, L. R.; An, K.; Komvopoulos, K.; Somorjai, G. A. *J. Phys. Chem. C* **2012**, 116, 17540-17546.
8. Baker, L. R.; Kennedy, G.; Krier, J.M.; Van Spronsen, M.; Onorato, R.M.; Somorjai G. A. *Catal. Lett*., **2012**, 142, 1286-1294.
9. Aliaga, C.; Park, J. Y.; Yamada, Y.; Lee, H. S.; Tsung, C. K.; Yang, P.; Somorjai, G. A. *J. Phys. Chem. C.* **2009**, 113, 6150-6155.
10. Li, D.; Wang, C.; Tripkovic, D.; Sun, S.; Markovic, N. M.; Stamenkovic, V. R.; *ACS Catal.* **2012**, 2, 1358-1362.
11. Choi, S.I.; Xie, S; Shao, M.; Odell, J. H.; Lu, N.; Peng, H. C.; Protsailo L.; Guerrero S.; Park, J.; Xia, X.; Wang J.; Kim M. J. Xia, Y. *Nano Lett.* **2013**, 13, 3420-3425.
12. Mazumber, V.; Sun, S.; *J. Am. Chem. Soc.* **2009**, 131, 4588-4589.

13. Yang, S.; Park, N. Y.; Han, J. W.; Kim, C.; Lee, S.C.; Lee. H; *Chem. Comm.* **2012**, 48, 257-259.

14. Blavo, S. O.; Qayyum, E.; Baldyga, L. M.; Castillo, V. A.; Sanchez, M. D.; Warrington, K.; Barakat, M. A.; Kuhn, J. N.; *Top. Catal.* **2013**, 56, 1835-1842.

15. Vidal-Iglesias, F.J.; Solla-Gullón, J.; Herrero, E.; Montiel, V.; Aldaz, A.; Feliu, J.M. *Electrochem. Comm*. **2011**, 13, 502-505.

16. Bard, A. J.; Faulkner, L. R. "Electrochemical Methods: Fundamentals and Applications", John Wiley and Sons, New York, 2nd ed. 2000.

17. Brett, C. M. A.; Oliviera-Brett, A. M., "Electrochemistry: Principles, Methods and Applications" Oxford University Press, Oxford, 1993.

18. Gosser, D. K. "Cyclic Voltammetry: Simulation and Analysis of Reaction Mechanism" VCH Publisher, New York, 1993.

19. Hamann, C. H.; Hamnett, A.; Vielstich, W. "Electrochemistry" Wiley, 1998.

20. Solla-Gullón, J.; Vidal-Iglesias, F.J.; Herrero, E.; Feliu, J.M.; Aldaz, A. Polymer Electrolyte Fuel Cells: Science, Applications, and Challenges, Chapter 3: Electrocatalysis on Shape-Controlled Pt Nanoparticles, ed. Alejandro A. Franco, Pan Stanford Publishing Pte. Ltd 2013.

21. Solla-Gullón, J.; Rodríguez, P.; Herrero, E.; Aldaz, A.; Feliu, J. M*. Phys. Chem. Chem. Phys.* **2008**, 10, 1359-1373.

22. Markovic, N. M.; Ross, P.N., *Surf. Sci. Rep*., **2002**, 45, 117-129.

23. Wieckowski, A.; Savinova, E.; Vayenas, C. "Catalysis and electrocatalysis at nanoparticle surfaces" Marcel Dekker, New York, 2003.

24. Clavilier, J.; Orts, J.; Gómez, R.; Feliu, J.M.; Aldaz, A., On the Nature of the Charged Species Displaced by CO Adsorption from Platinum Oriented

Electrodes in Sulpuric Acid Solution. Conway, B. E.; Jerkiewicz, G., Eds. The Electrochemical Society, INC.; Pennington, NJ, 1994; Vol 94-21, pp 167-183.

25. Feliu, J.M.; Orts, J.M.; Fernández-Vega, A.; Aldaz, A.; Clavilier, J. *J. Electroanal. Chem.* **1990**, 296, 191–201.
26. Feliu, J.M.; Orts, J. M.; Gómez, R.; Aldaz, A.; Clavilier, J. *J. Electroanal. Chem*. **1994**, 372, 265-268.
27. Orts, J. M.; Gómez, R.; Feliu, J.M.; Aldaz, A.; Clavilier J., *Electrochim. Acta*, **1994**, 39, 1519-1524.
28. Mayrhofer, K. J.J.; Arenz, M.; Blizanac, B.B.; Stamenkovic, V.; P.N. Ross, P.N.; Markovic, N. M*. Electrochim. Acta*, **2005**,50, 5144-5154.
29. Koper, M. T. M.; Lai, S. C. S.; Herrero, E., Mechanisms of the oxidation of carbon monoxide and small organic molecules at metal electrodes, in: M.T.M. Koper (Ed.), Fuel Cell Catalysis, A Surface Science Approach, John Wiley & Sons, Inc, Hoboken, NJ, 2009, pp. 159–208.
30. Arán-Ais, R.M.; Vidal-Iglesias, F.J.; Farias, M.J.; Solla-Gullón, J., Montiel, V.; Herrero, E.; Feliu, J.M., J. *Electroanal Chem.* **2017**, 793, 126-136.
31. Solla-Gullón, J.; Vidal-Iglesias, F. J.; Herrero, E.; Feliu, J. M.; Aldaz, A. *Electrochem. Comm.* **2006**, 8, 189-194.
32. Woods, R. and Bard, A.J. (Ed.) Electroanalytical Chemistry, vol 9., Marcel Dekker, New York, 1976, p.l.
33. Chen, Q. S.; Solla-Gullon, J.; Sun, S. G.; Feliu, J. M. *Electrochim. Acta* **2010**, *55*, 7982.
34. Rodríguez, P.; Herrero, E.; Solla-Gullón, J.; Vidal-Iglesias, F.J.; Aldaz, A.; Feliu, J. M. *Electrochim Acta*, **2005**, 50, 3111-3121.

35. Rodríguez, P.; Herrero, E.; Solla-Gullón, J.; Vidal-Iglesias, F.J.; Aldaz, A.; Feliu, J. M. *Electrochim. Acta*, **2005**, 50, 4308-4317.

36. Clavilier, J.; Sun, G.; Armand, D.; Petit, M. *J. Electroanal. Chem*.,**1986**, 205, 267-277.

37. Clavilier, J.; Faure, R.; Guinet, G.; Durand, R. *J. Electroanal. Chem*. **1980**, 107, 211- 216.

38. Clavilier, J. "Interfacial electrochemistry. A. Wieckowski ed. Marcel Decker, New York, pp 231.

39. Clavilier, J. Durand, R.; Guinet, G.; Faure, R. *J. Electroanal. Chem*. **1981**, 127, 281-287.

40. Rodes, A.; El Achi, K.; Zmakhchari, M. A.; Clavilier, J.: *J. Electroanal. Chem*. **1990**, 284, 245-253.

41. Clavilier, J.; Armand, D.; Wu, B. L. *J Electroanal. Chem*, **1982**, 135,159-166.

42. Rodes, A. Tesis Doctoral, Universidad de Alicante, 1991.

43. Clavilier, J.; Flame-Annealing and Cleaning Technique. In Interfacial Electrochemistry, Wieckowski, A., Ed. Marcel Dekker, Inc.: New York, 1999, pp 231-248.

44. Herrero, E.; Clavilier, J.; Feliu, J. M.; Aldaz, A. *J. Electroanal. Chem.* **1996**, 410, 125-127.

45. Wang, Z. L. "Characterization of Nanophase Materials" 2000, Wiley-VCH Verlag GmbH.

46. Arán-Ais, R. M.; Dionigi, F.; Merzdorf, T.; Gocycla, M.; Heggen, M.; Dunnin-Borkowski, R. E.; Gliech, M.; Solla-Gullón, J.; Herrero, E.; Feliu, J. M.; Strasser P. *Nano Lett.* **2015**, 15, 7473-7480.

Publications

Chapter 4.

Synthesis of Pt nanoparticles in water-in-oil microemulsion: on the effect of HCl on their surface structure

Abstract: The synthesis of shape-controlled nanoparticles is currently a hot research topic. However, from an applied point of view, it still lacks of easy, cheap and scalable methodologies. In this communication we report, for the first time, the synthesis of cubic platinum nanoparticles with a very high yield using a water-in-oil microemulsion method, which, unlike others, such as the colloidal method, fulfills the previous requirements. This shape/surface structure control is determined by the concentration of HCl in the water phase of the microemulsion. The results here reported show that the optimal HCl percentage in the water phase is about 25% to obtain the highest amount of cubic nanostructures. Ammonia electro-oxidation is used as surface structure sensitive reaction to illustrate HCl surface structure effect. Moreover, in situ-electrochemical characterization has been performed to study the nanoparticle surface structure.

4.1. Introduction

The electrochemical properties of nanoparticles are mainly determined by their bulk/surface composition, size, geometry and surface structure.[1-9] This last parameter is of great importance as many electrochemical reactions of interest are well-established to be structure sensitive. That is why during the last decade there has been an increasing interest over the control of the metal nanoparticles shape,[2] with the idea that through its control, the arrangement of the atoms at the surface can be tuned and consequently modify its catalytic activity. From the pioneer work of El-Sayed et al.[7] in which cubic and tetrahedral Pt nanoparticles were prepared with H_2 in presence of sodium polyacrylate, many other methods have been developed. Thus, shape-controlled nanoparticles of different metals as well as core-shell and alloyed structures have been successfully synthesized. However, due to its unique catalytic properties, Pt has been the metal attracting the widest attention by far.[3-7] Unfortunately, these synthetic procedures always require the presence of capping agents and most of them also high temperatures or long growth times, which makes them difficult to scale up. Consequently, the development of a fast, easy, cost-effective, at room temperature and scalable procedure of synthesis of shape-controlled metal nanoparticles would be of great importance.

Water-in-oil microemulsion is, among others, a very interesting candidate because it allows the synthesis of a wide number of nanoparticles of uniform size at room temperature in a very fast and economical way. Unfortunately, the control over the shape/surface structure of the nanoparticles, in particular noble metal nanoparticles (Pt, Au, Pd, etc...), is still very limited. In this sense, in previous contributions, we have shown that by using different surface modifiers (iodine and

bromide), for Au nanoparticles [10,11], or by changing the strength of the reducing agent (hydrazine or $NaBH_4$), for Pt nanoparticles[11] both prepared in water-in-oil microemulsion, we were able to induce slight modifications on the surface structure of the nanoparticles although without significant changes in their quasi-spherical shape as observed by TEM.

In this contribution, we show for the first time that cubic Pt nanoparticles can be easily prepared using a water-in-oil microemulsion by including specific amounts of HCl in the water phase of the microemulsion. In addition, the percentage of HCl (HCl%) will control the final shape of the nanoparticles. The size and shape of such Pt nanoparticles were evaluated by TEM measurements and the surface structure characterized by using different electrochemical probes. Finally, the electrocatalytic properties of the nanoparticles were tested using ammonia electro-oxidation in alkaline medium, which has shown to be extremely sensitive to the presence of (100) surface sites. [12-16]

4.2. Methodology

Pt nanoparticles were synthesized by reducing H_2PtCl_6 with sodium borohydride using a water-in-oil (w/o) microemulsion in a similar methodology to that previously reported.[17] (Experimental details are included in the Supporting Information). This procedure allows easily clean the nanoparticles preserving the initial surface structure of the nanoparticles. Different HCl% (from 0 to 37%) were incorporated to the water phase of the microemulsion. Irrespectively of the amount of HCl, the complete reduction took place in few minutes which is indicated by the color change of the solution from light yellow to black. After complete reduction, the

nanoparticles were collected and cleaned as described previously and stored in an ultra-pure water suspension.[17]

4.3. Results

Figure 4-1 shows the voltammetric response of a collection of Pt nanoparticles prepared with different HCl% obtained in 0.5 M H_2SO_4. It is well-established that the particular voltammetric profile in the so-called hydrogen region is directly related to their specific surface structure (nature and density of the surfaces sites).[17] Thus, the voltammetric features at 0.12, 0.27, 0.37 and 0.53 V vs RHE are characteristic of the presence of (110) sites, (100) steps and terrace borders, (100) terraces or wide domains and (111) sites, respectively. The main trend observed in Figure 4-1 is the increase of (100) sites, especially the (100) terraces, when the amount of HCl increases up to 25%. The increase of this type of surface sites is counterbalanced by a decrease of the (110) and (111) sites. Interestingly, the amount of (111) sites is nearly negligible for the nanoparticles prepared with a 25% HCl. For higher HCl concentrations, the amount of (100) terraces again decreases while the other orientations concurrently increase.

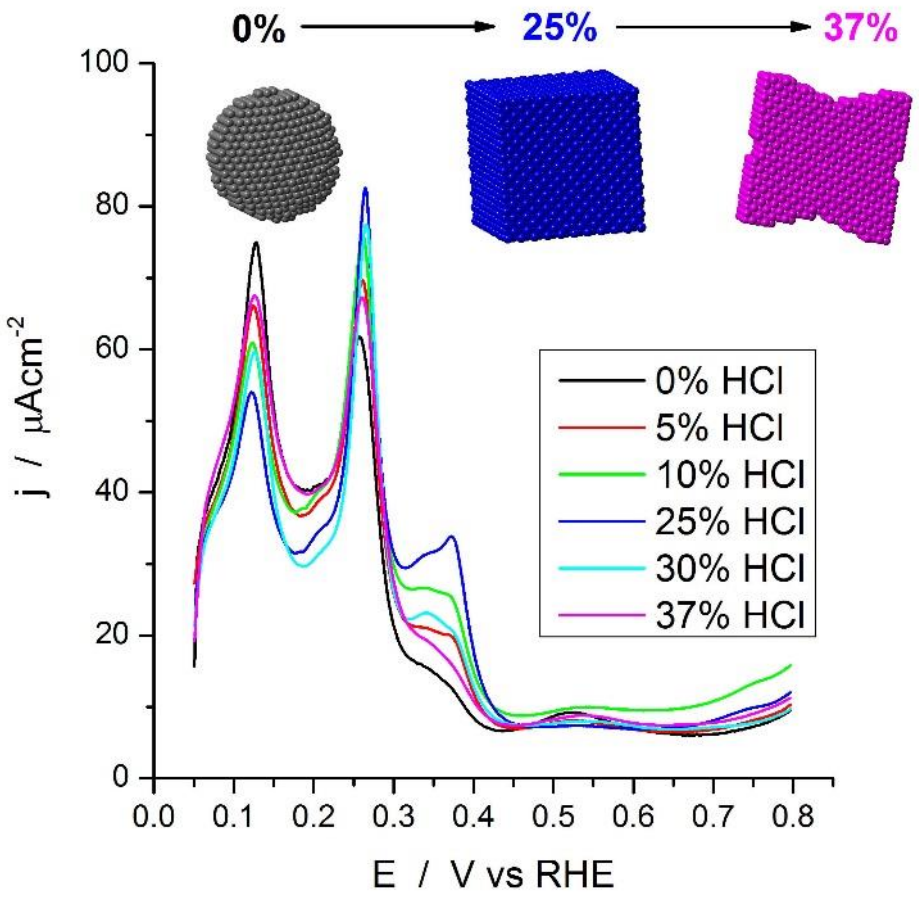

Figure 4-1. Voltammetric profile for platinum nanoparticles prepared by water-in-oil microemulsion in the presence of different amounts of HCl. Test solution: 0.5 M H_2SO_4. Scan rate: 50 mVs^{-1}.

Previous contributions pointed out that a voltammetric profile similar to that obtained with a 25% of HCl is characteristic of cubic Pt nanoparticles.[13,18] To verify this point, TEM measurements were done. Figure 4-2 shows a representative TEM image of the Pt nanoparticles obtained with a 25% HCl. The presence of Pt cubes with a particle size of about 12-14 nm is confirmed. These cubes are ideally enclosed by six {100} faces,[19] which appears clearly reflected in its voltammetric profile in the potential range between 0.3-0.45 V (Figure 4-1, dark blue line). The evolution of the

shape of the nanoparticles in the entire range of HCl% is shown in the supporting information, Figure S1. For HCl% between 0 and 25%, a clear evolution from quasi-spherical to cubic particles is observed. Liz-Marzán and coworkers recently evidenced a similar observation on Au@Ag nanoparticles. They observed, in presence of halide ions, a preferential formation of Ag {100} facets on gold, regardless of the starting gold morphology, as predicted by density functional theory (DFT) surface energy calculations.[20] In addition, the particle size increased from 3-5 nm (0% HCl) to 12-14 nm (25% HCl). However, from this % of HCl to the maximum one studied (37%), TEM images show an evolution from cubes to bone-like Pt nanoparticles. This evolution could be ascribed to the HCl etching properties[21]. In fact, some etching can already be observed for some cubes and is marked with red open circles in Figure 4-2. In terms of particle size, it remains nearly constant (about 12-14 nm) for these higher HCl percentages.

In order to quantitatively measure the amount of (100) sites at the surface of the different Pt nanoparticles, two different methods have been employed, hydrogen adsorption/desorption deconvolution[18] and germanium irreversible adsorption.[18,22] However, it is important to note the differences between these two approaches. Thus, while for the former all sites with (100) geometry, that is both step and terraces can be quantified, in the latter only those having wide enough surface domains for Ge to be adsorbed (each atom needs four platinum atoms) will be detected. Consequently, this second method will always give lower values because both (100) steps and terraces with less than 4 Pt atoms will be undetectable. Figure 4-3 shows the percentage of (100) surface sites obtained for the Pt nanoparticles prepared with different amounts of HCl.

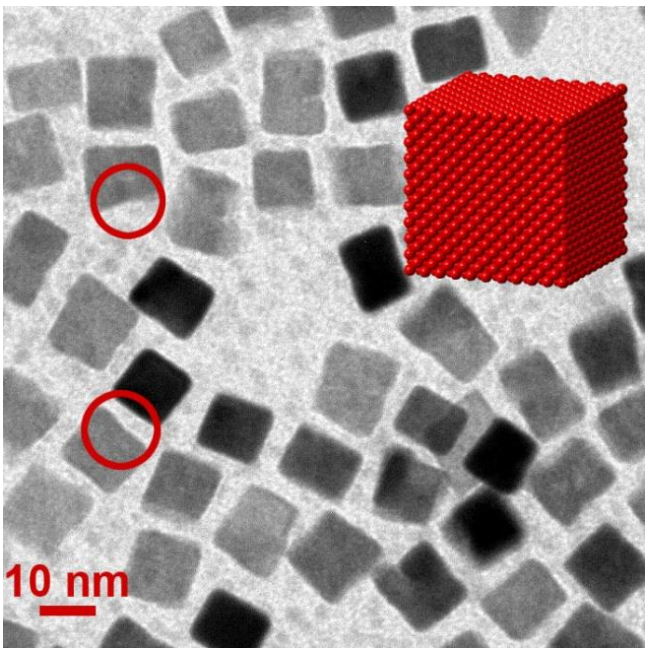

Figure 4-2. TEM image of platinum nanoparticles prepared by water-in-oil microemulsion in the presence 25% HCl in the aqueous phase. Red open circles show the etching effect of HCl.

c

Figure 4-3. Amount of (100) sites measured by Ge irreversible adsorption (solid black squares) and by hydrogen adsorption/desorption deconvolution (open red circles) for different HCl% in the aqueous phase of water-in-oil microemulsion.

As expected, the amount of (100) surface sites provided by the deconvolution analysis is always higher that that obtained with the Ge analysis. However, both analyses show a similar trend, that is, an increase of the (100) sites from 0 to 25 HCl% and then a clear decrease from 25 to 37%. In addition, it is important to point out the good agreement between these two analyses for the samples containing a higher

fraction of (100) terraces (from 15 to 25 HCl%) whereas for those samples containing a higher fraction of (100) step sites (from 0 to 15% and from 25 to 37%), important differences are found as expected from the particular requirements of the analysis. In fact, from both analyses, it is possible to estimate the (100) terraces to total (100) sites ratio on each Pt sample. Thus, for instance, whereas in the range of 15 to 37% of HCl, the total number of (100) surface sites is rather similar (47-37%), the percentage of (100) terraces is very different ranging from a 44% (25% HCl) to a 15% (37% HCl). Therefore, nearly all (100) sites for the 25% HCl nanoparticles are present as wide (100) domains, while for the 37% HCl nanoparticles (100) steps and defects are more abundant than (100) wide terraces. Finally, in terms of the highest amount of (100) surface sites, the value of (100) sites for the 25% HCl is similar (44%) to those previously reported for cubic nanoparticles synthesized with the colloidal method.[3,23]

To understand which factors are responsible for the formation of the cubic Pt nanostructures in presence of HCl, additional experiments were performed in which the independent effect of the presence of Cl^- ions or protons was evaluated. Thus, for the former, the synthesis was carried out with the addition of NaCl in the aqueous phase with a Cl^- concentration equal to that of 15% HCl. On the other hand, to study the effect of protons, another synthesis was undertaken but with a 15% $HClO_4$ in the aqueous phase (perchlorate anions are known to be weakly adsorbed on Pt surfaces). From the voltammetric response of these samples (see figure S4), it is evident that none of these experiments induced the formation of a preferential (100) surface structure. Thus, a combined effect of Cl^- ions and low pH values seems to be the responsible for the formation of the Pt cubes. In relation to the individual effects of protons and chloride in the reduction time, it was observed that increasing amounts of the latter made the reaction more sluggish but always within 10 min, while changes in

the pH did not have any significant effect in the reduction time. More work is in progress to understand the particular effect of these species on the growth rate of the nanoparticles.

To evaluate the electrocatalytic properties of the Pt nanoparticles, ammonia electro-oxidation in alkaline solution has been studied. This is an interesting reaction not only due to its possible application as ammonia-based low-temperature fuel cells but also as source of production of high-purity hydrogen, among others. Very interestingly, this anodic reaction has been shown to be extremely sensitive to the surface structure on platinum, taking place almost exclusively on (100) sites and being also sensitive to the width of the (100) terraces.[15,16] In fact, cubic Pt nanoparticles prepared using colloidal routes have already illustrated how the electrocatalytic activity can be optimized by controlling the surface structure of the catalytic material. Consequently, this reaction is an excellent candidate to test the electrocatalytic properties of the different samples. Figure 4-4A shows the voltammetric response of the collection of Pt samples towards ammonia oxidation. The results obtained clearly show that the activity for the different nanoparticles follow the same trend than that observed for the amount of (100) surface sites at the nanoparticles measured by germanium irreversible adsorption. Remarkably, a six-fold increase in the ammonia oxidation current density is observed from 0% to 25% HCl. However, it is worth noting that this reaction is also very sensitive to the width of the (100) terraces. Thus, for instance, and despite the total amount of (100) sites of the sample prepared in presence of 5% HCl is lower than that obtained with the samples prepared in the range between 30-37% of HCl. Their activities towards ammonia oxidation are rather similar in agreement with the analysis of the (100) terraces of the samples (Figure 4-3), which shows that the percentage of (100) sites for these Pt samples is similar.

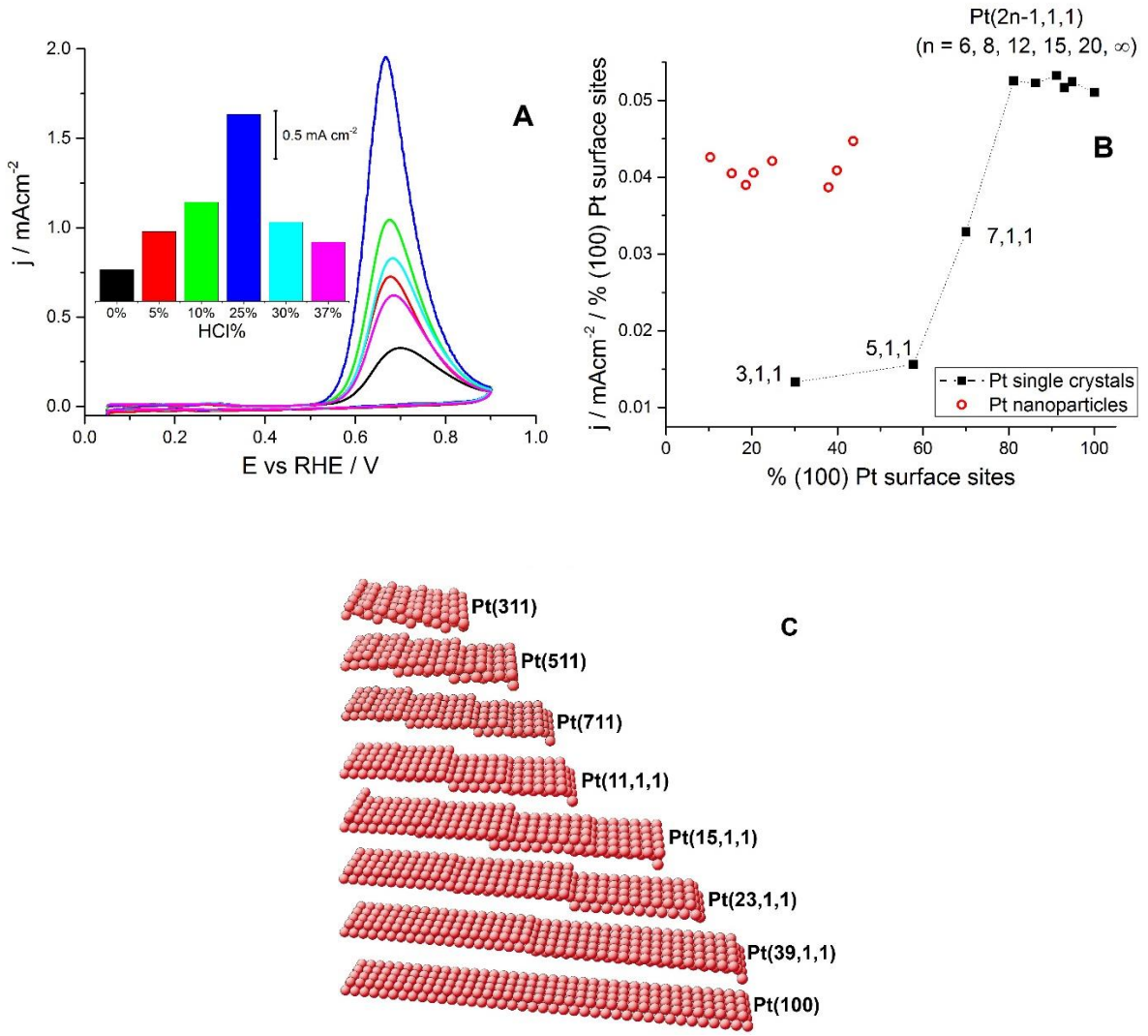

Figure 4-4. (A) Voltammetric profiles for ammonia oxidation with platinum nanoparticles prepared by water-in-oil microemulsion in the presence of different amounts of HCl. Inset shows the current density of the main peak versus the HCl%. (B) Normalized current density for Pt(2n-1,1,1) single crystals ((100) terraces with (111) steps) and platinum nanoparticles prepared with different amounts of HCl in the aqueous phase of the microemulsion. Test solution: 0.2 M NaOH + 0.1 M NH_3. Scan rate: 10 mVs^{-1}. (C) Atomic representation of stepped Pt surfaces with (100) terraces and (111) steps.

Moreover, in terms of the maximum current densities, the Pt nanoparticles prepared with 25% HCl (about 1.96 mA·cm-^{2}) show higher values than those reported for Pt nanoparticles prepared with a colloidal method using sodium polyacrylate.[12-14] Consequently, this current density is at present the highest one reported so far in the literature for ammonia oxidation at room temperature.

Finally, with the objective of analyzing in more detail the effect of the size of (100) domains present at the surface of the Pt nanoparticles, we have normalized their catalytic activity to the amount of wide (100) sites determined by Ge irreversible adsorption, shown in Figure 3 black squares. A similar rationalization was also done with Pt single crystals with stepped surfaces (Pt(2n-1,1,1) single crystals ((100) terraces with (111) steps)) (Fig. S5, Supporting Information). Both calculations are plotted and compared in Figure 4-4B. For the stepped Pt surfaces, it is clear the tremendous influence of the (100) terrace width. Larger (100) terraces are proportionally much more active than shorter terraces denoting a clear sensitivity to the long-range order of (100) surface domains. Nevertheless, it is also important to stress that this long-range order effect is particularly sensitive to the transition between 3 (Pt (511)) to 6 (Pt (11,1,1)) terrace atoms. However, for surfaces with a width of 6 or more atoms width terraces the normalized current densities are independent of the terrace width. In the case of the Pt nanoparticles, Figure 4-4B (red open cycles), we observe that the activity normalized to the (100) wide sites is nearly the same, and similar to those single crystals having terrace width of 4<n<6 atoms. This fact could be related to the presence of (100) domains with these dimensions on the nanoparticles. However, one should take into account that due to the lower percentage of (100) terraces on the nanoparticles, their maximum activity (≈ 2 mA·cm^{-2}) is lower than that expected from stepped single crystals of similar (100) terrace width (fig. S5).

4.4. Conclusions

In conclusion, this work shows a fast, easy, room temperature and scalable procedure of synthesis of cubic Pt nanoparticles based on the reduction of a Pt precursor by $NaBH_4$ in a water-in-oil microemulsion in presence of HCl. The percentage of HCl is the key point to control the shape/surface structure of the Pt nanoparticles. TEM and cyclic voltammetry measurements confirm the presence of Pt cubes with a preferential (100) surface structure. Different electrochemical probes have been used to quantify the total amount of (100) surface sites as well as to quantify the amount of (100) terraces present at the nanoparticles. The optimal amount of HCl was found to be between 15-25%, after which the samples show a decrease in the number of (100) wide domains as well as a bone-like shape. The electrocatalytic activity of the samples was tested towards ammonia oxidation. The activity reported with the 25% HCl was about 6-times higher than that obtained with the 0% HCl. This activity is currently the largest quantified current density so far in the literature. More work is currently in progress to extend this methodology to prepare other shape-controlled metal nanoparticles such as Pd or Rh as well as to obtain shape-controlled Pt alloys. In particular, the use of shape-controlled Pt alloys for the oxygen reduction reaction is being the subject of an intensive research in the last years.[24-26]

4.5. Associated content

4.5.1. Supporting Information

Experimental details describing: NPs syntheses, TEM analyses, area normalization, effect of Cl^- and pH on the shape of the Pt nanoparticles and ammonia oxidation on several Pt single crystals. This material is available in the *Annex III* of the Annexes section of the present Doctoral Thesis.

4.6. References

1. Long, N. V.; Chien, N. D.; Hayakawa, T.; Hirata, H.; Lakshminarayana, G.; Nogami, M. *Nanotechnology* **2010**, *21*, 1-16.
2. Tao, A. R.; Habas, S.; Yang, P. *Small* **2008**, *4*, 310-325.
3. Vidal-Iglesias, F. J.; Aran-Ais, R. M.; Solla-Gullon, J.; Herrero, E.; Feliu, J. M. *ACS Catal.* **2012**, *2*, 901-910.
4. Zhou, Z. Y.; Shang, S. J.; Tian, N.; Wu, B. H.; Zheng, N. F.; Xu, B. B.; Chen, C.; Wang, H. H.; Xiang, D. M.; Sun, S. G. *Electrochem. Commun.* **2012**, *22*, 61-64.
5. Narayanan, R.; El-Sayed, M. A. *Nano Lett.* **2004**, *4*, 1343-1348.
6. Narayanan, R.; El-Sayed, M. A. *J. Phys. Chem. B* **2004**, *108*, 5726-5733.
7. Ahmadi, T. S.; Wang, Z. L.; Green, T. C.; Henglein, A.; El-Sayed, M. A. *Science* **1996**, *272*, 1924-1925.
8. Tian, N.; Zhou, Z.-Y.; Sun, S.-G.; Ding, Y.; Wang, Z. L. *Science* **2007**, *316*, 732-735.
9. Xiao, J.; Liu, S.; Tian, N.; Zhou, Z.-Y.; Liu, H.-X.; Xu, B.-B.; Sun, S.-G. *J. Am. Chem. Soc.* **2013**, *135*, 18754-18757.
10. Mihaly, M.; Fleancu, M. C.; Olteanu, N. L.; Bojin, D.; Meghea, A.; Enachescu, M. *C. R. Chim.* **2012**, *15*, 1012-1021.
11. Hernández, J.; Solla-Gullón, J.; Herrero, E. *J. Electroanal. Chem.* **2004**, *574*, 185-196.
12. Vidal-Iglesias, F. J.; Solla-Gullón, J.; Montiel, V.; Feliu, J. M.; Aldaz, A. *J. Power Sources* **2007**, *171*, 448-456.
13. Vidal-Iglesias, F. J.; Solla-Gullón, J.; Rodríguez, P.; Herrero, E.; Montiel, V.; Feliu, J. M.; Aldaz, A. *Electrochem. Commun.* **2004**, *6*, 1080-1084.

14. Solla-Gullón, J.; Vidal-Iglesias, F. J.; Rodríguez, P.; Herrero, E.; Feliu, J. M.; Clavilier, J.; Aldaz, A. *J. Phys. Chem. B* **2004**, *108*, 13573-13575.

15. Vidal-Iglesias, F. J.; Garcia-Araez, N.; Montiel, V.; Feliu, J. M.; Aldaz, A. *Electrochem. Commun.* **2003**, *5*, 22-26.

16. Vidal-Iglesias, F. J.; Solla-Gullón, J.; Montiel, V.; Feliu, J. M.; Aldaz, A. *J. Phys. Chem. B* **2005**, *109*, 12914-12919.

17. Solla-Gullón, J.; Vidal-Iglesias, F. J.; López-Cudero, A.; Garnier, E.; Feliu, J. M.; Aldaz, A. *Phys. Chem. Chem. Phys.* **2008**, *10*, 3689-3698.

18. Solla-Gullón, J.; Rodríguez, P.; Herrero, E.; Aldaz, A.; Feliu, J. M. *Phys. Chem. Chem. Phys.* **2008**, *10*, 1359-1373.

19. Zhou, Z.-Y.; Tian, N.; Huang, Z.-Z.; Chen, D.-J.; Sun, S.-G. *Faraday Discuss.* **2009**, *140*, 81-92.

20. Gómez-Graña, S.; Goris, B.; Altantzis, T.; Fernández-López, C.; Carbó-Argibay, E.; Guerrero-Martínez, A.; Almora-Barrios, N.; López, N.; Pastoriza-Santos, I.; Pérez-Juste, J.; Bals, S.; Van Tendeloo, G.; Liz-Marzán, L. M. *The Journal of Physical Chemistry Letters* **2013**, *4*, 2209-2216.

21. Liu, M.; Zheng, Y.; Zhang, L.; Guo, L.; Xia, Y. *J. Am. Chem. Soc.* **2013**, *135*, 11752.

22. Rodríguez, P.; Herrero, E.; Solla-Gullón, J.; Vidal-Iglesias, F. J.; Aldaz, A.; Feliu, J. M. *Electrochimica Acta* **2005**, *50*, 4308-4317.

23. Vidal-Iglesias, F. J.; Solla-Gullon, J.; Herrero, E.; Aldaz, A.; Feliu, J. M. *Angew. Chem. Int. Edit.* **2010**, *49*, 6998-7001.

24. Zhang, J.; Yang, H.; Fang, J.; Zou, S. *Nano Lett.* **2010**, *10*, 638-644.

25. Cui, C.; Gan, L.; Li, H. H.; Yu, S. H.; Heggen, M.; Strasser, P. *Nano Lett.* **2012**, *12*, 5885-5889.

26. Choi, S. I.; Xie, S.; Shao, M.; Odell, J. H.; Lu, N.; Peng, H. C.; Protsailo, L.; Guerrero, S.; Park, J.; Xia, X.; Wang, J.; Kim, M. J.; Xia, Y. *Nano Lett.* **2013**, *13*, 3420-3425.

Chapter 5.

Synthesis and electrocatalytic properties of H_2SO_4-induced (100) Pt nanoparticles prepared in water-in-oil microemulsion

Abstract: The increasing number of applications for shape-controlled metal nanoparticles leads to the need of easy, cheap and scalable methodologies. In this communication we report, the synthesis of (100) preferentially oriented platinum (Pt) nanoparticles with 9 nm particle size using a water-in-oil microemulsion method. The specific surface structure of the nanoparticles is induced by the presence of H_2SO_4 in the water phase of the microemulsion. Interestingly, the results here reported will show how increasing amounts of H_2SO_4 lead to the formation of Pt nanoparticles containing a higher amount of (100) sites on their surface. This preferential surface orientation has been confirmed electrochemically by using the so-called hydrogen adsorption/desorption process. In addition, TEM measurements have confirmed the presence of cubic-like Pt nanoparticles. Finally, the electrocatalytic properties of the Pt nanoparticles have been evaluated towards ammonia and CO electro-oxidations as (100) structure sensitive reactions.

5.1. Introduction

Several methodologies for shape control of metal nanoparticles have been developed in the past decade with the main objective of controlling the specific arrangements of the atoms at their surface, that is, their surface structure.[1-4] In this way, as widely demonstrated with metal single crystals as model electrodes, the catalytic properties of the metal nanostructures can be tuned and optimised for a particular reaction. Among others, and due to its unique catalytic properties, Pt nanoparticles have been the focus of numerous studies from which their remarkable surface structure sensitivity has been illustrated and discussed for several reactions of interest.[1-5]

On the other hand, from a more applied point of view, it would be desirable to have a simple, fast and economically viable methodology for the preparation of such shape-controlled metal nanoparticles to be then scalable for large scale applications. However, most of the developed synthetic routes do not fulfil with these requirements and consequently, the scalability still remains a challenge. In this regard, in a very recent publication, we have extended the use of water-in-oil microemulsions, traditionally employed for the preparation of metal nanoparticles with controlled atomic composition and size, for the preparation of shape-controlled Pt nanoparticles. In particular, we have reported that the addition of determined amounts of HCl in the water phase of the microemulsion led to the formation of Pt nanoparticles with a bell-shaped preferential (100) surface structure with a maximum of the (100) character at about 25% of HCl.[6] This approach opens new possibilities in terms of scalability because the handling of the water-in-oil microemulsions is easy, fast, economic and frequently performed at room temperature. In this communication, we will show that

H_2SO_4 can be also used as effective (100) surface modifier during the preparation of Pt nanoparticles in microemulsion (see experimental section for details). The resulting Pt nanoparticles will be electrochemically characterized and their electrocatalytic properties evaluated towards carbon monoxide and ammonia electro-oxidation as (100) structure sensitive reactions.

5.2. Results and Discussion

Figure 5-1 shows the positive-going sweep voltammetric profiles for the nanoparticles prepared in the absence and presence of increasing amounts of H_2SO_4 (6.25%, 12.5% and 25%) in 0.5 M H_2SO_4. These voltammetric profiles show the hydrogen and anion adsorption/desorption region, which is well established to reveal the actual nanoparticles' surface orientation at an atomic level.[7] Very briefly, in a typical voltammogram, there are four main peaks located at 0.12, 0.27, 0.37 and 0.53 V vs RHE, which are related to the presence of (110) sites, (100) steps and terrace borders, (100) terraces or wide domains and (111) terraces, respectively. As it is clearly observed, when increasing the amount of H_2SO_4, the features assigned to the (100) surface sites, both steps (0.27 V) and terraces (0.37 V), increase. On the contrary, the contribution related to the presence of (110) sites on the surface of the Pt nanoparticles diminishes thus counterbalancing the (100) contributions. This counterbalance between the (110) and (100) sites with the addition of H_2SO_4 can be easily followed by analysing the current density ratio of the signal at 0.12 and 0.27 V, respectively, as a function of the % of H_2SO_4. The evolution of both contributions leads to the conclusion that the higher the amount of H_2SO_4, the higher the amount of (100) sites is. Unfortunately, the maximum amount of H_2SO_4 used had to be limited to 25%

because of instability problems of the water-in-oil microemulsion for higher concentrations. Finally, a similar trend, i.e. decrease for increasing amounts of H_2SO_4, is also observed for the (111)-related peak, although this signal is less visible due to the low (111) character of these Pt nanoparticles.

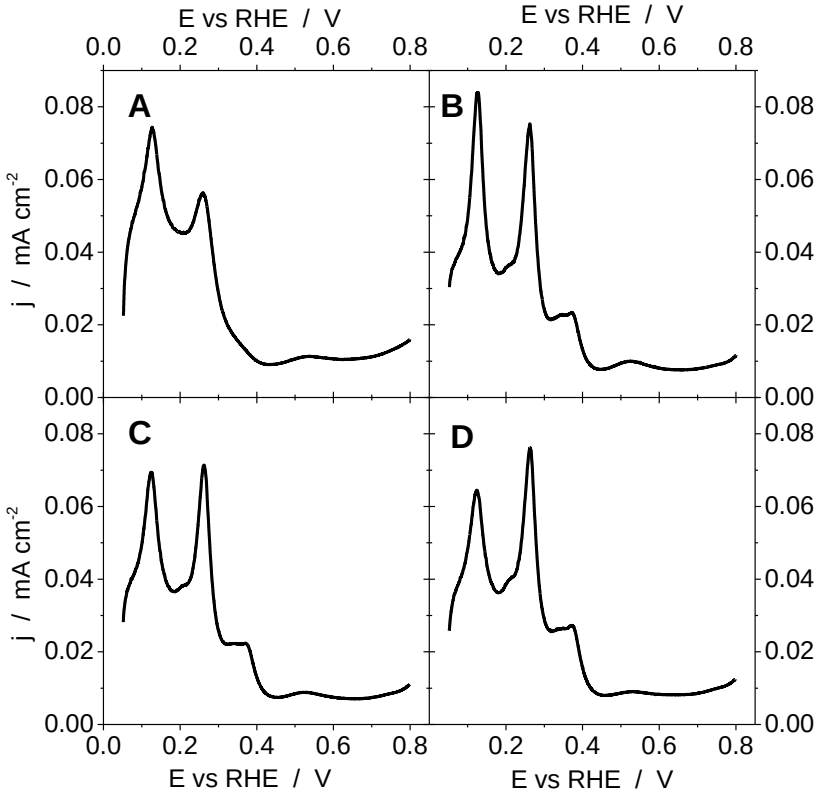

Figure 5-1. Voltammetric profiles for Pt nanoparticles prepared by water-in-oil microemulsion in the absence (A) and presence of different amounts of H_2SO_4 (6.25% (B), 12.5% (C) and 25% (D)). Test solution: 0.5 M H_2SO_4. Scan rate: 50 mVs^{-1}.

The voltammetric profiles reported here as a consequence of the presence of H_2SO_4 in the synthesis step are qualitatively similar to those obtained with Pt nanoparticles prepared in similar water-in-oil microemulsions but in the presence of HCl[6] and with Pt nanoparticles prepared with different capping materials (sodium

polyacrylate (NaPa),[8-10] tetradecyltrimethylammonium bromide (TTAB),[11-13] poly(vinylpyrrolidone) (PVP)[14, 15] or oleic acid/oleylamine[15]) by means of various colloidal routes, in all of which cubic Pt nanoparticles were synthesised. In this regard, it is important to recall that, by simple analogy with the unit stereographic triangle of a fcc metal, a stereographic triangle with shaped fcc metal nanoparticles can be made in which the three apexes represent the coordinates of polyhedral nanocrystals bounded by basal facets (a cube, octahedron and rhombic dodecahedron enclosed by (100), (111) and (110) faces, respectively).[16-18] Thus, a preferential (100) surface structure is the expected orientation from cubic Pt nanoparticles. Figure 5-2 shows representative TEM images of the nanoparticles prepared in the presence of different amounts of H_2SO_4. These TEM images were obtained by placing a drop of a diluted water suspension of the clean nanoparticles onto a Formvar-covered copper grid to avoid a serious damage of the carbon film by the H_2SO_4. However, this resulted in an important agglomeration of the samples. In any case, as shown in figure 5-2, nanoparticles tend to have a cubic-like shape, especially those prepared with the highest H_2SO_4 percentage (Figure 5-2C and 5-2D). The particle size is quite similar for the three different amounts of H_2SO_4 (9.2 ± 1.8, 8.4 ± 1.8 and 9.0 ± 1.7 nm for the 6.25, 12.5 and 25% H_2SO_4, respectively). Interestingly, this particle size is smaller than those prepared in a similar microemulsion but in the presence of HCl where the particle size of the Pt nanoparticles with the highest amount of (100) sites was found to be about 13 nm.[6] This fact is very relevant from an applied point of view where the electrocatalytic activity is frequently expressed in terms of mass activity ($mA \cdot mg_{Pt}$). Thus, in a cubic Pt nanoparticle model, a 4 nm particle size decrease represents a 66% decrease in Pt mass which remarkably reduces the cost of the process. The Pt nanoparticles prepared in microemulsion in the absence of H_2SO_4 have been widely

studied in some of our previous contributions and are characterized by a particle size of about 5 nm and a polyoriented surface structure[7,19] as illustrated in figure 5-1A.

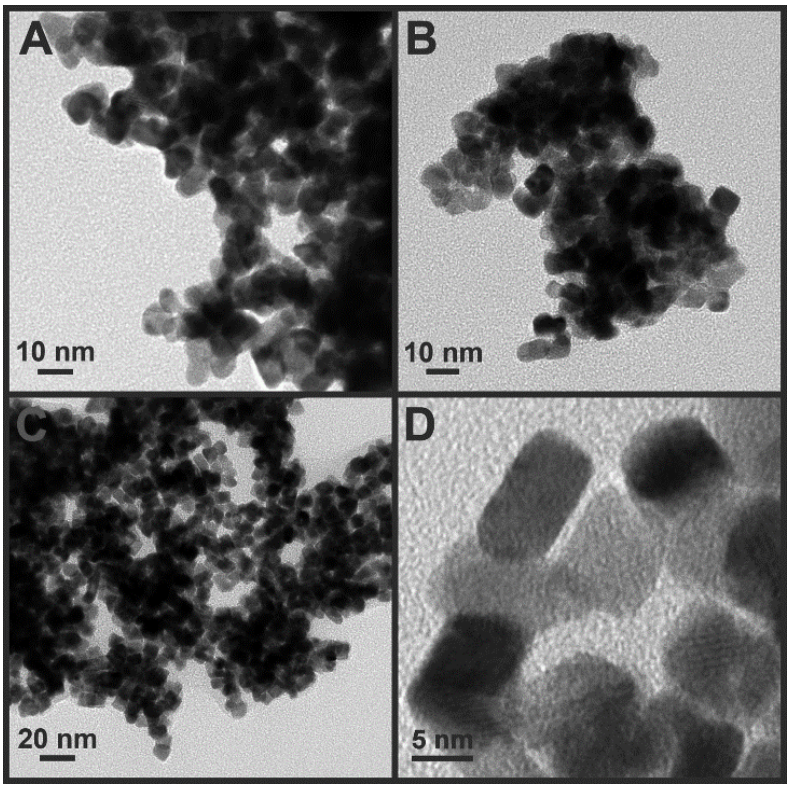

Figure 5-2. TEM image of platinum nanoparticles prepared by water-in-oil microemulsion in the presence of 6.25 (A), 12.5 (B) and 25% (C and D) H_2SO_4 in the aqueous phase.

Furthermore, to quantitatively estimate of the amount of (100) sites at the surface of the different Pt nanoparticles, the voltammetric profiles reported in figure 1 were subjected to a deconvolution process following a similar approach to that reported in previous contributions.[6,7] The results obtained are shown in figure 5-3 (solid squares). This analysis allows us to determine the total fraction of (100) surface

sites, that is, both step and terrace contributions, to be properly estimated. Thus, as expected from the voltammetric responses, the total amount of (100) surface sites clearly increases and reaches a maximum value close to a 50% of the surface. However, from a fundamental point of view, it is of great importance to discriminate between (100) surface steps and terraces. Previous knowledge from Pt stepped surfaces evidenced that the electrochemical reactivity on steps and terraces can be markedly different.[21-23] In previous contributions, we reported that the adsorption-desorption of Ge of Pt surfaces, both model and nanoparticulated electrodes, can be used to determine the amount of (100) terrace domains with a width $\geq$ 4 Pt atoms (each Ge atom requires four platinum atoms to be adsorbed).[7, 24, 25] Figure 5-3 (open circles) shows the percentage of (100) surface domains obtained for the Pt nanoparticles prepared with different amounts of H_2SO_4. A simple inspection of the results obtained with the different approaches allows us estimating the (100) terraces to total (100) sites ratio on each Pt sample which ranges from a 50% to a maximum value of 65% for those Pt nanoparticles prepared in the presence of a 25% of H_2SO_4.

Finally, the electrocatalytic properties of the Pt nanoparticles were evaluated using two different (100) structure sensitive electrochemical reactions: ammonia electro-oxidation on alkaline solution and CO stripping in acidic solution. Ammonia electro-oxidation is well-known to be extremely sensitive to the Pt surface structure, taking place almost exclusively on (100) sites and in particular on (100) two-dimensional domains.[26] This surface structure sensitivity has been illustrated not only on model Pt single crystal surfaces, both with stepped and basal orientations, but also in an important number of (100) oriented Pt nanostructures prepared by different methodologies. [6,8,27-30] In all cases, the use of (100) oriented Pt nanoparticles resulted

in enhanced electrocatalytic activities towards ammonia oxidation in comparison with polyoriented Pt nanoparticles.

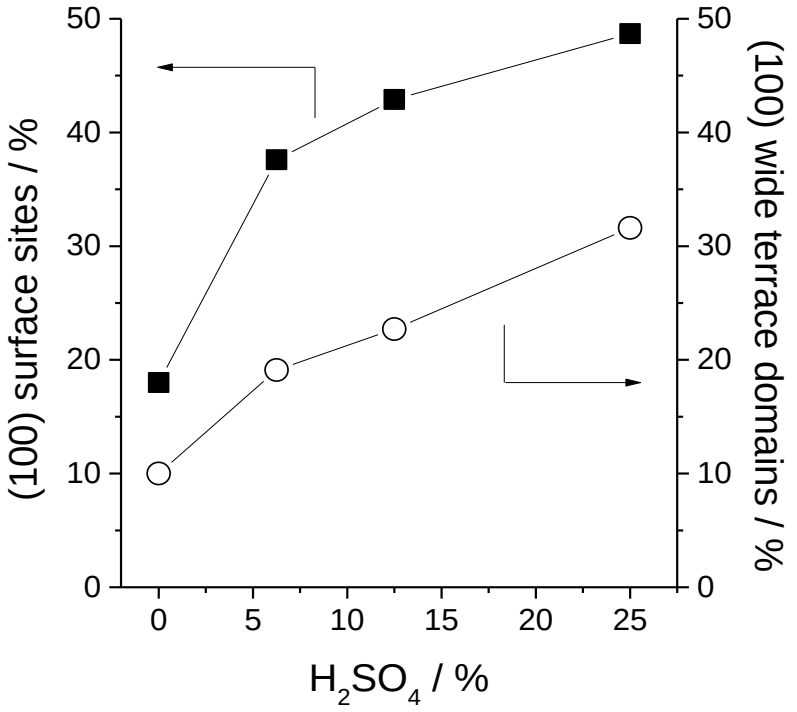

Figure 5-3. Amount of (100) sites measured by hydrogen adsorption/desorption deconvolution (solid squares) and by Ge irreversible adsorption (open circles) for different H_2SO_4% in the microemulsion.

Figure 5-4A shows the electrocatalytic activity toward ammonia oxidation of the nanoparticles prepared in the absence and presence of 6.25, 12.5 and 25% H_2SO_4 in the water phase of the microemulsion. In full agreement with the results shown in figures 5-1 and 5-3, those Pt nanoparticles containing a higher fraction of (100) surface sites display the best catalytic activity. This maximum activity is more than 3-times higher than that obtained with the polyoriented Pt nanoparticles. Interestingly, as evidenced in figures 5-4B and 5-4C, the ammonia oxidation activity (peak current density) is in excellent correlation with the amount of (100) terraces estimated from Ge analysis while this correlation is not so good if the total amount of (100) surface sites is estimated from the deconvolution analysis, in which all (100) surface sites are taken into account. This experimental feature again points out the extremely sensitivity of the ammonia oxidation reaction to the surface domains with a (100) symmetry.

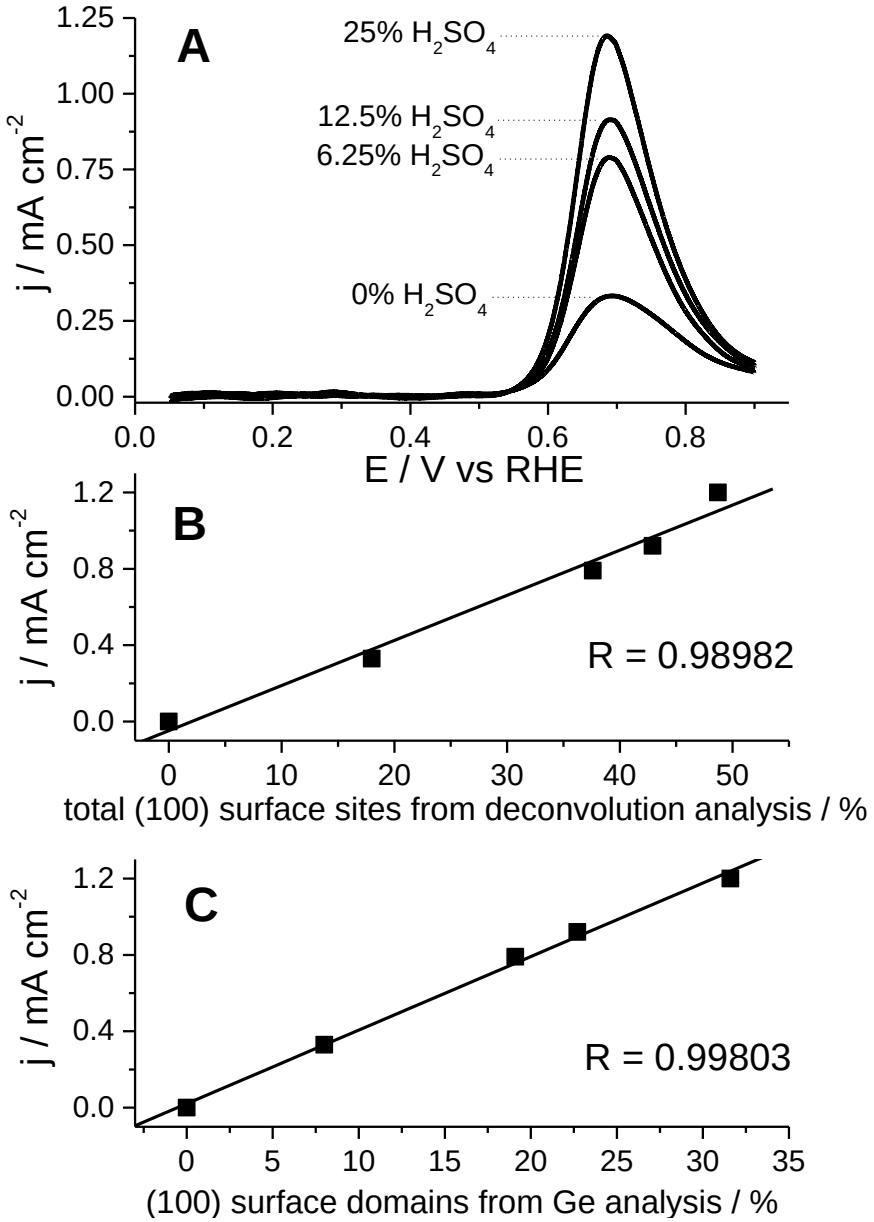

Figure 5-4. (A) Voltammetric profiles for ammonia oxidation with platinum nanoparticles prepared by water-in-oil microemulsion in the absence and presence of different amounts of H_2SO_4. Test solution: 0.2 M NaOH + 0.1 M NH_3. Scan rate: 10 $mV \cdot s^{-1}$. Linear fitting between the peak current density and (B) total amount of (100) surface sites and (C) amount of (100) surface domains.

Irreversible CO monolayer oxidation, also called CO stripping, is one of the most studied reactions in Electrocatalysis, not only because CO is a common poisoning intermediate in most of the C1 and C2 molecule organic oxidations, but also because it has been widely used as a surface probe molecule in fundamental studies.[31-34] CO monolayer oxidation is also known to be structure sensitive on Pt surfaces but with a minor structural sensitivity than ammonia electro-oxidation.[22, 34, 35] In fact, in case of Pt nanoparticles, all surface sites contribute to the reaction although the CO oxidation peak coming from the (100) terraces is relatively well-separated from the others and appears at a higher potential value.[11, 36, 37] Figure 5-5 shows the CO stripping voltammograms obtained with the different Pt nanoparticles. The response of the polyoriented Pt nanoparticles, dotted line, shows a single and broad oxidation peak centered at 0.72 V, while those prepared in the presence of H_2SO_4 show two different peaks located at 0.70 and 0.75 V. From previous contributions with shaped Pt nanoparticles, it was established that the second of these two peaks is ascribed to the presence of (100) surface domains.[11, 37] Thus, as figure 5-5 shows, the increasing amount of (100) surface domains sites with the amount of H_2SO_4 results in a clear intensification of this second contribution in relation to the first one.

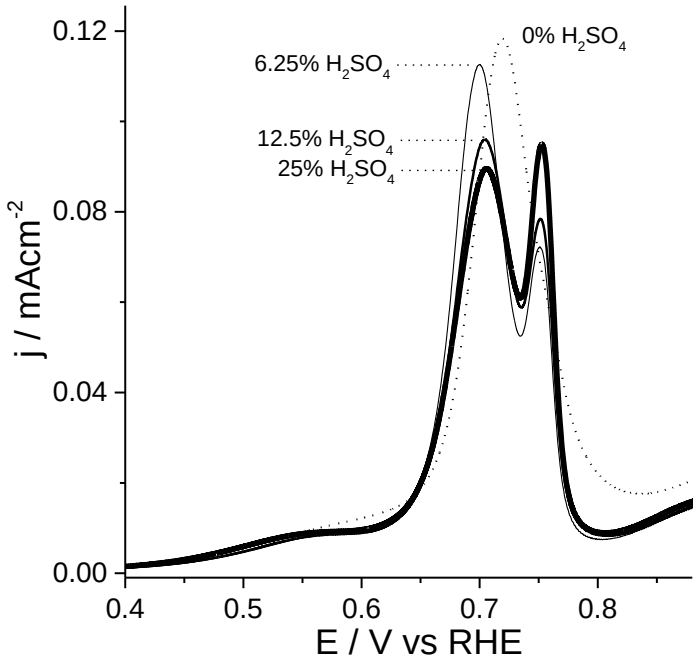

Figure 5-5. CO monolayer voltammograms obtained with platinum nanoparticles prepared in water-in-oil microemulsion in the absence (dotted line) and presence (solid lines) of different amounts of H_2SO_4. Test solution: 0.5 M H_2SO_4. Scan rate: 20 mVs^{-1}.

5.3. Conclusion

In conclusion, this communication shows a simple, fast, economical and scalable route for the synthesis of Pt nanoparticles with a preferential (100) surface structure and a particle size about 9 nm. The methodology is based on the chemical reduction of a platinum precursor by $NaBH_4$ in a water-in-oil microemulsion in the presence of H_2SO_4 in the water phase of the microemulsion. It has been found that

the (100) character of the samples increases with the amount of H_2SO_4. The maximum amount of H_2SO_4 that can be used without altering the stability of the microemulsion is 25%. The resulting Pt nanoparticles approximately contain a 50% of (100) surface sites, 35% of which are wide surface domains with width $\geq$ 4 Pt atoms. The preferential surface structure of the different nanoparticles has been electrochemically characterized by means of some structure sensitive reactions such as hydrogen and anion adsorption/desorption process and Ge adsorption desorption. Finally, the electrocatalytic properties of the samples have been evaluated towards ammonia and carbon monoxide electro-oxidations.

5.4. Experimental remarks

Pt nanoparticles were synthesized by reducing H_2PtCl_6 with sodium borohydride ($NaBH_4$) using a water-in-oil (w/o) microemulsion of water (3%)/polyethylene glycol dodecyl ether (BRIJ®30) (16.5%)/n-heptane (80.5%) as previously reported.[19] Values in brackets represent the volume percentage of each compound. The concentration of the H_2PtCl_6 solutions was always 0.1 M although, to evaluate the effect of the presence of H_2SO_4, these were prepared using aqueous solutions containing a certain percentage of this acid. The percentages studied were 0% (absence of H_2SO_4), 6.25%, 12.5% and 25% H_2SO_4). These H_2SO_4 percentages are expressed in wt/wt ratio. For higher concentrations of the acid, the microemulsion system became unstable. The reduction of platinum was achieved by adding solid $NaBH_4$ to the water-in-oil microemulsion solution. The amount of $NaBH_4$ added was that to have a 1 M concentration solution in the water phase ($NaBH_4$/Pt molar ratio of 10). After complete reduction, which takes place in few minutes, acetone was added

to the solution to cause phase separation. Afterwards, the Pt nanoparticles were cleaned with successive acetone, acetone-water mixtures and water washes to finally achieve a water suspension with clean nanoparticles. Finally, the nanoparticles were stored in ultrapure water as a suspension.

The electrochemical experiments were performed in a three-electrode electrochemical cell using a VMP3 multichannel potentiostat (BioLogic) working with a NStat configuration (1 counter electrode, 1 reference electrode and N working electrodes working simultaneously). The counter electrode was a platinum wire. Potentials were measured against a reversible hydrogen electrode (RHE) connected to the cell through a Luggin capillary. Before each experiment, the gold collector electrodes used to deposit the Pt NPs over were mechanically polished with alumina and rinsed with ultra-pure water to eliminate NPs from previous experiments. The active surface area of the Pt NPs was determined by the charge involved in the so-called hydrogen UPD region (between 0.06 V and 0.6 V) after the subtraction of the double layer charging contribution and assuming the calibration ratio (UPD charge) / (Pt surface area) as 0.23 $mC \cdot cm^{-2}$.[38]

5.5. References

1. Solla-Gullon J.; Vidal-Iglesias, F.J.; J. M. Feliu, J.M. *Annu. Rep. Prog. Chem., Sect. C*. **2011**, 107, 263-297.
2. Burda, C.; Chen, X.; Narayanan, R.; El-Sayed, M.A. *Chem. Rev.* **2005**, 105, 1025-1102.
3. Xia, Y.; Xiong, Y.; B. Lim, B.; S. E. Skrabalak S.E. *Angew. Chem. Int. Edit.* **2009**, 48, 60-103.
4. Tao, A.R.; S. Habas, S.; P. Yang P. *Small*. **2008**, 4, 310-325.
5. Koper, M. T. M. *Nanoscale*. **2011**, 3, 2054-2073.
6. Martínez-Rodríguez, R.A.; Vidal-Iglesias, F.J.; Solla-Gullon, J.; Cabrera, C.R.; Feliu, J.M. *J. Am. Chem. Soc.* **2014**.
7. Solla-Gullón, J.; Rodríguez, P.; Herrero, E.; Aldaz, A.; Feliu, J.M. *Phys. Chem. Chem. Phys.* **2008**, 10, 1359-1373.
8. Vidal-Iglesias, F.J.; Solla-Gullón J.;, Rodríguez, P.; Herrero, E.; Montiel, V.; Feliu, J.M.; Aldaz A. *Electrochem. Commun.* **2004**, 6, 1080-1084.
9. Vidal-Iglesias, F.J.; Aran-Ais, R.M.; Solla-Gullon, J.; Herrero, E.; Feliu, J.M. *ACS Catal.* **2012**, 2, 901-910.
10. Sanchez-Sanchez, C.M.; Solla-Gullon, J.; Vidal-Iglesias, F.J.; Aldaz A.; , Montiel, V.; Herrero, E. *J. Am. Chem. Soc.* **2010**, 132, 5622-5624.
11. Urchaga, P.; Baranton, S.; Coutanceau, C.; Jerkiewicz, G. *Langmuir*. **2012**, 28, 3658-3663.
12. Urchaga, P.; Baranton, S.; Napporn, T.W.; Coutanceau, C. *Electrocatalysis*. **2010**, 1-4.
13. Coutanceau, C.; Urchaga, P.; Brimaud, S.; Baranton, S. *Electrocatalysis*. **2012**, 3, 75-87.

14. Monzó, J.; Koper, M. T. M.; Rodriguez, P. *ChemPhysChem*. **2012**, 13, 709-715.
15. Yang, H.; Tang, Y.; Zou, S. *Electrochem. Commun.* **2014**, 38, 134-137.
16. Zhou, Z.Y.; Tian, N.; Huang, Z.Z.; Chen, D.J.; Sun, S. G. *Faraday Discuss.* **2009**, 140, 81-92.
17. Tian, N.; Zhou, Z.Y; Sun S.G. *J. Phys. Chem. C*. **2008**, 112, 19801-19817.
18. Proussevitch, A.A.; Sahagian, D.L. *Computers & Geosciences*. **2001**, 27, 441-454.
19. Solla-Gullón, J.; Vidal-Iglesias,F.J.; López-Cudero, A.; Garnier, E.; Feliu, J.M.; Aldaz, A. *Phys. Chem. Chem. Phys.* **2008**, 10, 3689-3698.
20. Kuzume, A.; Herrero, E.; Feliu, J.M. *J. Electroanal. Chem.* **2007**, 599, 333-343.
21. Lebedeva, N.P.; Rodes, A.; Feliu, J.M. Koper, M.T.M.; van Santen R.A. *J. Phys. Chem. B*. **2002**, 106, 9863-9872.
22. Lebedeva, N.P.; Koper, M.T.M.; Herrero, E.; J. M. Feliu, J.M.; van Santen, R.A. *J. Electroanal. Chem.* **2000**, 487, 37-44.
23. Vidal-Iglesias, F.J.; Solla-Gullón, J.; Montiel, V.; Feliu, J.M.; Aldaz, A.; *J. Phys. Chem. B*. **2005**, 109, 12914-12919.
24. Rodríguez, P.; Herrero, E.; Solla-Gullón, J.; Vidal-Iglesias, F.J.; Aldaz, A.; Feliu, J.M. *Electrochim. Acta*. **2005**, 50, 3111-3121.
25. Rodríguez, P.; Herrero, E.; Solla-Gullón, J.; Vidal-Iglesias, F.J.; Aldaz, A.; Feliu, J.M. *Electrochim. Acta*. **2005**, 50, 4308-4317.
26. Vidal-Iglesias, F.J.; Garcia-Araez, N.; Montiel, V.; Feliu, J.M.; Aldaz A. *Electrochem. Commun.* **2003**, 5, 22-26.
27. Bertin, E.; Garbarino, S.; Guay, D.; Solla-Gullón, J.; Vidal-Iglesias, F.J.; Feliu, J.M. *J. Power Sources*. **2013**, 225, 323-329.

28. Le Vot, S.; Roué, L.; Bélanger, D. *J. Electroanal. Chem.* **2013**, 691, 18-27.
29. Rosca, V.; Duca, M.; de Groot, M.T.; Koper, M. T. M. *Chem. Rev.* **2009**, 109, 2209-2244.
30. Solla-Gullón, J.; Vidal-Iglesias, F.J.; Rodríguez, P.; Herrero, E.; Feliu, J.M. Clavilier, J.; Aldaz, A. *J. Phys. Chem. B*. **2004**, 108, 13573-13575.
31. Maillard, F.; Savinova, E.R.; Stimming, U. *J. Electroanal. Chem.* **2007**, 599, 221-232.
32. Wieckowski, A.; Savinova, E.R.; Vayenas, C.G. Catalysis and electrocatalysis at nanoparticle surfaces, CRC Press, New York, **2003**.
33. Markovic, N.M.; Ross, P.N. *Surf. Sci. Rep.* **2002**, 45, 117-229.
34. Koper, M.T.M.; Lai, S. C. S. ; Herrero, E. in *Mechanisms of the Oxidation of Carbon Monoxide and Small Organic Molecules at Metal Electrodes, Vol.* (Ed. M. T. M. Koper), John Wiley & Sons, Inc, Hoboken, NJ, **2009**, pp.159-208.
35. Vidal-Iglesias, F.J. ; Solla-Gullón, J. ; Campina, J.M.; Herrero, E. ; Aldaz, A.; Feliu, J.M. *Electrochim. Acta*. **2009**, 54, 4459-4466.
36. Brimaud, S.; Pronier, S.; Coutanceau, C.; Léger, J. M. *Electrochem. Commun.* **2008**, 10, 1703-1707.
37. Solla-Gullón, J.; Vidal-Iglesias, F.J.; Herrero, E.; Feliu, J.M.; Aldaz, A. *Electrochem. Commun.* **2006**, 8, 189-194.
38. Chen, Q.S.; Solla-Gullón, J.; Sun, S.G.; Feliu, J.M. *Electrochim. Acta*. **2010**, 55, 7982-7994.

Chapter 6.

Electrochemical characterization of platinum nanoparticles prepared in water-in-oil microemulsion in the presence of different modifiers and metal precursors

Abstract: In this manuscript, Pt nanoparticles have been synthesized using water-in-oil microemulsions in the presence of different modifiers and metal precursors to obtain preferentially oriented nanoparticles. Preferentially oriented cubic nanoparticles, enriched in (100) sites, were mainly prepared for specific concentrations of HCl, HBr, H_2SO_4 and H_3PO_4. On the other hand, citric and oxalic acids increased the amount of (111) sites, although not significantly. Nanoparticles have been electrochemically characterised by hydrogen and Ge ads/desorption processes as well as CO stripping. Finally, the electrocatalytic activity of the nanoparticles having the highest (100) percentage was evaluated towards ammonia oxidation confirming the electrochemical characterization results. The results obtained indicate that, 15% HCl-modified Pt nanoparticles using K_2PtCl_4 as metal precursor displayed the highest amount of (100) sites, 46.7%, and gave the highest peak current density for ammonia oxidation, around 5 times that of a polyoriented Pt.

6.1. Introduction

The interest towards the synthesis of shape-controlled metallic nanoparticles has rapidly increased over the last years due to their particular properties. Concerning their catalytic and electrocatalytic properties, the control over the shape directs the orientation of the atoms at the surface of the nanoparticles, and thus, the electrocatalytic activity towards many electrocatalytic reactions which are structure sensitive reactions, can be conveniently tuned. [1-7]

In Electrocatalysis, one of the most studied metals is platinum (Pt) due to its interesting catalytic properties over many electrochemical reactions of high interest such as carbon monoxide [8-10], ammonia [11-13], methanol [14-16], ethanol [16-17] or formic acid [15, 18] oxidations and oxygen [19-27] or nitrite [28-30] reductions. Interestingly, all of these electrochemical reactions are structure sensitive. Therefore, by controlling the shape of the nanoparticle and thus, their surface structure, remarkable improvements have been reported for carbon monoxide [9-10, 31], ammonia [31-34] or methanol [15, 35] oxidations and oxygen reduction[19] among others. In the particular case of the ammonia oxidation in alkaline medium, Pt nanocubes, ideally enclosed by 6 (100) faces, have shown higher catalytic activity over other kind of Pt nanostructures. This behavior is due to the structure sensitivity to (100) surface planes on which the ammonia oxidation process occurs preferentially. [11-12]

The importance of the control over the shape of the nanoparticles has made that a wide variety of methods have been reported to synthesize metallic nanoparticles with well-defined structures. For Pt, there is a plethora of shapes that had been obtained, such

as cubes [33-34, 36-38], tetrahedra [37] or octahedra [36] among many others. However, most of these methods require complicated protocols, the need of heat or the use of hazardous materials, making them difficult to be scaled up. From an industrial point of view, synthesis protocols for electrocatalysts' mass production have to fulfill several requirements, so these have to be fast and easy while, if possible, avoiding the need of heating and of expensive reagents.

In a recent communication, we reported a new methodology to prepare cubic Pt nanoparticles with a high yield using a water-in-oil (w/o) microemulsion method [34]. The formation of the cubic Pt nanoparticles was achieved by adding HCl in the aqueous phase of the w/o microemulsion. In that work, a high concentration of HCl was the key point to modify the shape/surface structure of the nanoparticles. Interestingly a volcano-shaped curve was obtained when correlating the quality of the cubic shape and the amount of HCl, being a 25% HCl the optimum concentration. In a similar way, Pt cubes were also obtained by controlling the amount of H_2SO_4 added as modifier to the aqueous phase of the w/o microemulsion. [33] In this latter case, the mean size of the Pt cubes was relative smaller than that of the Pt nanocubes synthesized using HCl as surface modifier. Both methods confirmed that HCl and H_2SO_4 act as surface modifiers and had a control over the surface structure when added in the aqueous phase of the w/o microemulsion. Conversely to other synthesis protocols these do fulfill the above-mentioned requirements to be scaled up and applied in industry.

On the other hand, cyclic voltammetry is a powerful tool to characterize the surface orientation of platinum surfaces. [39] For this metal, a voltammogram in H_2SO_4 provides direct qualitative information about the surface structure. It is important to recall that it is

the surface structure what determines the resulting catalytic activity. In addition some electrochemical reactions such as Bi and Ge irreversible adsorptions can be used to measure the amount of sites from nanoparticles with an orientation (111) and (100), respectively, based on previous calibrations performed with well-defined surfaces (single crystals). [39] Unlike Transmission Electron Microscopy (TEM) where only a small number of nanoparticles are studied, cyclic voltammetry provides representative information of the sample. Additionally, it is worth noting that shape is only an indicator of the surface structure but the surface of a nanoparticle can be perturbed without noticing a difference in a regular TEM image. [40] Interestingly, advanced microscopic techniques such as spherical-aberration-corrected transmission electron microscopy, can be used to provide atomic-resolution information about the local topologies of active sites [41]. Unfortunately, this type of analysis is still quite unusual, very time consuming, again statistically unrepresentative as a limited number of nanoparticles is analyzed and obviously, requires very expensive instrumentation not easily available.

The present manuscript extends the study of the effect of the presence of different surface modifiers towards the synthesis of shaped Pt nanoparticles, mainly cubes, also covering the effect of using different metal precursors. In all cases, the surface modifiers have been incorporated to the water phase of the w/o microemulsion. The synthesized Pt nanoparticles have been characterized by TEM and also electrochemically using the so-called hydrogen adsorption/desorption process and germanium irreversible adsorption to quantify the amount of (100) sites. CO stripping and ammonia electrooxidations have been also studied as test reactions in order to determine the catalytic activity.

6.2. Results

As previously indicated in the introduction, we recently reported the synthesis of Pt nanocubes with a very high yield by adding HCl into the aqueous phase of the w/o microemulsion. In that manuscript the concentration of HCl used ranged from 0 to 37 % and the optimum for the preparation of those shaped nanoparticles was located at 25 %. Nevertheless, the effect of other hydrogen halides was not evaluated. Thus, first of all, the effect on the shape of the Pt nanoparticles using HBr and HI has been also evaluated.

The first modifier to be evaluated was HBr. It has been previously reported that Br^- selectively adsorb onto {100} facets of Pd nanocrystals. [42] This selective adsorption stabilizes these facets during the growth of the nanoparticles and then Pd nanocubes, which are enclosed by six {100} facets, are obtained. [43-44] Figure 6-1A shows a collection of the positive scans of the CV response for Pt nanoparticles prepared with different concentrations of HBr in the water phase of the w/o microemulsion. As usual, the voltammetric profile of a platinum surface in a 0.5 M H_2SO_4 solution gives us significant information concerning the nature and quantity of the different surface sites. In brief, four different contributions can be observed. These are centred approximately at 0.12, 0.27, 0.37 and 0.53 V vs RHE and are ascribed to the presence of (110) sites, (100) steps and terrace borders, (100) terraces and wide (100) domains and (111) sites, respectively. As it is observed, when increasing the HBr concentration from 0 to 25 %, the contribution due to the (100) terraces remarkably increases, together with the band at 0.27 V due to (100) steps and terrace borders. In general terms, the increase of both (100)-related contributions comes together with a decrease in the (110) contribution, as well as that due to the (111) sites, although this latter signal is very weak in all cases. Interestingly,

as in the case of HCl as modifier, the maximum for (100) sites is also observed at 25%. After this maximum is reached, increasing amounts of HBr cause a sudden decrease in the (100) terrace contribution, but not in that due to (100) small sites, which grows even more, unlike the behaviour previously reported when using HCl.[34] In addition, the other two contributions, related to (110) and (111) sites, also grow.

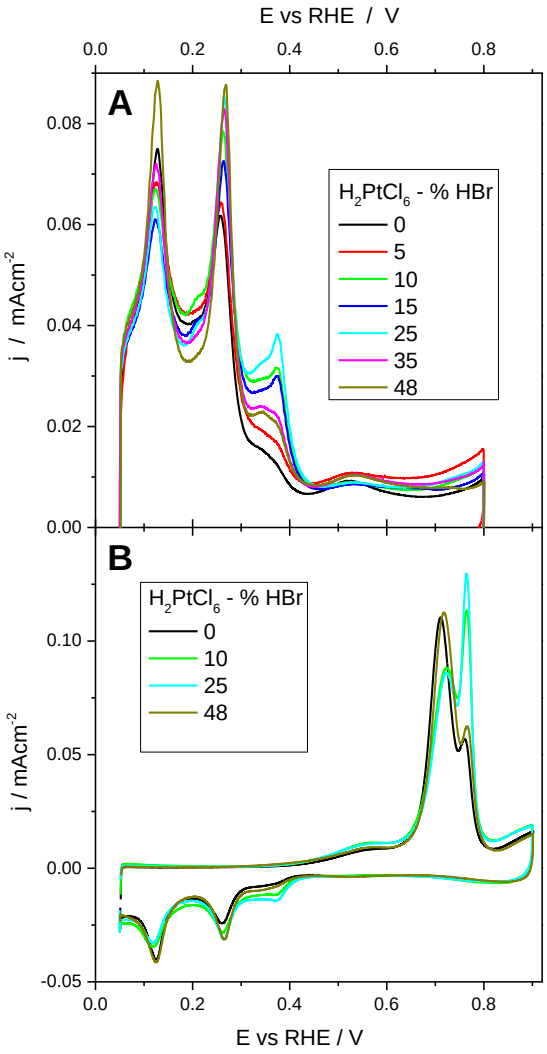

Figure 6-1. (A) Voltammetric profiles of Pt nanoparticles synthesized using different concentration of HBr in the water phase of w/o microemulsions. Scan rate 50 mV s^{-1}. (B) CO monolayer oxidation. Scan rate 20 mV s^{-1}. Test solution 0.5 M H_2SO_4.

Figure 6-1B shows the CO stripping oxidation in H_2SO_4 for the samples prepared in the presence of HBr. For sake of clarity, only the voltammetric behaviour of some samples is shown. CO stripping is also a structure sensitive reaction, and it has been previously reported the different voltammetric behaviour of different nanoparticles with different surface structures.[10] In the voltammograms shown in figure 6-1B, two different peaks are observed for its oxidation, being centred at 0.73 and 0.78 V, being the latter ascribed to the presence of preferential (100) domains.[10] In this way the trend observed for the (100) terrace contribution centred at 0.37 V in H_2SO_4 (fig. 6-1A) is reflected for this CO contribution, increasing from 0 to 25 % and then decreasing for higher HBr concentrations in the water phase. Evidently, the increase of the sharp peak is compensated with a decrease of the other voltammetric feature and vice versa.

In this regard, S.G. Sun's group has recently reported that, in the presence of 1 mM HBr, the potential at which the surface oxidation of a Pt(100) surface starts is shifted to more positive potentials (from 0.6 to 0.9 V vs RHE [45]) thus reflecting a strong bromide-Pt(100) interaction and concluded that the origin of protecting the long-range ordered (100) structure by HBr is mainly through the inhibition of oxygen adsorption. The conclusions from that manuscript clearly agree with our finding. Thus, during the growth of the nanoparticles, bromide is adsorbed on the (100) surfaces thus inducing the preferential formation of nanocubes.

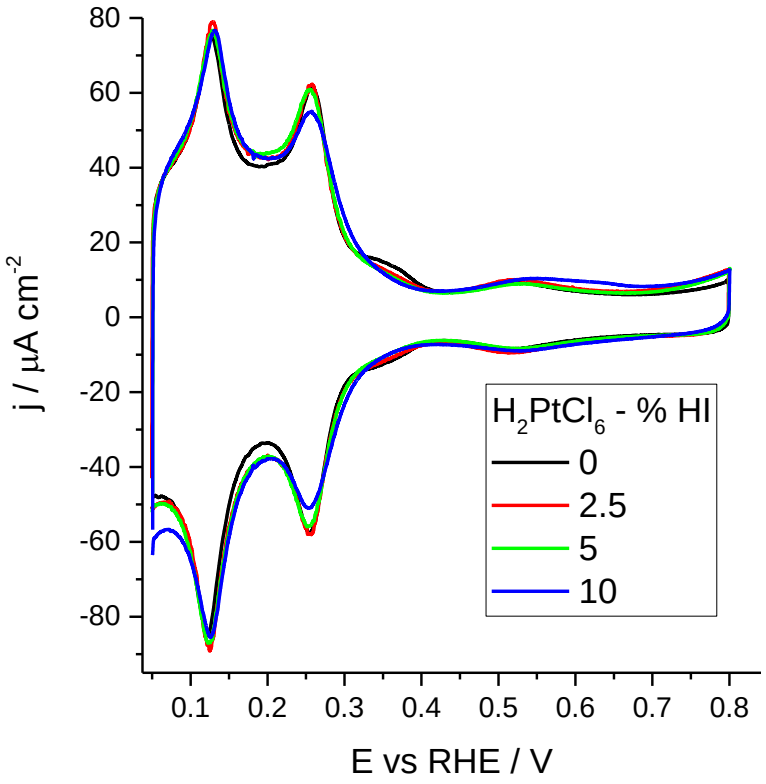

Figure 6-2. Voltammetric profiles of Pt nanoparticles synthesized using different concentration of HI in the water phase of w/o microemulsions. Scan rate 50 mV s^{-1}. Test solution 0.5 M H_2SO_4.

With the same objective, the effect of the addition of different concentrations of HI up to 10% w/w has been also explored. However, for 10% or higher HI amounts, the platinum precursor was not completely reduced while working in the same experimental conditions as those used throughout the manuscript for all the syntheses. Figure 6-2 shows the voltammograms in H_2SO_4 of the nanoparticles prepared in the absence and

presence of HI in the water phase of the microemulsion. The voltammetric profiles indicate a clear diminution of both (100) step and terrace contributions with increasing amounts of HI. In this case, the lower concentration has been reduced to 2.5 %, giving similar results in comparison with the 5 % and 10 %. In fact, the voltammograms recorded for the 3 types of nanoparticles prepared in the presence of HI show the typical profile of a polyoriented platinum surface. Although much lower concentrations have been used for HI in comparison with HCl or HBr, the results are nevertheless very clear concerning the lack of any preferential orientation. For both HCl and HBr the preferential (100) orientation is very similar and it is also quite clear for a 10% of the corresponding hydrogen halide, conversely to the effect of HI.

In the case of palladium, the use of KBr into a polyol system led to the formation of nanocubes and nanobars (enclosed by {100} facets) while the use of KCl had a different effect, cuboctahedra being mainly formed.[46] However, the use of KI resulted in much smaller nanoparticles with poorly defined shape due to the much stronger chemisorption of I^- on the nanocrystal surface, being the adsorption strength order $Cl^- < Br^- < I^-$ [47-48]. This result is similar to that observed in our case for platinum nanoparticles. In the case of HI-modified platinum nanoparticles, the mean size is around 5 nm, while in the case when HCl or H_2SO_4 is used as surface modifier, the mean size is significantly higher (about 12-14 nm [34] and 9 nm [33], respectively). Thus, probably I^- adsorbs very strongly on all the different orientations and consequently no preferential orientation is observed, which may also explain the smaller size of the nanoparticles prepared in the presence of HI.

Besides using hydrogen halides as surface modifiers, H_2SO_4 was also reported to cause a preferential (100) orientation in the synthesized nanoparticles [33], similarly to that shown for HCl and HBr. In this contribution, a different multiprotic acid was used, but reducing considerably the strength of the acid to analyses its possible effect on the resulting shape/surface structure of the nanoparticles. For this purpose, phosphoric acid was employed. The purity of this acid was 85 % and micellar solution showed good stability and both metal precursor dissolution and chemical reduction reaction could be effectively achieved even at that high acid concentration. The results obtained, figure 6-3, show a polyoriented profile for the nanoparticles prepared in the absence of modifier (0 % H_3PO_4) which evolves to a slightly preferential (111) voltammogram for increasing H_3PO_4 contents up to a 10 %. Thus, the contribution at 0.51 V is maximum at the expense of the two (100) contributions, which diminish. The (110) contribution becomes also lower, but so slightly that its change can be neglected. Nevertheless, if the phosphoric acid concentration is further increased, the (100) signals become progressively more intense up to the maximum H_3PO_4 concentration in the water phase, thus showing a clear voltammetric behaviour of preferentially oriented (100) nanoparticles. Together with this (100) increase, from the 10 % to the 85 % H_3PO_4, the (110) and (111) contributions diminish.

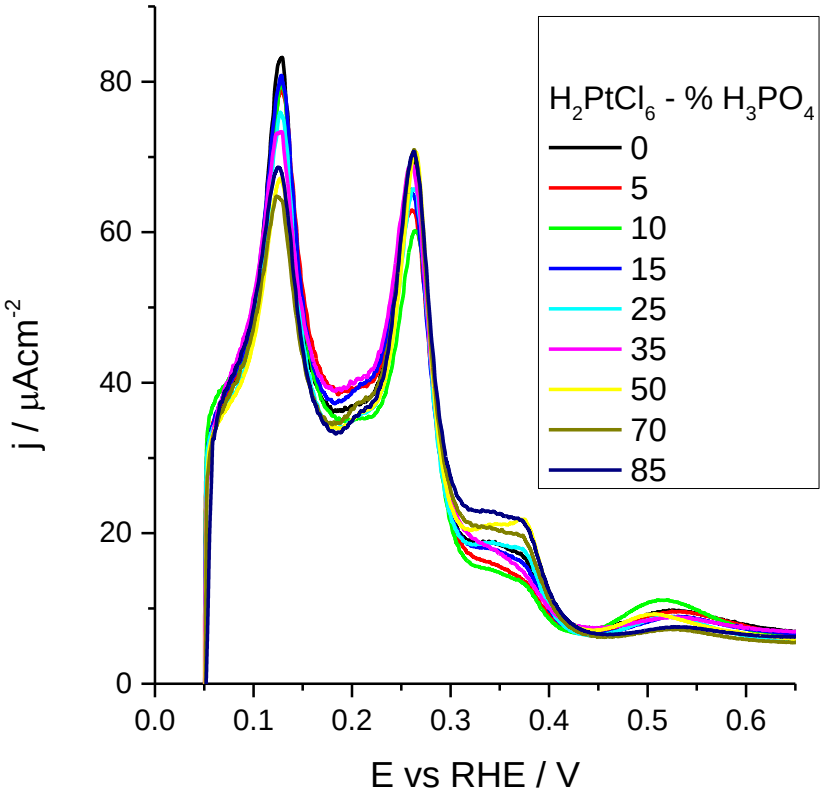

Figure 6-3. Voltammetric profiles of Pt nanoparticles synthesized using different concentration of H_3PO_4 in the water phase of w/o microemulsions. Scan rate 50 mV s^{-1}. Test solution 0.5 M H_2SO_4.

Important contributions have been also published in the last years concerning the use of different organic molecules to guide metal crystals to a preferential nanoparticle shape. For example, Chiu et al. reported the preparation of platinum nanoparticles using many different modifiers such as ascorbic acid, catechol, hydroquinone, syringol or resorcinol among others. [49] The authors concluded that negative electrostatic potential

on the aromatic ring is prerequisite to display binding selectivity to Pt (111), while a neutral to positive one prefers Pt (100). In addition, they claimed that the geometric matching between molecular binding sites and surface lattices plays a role as well in facet selectivity. In addition, Ruan et al. recently studied the synthesis of platinum nanoparticles in the presence of different peptides.[50] They observed that those with phenylalanine gave high tetrahedral yields. Similarly but for Pd, Lim et al. reported that citrate or citric acid could selectively stabilize {111} facets and thus, favour the formation of Pd nanocrystals enclosed by {111} facets, such as octahedrons.[51]

Accordingly, we have evaluated some organic acids at certain concentrations in order to evaluate their effect as surface modifiers. The selection of citric, oxalic and ascorbic acids as modifiers has been made due to the fact that those are well known in the case of Pd for the synthesis of octahedra and cubes. [52-54] The percentages used for citric acid, ascorbic acid and oxalic acid have been 9, 8 and 4% respectively. These values are in the range of those used in bibliography.[51] The other parameters of synthesis have been the same as in previous experiments.

Figure 6-4 shows the voltammograms recorded for the different nanoparticles modified with those organic acids. The effect of these modifiers is very small, but as in the case of Pd [51] they cause a moderate increase in the amount of (111) sites, although to a much lower extent. This (111)-site growth comes together with a diminution of the (100)-terrace contribution. The maximum increase of (111) sites is recorded for citric acid, which is in agreement with molecular dynamics simulations performed for Pd, for which the strong interaction of the OH functional group in the citric acid molecule with the

Pd(111) surface, explains why nanoparticles synthesized in its presence are dominated by (111) facets.[55]

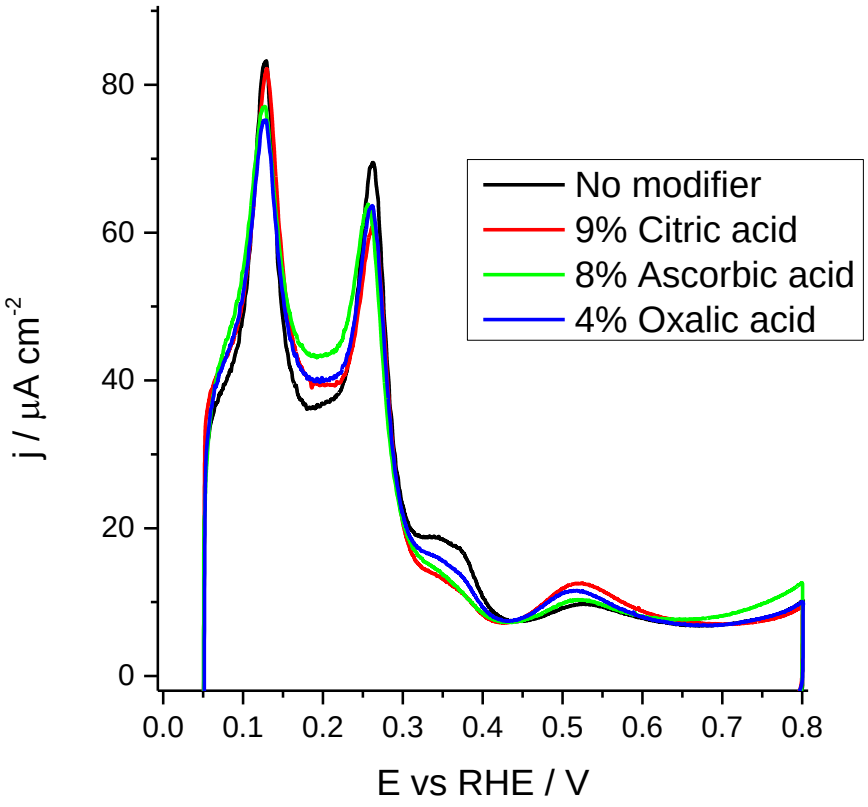

Figure 6-4. Voltammetric profiles of Pt nanoparticles synthesized using three different organic acids in the water phase of w/o microemulsions. Scan rate 50 mV s^{-1}. Test solution 0.5 M H_2SO_4.

The nanoparticles prepared up to this point as well as those previously reported with this methodology [33-34] have been synthesised using H_2PtCl_6 as metal precursor. Consequently, the effect of using a different platinum source has also been analysed.

This synthesis was exclusively performed with those modifiers which gave the most satisfactory results with H_2PtCl_6 as platinum precursor. Thus, nanoparticles were synthesized using K_2PtCl_4 as platinum source in the presence of different concentrations of HCl and H_2SO_4, being their electrochemical characterization shown in figures 6-5 and 6-6, respectively. Figure 6-5A shows the voltammetric profiles in 0.5 M H_2SO_4 of the Pt nanoparticles synthesized using HCl as surface modifier up to a maximum concentration of 20%. An impressive change in the so-called hydrogen region is clearly observed when the amount of HCl used in the synthesis is increased (for sake of comparison, the voltammetric profile of the nanoparticles synthesized with K_2PtCl_4 in the absence of HCl is also plotted). The relative increase of the peaks at 0.27 and especially at 0.37 V vs RHE denotes a clear change in the surface structure produced by the addition of HCl up to a 15%. Those two contributions (related to (100) Pt steps and terraces and wide domains) remarkably increase with the HCl concentration up to that 15%. The increase of (100) sites up to that optimum 15% is counterbalanced with the diminution of the (110) and (111) signals, although the latter is considerable weaker. For higher HCl amounts (20% HCl), the (100) quality is drastically affected. Thus, for the sample prepared in the presence of a 20% HCl, the peaks corresponding to the (100) contributions decrease in intensity while the (110)-site related signal increases, thus confirming the loss of quality concerning the (100) preferential orientation. It is important to highlight that the (100) quality of the 15% HCl-modified Pt nanoparticles is significantly better that that previously obtained in the presence of 25% HCl using H_2PtCl_6 as platinum precursor [34] and with a significant lower amount of surface modifier.

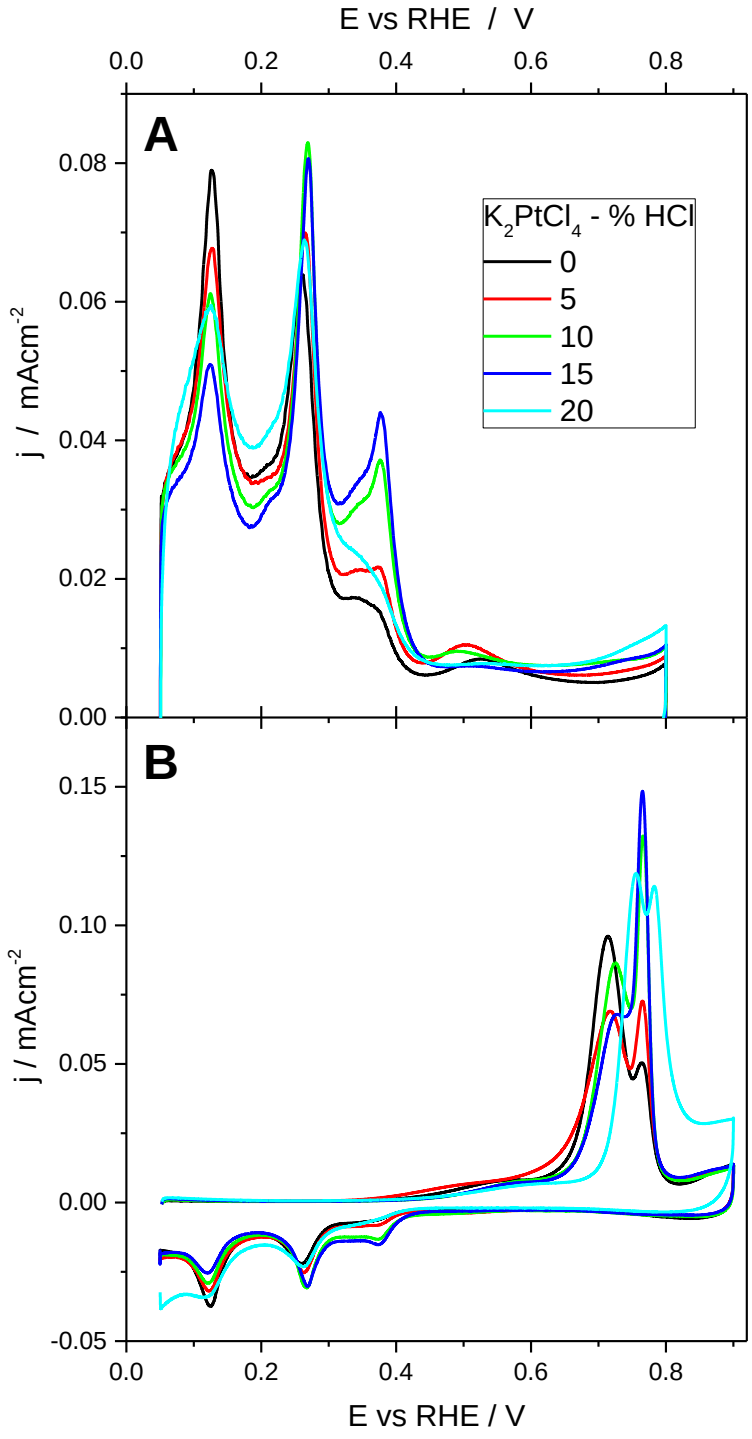

Figure 6-5. (A) Voltammetric profiles of the Pt nanoparticles using K_2PtCl_4 as Pt precursor in the presence of different HCl percentages. Scan rate 50 mVs^{-1}. (B) CO monolayer oxidation. Scan rate 20 mVs^{-1}. Test solution 0.5 M H_2SO_4.

Similarly, the CO stripping on these nanoparticles (showed in Figure 6-5B) although less sensitive, also confirms those previous results. The relative decrease of the peak centered at 0.73 V and the consecutive increase of the sharp peak at 0.78 V vs RHE clearly highlights the increase of the Pt (100) terraces sites and wide domains for the samples prepared using K_2PtCl_4 as platinum source and with HCl up to 15%.

The use of H_2SO_4 as surface modifier also denotes a relative change in the surface structure of the Pt nanoparticles using K_2PtCl_4 as Pt precursor (figure 6-6). Previous results for H_2SO_4-modified Pt nanoparticles using H_2PtCl_6 as modifier showed that the synthesis was very sensitive to the amount of modifier added, and that the amount of (100) sites progressively grows with the acid concentration. The maximum was obtained for a 25% (in volume) H_2SO_4, which corresponds to a 38% w/w, before the system became unstable. In the case of using K_2PtCl_4 as metal precursor, a 50 % H_2SO_4 could be reached, being the quality of the sample in relation to the amount of (100) sites very similar for both metal precursors at the best mentioned concentrations, as shown in figure 6A and reference [33]). Figure 6-6B shows the CO monolayer stripping voltammograms for which the growth of the two (100) signals in figure 6-6A can be followed with the second CO oxidation peak, which is centered at 0.75 V.

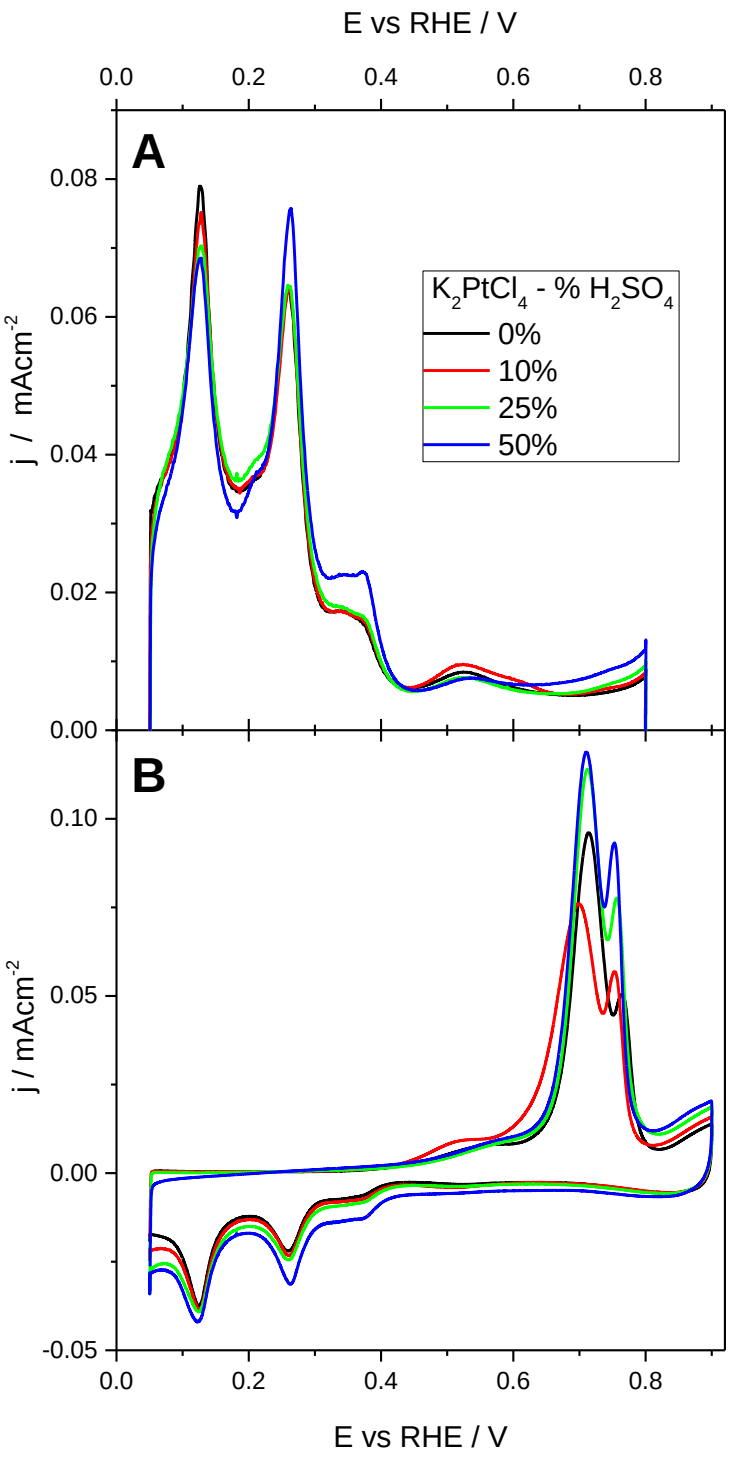

Figure 6-6. (A) Voltammetric profile of the Pt nanoparticles synthesized using H_2SO_4 at different concentrations. Scan rate 50 mVs^{-1}. (B) CO monolayer oxidation at 20 mVs^{-1}. Test solution 0.5 M H_2SO_4.

So far, we have qualitatively analyzed the amount of (100) sites. Nevertheless, the amount of this type of site can be conveniently quantitatively measured through germanium irreversible adsorption as described in previous contributions. [39, 56] Briefly, the glassy carbon electrode with the platinum nanoparticles attached was transferred with a drop of a 10^{-2} M GeO_2 and 1 M NaOH solution into an electrochemical cell with 0.5 M H_2SO_4. The contact with the solution was performed at controlled potential, 0.1 V vs RHE. From the voltammogram obtained, the area due to the germanium contribution was obtained by integration and from that area, the (100)-site percentage could be obtained by using the calibration expression found in literature, which was obtained with model surfaces (single crystals). [56]

Table 6-1 presents the values obtained for the quantification of (100) sites, given in percentages, for the most preferentially oriented samples according to their cyclic voltammograms in H_2SO_4. In addition, the data for the HCl and H_2SO_4 modified Pt nanoparticles prepared with H_2PtCl_6 as metal precursor and reported previously [33-34] are also included.

Table 6-1. Relative percentage of (100) sites measured by Ge irreversible adsorption for different additives in the aqueous phase of water-in-oil microemulsion

Additive	**% (100) sites**
Metal precursor H_2PtCl_6	
25% HCl	44.0[10c]
38% H_2SO_4	35.0[10c]
25% HBr	44.9
85% H_3PO_4	29.2
Metal precursor K_2PtCl_4	
15% HCl	46.7

From the results shown in table 6-1, it is confirmed that the nanoparticles with the highest amount of (100) sites are those prepared using K_2PtCl_4 as metal precursor and a 15% HCl as surface modifier. This result was somehow expected from the voltammograms in H_2SO_4 shown previously and particularly, from the contribution located at 0.37 V, for which this sample showed the largest and most defined peak. All the samples prepared in the presence of K_2PtCl_4 and HCl were analyzed with this Ge quantification method and a volcano shape curve similar to that reported previously [34]

was obtained when comparing the amount of (100) sites with the HCl percentage. Thus, percentages of 18.6, 19.1, 40.8, 46.7 and 28.9 % sites with (100) geometry were obtained for non-modified and 5, 10, 15 and 20 % HCl with K_2PtCl_4 as metal precursor (result not shown).

In parallel, all samples were also analyzed by TEM. Although CV gives a complete behavior of the sample and the response is a direct reflect of all surface sites present at the surface of the nanoparticles, TEM also gives qualitative information concerning the quality of the sample. Thus, samples displaying a high amount of (100) sites are expected to be preferentially cubic, as a cube is ideally enclosed by 6 (100) faces. TEM analysis of the samples was not an easy task. TEM grids were prepared collecting the samples before adding acetone, which causes phase separation and makes the nanoparticles precipitate and then agglomerate. This agglomeration has to be avoided in order to obtain high quality TEM images. Unfortunately, the acids used as surface modifiers are in such a high concentration in many of the samples that the grid is damaged during the TEM sample preparation. In some of the cases the sample cannot be analyzed due to this problem and in others, small grey dots that look like quasi spherical nanoparticles are clearly observed. EDX experiments confirmed that those grey dots were not platinum.

Figure 6-7 shows some representative TEM figures obtained for some of the samples of interest. Figure 6-7A shows the quasi spherical shape of HI-modified nanoparticles synthesized using H_2PtCl_6 as metal precursor. As deduced from the voltammogram CVs shown in figure 6-2, the presence of HI does not originate any preferential orientation and the mean size is smaller. On the other hand, figures 6-7B, 6-6-7C and 6-7D show the cubic shapes obtained with 10% HBr and 15% HCl-modified

platinum nanoparticles prepared using H_2PtCl_6 and K_2PtCl_4, respectively, as metal precursor. As it is observed, both samples show good quality cubes, but voltammograms shown in figure 6-1 and figure 6-5 make clear that the latter are better (100) preferentially oriented. In addition, in figure 6-7D the previously mentioned problem concerning the sample preparation for acid-rich samples is observed, especially at the top of the image as small grey dots that without any EDX analysis could be taken as much smaller Pt nanoparticles without any preferential orientation. An explanation for the higher amount of (100) terrace sites could be also justified considering the particle size of the nanoparticles. In fact, the larger the nanoparticles, the wider can be the (100) surface domains. In fact, H_2SO_4 and HCl modified nanoparticles obtained from H_2PtCl_6 and HCl modified nanoparticles from K_2PtCl_4 have a mean particle size of about 9, 12-14 and 17 nm, respectively.

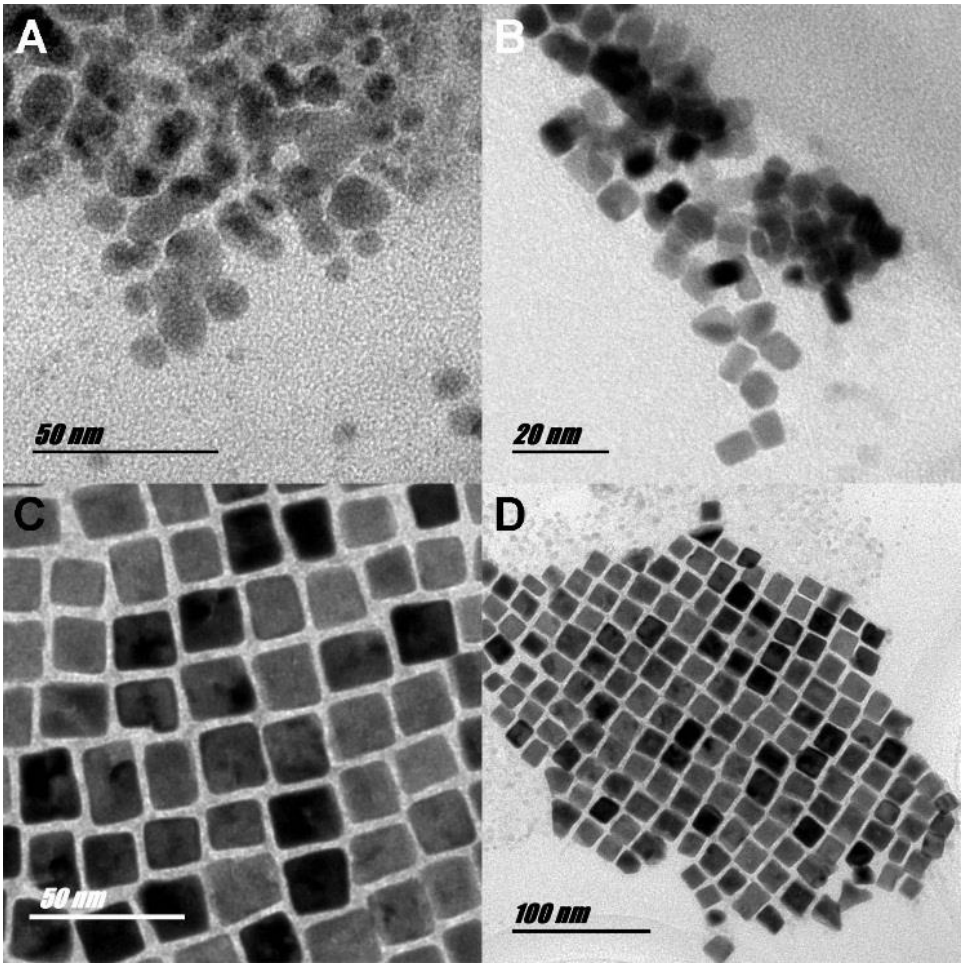

Figure 6-7. Pt nanoparticles synthesized using w/o microemulsion with H_2PtCl_6 as metal precursor prepared in the presence of (A) 2.5% HI, (B) 10% HBr and (C) and (D) using K_2PtCl_4 as metal precursor with 15% HCl.

The present results point out that we can prepare preferentially oriented cubic nanoparticles with a high yield using some acids as surface modifiers. The importance of preparing this type of catalysts lies in the fact that many electrochemical reactions of high interest are structure sensitive, so these cubic nanoparticles could be chosen as better catalysts for electrochemical reactions in which (100) sites are favorable. Ammonia

electrooxidation is one of the most structure sensitive reactions which takes place almost exclusively on (100) sites. [12-13] In fact, this reaction is so sensitive that it can also be used as a tool to get information about the quality and amount of (100) sites. [34] For this study, the nanoparticles containing a high amount of (100) sites, were used as electrocatalysts and the results are given in figure 6-8. For sake of comparison, the data corresponding to quasi-spherical nanoparticles (HI modified) which give the lowest current densities, are also shown. As it is observed, the Pt nanoparticles synthesized using K_2PtCl_4 as metal precursor and using a 15% HCl as surface modifier displayed the best catalytic activity for ammonia oxidation in terms of peak current density. This result was expected from the Ge data (table 1), for which this catalyst was the one with the highest (100) percentage. In addition, the data for 25% HBr, 25% HCl and 47% H_2SO_4-modified platinum nanoparticles are also very satisfactory.

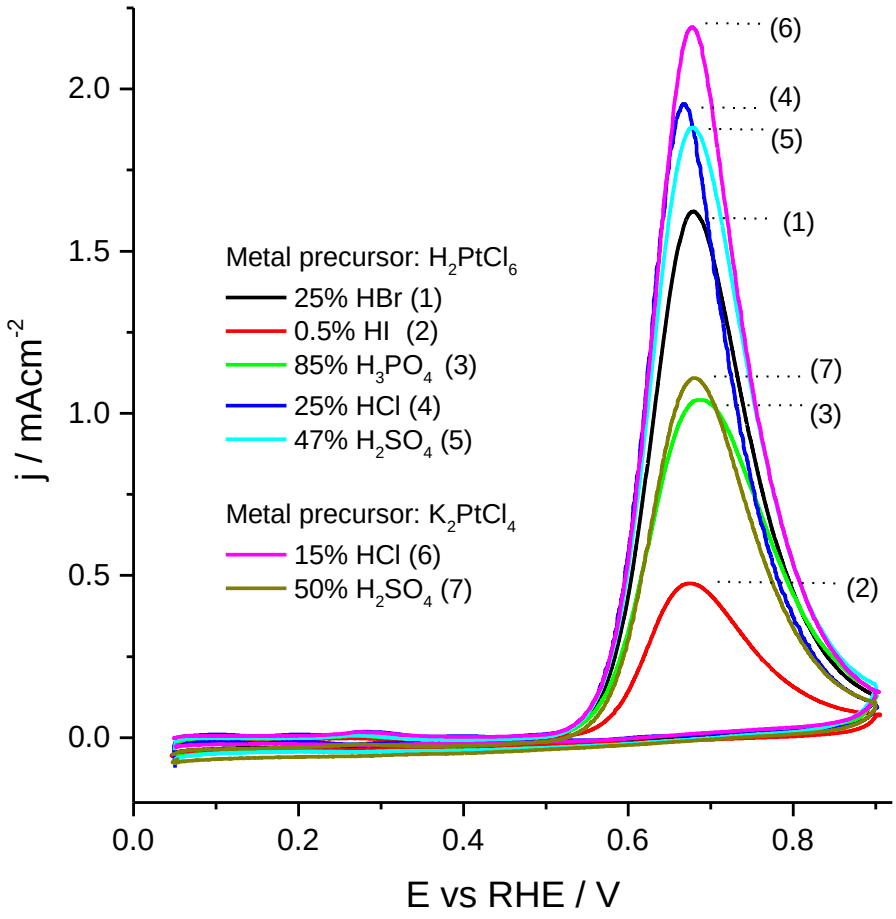

Figure 6-8. Voltammetric profiles for ammonia electrooxidation for different Pt nanoparticles synthesized using different acid concentrations in the aqueous phase of the w/o microemulsion and different metal precursors. Scan rate 10 mV s^{-1}. Test solution: 0.2 M NaOH + 0.1 M NH_3.

6.3. Conclusions

Pt nanoparticles with preferential shapes were synthesized using different acids and using different Pt precursors in water-in-oil microemulsions. On the one hand, the effect of different inorganic acids was analysed. First of all, several hydrogen halides were used. Specifically, HBr and HI were used and compared with the effect of HCl, which had been already studied in a previous publication.[34] HBr, as in the case of HCl, gave nanoparticles with a high proportion of (100) sites and showed a preferential cubic shape as observed by TEM. On the contrary HI-modified Pt nanoparticles did not show a preferential surface structure and their CV in H_2SO_4 solution is characteristic of a polyoriented surface. In addition, H_2SO_4, had also been used previously as a successful modifier toward the synthesis of preferentially oriented cubic nanoparticles.[33] In this manuscript, the effect of a weaker multiprotic acid, H_3PO_4, was also evaluated, yielding nanoparticles with a slightly higher percentage of (100) sites than a polyoriented surface but poorer results than in the case of H_2SO_4.

On the other hand, some organic modifiers were used in order to obtain (111)-rich nanoparticles. Similar organic molecules had been successfully used for synthesising (111)-rich palladium nanoparticles, although not in microemulsion. For this purpose, citric, ascorbic and oxalic acids were used as modifiers. Although an increase in the number of (111) sites was accomplished, this improvement was quite subtle.

Finally, the nature of the Pt source was also explored. Thus, the metal precursor H_2PtCl_6 used for the previous experiments was replaced by K_2PtCl_4 and employed together with those modifiers giving the best results (HCl and H_2SO_4). Although the latter

did not significantly improve the results obtained with the H_2PtCl_6 as metal precursor, HCl yielded very well-defined cubic nanoparticles, with the highest (100) percentage among those obtained with this methodology with the different used modifiers. Finally, the nanoparticles having the highest amounts of (100) sites were tested towards ammonia electrooxidation and, as expected, the highest peak current density was obtained with the 15% HCl modified Pt nanoparticles prepared with K_2PtCl_4 as metal precursor.

6.4. Experimental remarks

Pt nanoparticles were synthesized in a similar methodology to that previously reported [34], using a w/o microemulsion of water/polyethylene glycol dodecyl ether (Brij®L4, Sigma-Aldrich)/n-heptane (99.86% p.a. from Acros Organics) with a volume percentage of 3, 16.5 and 80.5 %, respectively. In the water phase the metal precursor (constant 0.1 M concentration) together with the surface modifier were added. In this manuscript, two different Pt precursors have been used, H_2PtCl_6 (40% weight Pt Acros Organics) and K_2PtCl_4 (99.99% Acros Organics). The different modifiers that have been used are the following: hydrochloric acid (HCl 37% p.a. from Panreac), sulfuric acid (H_2SO_4 95-97%, p.a. from Merck), bromhydric acid (HBr 48% ACS reagent from Acros Organics), iodhydric acid (HI 57% from Sigma Aldrich) phosphoric acid (H_3PO_4 85%, p.a. from Merck), citric acid (99.7% from Prolabo), ascorbic acid (reagent grade from Sigma-Aldrich) and oxalic acid ($(COOH)_2$ x $2H_2O$ ACS, ISO, Reagent) from Merck. Once the microemulsion was prepared and ultrasonically mixed, $NaBH_4$ (Reagent Plus 99% from Sigma Aldrich) as solid was added as reducing agent. The amount of the reducing agent

was that necessary for a 1 M concentration in the water phase. The complete reduction usually takes place in a couple of minutes in the absence of any surface modifier. Nevertheless, in the presence of the modifiers, the process could take up to 8 minutes to make the micellar solution become black. Thirty minutes after the reducing agent was added, acetone was added to the solution to cause phase separation. Once the nanoparticles precipitated, they were washed several times with acetone and ultrapure water (Millipore, 18.2 MΩ cm) in order to remove the modifiers and the surfactant. Finally, the nanoparticles were stored in ultrapure water as a suspension. The concentration of the different modifiers was limited to the as-purchased reagent concentration except when the nature and high acid concentration of the acid cause instability of the micellar solution. For example, in the case of HBr the concentrations varied from 0% (pure water) to 48% (commercial solution). However, for HI the maximum concentration used in the water phase was 10%. Concentrations of the modifiers throughout the manuscript are expressed in w/w %.

Surface characterisation of the nanoparticles was performed by Transmission Electron Microscopy (TEM). TEM allowed the shape and the size distribution of the samples to be estimated. These experiments were performed with a JEOL, JEM-2010, working at 200 kV. Electrochemical measurements were performed using a three-electrode electrochemical cell using a VMP3 multichannel potentiostat (BioLogic) with a NStat configuration (1 counter electrode, 1 reference electrode and up to 8 working electrodes working simultaneously). The counter electrode was a platinum wire and the reference electrode was a reversible hydrogen electrode (RHE) connected to the cell through a Luggin capillary. Gold collector electrodes, on which the nanoparticles were

deposited, were used as working electrodes. Before each experiment, the working electrode was mechanically polished with alumina and rinsed with ultra-pure water to eliminate the impurities. After checking the cleanness of the gold surface, a drop (≈ 5 µl) was drop-casted on the surface and dried in an argon atmosphere. The active surface area of the Pt NPs was determined by the charge involved in the so-called hydrogen UPD region (between 0.06 V - 0.6 V) after the subtraction of the double layer charging contribution and using the value of 230 µC cm^{-2}. [57]

6.5. References

1. Solla-Gullon, J.; Vidal-Iglesias, F. J.; Feliu, J. M.; *Annual Reports on the Progress of Chemistry, Section C: Physical Chemistry,* **2011,** 107, 263-297.
2. Koper, M. T. M.; *Nanoscale* **2011,** 3, 2054-2073.
3. J. Solla-Gullón, F. J. V.-I., E. Herrero, J. M. Feliu, A. Aldaz, Electrocatalysis on Shape-Controlled Pt Nanoparticles. In *Polymer Electrolyte Fuel Cells: Science, Applications, and Challenges*, Franco, A. A., Ed. Pan Stanford Publishing Pte Ltd: Boca Raton, Florida, 2013; pp 93-52.
4. Bing, Y.; Liu, H.; Zhang, L.; Ghosh, D.; Zhang, J.; *Chem. Soc. Rev.* **2010,** 39, 2184-2202.
5. Peng, Z.; Yang, H.; *Nano Today* **2009,** 4, 143-164.
6. Chen, J.; Lim, B.; Lee, E. P.; Xia, Y.; *Nano Today,* **2009,** 4, 81-95.
7. You, H.; Yang, S.; Ding, B.; Yang, H.; *Chem. Soc. Rev.* **2013,** 42, 2880-2904.
8. Mayrhofer, K. J. J.; Arenz, M.; Blizanac, B. B.; Stamenkovic, V.; Ross, P. N.; Markovic, N. M.; *Electrochimica Acta* **2005,** 50, 5144-5154.
9. Brimaud, S.; Pronier, S.; Coutanceau, C.; Léger, J. M.; *Electrochem. Commun.* **2008,** 10, 1703-1707.
10. Solla-Gullón, J.; Vidal-Iglesias, F. J.; Herrero, E.; Feliu, J. M.; Aldaz, A.; *Electrochem. Commun.* **2006,** 8, 189-194.
11. Rosca, V.; Koper, M. T. M.; *Phys. Chem. Chem. Phys.* **2006,** 8, 2513-2524.
12. Vidal-Iglesias, F. J.; Solla-Gullón, J.; Montiel, V.; Feliu, J. M.; Aldaz, A.; *J. Phys. Chem. B* **2005,** 109, 12914-12919.

13. Vidal-Iglesias, F. J.; Garcia-Araez, N.; Montiel, V.; Feliu, J. M.; Aldaz, A.; *Electrochem. Commun.* **2003,** 5, 22-26.
14. Tripkovic, A. V.; Gojkovic, S. L. J.; Popovic, K. D.; Lovic, J. D.; *Journal of the Serbian Chemical Society* **2006,** 71, 1333-1343.
15. Solla-Gullón, J.; Vidal-Iglesias, F. J.; López-Cudero, A.; Garnier, E.; Feliu, J. M.; Aldaz, A.; *Phys. Chem. Chem. Phys.* **2008,** 10, 3689-3698.
16. Han, S. B.; Song, Y. J.; Lee, J. M.; Kim, J. Y.; Park, K. W.; *Electrochem. Commun.* **2008,** 10, 1044-1047.
17. Buso-Rogero, C.; Grozovski, V.; Vidal-Iglesias, F. J.; Solla-Gullon, J.; Herrero, E.; Feliu, J. M.; *J. Mater. Chem. A,* **2013,** 1, 7068-7076.
18. Wang, C.; Daimon, H.; Lee, Y.; Kim, J.; Sun, S.; *J. Am. Chem. Soc.* **2007,** 129, 6974-6975.
19. Sanchez-Sanchez, C. M.; Solla-Gullon, J.; Vidal-Iglesias, F. J.; Aldaz, A.; Montiel, V.; Herrero, E.; *J. Am. Chem. Soc.* **2010,** 132, 5622-5624.
20. Wieckowski, A., *Interfacial electrochemistry : theory, experiment, and applications*. Marcel Dekker: New York, 1999; p xviii, 966 p.
21. Markovic, N. M.; Gasteiger, H. A.; Ross, P. N.; *J. Phys. Chem.* **1995,** 99, 3411-3415.
22. Gewirth, A. A.; Thorum, M. S.; *Inorg. Chem.* **2010,** 49, 3557-3566.
23. Adzic, R. R., Recent advances in the kinetics of oxygen reduction. In *Electrocatalysis*, Lipkowski, J.; Ross, P. N., Eds. Wiley-VCH: New York, 1998; pp 197-242.

24. Gomez-Marin, A. M.; Rizo, R.; Feliu, J. M.; *Catal. Sci. Technol.* **2014,** 4, 1685-1698.
25. Kuzume, A.; Herrero, E.; Feliu, J. M.; *J. Electroanal. Chem.* **2007,** 599, 333-343.
26. Bandarenka, A. S.; Hansen, H. A.; Rossmeisl, J.; Stephens, I. E. L.; *Phys. Chem. Chem. Phys.* **2014,** 16, 13625-13629.
27. Maciá, M. D.; Campina, J. M.; Herrero, E.; Feliu, J. M.; *J. Electroanal. Chem.* **2004,** 564, 141-150.
28. Duca, M.; Figueiredo, M. C.; Climent, V.; Rodriguez, P.; Feliu, J. M.; Koper, M. T. M.; *J. Am. Chem. Soc.* **2011,** 133, 10928-10939.
29. Duca, M.; Cucarella, M. O.; Rodriguez, P.; Koper, M. T. M.; *J. Am. Chem. Soc.* **2010,** 132, 18042-18044.
30. Duca, M.; Rodriguez, P.; Yanson, A. I.; Koper, M. T. M.; *Top. Catal.* **2014,** 57, 255-264.
31. Solla-Gullón, J.; Vidal-Iglesias, F. J.; Rodríguez, P.; Herrero, E.; Feliu, J. M.; Clavilier, J.; Aldaz, A.; *J. Phys. Chem. B* **2004,** 108, 13573-13575.
32. Vidal-Iglesias, F. J.; Solla-Gullón, J.; Rodríguez, P.; Herrero, E.; Montiel, V.; Feliu, J. M.; Aldaz, A.; *Electrochem. Commun.* **2004,** 6, 1080-1084.
33. Martínez-Rodríguez, R. A.; Vidal-Iglesias, F. J.; Solla-Gullón, J.; Cabrera, C. R.; Feliu, J. M.; *ChemPhysChem.* **2014,** 15, 1997-2001.
34. Martínez-Rodríguez, R. A.; Vidal-Iglesias, F. J.; Solla-Gullon, J.; Cabrera, C. R.; Feliu, J. M.; *J. Am. Chem. Soc.* **2014,** 136, 1280-1283.
35. Susut, C.; Tong, Y.; *Electrocatalysis* **2011,** 2, 75-81.

36. Song, H.; Kim, F.; Connor, S.; Somorjai, G. A.; Yang, P.; *J. Phys. Chem. B* **2005,** 109, 188-193.
37. Chiu, C.-Y.; Li, Y.; Ruan, L.; Ye, X.; Murray, C. B.; Huang, Y.; *Nat. Chem.* **2011,** 3, 393-399.
38. Ahmadi, T. S.; Wang, Z. L.; Green, T. C.; Henglein, A.; El-Sayed, M. A.; *Science* **1996,** 272, 1924-1926.
39. Solla-Gullón, J.; Rodríguez, P.; Herrero, E.; Aldaz, A.; Feliu, J. M.; *Phys. Chem. Chem. Phys.* **2008,** 10, 1359-1373.
40. Vidal-Iglesias, F. J.; Solla-Gullón, J.; Herrero, E.; Montiel, V.; Aldaz, A.; Feliu, J. M.; *Electrochem. Commun.* **2011,** 13, 502-505.
41. Gontard, L. C.; Chang, L. Y.; Hetherington, C. J. D.; Kirkland, A. I.; Ozkaya, D.; Dunin-Borkowski, R. E.; *Angew. Chem. Int. Ed.* **2007,** 46, 3683-3685.
42. Xiong, Y.; Cai, H.; Wiley, B. J.; Wang, J.; Kim, M. J.; Xia, Y.; *J. Am. Chem. Soc.* **2007,** 129, 3665-3675.
43. Lim, B.; Kobayashi, H.; Camargo, P. H. C.; Allard, L. F.; Liu, J.; Xia, Y.; *Nano Research* **2010,** 3, 180-188.
44. Jin, M.; Liu, H.; Zhang, H.; Xie, Z.; Liu, J.; Xia, Y.; *Nano Research,* **2011,** 4, 83-91.
45. Xu, C.-D.; Ye, J.-Y.; Chen, L.; Chen, D.-H.; Li, J.-T.; Zhen, C.-H.; Sun, S.-G.; *Electrochimica Acta* **2015,** 162, 129-137.
46. Wu, B.; Zheng, N.; *Nano Today* **2013,** 8, 168-197.
47. Soriaga, M. P.; Schimpf, J. A.; Carrasquillo, A.; Abreu, J. B.; Temesghen, W.; Barriga, R. J.; Jeng, J. J.; Sashikata, K.; Itaya, K.; *Surf. Sci.* **1995,** 335, 273-280.

48. Carrasquillo Jr, A.; Jeng, J.-J.; Barriga, R. J.; Temesghen, W. F.; Soriaga, M. P.; *Inorganica Chimica Acta* **1997,** 255, 249-254.
49. Chiu, C.-Y.; Wu, H.; Yao, Z.; Zhou, F.; Zhang, H.; Ozolins, V.; Huang, Y.; *J. Am. Chem. Soc.* **2013,** 135, 15489-15500.
50. Ruan, L.; Ramezani-Dakhel, H.; Chiu, C.-Y.; Zhu, E.; Li, Y.; Heinz, H.; Huang, Y.; *Nano Lett.* **2013,** 13, 840-846.
51. Lim, B.; Xiong, Y.; Xia, Y.; *Angew. Chem. Int. Edit.* **2007,** 46, 9279-9282.
52. Shao, M.; Yu, T.; Odell, J. H.; Jin, M.; Xia, Y.; *Chem. Commun.* **2011,** 47, 6566-6568.
53. Xiong, Y.; Xia, Y.; *Advanced Materials (Weinheim, Germany)* **2007,** 19, 3385-3391.
54. Lim, B.; Jiang, M.; Tao, J.; Camargo, P. H. C.; Zhu, Y.; Xia, Y.; *Adv. Funct. Mater.* **2009,** 19, 189-200.
55. Yue, J.; Du, Z.; Shao, M.; *Chem. Phys. Lett.* **2016,** 659, 159-163.
56. Rodríguez, P.; Herrero, E.; Solla-Gullón, J.; Vidal-Iglesias, F. J.; Aldaz, A.; Feliu, J. M.; *Electrochimica Acta* **2005,** 50, 3111-3121.
57. Chen, Q. S.; Solla-Gullon, J.; Sun, S. G.; Feliu, J. M.; *Electrochimica Acta* **2010,** 55, 7982-7994.

Other Results

Chapter 7.

Electrochemical behavior of shape-controlled Pt-Rh nanoparticles for ammonia oxidation in alkaline medium for direct alkaline fuel cell application

Abstract: The interest for the development of nanostructures prepared with two or more elements are becoming interesting due to the increment in their uses in different sectors including catalysis as one of the most frequently studied. However, the design of scalable and also, low-cost processes for the synthesis of nanostructures is a current challenge that needs to be evaluated in order to optimize the methods and consequently make it available to the new technology development. On this basis, we have previously working with a methodology to prepare cubic shaped Pt nanoparticles with an easy, cheap and scalable methodology. However, this method has been never studied in the preparation of shaped controlled bimetallic nanostructures. In this work, a method similar to that previously described were tested by adding a rhodium precursor to synthesize shaped controlled Pt/Rh nanoparticles. Bimetallic nanostructures were, characterized and electrochemical evaluated under two different structure-sensitive reaction including ammonia and ethanol oxidation in alkaline media. In this chapter, we show for the first time the electrochemical behavior of preferentially cubic Pt/Rh nanoparticles synthesized with water-in-oil microemulsion using a high concentration of acids in the water phase, towards the ammonia and ethanol oxidation reaction. The effect of different Pt precursors and of the ratio Pt/Rh is evaluated.

7.1. Introduction

Nanomaterials are increasingly becoming more important due to the increment in their uses for different industrial sectors. One of them deals with catalysis, in which nanomaterials are highly demanded due to the properties presented at this scale. In addition, nanomaterials have also helped in the development of new technologies with applications in many fields such as electronics, materials, transportation, storage and energy production, agriculture and health care.[1-3]

As a catalyst, platinum (Pt) has received wide attention due to its well-known catalytic properties. Moreover, many of the studies in this field have focused on many reactions cataloged as structure-sensitive, which means that catalytic activity depends on how the atoms are arranged on the catalyst surface.[4-9] On this basis, control over the surface structure of the catalytic materials is a current issue of paramount importance today.

On the other hand, bimetallic nanoparticles are known to exhibit in some cases improved catalytic properties that can be related to their higher reactivity as well as to a higher poison tolerance, which increase the catalyst activity and life.[10-13] For the particular case of NH_3 oxidation, Pt-based bimetallic structures have been studied in the form of bulk material with metals such as Ir, Ru, Ni or Cu [14,15] as well as Pt-based bimetallic nanoparticles made with Ir, Rh, Ru Pd and oxides such as SnO_x.[16,17] Authors concluded that the presence of metals such as Rh and Ir improve the catalytic properties of Pt by a slight increase in the current density for NH_3 oxidation at low potential.[15,16]

The electrochemical oxidation of ethanol in alkaline medium is another structure-sensitive reaction in which shaped-controlled Pt nanoparticles[18,19], as well

as Pt-based bimetallic nanostructures[20-22], have shown an improvement in their catalytic performance. The interest of studying ethanol oxidation aims from the fact that it could be a prominent candidate as fuel for alcohol fuel cells, due to several benefits including abundance, agricultural origin, low toxicity and high energy density.[23-31] However, the electrochemical oxidation of ethanol is a complex process, for which many studies have concluded that the addition of a second element to the Pt catalyst improves the catalytic activity in terms of, for example, accelerating the oxidation of CO adsorbate, in the case of Pt-Ru structures[32,33] or promoting the C-C bond breaking assigned mostly to Pt-Rh structures[22,31,33-37].

Taking into consideration that Pt-based bimetallic structures prepared with metals such as Rh and Ru increase the catalytic performance for some electrochemical reactions, it would be interesting to evaluate the performance of shape-controlled Pt-based bimetallic nanoparticles. In particular, for the case of NH_3 oxidation, this interest is supported by the fact that it is a structure-sensitive reaction and that Pt/Rh have been reported catalytic performance by decreasing the onset potential.[16,46] However, the synthesis of Pt-based bimetallic nanostructures with control over their shape has not been reported yet.

On this basis, in this work, we propose to synthesize shape-controlled Pt-Rh bimetallic nanoparticles by using a similar method to that previously published for shaped controlled Pt nanoparticles.[38-40] This method consists in the use of w/o microemulsion in which the acid is added into the aqueous phase as a shape-directing agent. The concentration at which the acids were tested was determined by the optimum concentration at which preferentially cubic pure Pt nanoparticles were previously obtained. In this way, the concentrations (% weight/volume) of the

evaluated acids (HCl, H_2SO_4 and HBr) was 20, 50 and 25 % respectively. The atomic composition of the bimetallic nanostructures synthesized is another parameter evaluated in this work. Furthermore, the change of the Pt precursor was also evaluated by testing the use of K_2PtCl_4 instead of H_2PtCl_6, which was previously evaluated as Pt precursor together with HCl as a shape-directing agent in the synthesis of preferential cubic Pt nanoparticles by using w/o microemulsions.[40]

Ethanol and NH_3 oxidation were used to evaluate and compare the catalytic performance of the synthesized shape-controlled Pt/Rh bimetallic nanostructures with a preferential cubic Pt shape. Also, in order to evaluate the stability of the bimetallic nanostructures towards NH_3 oxidation, chronoamperometric measurements were also performed.

7.2. Methodology

7.2.1. Synthesis and physicochemical characterization of Pt/Rh nanoparticles

As mentioned before, Pt/Rh nanoparticles were synthesized by reduction of 0.1 M solution of the metal precursors (H_2PtCl_6 or K_2PtCl_4 and $RhCl_3$) by using w/o microemulsion prepared with the metal precursors solution, which is the aqueous phase (3% percent in volume), polyethylene glycol dodecyl ether (BRIJ®30) (16.5%), and n-heptane (80.5%). When H_2PtCl_6 was used as Pt precursor, the aqueous solution was prepared with a certain concentration of the evaluated acids (HCl, H_2SO_4 and HBr) 20, 50 and 25 % w/v respectively. On the other hand, for the case of K_2PtCl_4 as Pt precursor, an aqueous solution containing 15% HCl was prepared. The Rh

precursor solution was prepared at the corresponding concentration at which the Pt precursor was prepared in order to combine both solutions with the same concentration of the same acid.

Pt/Rh nanoparticles were prepared by using, in some cases, up to six different volume metal ratios including 100/0, 90/10, 75/25, 50/50, 25/75 and 0/100 where 100/0 and 0/100 represent pure Pt and Rh nanoparticles, respectively. After the addition of the solutions containing the precursors in the w/o microemulsion, sonication and continuously magnetic stirring was allowed to keep homogeneity. After a few minutes and after checking the w/o microemulsion stability, the reducing agent ($NaBH_4$) was added as a powder in a molar concentration approximately 10 times higher than that of the precursors in order to ensure their reduction. After complete reduction, acetone was added to the solution to cause phase separation. Afterward, these Pt-Rh were cleaned as previously reported[16,41] (see also section 3.1.4) with successive acetone and ultra-pure water (18.2 mΩ*cm) washes to finally be ready for electrochemical measurements.

In order to get information about the shape and size of the synthesized nanoparticles, Transmission Electron Microscopy (TEM) analysis was performed with a JEOL, JEM-2010 microscopy working at 200 kV. This equipment also allowed to perform Energy Dispersive analysis by X-Rays (EDX) with OXFORD, INCA model system, which gives information related to the composition of the nanoparticles.

7.2.2. Preparation of the electrochemical measurements

The electrochemical measurements, including cyclic voltammetry (CV) as well as chronoamperometry methods (CA), were carried out with a Bio-Logic multi-potentiostat model VMP3 with multichannel for the analysis up to 8 working electrodes under the same experimental conditions. The electrochemical behavior of the nanoparticles was evaluated as previously reported.[12,16,41-43] In summary, nanoparticles were deposited on a previously polished polycrystalline gold disc electrode (5mm diameter) by depositing a drop of about 5-10 µL of the nanoparticle suspension in water on top of the surface of the gold disc. A multiple working electrode electrochemical cell setup was used (See figure 3.5 B from the experimental chapter). The configuration remains similar to that of a three-electrode electrochemical cell but in this particular case, multiple working electrodes were measured at the same time under the same experimental conditions, sharing the counter and reference electrodes. The counter electrode was a large spiral Pt wire and the reference electrode was a reversible hydrogen electrode (RHE) connected to the cell through a luggin capillary.

The electrochemical characterization of the nanoparticles was performed in a 0.5 M H_2SO_4 solution at room temperature. The electrolyte solution was prepared from Milli-Q water and Merck p.a. (H_2SO_4) every day an experiment was carried out. The electrochemical measurements to study the performance towards NH_3 oxidation were carried out in 0.1 M NH_3 alkaline solution, prepared by addition of $(NH_4)_2SO_4$ with 0.2 M NaOH solution. The electrochemical oxidation of ethanol was performed in 0.2 M CH_3CH_2OH in 0.1 M NaOH prepared with ethanol (Merck p.a.). All the solutions

prepared for electrochemical analyses were deoxygenated by bubbling Ar for approximately 10 min.

Prior to the analysis of each test for NH_3 and ethanol oxidation, nanoparticles they were cleaned by CO adsorption and stripping after which the base voltammograms were recorded in 0.5 M H_2SO_4 in order to calculate the real surface area with the clean surface. The real surface area was measured from the charged involved in the so-called hydrogen adsorption-desorption region, for which the charge for the Pt and Rh are 210 and 221 $\mu C*cm^{-2}$, respectively.[44] For Pt/Rh nanoparticles the weighted arithmetic mean between the two pure metals was used.[16] As a brief example, for Pt_{75}/Rh_{25} mass ratio was calculated by the weighted arithmetic mean. ($[0.75 \cdot 210\ \mu C \cdot cm^{-2} + 0.25 \cdot 221\ \mu C \cdot cm^{-2}] / 2 = 212.75\ \mu C \cdot cm^{-2}$)

7.3. Results

7.3.1. Electrochemical characterization of Pt-Rh nanoparticles

The voltammetric profiles for pure Pt and pure Rh nanoparticles as well as those for Pt/Rh nanoparticles with different atomic ratio are shown in figure 7-1 for the three shape modifiers and the two precursors studied. For the pure Pt nanoparticles regardless of the studied acid, the presence of preferentially (100) ordered domains is denoted by the presence of a signal at 0.37 V. In addition, other sites such as edges, steps or defects with (110) and (100) symmetry with signals at 0.125 V and 0.26 V, are shown. This confirms the presence of preferentially cubic Pt nanoparticles, as previously reported. [38-40] In fact, the modifiers and their concentration were those that

previously showed to yield high (100) percentage Pt nanoparticles, as a starting point to prepare cubic Pt/Rh nanoparticles.

The voltammetric profiles of the nanoparticles chill from the typical features of Rh to that of Pt. This behavior can be followed by simple-spectra of the well-known hydrogen adsorption-desorption region which shows up the evolution of the voltammetric profiles as the Pt percentage increase. Also, as Pt concentration increases a shift of the hydrogen adsorption peaks to more positive potentials values is observed. [38] In addition, the onset potential for oxide formation takes places at higher potentials as the Pt percentage increases. Finally, figure 7-1(d) shows the voltammetric profiles for the Pt/Rh nanoparticles synthesized with K_2PtCl_4 as Pt precursor (instead of H_2PtCl_6), with 15% HCl. As mentioned before, the voltammetric profile of pure Pt denotes the presence of preferentially (100) ordered domains at 0.37 V but in this particular case, the current intensity for the peaks of the (100) sites contribution are relatively higher than in the samples prepared by using H_2PtCl_6 as Pt precursor. Also, the voltammetric profile for the poly-oriented Pt_{75}/Rh_{25} nanoparticles (green line) was inserted, in order to compare their electrochemical behavior with the shape-controlled Pt_{75}/Rh_{25} nanoparticles (red line) synthesized in this research work. By comparing both voltammetric profiles, it is noticeable that shape-controlled Pt_{75}-Rh_{25} nanoparticles show an increase of both contributions attributed to the presence of (100) surface domains, with higher current intensity to that recorded for the polyoriented Pt_{75}/Rh_{25} nanoparticles.

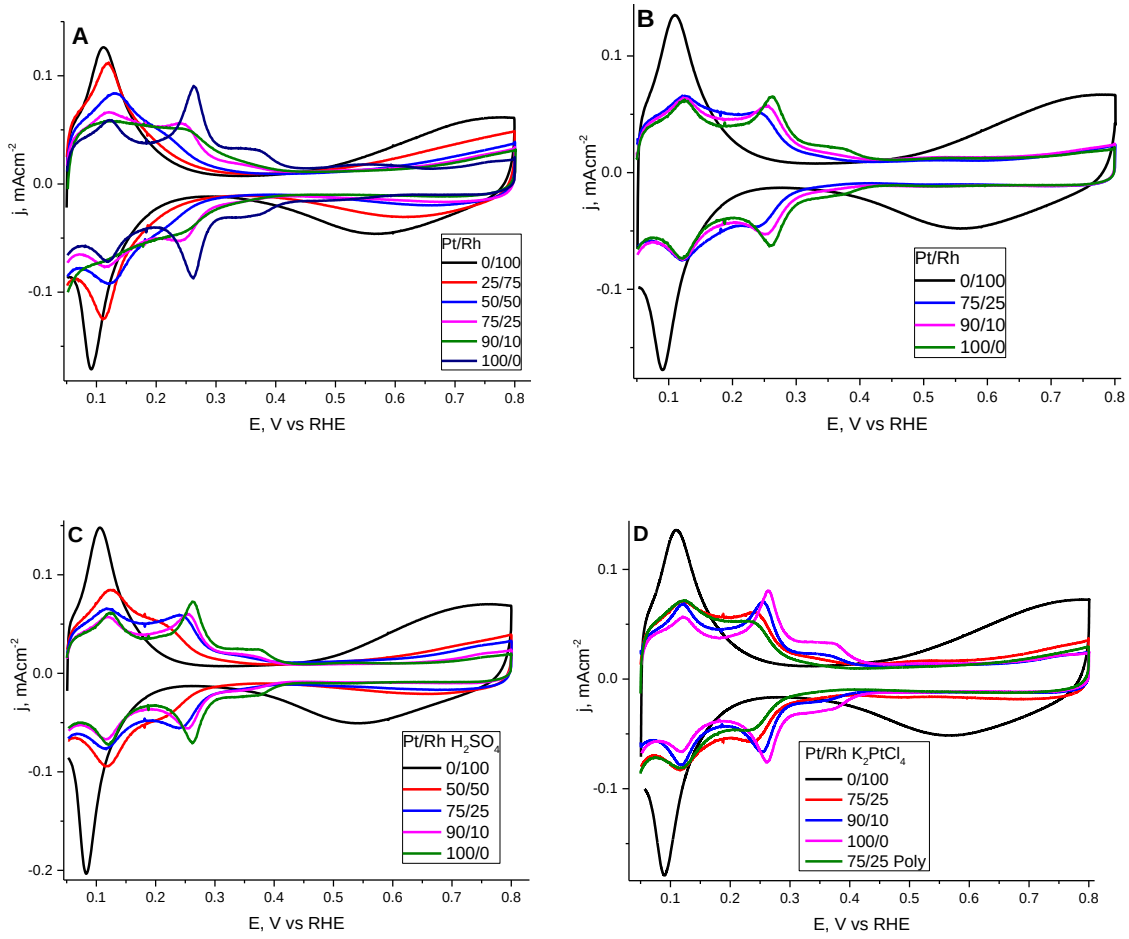

Figure 7-1. Voltammetric profiles of Pt/Rh nanoparticles synthesized using (A) 20% HCl, (B) 25% HBr, (C) 50 % H_2SO_4 and (D) Pt/Rh nanoparticles by using K_2PtCl_4 as Pt precursor with 15% HCl. Test solution 0.5 M H_2SO_4. Scan rate 50 mVs^{-1}.

7.3.2. Ammonia oxidation in Pt/Rh nanoparticles

Figure 7-2 shows the voltammetric profiles for ammonia oxidation of the different Pt/Rh samples previously characterized and shown in figure 7-1. Voltammograms for the different pure Rh nanoparticles synthesized showed no apparent NH_3 oxidation. These results shown are expected, according to the results of Vooys et al.[46] who concluded that on this metal NH_3 is dehydrogenated at significantly lower potentials than on Pt, leading a poisoned surface with N_{ads}. This behavior could explain that as the Rh atomic ratio concentration increases, a decrease in current density is observed. Thus, Rh does not seem to have a positive effect. As the higher its percentage, the lower the current density is. However, giving more attention, a decrease in the onset potential is observed, being slightly more evident in the case of 50% H_2SO_4 used as a surface modifier and H_2PtCl_6 as Pt precursor [Figure 7-2 (C)]. This fact can be very interesting from the practical point of view where NH_3 oxidation is performed at potentiostatic conditions.

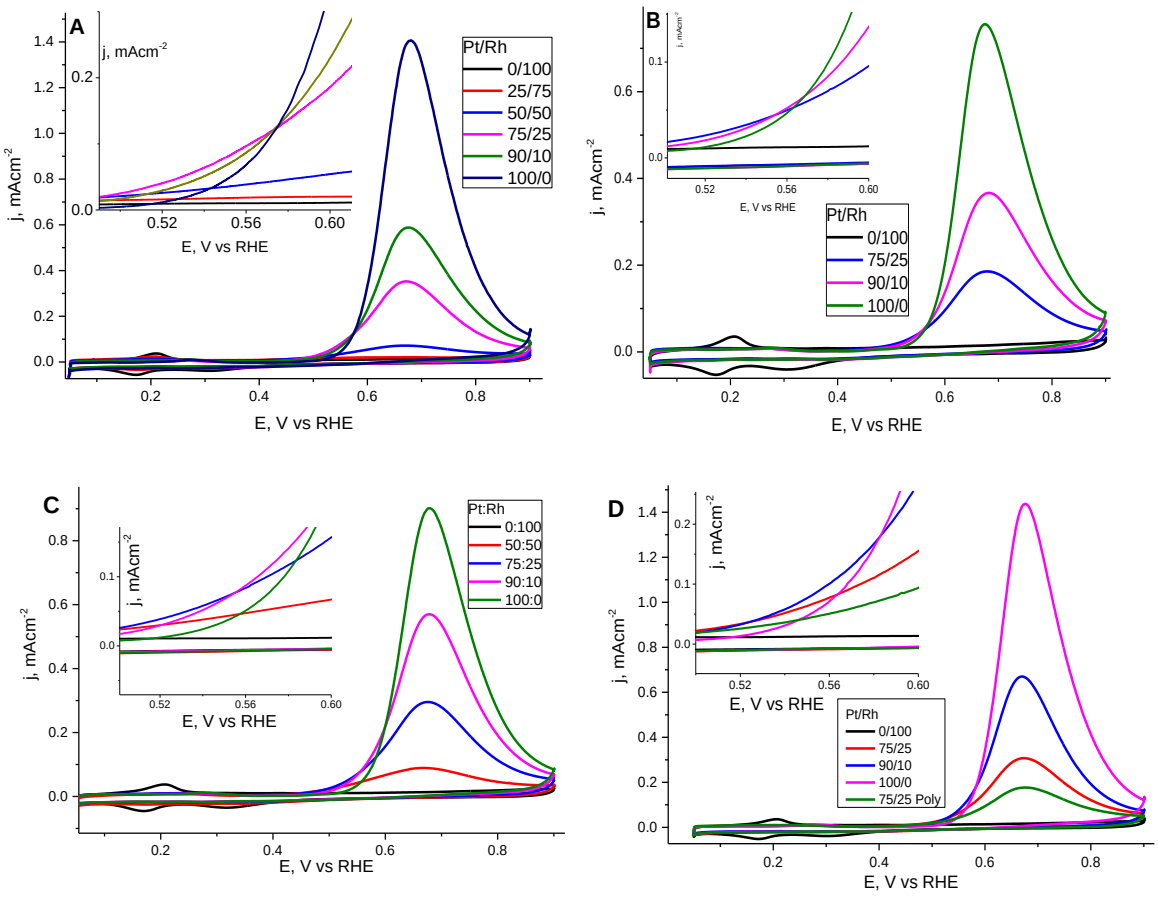

Figure 7-2. Voltammetric profiles for ammonia oxidation in Pt/Rh bimetallic nanoparticles synthesized with (A) 20% HCl (B) 25% HBr (C) 50% H_2SO_4 using H_2PtCl_6 as Pt precursor and (D) Pt/Rh bimetallic nanoparticles prepared with K_2PtCl_4 in 15 %HCl. Test solution 0.1 M NH_3 and 0.2 M NaOH at 10 $mV*s^{-1}$. Inset: Currents for the positive scan in the onset potential region.

Chronoamperometric measurements were performed to analyze the nanoparticles behavior in long experiments at a constant potential which is interesting from an applied point of view. In figure 7-3 the chronoamperometric profiles at different potential, ranging from 0.55 to 0.60 V, can be observed for the Pt/Rh samples prepared with 20% HCl. In the profile at 0.55 V, it is noticeable an increment in the current density for the samples prepared with Pt_{90}/Rh_{10} and Pt_{75}/Rh_{25} in comparison with the

pure Pt nanoparticles, which are the most catalytic towards NH_3 oxidation reaction according to the voltammetric results in this study. The displacement of the onset potential to lower values confirms again that the presence of Rh promotes the NH_3 oxidation, shifting it to lower potential. Another important aspect to remark in the chronoamperometric measurement at 0.55 V is the difference of the current values for the performance of the shape-controlled Pt_{75}/Rh_{25} nanoparticles versus the performance of the poly-oriented Pt_{75}/Rh_{25} nanoparticles. The difference in current density between these two samples, made with the same atomic composition, is ascribed to the presence of controlled-shape bimetallic nanostructures that improve their catalytic performance by providing the specific sites, thus enhancing the NH_3 electrochemical oxidation.

When the chronoamperometric measurements were carried out at higher potentials, preferentially cubic Pt nanoparticles highest current densities. It is also worth highlighting that the catalytic performance decreases as Rh percentage increases, as previously observed in the NH_3 oxidation voltammetric profiles (Figure 7-2).

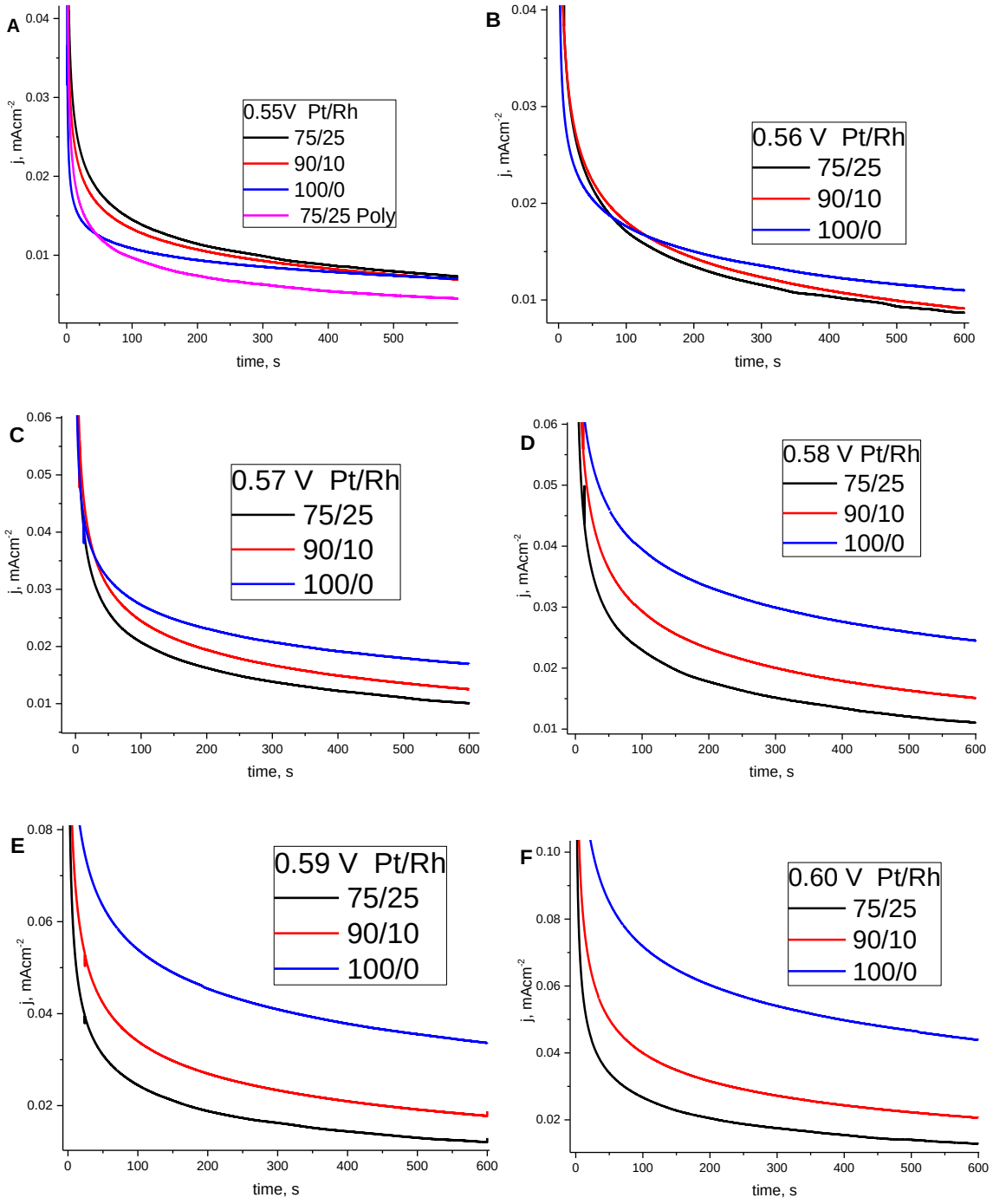

Figure 7-3. Chronoamperometric measurements of (A) 0.55, (B) 0.56, (C) 0.57, (D) 0.58, (E) 0.59 (F) 0.60 V for the Pt/Rh nanoparticles synthesized with 20% HCl. Test solution 0.1 M NH_3 and 0.2 M NaOH.

Similar electrochemical behavior was observed for the Pt/Rh nanoparticles synthesized with 25% HBr, 50% H_2SO_4 as well as for the Pt/Rh nanoparticles synthesized by using K_2PtCl_4 as Pt precursor with 15% HCl. At 0.55 V, the samples prepared with Pt_{75}/Rh_{25} and Pt_{90}/Rh_{10} obtained respectively, the highest current density in comparison with the pure preferential cubic Pt nanoparticles. For the particular case of the Pt/Rh nanoparticles prepared with 50% H_2SO_4, the sample prepared with Pt_{90}/Rh_{10} obtained the highest current density. However, at 0.6 V the different samples of the preferential cubic Pt nanoparticles obtained the highest current density in comparison with any of the bimetallic Pt/Rh nanoparticles. Also, as previously seen, a decrease in the current density is reported as the reduction of the atomic concentration of Pt.

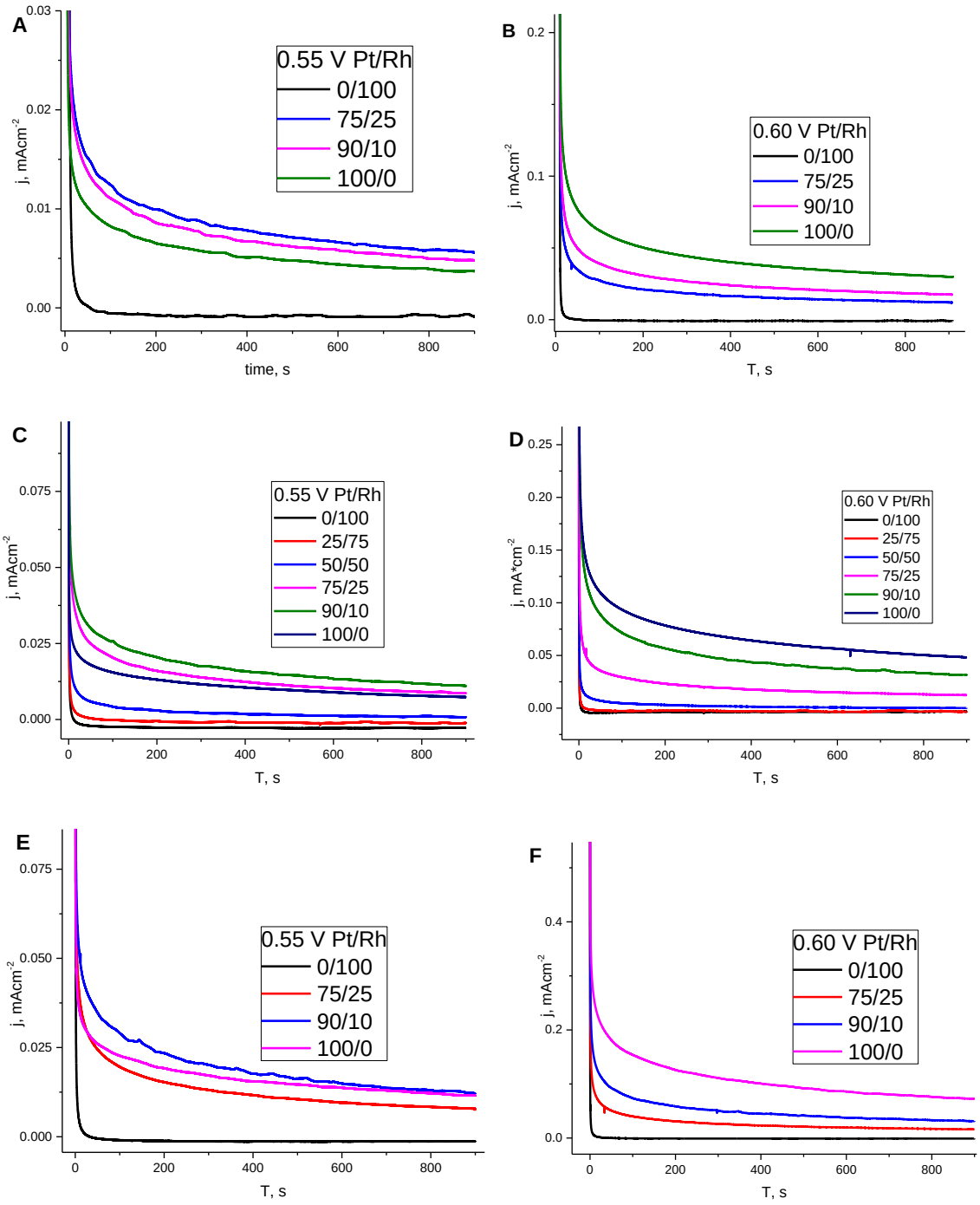

Figure 7-4. Chronoamperometric measurements at 0.55 V (A, C and E) and 0.60 V (B, D and F), for Pt/Rh nanoparticles synthesized with (A, B) 25% HBr (C, D) 50% H_2SO_4 using H_2PtCl_6 as Pt precursor and (E, F) Pt/Rh nanoparticles synthesized with K_2PtCl_4 as Pt precursor with 15 % HCl. Test solution 0.1 M NH_3 and 0.2 M NaOH.

As previously mentioned, and shown in the figure 7-3 (A), the catalytic performance of Pt_{75}/Rh_{25} bimetallic nanostructures synthesized in the presence of surface modifiers was compared with poly-oriented Pt_{75}/Rh_{25} bimetallic nanoparticles synthesized with a similar method in the absence of any surface modifier (Figure 7-5). The voltammetric profiles for the ammonia oxidation showed that the catalytic performance is nearly two times lower than that of the shape-controlled bimetallic nanoparticles. This fact also suggests the possible structure control over the bimetallic nanostructures synthesized in this work in the presence of surface modifiers. The improvement of the electrochemical oxidation for the shaped controlled bimetallic nanoparticles also was confirmed by chronoamperometric measurements (figure 7.5(B)) in which were also obtained the highest current densities.

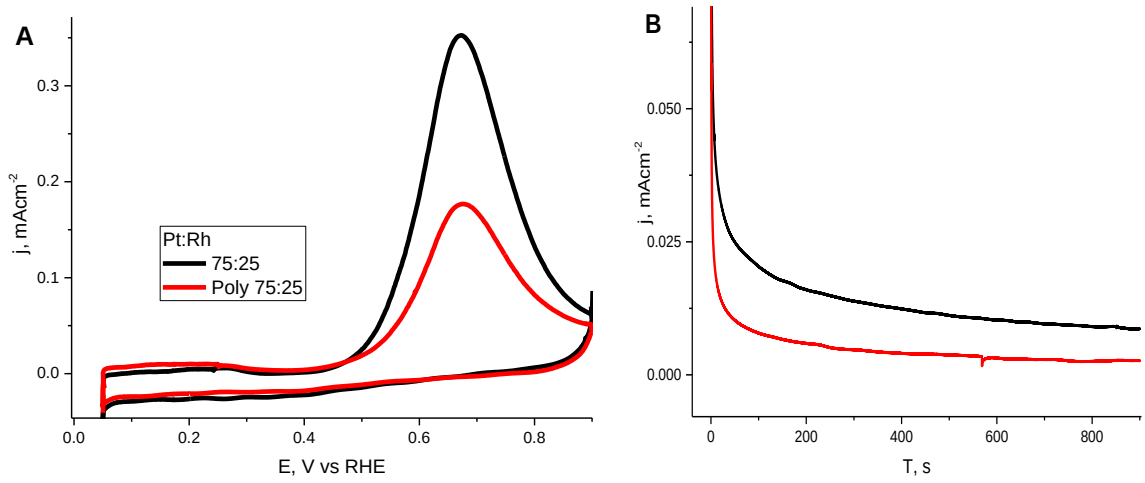

Figure 7-5. (A) Voltammetric profile for ammonia oxidation at $50mV*s^{-1}$ on shape controlled (black) and poly-oriented (red) Pt_{75}/Rh_{25} nanoparticles and (B) the chronoamperometric measurements for 600s at 0.55 V. Test solution 0.1 M NH_3 and 0.2 M NaOH.

7.3.3. Ethanol oxidation in Pt/Rh nanoparticles

The electrochemical behavior of the synthesized bimetallic Pt/Rh nanoparticles toward ethanol oxidation in alkaline medium also showed interesting results. The high activity reported above at 0.7 V, with current densities above 6 $mA \cdot cm^{-2}$ made that CV were affected by the ohmic drop. Thus, electrochemical measurements were obtained by using ohmic drop compensation.

In addition, it is convenient to deposit on the support electrode small amounts of catalyst. It was found that there were diffusion problems of the reactant (ethanol) through the catalyst layer. Thus, experiments had to be performed with balanced amounts of catalyst that had a proportional behavior between the nanoparticles deposited (electroactive surface area) and the current density of the ethanol oxidation peak. Only then, a proper comparison between the different nanoparticles could be performed.

Figure 7-6 (A) shows the voltammetric profiles for the Pt/Rh nanoparticles synthesized with 20% HCl, using H_2PtCl_6 as Pt precursor, and those of Pt/Rh nanoparticles synthesized with K_2PtCl_4 as Pt precursor in 15% HCl (Figure 7-6(B)). In both cases, for lower atomic concentrations of Rh into the bimetallic nanostructures, both an increase of the current density[19] and a lower onset potential are observed. Specifically, in the case of Pt using 20% HCl and H_2PtCl_6 as Pt precursor, Pt_{50}/Rh_{50} and Pt_{75}/Rh_{25} had nearly the same onset potential, although the later was considerably more active. In the case of using 15 % HCl and K_2PtCl_4 as Pt precursor, both Pt_{75}/Rh_{25} and Pt_{90}/Rh_{10} had nearly the same onset potential, slightly lower for the former although having a lower peak current density than the latter.

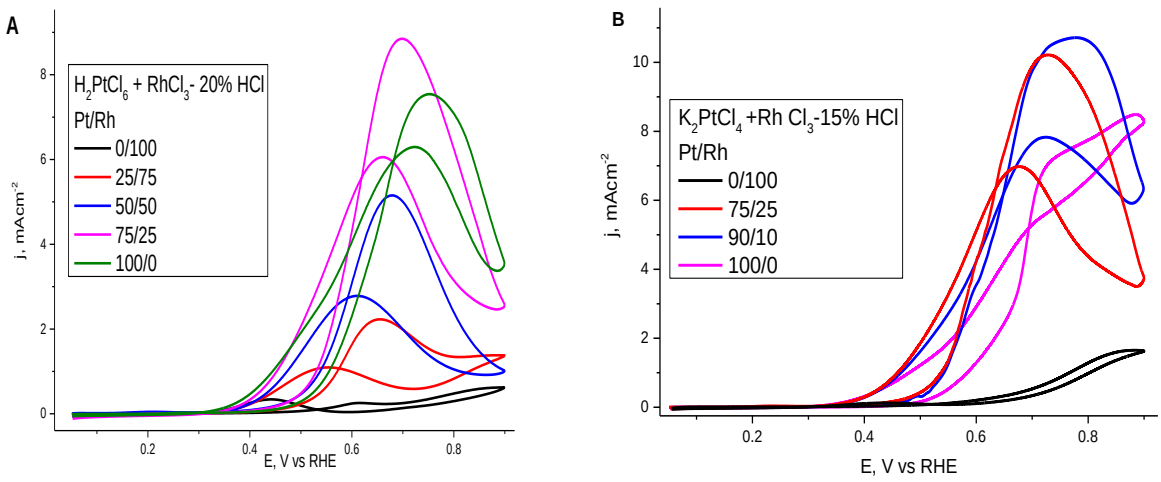

Figure 7-6. Voltammetric profile of the bimetallic Pt/Rh nanoparticles synthesized with (A) 20% HCl using H_2PtCl_6 as Pt precursor and the (B) synthesized with 15% HCl with K_2PtCl_4 as Pt precursor. Test solution 0.2 M NaOH + 0.1 M ethanol at 20 $mV \cdot s^{-1}$.

A summary of the bimetallic Pt_{75}/Rh_{25} nanoparticles towards ethanol oxidation is shown in figure 7-7. In this figure, the voltammetric profiles obtained for the bimetallic nanostructures are compared with the performance for the synthesized pure Pt nanoparticles with preferential cubic shape. It is noticeable the increment of the current density as well as the decrease to lower potentials of the onset potential. This means that control over the shape of the Pt/Rh structures improves their activity as previously observed with the NH_3 oxidation. In terms of catalytic performance, the samples prepared with Pt_{75}/Rh_{25}, were, in summary, the best samples for the ethanol oxidation reaction in this work. The sample synthesized by using K_2PtCl_4 as Pt precursor in the presence of 15% HCl, showed the highest peak current density close to ≈10.5 $mA \cdot cm^{-2}$. The inset figure shows a zoomed section of the voltammogram (positive going sweep) showing that in terms of the onset potential, Pt_{75}/Rh_{25} prepared with 25% HCl is slightly better and exhibits the lowest value. In this figure, it is also clearly observed

that all the bimetallic nanostructures samples have a lower onset potential than the preferentially cubic pure Pt nanoparticles.

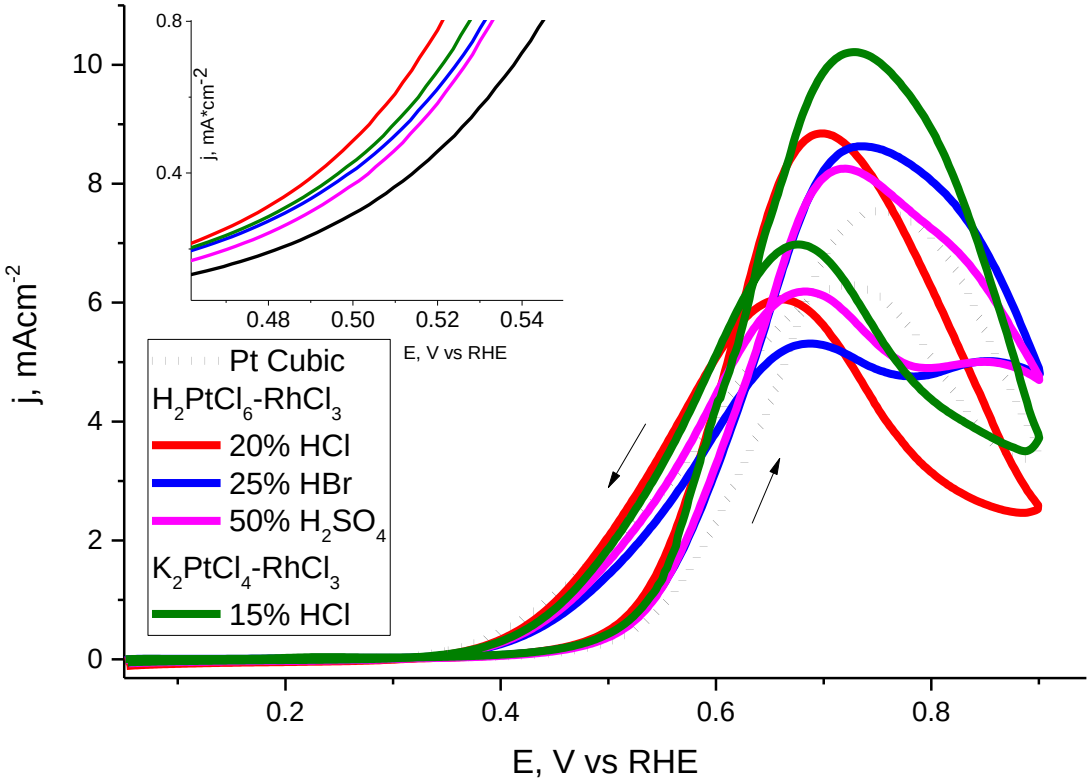

Figure 7-7. Summary of the voltammetric profiles of the bimetallic Pt_{75}/Rh_{25} nanoparticles towards ethanol oxidation. Test solution 0.2 M NaOH + 0.1 M ethanol at 20 $mV \cdot s^{-1}$.

7.3.4. Physicochemical characterization

TEM images were used to confirm the shape of the bimetallic structures, and EDX analyses, were used to determine the atomic composition. Figure 7-8, 7-9, 7-10 and 7-11 show the TEM images and the EDX analysis for Pt_{75}/Rh_{25} synthesized by

using different acids as surface modifier with H_2PtCl_6 as Pt precursor and the Pt_{75}/Rh_{25} synthesized with K_2PtCl_4 as Pt precursor prepared in 15% HCl (Figure 7-11). Particularly, Pt_{75}/Rh_{25} prepared with 20% HCl (figure 7-8) was the sample with the TEM images in which some structures show the most preferential cubic shape related to the higher amount of (100) sites nanoparticles. The rest of the studied Pt_{75}/Rh_{25} show TEM images with not well-defined geometrical structure. The EDX measurements revealed that the atomic composition is very close to the nominal composition as expected form the synthesis. Evidently, the peaks due to C, Si, and Cu come from the TEM grid.

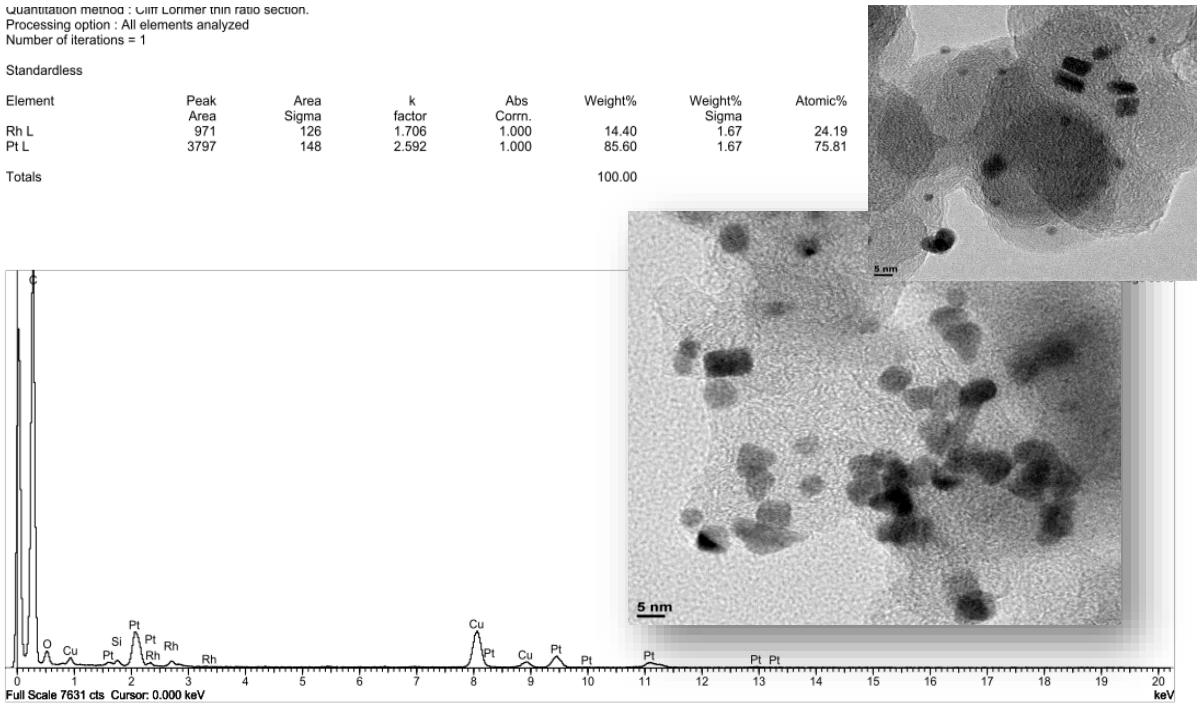

Figure 7-8. EDX measurements and the corresponding TEM images of the Pt_{75}/Rh_{25} samples prepared with 20% HCl.

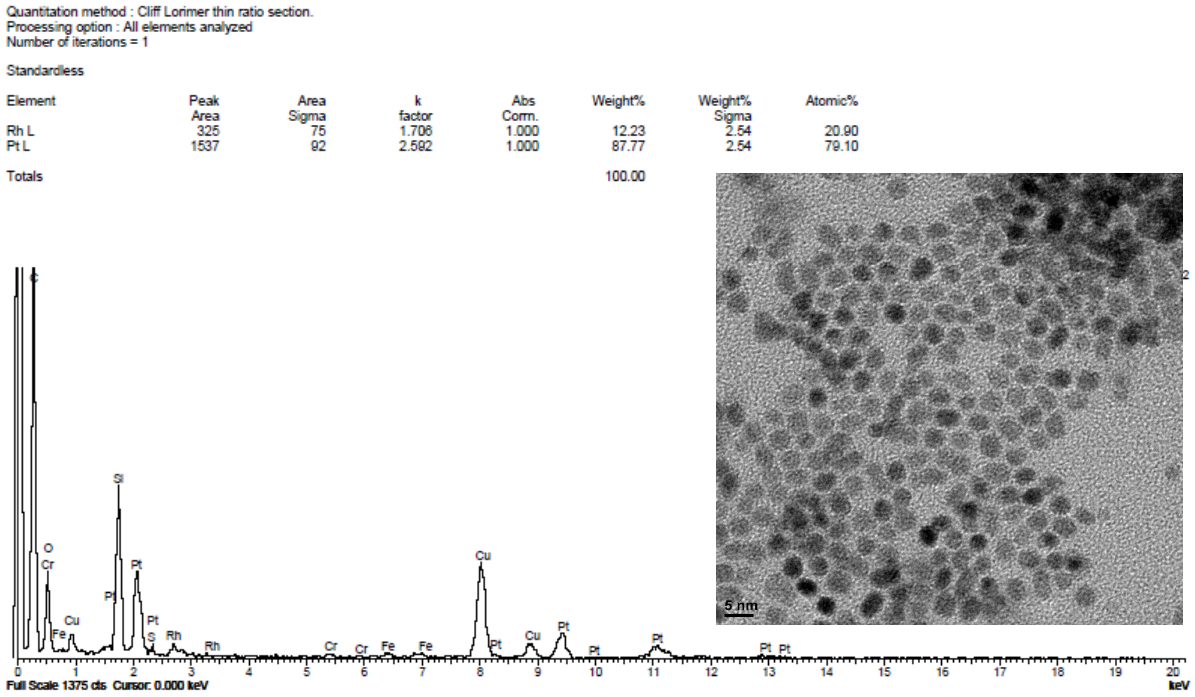

Figure 7-9. EDX measurements and the corresponding TEM images of the Pt_{75}/Rh_{25} samples prepared with 25% HBr.

Quantitation method : Cliff Lorimer thin ratio section.
Processing option : All elements analyzed
Number of iterations = 1

Standardless

Element	Peak Area	Area Sigma	k factor	Abs Corrm.	Weight%	Weight% Sigma	Atomic%
Rh L	478	132	1.706	1.000	12.38	3.05	21.13
Pt L	2226	110	2.592	1.000	87.62	3.05	78.87
Totals					100.00		

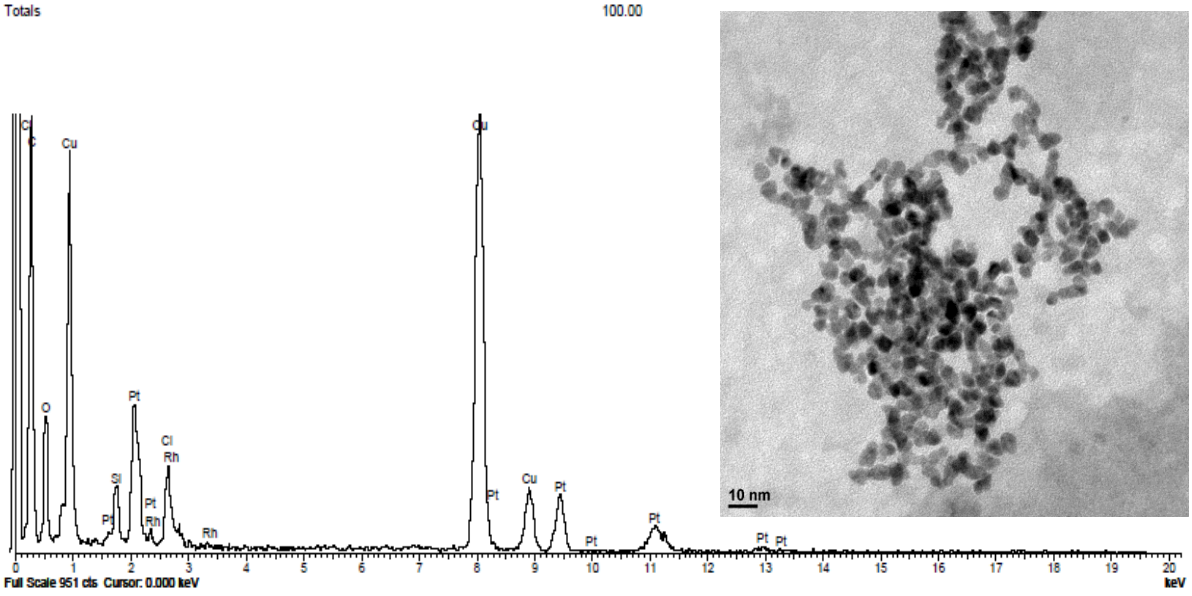

Figure 7-10. EDX measurements and the corresponding TEM images of the Pt_{75}/Rh_{25} samples prepared with 50% H_2SO_4.

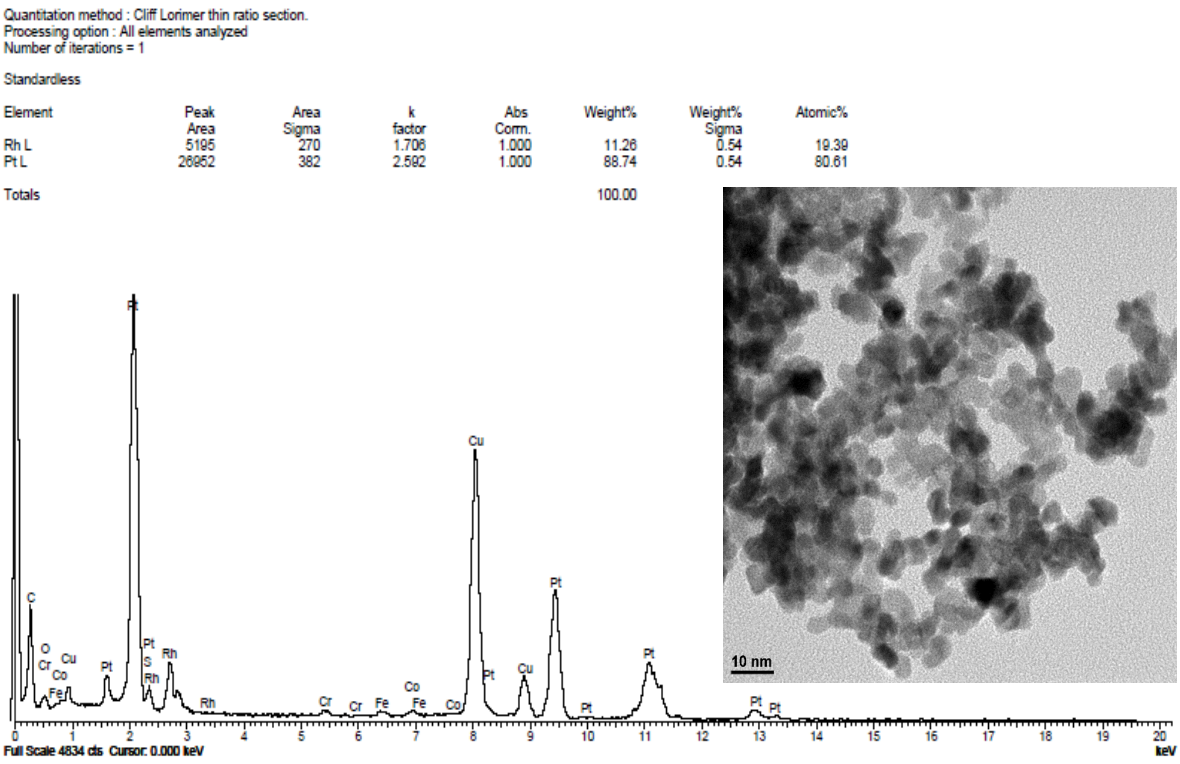

Figure 7-11. EDX measurements and the corresponding TEM images of the Pt_{75}/Rh_{25} samples prepared with15 % HCl and K_2PtCl_4 as Pt precursor.

Table 7-1 summarizes the results obtained by EDX for the different Pt_{75}/Rh_{25}, and which share similar results.

Table 7-1. Atomic composition measured by EDX of the bimetallic Pt_{75}/Rh_{25} nanoparticles

Pt precursor	Surface modifier	EDX Atomic Composition Pt/Rh ratio
H_2PtCl_6	20% HCl	75.81/24.19
	25% HBr	79.10/20.90
	50% HCl	78.87/21.13
K_2PtCl_4	15 % HCl	80.81/19.39

7.4. Conclusions

In this work, we have successfully synthesized, for the first time, shape-controlled bimetallic Pt/Rh nanoparticles by using the w/o microemulsion method with the addition of different acids to evaluate the surface modifier capacity. The physicochemical characterization confirms that in some cases, acids successfully worked as shape directing agents for the preparation of shape-controlled Pt/Rh bimetallic structures in which TEM images were useful to report the presence of some shaped controlled nanostructures. In the particular case of the bimetallic structures

synthesized with 20% HCl and H_2PtCl_6 as Pt precursor, TEM images reported some preferential cubic nanostructures. In terms of the composition of the bimetallic structures, EDX measurements confirmed that the values are relatively close to the nominal composition, as expected from the synthesis. However, a deeper physicochemical characterization can be employed in the future to confirm the surface structure and obtain a more accurate atomic surface composition.

For NH_3 oxidation, Pt_{75}/Rh_{25} and Pt_{90}/Rh_{10} showed interesting results in terms of the displacement of the onset potential to lower values when the samples were compared with the preferentially cubic pure Pt nanoparticles. However, in terms of catalytic performance, pure cubic Pt nanoparticles still have the best catalytic performance. On the other hand, for ethanol oxidation, bimetallic Pt_{75}/Rh_{25} samples showed the highest catalytic performance, obtaining the highest current density as well as lower onset potential, in comparison with the preferentially cubic Pt nanoparticles. As future work remains the evaluation of the use of the shaped bimetallic nanoparticles as real catalyst for a direct alkaline ethanol fuel cell system, in order to determine their catalytic performance as well as their long-term stability.

7.5. References

1. Roco, M.C. *J. Nanopart. Res.* **2011**, 13, 427-445.
2. Roco, M.C.; Hersam, M.C.; Mirkin, C. A. Nanotechnology Research Directions for Societal Needs in 2020 – 2011. (2011) Springer Netherlands.
3. Roco, M. C. Nanotechnology: From Discovery to Innovation and Socioeconomic Projects. Chemical Engineering Progress. 2011, 107. 21-27.
4. Adzic, R. R. in Modern of Electrochemistry, ed. R. E. White, J. O. M. Bockris and B. E. Conway, Plenum Press, New York, 1990, vol. 21, pp. 163-236.
5. Sriramulu, S.; Javi, T. D.; Stuve, E. M. Interfacial Electrochemistry: Theory, Experiments and Applications, ed. A. Wieckowski, Marcel Dekker, New York, 1998, pp 793.
6. Markovic, N. M. & Ross, P. N. Interfacial Electrochemistry: Theory, Experiments and Applications, ed. A. Wieckowski, Marcel Dekker, New York, 1998, pp 821.
7. Markovic, N. M. & Ross, P. N. *Surf. Sci. Rep*. **2002**, 45, 117-229.
8. Herrero, E.; Feliu, J.M.; Aldaz, A. Encyclopedia of Electrochemistry, ed. A. J. Bardand, M. Stratman, Wiley- VCH Verlag, Weinheim, 2003, vol. 2, pp. 443.
9. Koper, M.T.M.; Van Santen, R.A; Neurock, M. Catalysis and Electrocatalysis at nanoparticles Surfaces, ed. A. Wieckowski, E. R. Savinova and C G. Vayenas, Marcel Dekker, New York, 2003, pp 1-32.
10. Markovic, N.M.; Ross, Jr. P.N.; *Surf. Sci. Rep*. **2002**, 45, 117-229.
11. Vidal-Iglesias, F.J.; Al-Alk, A.; Watson, D.J.; Attard, G.A. *Electrochem. Commun.* **2006**, 8, 1147-1150.
12. Solla-Gullón, J.; Rodes, A.; Montiel, V.; Aldaz, A.; Clavilier, J.; *J. Electroanal. Chem*. **2003**, 554-555, 273-284

13. Fang, L.; Vidal-Iglesias, F. J.; Huxter, S.E.; Attard, G.A. *J. Electroanal. Chem*. **2008**, 622,73-78.
14. Endo, K.; Nakamura, K.; Katayama, Y.; Miura, T. *Electrochimica Acta*, **2004**, 49, 2503-2509.
15. Endo, K.; Katayama, Y.; Miura, T. *Electrochimica Acta*, **2004**, 49, 1635-1638.
16. Vidal-Iglesias, F.J.; Solla-Gullón, J.; Montiel, V.; Feliu, J.M.; Aldaz, A. *J. Power Sources,* **2007**, 171, 448-456.
17. Lomocso, T. L.; Baranova, E*. Electrochimica Acta*, **2011**, 56, 8551-8558.
18. Busó-Roguero, C.; Grozovski, V.; Vidal-Iglesias, F.J.; Solla-Gullón, J.; Herrero, E.; Feliu J.M. *J. Mater. Chem. A,* **2013**, 1, 7068-7076.
19. Busó-Roguero, C.; Solla-Gullón, J.; Vidal-Iglesias, F.J.; Herrero, E.; Feliu, J.M. *J. Solid State Electrochem*. **2016**, 20, 1095-1106.
20. Shen, S. Y.; Zhao, T. S. & Xu, J.B. *Int. J. Hydrog. Energy* **2010**, 35, 12911-12917.
21. Bergamaski, K.; Gonzalez, E.R.; Nart, F.C*. Electrochimica Acta*, **2008**, 53, 4396-4406.
22. Lima, F.H.B.; Profeti, D.; Lizcano-Valbuena, W.H.; Ticianelli, E.A.; Gonzalez, E.R. *J. Electroanal. Chem.* **2008**, 617, 121-129.
23. Badwal, S. P. S.; Giddey, S.; Kulkarni, A.; Goel, J.; Basu, S. *Applied Energy, **2015**,* 145, 80–103.
24. Gnansounou, E.; Dauriat, A. *J. Sci. Ind. Res.* **2005**, 64, 809-821.
25. Lamy, C.; Belgsir, E.; Leger, J. *J. Appl. Electrochem.* **2001**, 31, 799−809.
26. Li, G.; Pickup, P. G. *J. Power Sources,* **2006**, 161, 256−263.
27. Ribeiro, J.; Dos Anjos, D.; Leger, J.-M.; Hahn, F.; Olivi, P.; De´ Andrade, A.; Tremiliosi-Filho, G.; Kokoh, K*. J. Appl. Electrochem.* **2008**, 38, 653−662.

28. Wang, Y.; Zou, S.; Cai, W.-B. *Catalysts,* **2015**, 5, 1507−1534.
29. Sulaiman, J. E.; Zhu, S.; Xing, Z.; Qiaowan-Chang Q.; Shao, M. *ACS Catalysis,* **2017**, *7*, 5134-5141
30. Wang, H.; Jusys, Z. and Behm, R. J. *J. Phys. Chem. B.* **2004**, 108, 19413-19424.
31. Tu Mai, P.; Haze, A.; Chiku, M.; Higuchi, E.; Inoue, H. *Catalyst*, **2017**, 7, 246-256.
32. Gămara, G.A.; de Lima, R.B.; Iwasita, T. *J. Electroanal. Chem*. **2005**, 585, 128-131.
33. Morimoto, Y.; Yeager, E. B. *J. Electroanal. Chem.* **1998**, 444, 95-100.
34. Ianniello, R.; Schmidt, V.M.; Rodríguez, J.L.; Pastor, E.; *J. Electroanal. Chem.* **1999**, 471, 167-179.
35. Bergamaski, K.; Gomes, J. F.; Goi, B.E.; Coutanceau, C.; Léger, J-M. *Electrochimica Acta*, **2004**, 49, 3901-3908.
36. Souza, J.P.I.; Queiroz, S.L.; Bergamaski, K.; Gonzalez, E.R.; Nart, F.C. *J. Phys. Chem***. 2002**, 106, 9825-9830.
37. Cantane, D.A.; Ambrosio, W.F.; Chatenet, M.; Lima, F.H.B. *J. Electroanal Chem*. **2012**, 681, 56-65.
38. Martínez-Rodríguez, R. A.; Vidal-Iglesias, F. J.; Solla-Gullón, J.; Cabrera, C. R.; Feliu, J.M. *J. Am. Chem. Soc.* **2014**, 136, 1280-1283.
39. Martínez-Rodríguez, R. A.; Vidal-Iglesias, F. J.; Solla-Gullón, J.; Cabrera, C. R.; Feliu, J.M. *Chem. Phys. Chem.* **2014**, 15,1997-2001.
40. Martínez-Rodríguez, R. A.; Vidal-Iglesias, F. J.; Solla-Gullón, J.; Cabrera, C. R.; Feliu, J.M. *ChemElectroChem*. **2016**, 3, 1601-1608.

41. Solla-Gullón, J.; Montiel, V.; Aldaz, A.; Clavilier, J.; *J. Electroanal. Chem*. **2000**, 491, 69-77.

42. Solla-Gullón, J.; Montiel, V.; Aldaz, A.; Clavilier, *J. Electrochem. comm*. **2002**, 4, 716-721.

43. Solla-Gullón, J.; Montiel, V.; Aldaz, A.; Clavilier, *J. Electrochem. Soc*. **2003**, 150, E104-E109.

44. Bard, A.J. *Electroanalytical Chemistry: A Series of Advances*; Electroanalytical Chemistry, Vol. 9; M. Dekker: New York, 1976; Vol. Volume 9 /.

45. Rand, D.A.J.; Woods, R. *J. Electroanal. Chem*. **1972**, 35, 209-218.

46. de Vooys, A.C.A.; Koper, M.T.M.; van Santen, R.A. *J. Electroanal. Chem.* **2001**, 506, 127-137.

Chapter 8.

Preliminary electrochemical studies of adsorption of $(SO_4)^{-2}$ and Cl^- on main basal Pt single crystal electrodes towards understanding their effects in the synthesis of preferential shape Pt nanoparticles

Abstract: The synthesis of Pt nanoparticles with preferential shapes has received increasing attention in the last years due to the high number of structure-sensitive reactions. Commonly, in order to get the control over the shape at this scale the adsorption of specific adatoms or molecules on the nanoparticle surface during the synthesis process is required, thus favoring a particular pattern. Currently, a method to synthesize preferentially cubic Pt nanoparticles by using high concentrations of HCl and H_2SO_4 in water in oil (w/o) microemulsions is well documented. In the present work, we show the preliminary results of a fundamental electrochemical study about how the hydrogen and anion adsorption-desorption processes are influenced by both acids, aiming to understand how these ions could influence over the surface structure of the preferentially shaped Pt nanoparticles. The acid concentrations of these solutions were selected mimicking the synthesis conditions of the aqueous phase of the water-in-oil microemulsions in which shape-controlled nanoparticles were prepared. In this study, the three Pt basal planes [Pt (100), Pt (111) and Pt (110)], as well as a Pt poly-oriented surface, have been studied in order to evaluate the electrochemical behavior.

8.1. Introduction

Pt nanoparticles with preferential surface structures have been widely studied as prominent candidates to prepare high-performance electrocatalysts.[1-6] This is due to the surface structure sensitivity of many electrochemical reactions, several of them in the fuel cell research area. This means that the catalytic performance is strongly determined by the surface site properties of the structures on which the reaction occurs. To achieve the best performance, researchers have been dedicated to the search for new methods which could yield nanostructures with preferential shapes. For shape-controlled Pt nanoparticles, some well-known methods have been used, including colloidal synthesis[7-16], electrochemical reduction[17], and electron beam deposition[18].

In most of the cases, these methods require a surface modifier (capping agents, surfactants) to control the shape and size of the nanostructure. For the particular case of cubic Pt nanoparticles, the most used methods include the use of carboxylic acids[7,8], amines[9,10], cetyltrimethylammonium bromide (CTAB)[11,12], aromatic molecules[13] and polymeric surfactants such as polyvinylpyrrolidone (PVP)[14] and polyacrylic acid (PAA)[15,16] as shape directing agents.

On the other hand, common anions and small molecules have been proposed for the synthesis of shape-controlled Pt nanoparticles as an alternative to the search of polymer-free methods. Halide ions [Cl^-, Br^-, I^-] are some of the typical anions tested due to their strong tendency to adsorb on metallic surfaces.[19] Previous studies showed that chloride (Cl^-) and bromide (Br^-) anions promote the formation of crystal facets, specifically in the formation of shapes with (100) and (111) facets.[20-24] However, the mechanism behind this enhancement is still under discussion. Researchers suggest

that adsorption of halide ions may be critical for the growth of selective facets of the metal nanocrystals.

Deng-Xu et al. studied the adsorption of CTAB and Br^- on Pt (100) using cyclic voltammetry in order to gain insights in understanding the interaction with the electrode surface.[20] In that work, researchers demonstrated that adsorption of bromide ions on Pt (100) could protect the long-range order by inhibition of oxygen adsorption. Also, they predicted that CTAB is more favorable to yield Pt nanomaterials with long-range ordered (100) surface structures when it is employed as a shape-tuning agent.

In this work, a preliminary electrochemical study of the interaction between the three basal planes of Pt electrodes [Pt (100), Pt(111) and Pt (110)] with chloride (Cl^-) and sulfate (SO_4^{-2}) ions was performed to understand their shape directing effect as previously confirmed in the synthesis of preferentially cubic Pt nanoparticles.[22-24] The main objective is to understand the role of how these ions induce this shape selectivity. To make this possible, cyclic voltammetry (CV) was selected by using the mentioned Pt basal planes as working electrodes under the influence of different concentrations of HCl and H_2SO_4 as supporting electrolytes. In this way, this study pretends to determine the adsorption states characteristic of each surface arrangement in highly concentrated acidic solutions. Their electrochemical behavior is analyzed by using the three Pt basal planes under similar experimental conditions.

8.2. Methodology

8.2.1. Synthesis and cleaning of the Pt nanoparticles

In this study, three different shape-controlled Pt nanoparticles were evaluated. The nanoparticles with preferential spherical shape (Pt(poly)) were synthesized using the water-in-oil (w/o) microemulsion method as previously reported by Solla-Gullón et al.[25] by reducing H_2PtCl_6 in the presence of sodium borohydride. After complete reduction, acetone was added to the solution to cause phase separation. The black precipitate was washed several times with acetone and then with ultra-pure water to remove surfactant molecules.

On the other hand, the Pt nanoparticles with a preferential shape were prepared using the colloidal method proposed by El-Sayed et al.[15,16] In summary, a variable amount of PAA was added to a 10^{-4} M solution of the desired Pt precursor. The use of K_2PtCl_4 allows cubic shaped Pt nanoparticles with preferential (100) facets to be obtained whereas octahedral nanoparticles with preferential (111) facets could be synthesized with H_2PtCl_6. After 20 min of Argon (Ar) bubbling the Pt ions were reduced with H_2 bubbling in the solution for approximately 5 minutes. After complete reduction (12-24h), two pellets of NaOH were added to make the nanoparticles precipitate. After that, several washes with ultra-pure water were carried out.

8.2.2. Preparation of Pt single crystals and Pt nanoparticles electrodes

Platinum single crystal electrodes were oriented, cut and polished from small single crystal beads (2.5 mm diameter) following the procedure described by Clavilier et al.[26] The surfaces used were Pt (100), Pt (111), Pt (110) basal planes and a poly-

faceted Pt [Pt(poly)] electrode to check the influence of the selected probe reaction. The electrodes were flame-annealed, cooled down in a (H_2 + Ar) mixture and protected with water in equilibrium with this gas mixture to prevent contamination before immersion in the electrochemical cell, as described previously.[27]

The preparation of the electrodes with Pt nanoparticles was done by drop-casting, approximately 5µL of an aqueous suspension of the Pt nanoparticles onto a gold collector. The electrode was placed under Ar atmosphere to remove the water. By doing that, the nanoparticles get firmly attached to the gold collector and ready to be analyzed.

8.2.3. Electrochemical measurements

The electrochemical behavior of the Pt single crystal electrodes as well as that of the shape-controlled Pt nanoparticles was evaluated in a 0.5 M H_2SO_4 in order to check the quality of the surface structure of the samples.[28] The electrochemical measurements performed in hydrochloric acid (HCl) solution ranged concentrations from 1.8 to 35% w/w where 1.8 % w/w is equivalent to 0.5 M HCl. In the case of using H_2SO_4 as electrolyte, experiments were performed in the range from 5 to 50% w/w. A three-electrode electrochemical cell using a Pt coil as a counter electrode and a reversible hydrogen electrode (RHE) as reference electrode, was used. The electrolyte solution was bubbled with Ar before experiments and, during the electrochemical analysis, Ar flow was kept to have an oxygen-free atmosphere.

8.3. Results

8.3.1. Surface characterization of Pt single crystal electrodes and Pt nanoparticles in 0.5 M HCl

The electrochemical behavior was evaluated for the three Pt basal planes [Pt (100), Pt (111) and Pt (110)] and the poly-faceted Pt electrode. Figure 8-1 shows the voltammetric profiles of the studied Pt single crystal electrodes in 0.5 M HCl. There is a characteristic positive scan voltammogram for each Pt basal plane, which also shows a level of cleanliness of the system by simply visualizing the so-called hydrogen adsorption-desorption region, highlighting the peak sharpness. The presence of these contributions is indicative of the coupling between the H^+ and Cl^- adsorption-desorption processes, as previously reported.[29]

The Pt (100) electrode is the Pt basal plane with the most denoted contribution, represented by the sharpest peak and with a high intensity centered at 0.23 V vs RHE. For this surface, there are another two small contributions which take place at 0.54 V and 0.63 V that may be attributed to changes in the anion ad-layer.

For Pt (111) single crystal electrodes, three important contributions are observed. The most remarkable one is the peak at the same potential as that of the spike present for Pt (100) single crystal electrode. However, there is a huge difference in intensity, having in this case at least six times less current density for the wider Pt (111) single crystal electrode contribution. This confirms that Cl-H competitive adsorption leaves different contributions in both basal planes.[30] The other two small contributions take place at 0.46 V and 0.63 V. The sharp peak at 0.46 V has a characteristic reversible behavior and could reflect the building of an ordered layer as in the case of sulfuric acid. The most positive contribution for this surface shows a

non-reversible peak also similar to that shown in sulfuric acid solution which is attributed to the sulfate ionic pair adsorption [$(SO_4)^{-2}/(HSO_4)^-$]. [31-34]

For the Pt (110) single crystal electrode the main contribution is shown as a single wide peak at approximately 0.14 V. The intensity of the peak, measured in current density, is comparable with the intensity of the main contribution of the Pt (111) electrode. Finally, the analysis of the Pt (poly) electrode showed all the main contributions reported for the three Pt basal planes, including the peak at 0.15 V assigned to Pt (110) sites and a single peak at 0.23 V assigned to the presence of wide domains with (100) and (111) orientations. It is interesting to highlight that the current intensity of the Pt (110) contribution is relatively higher in comparison with the current density of the peaks assigned to the Pt (100) and Pt (111) contributions, while for the Pt (100) electrode the current intensity was very high. This behavior suggests that the sharp peak characteristic of the Pt (100) is very sensitive to the long-range order.

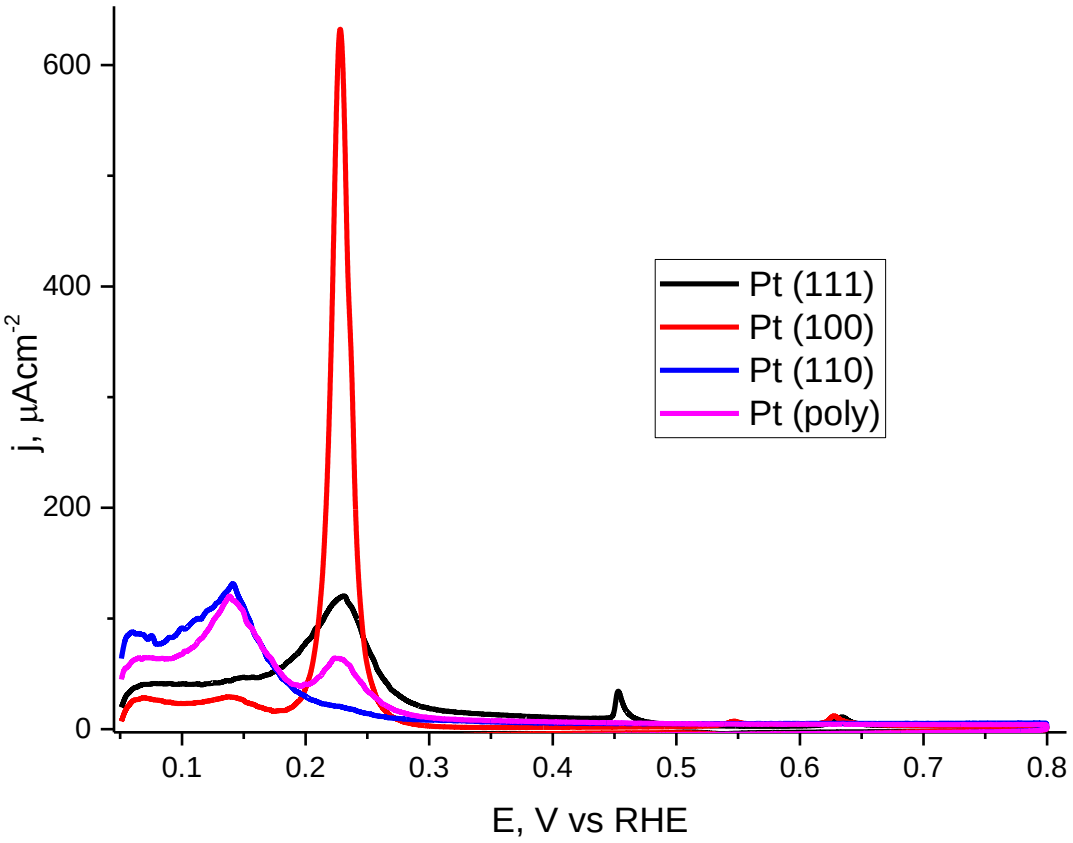

Figure 8-1. Voltammetric profile for the positive scan of basal plane of Pt single crystal and Pt polyfaceted electrode in 0.5 M HCl. Scan rate 50 mVs^{-1}.

Figure 8-2 shows, for the first time, the characteristic voltammetric profiles of the three evaluated shape-controlled Pt nanoparticles in 0.5 M HCl as supporting electrolyte. These Pt nanoparticles were previously cleaned using electrochemical oxidation of carbon monoxide (CO) monolayer, due to the tested evidence of its efficiency to achieve surface cleanliness.[35] In this particular case, the CO monolayer oxidation was performed in 0.5 M H_2SO_4, as previously reported. The effectivity of cleaning by using CO was confirmed by visualizing the sharpness, good definition, and symmetry of the adsorption states shown in the voltammetric profiles for all samples.

Unlike Pt single crystal electrodes, shape-controlled Pt nanoparticles are bound to have a higher number of different domains with a lower two-dimensional order. Thus, by comparing with the electrochemical behavior of the Pt basal planes, a first estimation of the presence of the different surface sites on the whole surface is provided.[36,37] Before the analysis in HCl, the three selected shape-controlled nanoparticles were previously examined in H_2SO_4, in order to confirm their surface structure.[28]

For each set of shape-controlled Pt nanoparticles, it is evident a characteristic behavior that makes their voltammetric profile be used as a fingerprint of their specific surface structure. However, for the particular case of Pt nano-octahedra, the case is not straightforward. An octahedra is ideally limited by (111) faces but edges should involve (110) sites. For these nanoparticles, the main contribution takes place at 0.14 V, due to the presence of (110) sites, but with a lower current density than the nanospheres. The low contribution from (111) sites, which is observed as a shoulder in the descending branch, at around 0.22 V, has to be related to the different long-range order present on single crystals and nanoparticles.

In contrast, preferential cubic Pt nanoparticles show two important contributions. The first contribution, centered at 0.150 V, is attributed to Pt (110) surface sites while the second one, which is a sharper peak with high current density at 0.23V is related to the presence of Pt (100) ordered domains as it is deduced from the potential at which the main contribution corresponding to the Pt (100) basal plane is reported. In addition, this peak could also be related to the presence of Pt (111) surface domains due to its location. However, Pt cubic structures are ideally enclosed

by six-(100) faces, thus the percentage of (111) in comparison with those (100) should be negligible.

Finally, the behavior of Pt nanospheres should be similar to that of a polyoriented surface. However, whereas the peak due to the (110) sites is the highest one, the peak due to the presence of both (100) and (111) sites is considerably lower. In fact, it is just a marked shoulder. Evidently, a Pt nanosphere is not a surface with virtually only (110) sites. The explanation for this behavior comes from the expected difference in long-range ordered domains. In a polyoriented Pt electrode, facets can be observed even with the naked eye, so much wider domains will be present in comparison with the nanospheres.

In summary, these voltammograms recorded at 0.5 M HCl can be used as a fingerprint of the specific surface structure of the evaluated shape-controlled Pt nanoparticles and can give an estimation of the different surface sites presented, in a similar way to that previously reported with H_2SO_4.[28]

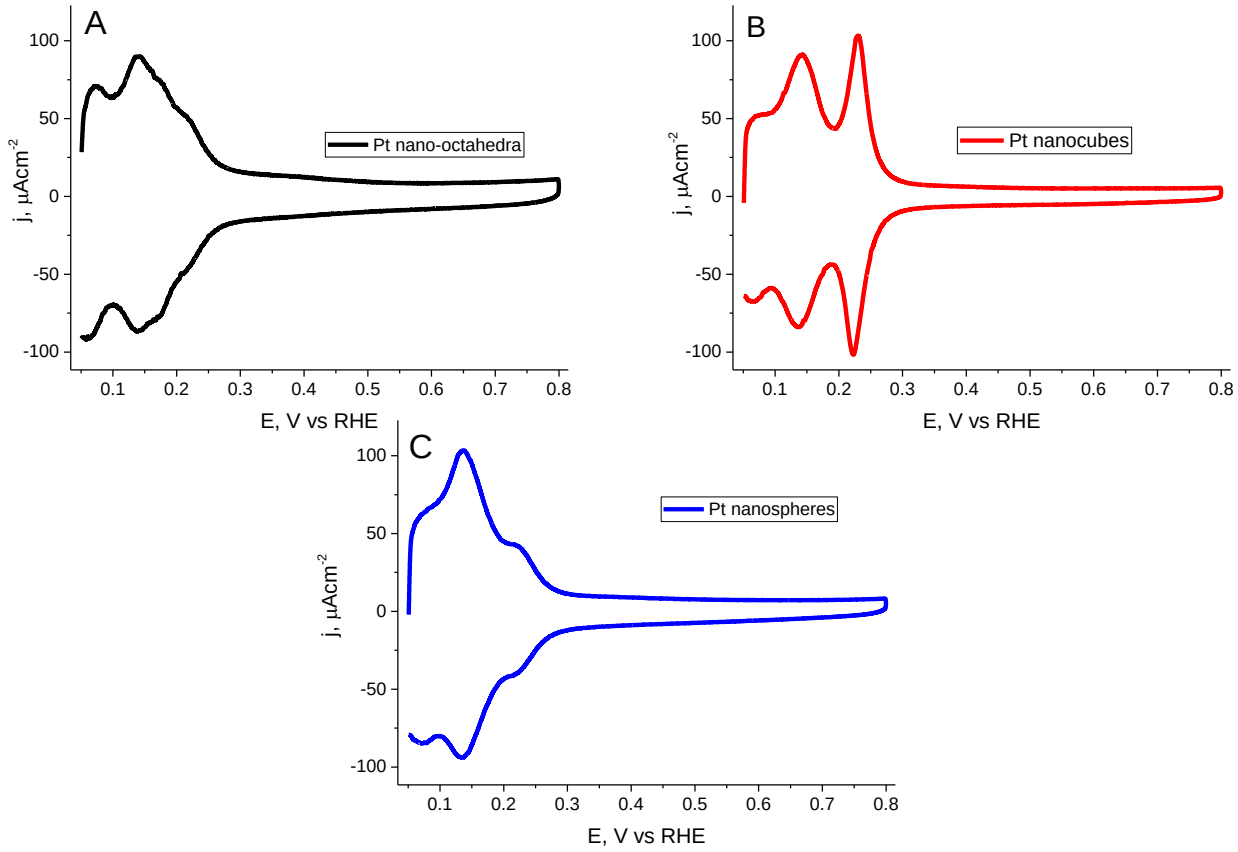

Figure 8-2. Voltammetric profiles for different shape-controlled Pt nanoparticles including (A) nano-octahedra (B) nanocubes and (C) nanospheres recorded in 0.5 M HCl. Scan rate: 50mVs^{-1}.

8.3.2. Evaluation of the electrochemical behavior of Pt single crystal electrodes under different HCl concentrations

The electrochemical behavior of the three Pt basal planes has been evaluated using different concentrations of HCl as supporting electrolyte and analyzing its influence in the voltammetric profiles. The evaluated HCl concentrations were similar to those used as a shape-directing agent in the synthesis of preferential cubic Pt nanoparticles with w/o microemulsion.[22] Figure 8-3 shows the corresponding

voltammograms for the Pt (100) basal plane electrode in different concentrations of HCl, increasing from 5 to 37 % w/w. It is evident the presence of two kinds of electrochemical behaviors with the increase of the Cl^- concentration. One of them implies the shift of the voltammogram to lower potentials and the second is the splitting of the main contribution, observed as a single peak at the lowest HCl concentration (5% wt) into two contributions, together with a decrease of the current intensity. The splitting of the main contribution into two different ones starts to be distinguishable when the concentration of HCl increases from 15% up to 37% and the potential difference steadily increases with the HCl concentration. This may be due to the presence of two different processes that should be related to the adsorption-desorption of weakly and strongly bonded H^+ or Cl^- on the Pt surface.[29] Also, another possibility could be the formation of adducts with the higher concentrations of HCl which are not been reported before, however could still as a hypothesis about the presence of another contribution.

In addition, the voltammetric profile of the Pt (100) electrode also shows two more characteristic small contributions in the so-called double layer region. These peaks are present at potentials between 0.3 V and 0.6 V and likely are due to phase transition on the adsorption Cl^- layer. With an increase of HCl concentration, these peaks also shows a displacement of potentials to lower values. The voltammetric profiles showed in the inset of the figure 8-3 show these peaks for the scan recorded at 20% HCl and the corresponding potentials obtained. As can be observed, both peaks show some irreversibility.

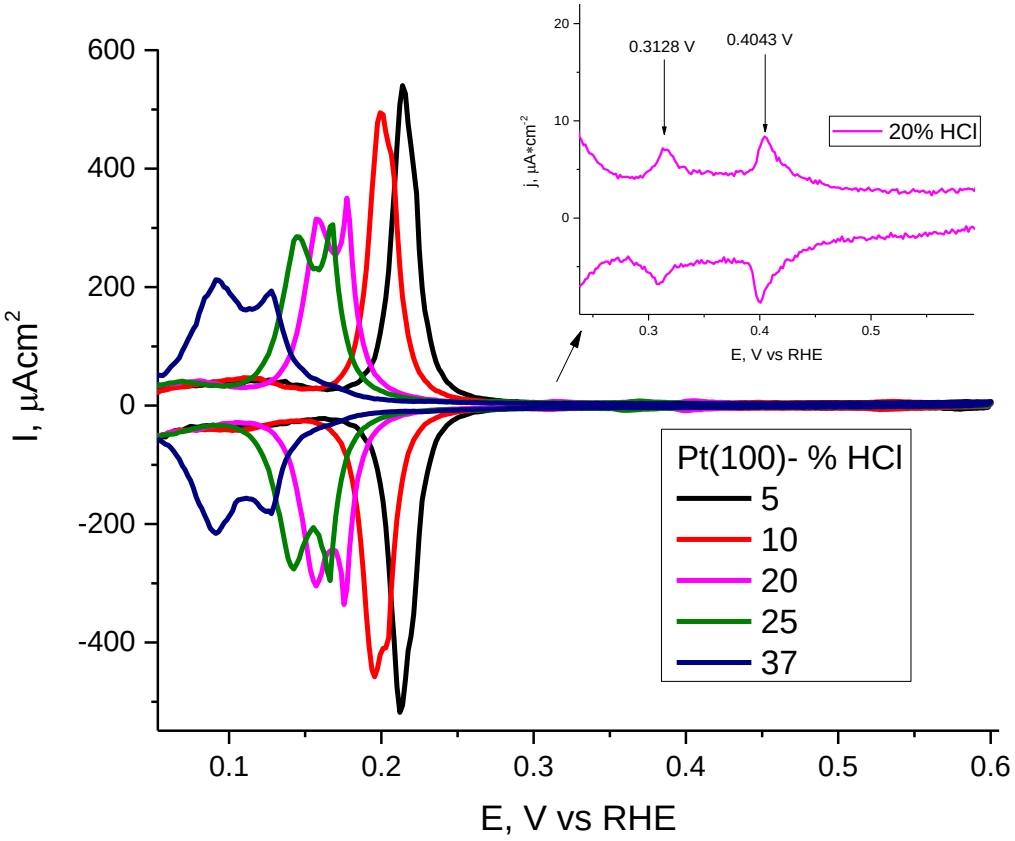

Figure 8-3. Voltammograms corresponding to the Pt (100) electrode in the presence of different concentrations of HCl at 50 mVs^{-1}. Inset: Zoomed image of the voltammetric region from 0.24 V to 0.59 V for the scan recorded with 20% HCl.

Figure 8-4 shows the plots of peak potentials values versus the logarithmic value of the H_2SO_4 activity. The slope of the graphical representation provides the value of the Esin-Markov coefficient related to the cross differentiation of the electrocapillary equation. This equation, as previously established, is determined by the number of electrons flowing to the electrode per adsorbed species at a constant potential, and at constant chemical potential.[33,38] For all the contributions reported in this particular case, a linear plot with a negative slope was obtained. The first two

linear plots (peak 1 and 2) are related to the contribution that splits into two peaks with the increase of HCl concentration. Both contributions (peaks 3 and 4) got similar values, maybe related to the adsorption of the same species as for the analogous case of Pt (111) evaluated in sulfate solutions by N. Garcia-Araez et al. (2008) [33], who found that both contributions showed a similar behavior obtaining the same Esin-Markov coefficient values from the graphical representation.

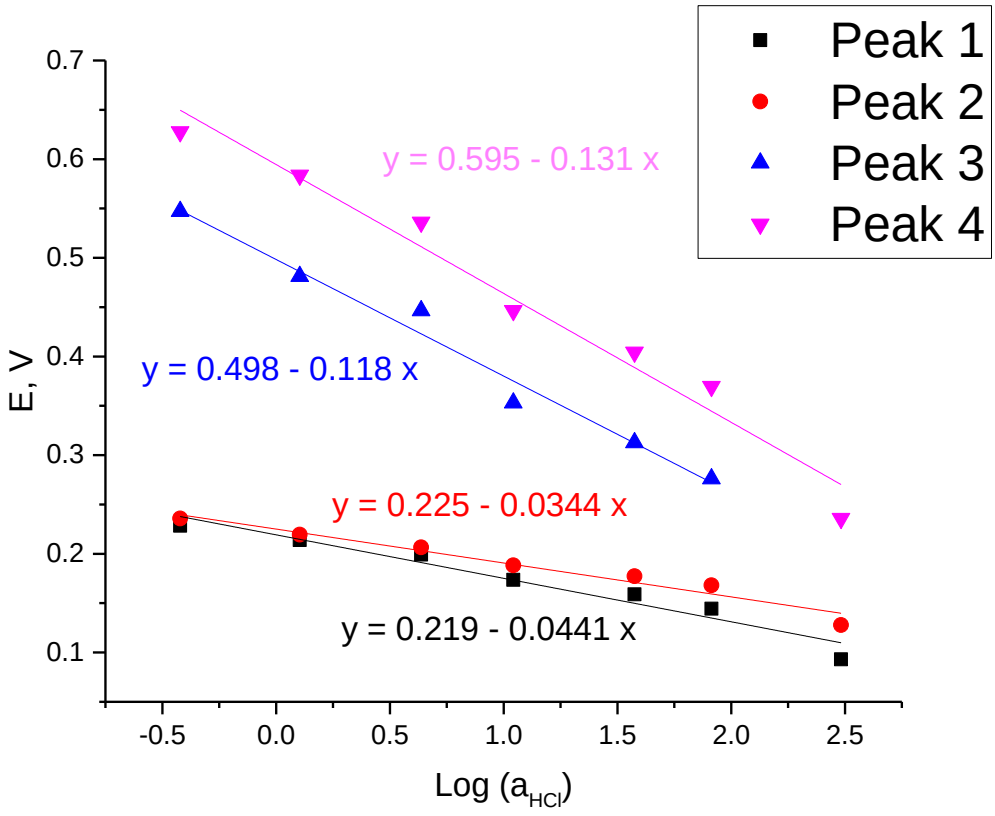

Figure 8-4. Graphical representation of the potential (V) of the different peaks observed for the Pt (100) versus the Log (a_{HCl}).

Pt (111) also shows a characteristic electrochemical behavior influenced by the different concentrations of HCl evaluated (figure 8-5 (A)). As in the case of the Pt (100),

four different contributions are observed. The interesting electrochemical behavior reported in this basal plane is based in the increase of the intensity of the two main contributions (peaks 1 and 2) with increasing the HCl concentration which is the opposite electrochemical behavior observed for the Pt (100) electrode. Figure 8-5 (B) shows the plot of the potential of the peaks versus the logarithmic value of HCl activity. In this case we have found that both peaks 1 and 2 have the same Esin-Markov coefficient that may be related to the adsorption of the same species, as previously reported for the Pt (100) plot. The last two small contributions do not show any remarkable electrochemical behavior.

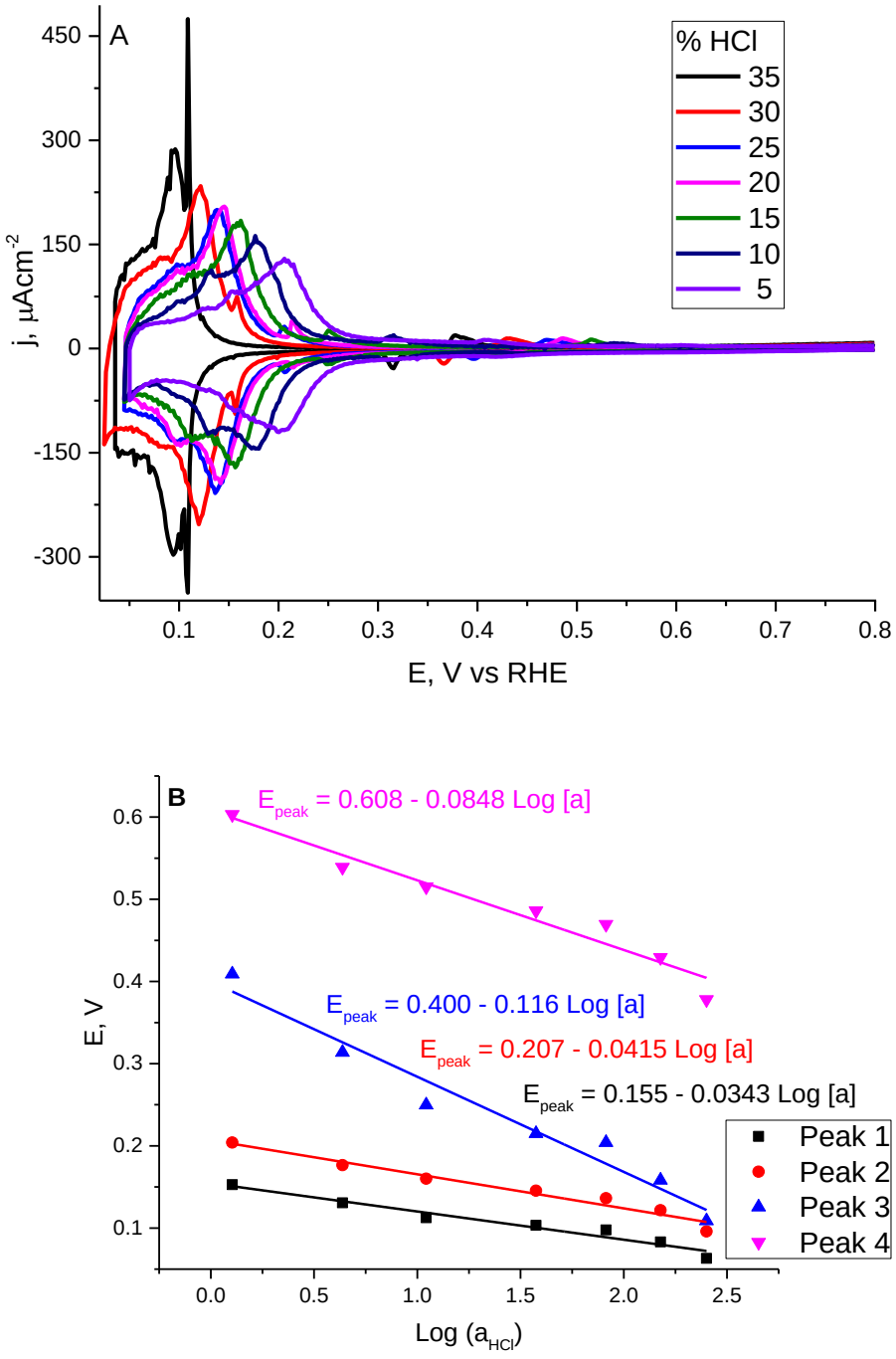

Figure 8-5. (A) Voltammetric profiles of Pt (111) electrode with different concentrations of HCl recorded at 50 mVs^{-1} and (B) plots of the corresponding potential of the maximum of each contribution detected in function of the Log (a_{HCl}).

Finally, Pt (110) and Pt (poly) electrodes show no significant changes in the voltammetric profiles when the electrochemical behavior under the influence of different concentrations of HCl (Figure 8-6) is analyzed. Only the shift of all the contributions to lower potentials as the concentration of HCl increases was noticed.

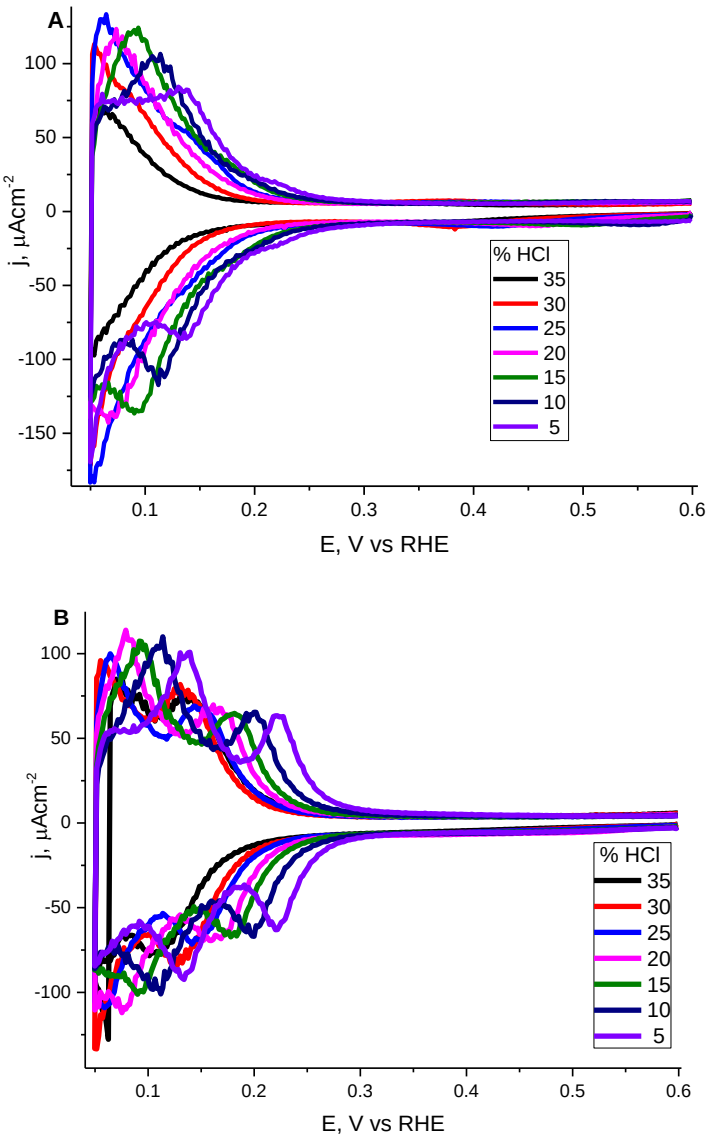

Figure 8-6. Voltammetric profiles of (A) Pt (110) single crystal and (B) Pt (poly) electrodes at different concentration of HCl. Scan rate 50 mV s^{-1}.

8.3.3. Evaluation of the electrochemical behavior of Pt single crystal electrodes under different concentrations of H_2SO_4

By studying the electrochemical behavior under different concentrations of H_2SO_4 as supporting electrolyte, it is observed, that Pt (111) showed the most interesting behavior in terms of a change of the contributions corresponding to the well-known sulfate adsorption region, previously studied.[28,30,32-34] At lower concentrations of H_2SO_4 (5% w/w), the electrochemical behavior is similar to that previously reported in 0.5 M H_2SO_4 [28], in which the main feature is the presence of a voltammetric sharp spike near 0.45 V, corresponding to the phase transition after completion of the main sulfate (SO_4^{-2}) adsorption process. Also, a small feature appearing at potentials higher than that of the spike is shown and called “the hump” as previously reported.[30,32]

By looking at the figure 8-7 (A) some effects on Pt (111) can be observed with the increase of H_2SO_4 concentration, including a shift of all the contributions towards lower potential, the presence of a new denotable contribution in the sulfate adsorption region which starts to be appreciable from 10% H_2SO_4 and the consecutive increase of its current intensity. The presence of the new contribution reported may be attributed to the sulfate (SO_4^{-2}) adsorption process which exhibits a subtle dependence on pH, as previously reported.[32,33] In the voltammetric profile corresponding to the 20% of H_2SO_4, the new contribution reaches a higher current intensity to that obtained by the voltammetric spike reported in the same scan. From there, the new contribution increases the current intensity consecutively until the percentage reaches the maximum evaluated (70% H_2SO_4).

Figure 8-7 (B) shows the plots peak potentials values versus the logarithmic value of the H_2SO_4 activity. In this graphical representation the peak 1 (main) and the peak 2 (spike) are parallel, consequently, it can be concluded that both features involve SO_4^{-2} adsorption. Another fact is associated to the increase of the slope (in absolute value) that could be related to that charge density is lower in these solution compositions, and the condition of constant charge may not be fully satisfied in this concentration range.

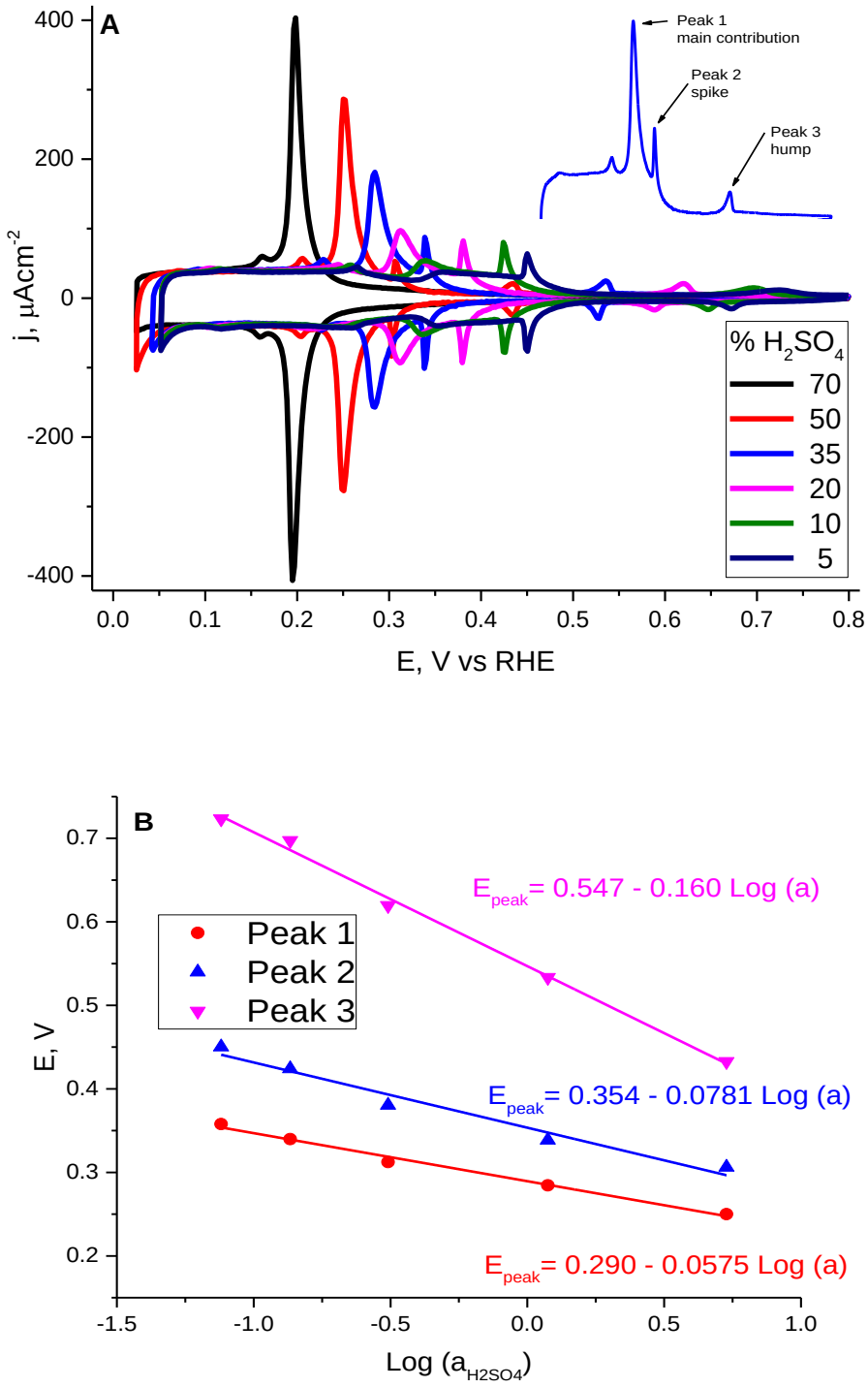

Figure 8-7. (A) Voltammetric profiles of Pt (111) electrode tested with different concentrations of H_2SO_4 at 50 mV s^{-1} and (B) Peak potential values of the contributions assigned to Pt (111) versus Log (a_{H2SO4}).

The characteristic behavior of Pt (110) with respect to the main contribution showed for this kind of single crystal, was also evaluated and the results are summarized in figure 8-8. At higher concentrations, it is noticeable the enlargement of the peak which probably corresponds to the split of two different contributions. In fact, at the highest concentrations, the presence of a shoulder in the descending branch of the main peak becomes quite clear. In terms of current intensity, a slight increase is observed when the electrolyte concentration increases from 5 to 35 %, after which decreases, especially in the case of 70 %, for which a significant decrease of the current intensity is observed.

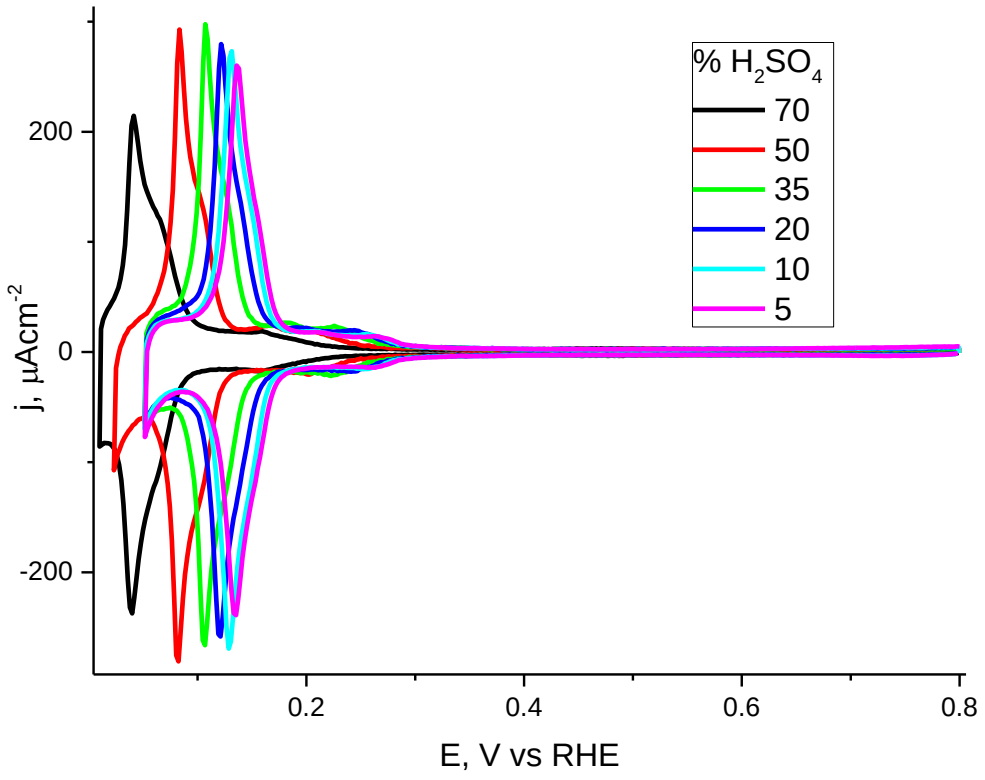

Figure 8-8. Voltammetric profiles of the Pt (110) single crystal electrode in the presence of different concentration of H_2SO_4.

Finally, for Pt (100) and Pt (poly) electrodes, only a displacement to lower potentials with the increase of H_2SO_4 concentration was reported as seen in figure 8-9. In the particular case of the Pt (100) electrode (figure 8-9 A), only small changes in the current density with no significative pattern were observed. It is also interesting to highlight that the small peak due to the presence of small fraction of (100) terrace border sites contribution shifts with the increase of the H_2SO_4 concentration in a higher degree than that due to (100) terraces (main peak). For the Pt (poly) electrode only three main contributions appear, the same as shown by testing the basal plane electrode in 0.5 M H_2SO_4.

Unfortunately, a deep analysis would be much more complicated as it could be for nanoparticles having all type of sites. As for the other defects, with increasing the H_2SO_4 concentration, the peaks shift to lower potentials. For the CV of 70% H_2SO_4, the concentration which takes place at a lower potential is not observed, as it overlaps with the hydrogen evolution. In addition, for the highest concentration more small contributions can be observed. This effect is clearly the result of a complex change of interactions in the adsorbed layer, taking into account the previous results for the three Pt basal planes and the fact that a polyoriented surface has contributions from all those three and also other from stepped and hinked surface-sites.

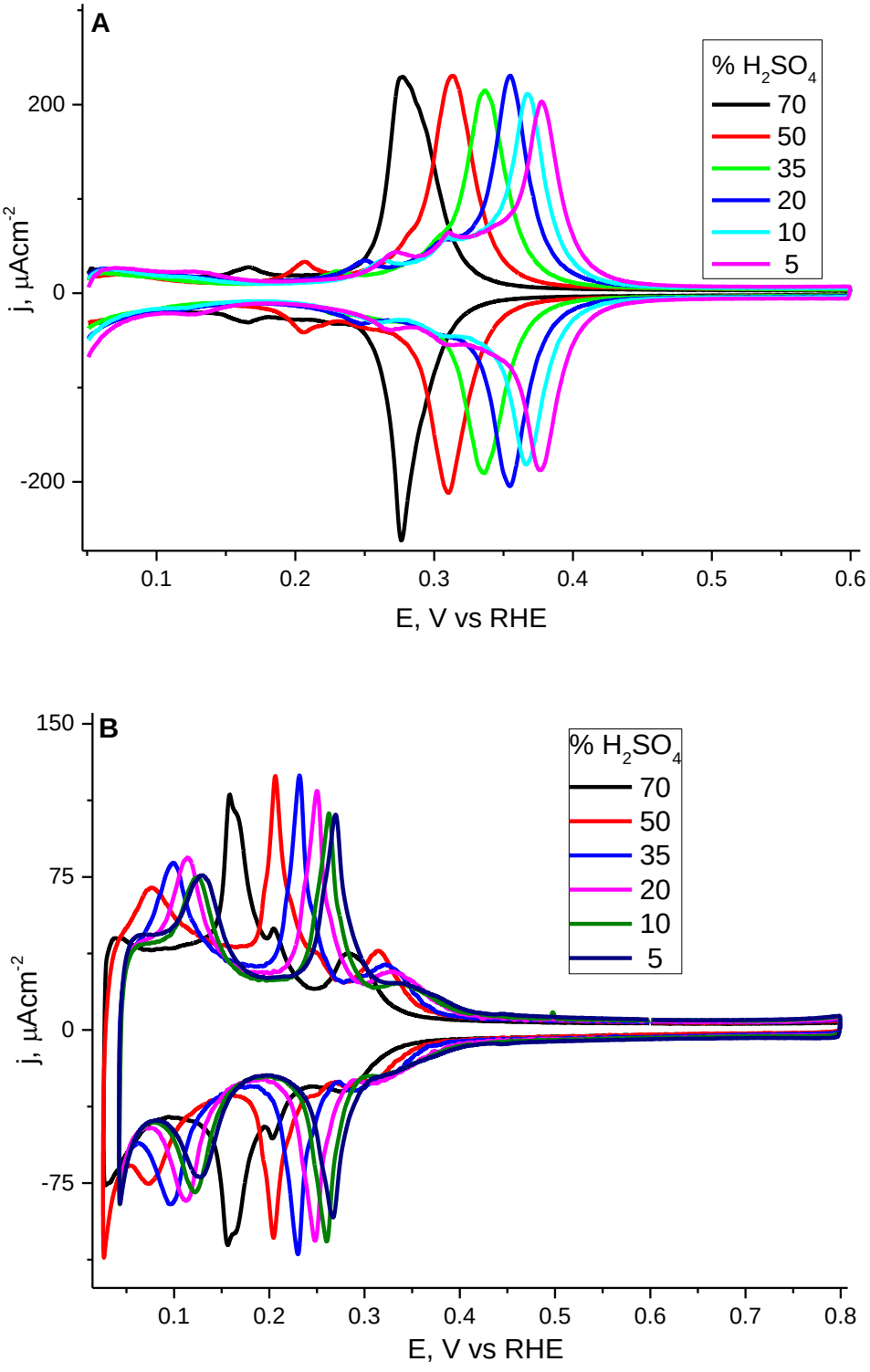

Figure 8-9. Voltammetric profiles of the (A) Pt (100) and (B) Pt (poly) electrodes in the presence of different concentrations of H_2SO_4.

8.3.4. Evaluating the presence of lower concentrations of HCl in $HClO_4$

A preliminary study about the Cl^- adsorption was prepared to observe their influence in $HClO_4$ as supporting electrolyte. The experiment consisted in comparing the voltammetric profiles of the Pt (100) electrode in 0.1 M $HClO_4$ with another scan in which a small concentration of HCl ($1x10^{-3}$ M) was added intentionally. As can be observed in figure 8-10, four different voltammetric profiles of Pt (100) were obtained. The first voltammogram (black line) corresponds, to the first scan of the Pt (100) in 0.1M $HClO_4$. This profile shows a similar electrochemical behavior to that reported by Rodes et al. (1991).[39] In this voltammogram only a small hydrogen state is reported near 0.30 V. At the same time the main adsorption state, centered at 0.36 V, presents a shoulder at 0.41 V, and the wide adsorption state spreading up to 0.70 V. An increase of the positive potential limit up to 1.3 V allows the observation of a well-marked oxygen adsorption peak near to 1.025 V preceded by a sharp small peak at 0.980 V, as previously reported.[39] The second scan performed (red line) shows the similar behavior to that discussed for the first scan but in this case, the main adsorption state presents lower current intensity, which may be assigned to the surface modification by reaching higher oxidation potentials. The oxygen adsorption peak obtained also shows a lower current intensity to that obtained in the first scan.

When a small amount of HCl was added to the $HClO_4$, a new voltammogram was recorded with the clean Pt (100) electrode. The first scan (blue line) shows that the hydrogen adsorption-desorption region, as well as the double-layer region, becomes similar to the voltammogram for Pt (100) in 5% HCl (figure 8-3). The sharp peak in the hydrogen region, observed in the positive sweep, is probably caused by the simultaneous rapid adsorption of Cl^- and the desorption of hydrogen, as previously

observed by similar experiment prepared by N. Markovic et al. (1986). [29] After adsorption process occurs, Cl^- diffuses away from the surface and then re-adsorbs slowly under diffusion control simultaneously with H desorption during the negative sweep potential, obtaining a peak with lower current intensity product from the mentioned process. The most significative change was observed in the oxygen region where the oxidation current peak shift to the positive direction around 200 mV in comparison to that observed without the Cl^- solution. In the negative-going potential scan only one reduction current peak is observed around 0.81 V with smaller intensity which is assigned to the reduction of Pt oxide formed in positive-going potential scan. It is obvious that the oxygen adsorption in the presence of chloride ions in solution is drastically inhibited.

A similar study performed with bromide ions showed also a similar electrochemical behavior and Xu C. D et al. (2015) [21] related to the Br^- oxidation/adsorption and $(Br_2)_{ad}$ reduction, respectively, together with oxygen adsorption and Pt oxide reduction. Analogous to that observation, this behavior is assigned obviously to the Cl^- oxidation/adsorption and $(Cl_2)_{ad}$ reduction, respectively. These preliminary experiments determined that HCl could protect the Pt (100) long-range ordered structure by inhibition of oxygen adsorption. This confirms newly the chlorides ions preference to the Pt (100) surface sites which advantage the Cl^- adsorption-desorption process and consequently adsorbed ions influence over the structure surface of the shape-controlled nanoparticles.

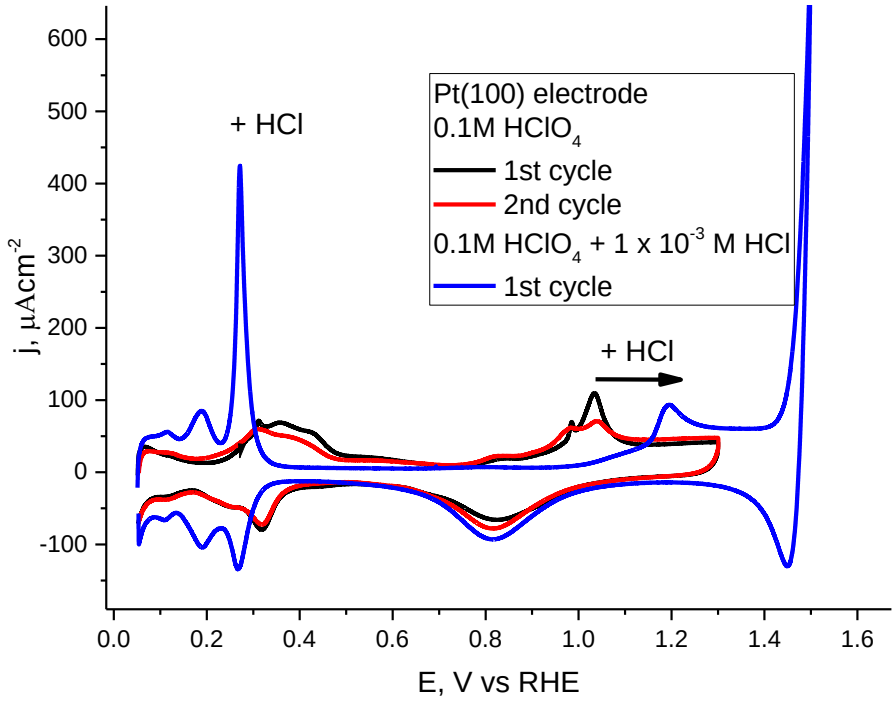

Figure 8-10. Cyclic voltammograms of Pt (100) electrode recorded in 0.1 M $HClO_4$ (black and red lines) and 0.1 M $HClO_4$ +1 mM HCl (blue line) solutions.

8.5. Conclusions

The electrochemical behavior of the three Pt basal planes are reported by using HCl and H_2SO_4 as supporting electrolytes. In addition, we have reported for the first time the electrochemical behavior of three different shape-controlled Pt nanoparticles in 0.5M HCl which could be used as a fingerprint profiles for the selected nanostructures. The analysis for the electrochemical behavior of the Pt basal planes electrodes using higher concentrations of HCl and H_2SO_4 as supporting electrolytes, confirmed in some extent a preferential adsorption of the Cl^- over the Pt (100). This research brings some preliminary results to understand the electrochemical behavior of the three main Pt basal plane electrodes under the presences of high concentrations

of chlorides and (bi)sulfate/sulfate ions. For the particular case of the Pt (100) electrode, a characteristic electrochemical response was observed under the influence of HCl concentrations similar to those used to synthesize shape-controlled Pt nanoparticles as previously reported. Also, this behavior confirms that well-ordered Pt (100) surface is strongly sensitive to the presence of Cl^- ions. For the analysis of the three Pt basal planes tested in the presence of high concentrations of H_2SO_4, it can be concluded that it is the Pt (111) the most influenced surface and that for all cases an increase of the acid concentration involves a shift of the different contribution towards more negative potentials.

In conclusion, a deeper experimental analysis is still necessary to reach some conclusions about the mechanism of how both acids induce the formation of shape-controlled Pt nanoparticles.

8.6. References

1. Wieckowski, A., Savinova, E. R., and Vayenas, C. G. (2003). *Catalysis and Electrocatalysis at Nanoparticle Surfaces* (Marcel Dekker, New York).
2. Vielstich, W., Lamm, A., and Gasteiger, H. (2003). *Handbook of Fuel Cells: Fundamentals*, *Technology and Applications* (John Wiley & Sons Ltd., Chichester, UK).
3. Zhang, J. (2008). *PEM Fuel Cell Catalysts and Catalyst Layers — Fundamentals and Applications* (Springer-Verlag London Ltd., London, UK).
4. Zhang, J., and Liu, H. (2009) *Electrocatalysis of Direct Methanol Fuel Cells*, (Wiley-VCH Verlag GmbH & Co. KGaA, Weinheim, Germany).
5. Koper, M. T. M. (2009) *Fuel Cell Catalysis: A Surface Science Approach*,
6. (John Wiley & Sons, Inc., Hoboken, EEUU).
7. Solla-Gullón, J.; Vidal-Iglesias, F.J.; Herrero, E.; Feliu, J.M.; Aldaz, A. Polymer Electrolyte Fuel Cells: Science, Applications, and Challenges, Chapter 3: Electrocatalysis on Shape-Controlled Pt Nanoparticles, ed. Alejandro A. Franco, Pan Stanford Publishing Pte. Ltd 2013.
8. Attard, G.A.; Jenkins, Ye. P. Vidal-Iglesias, F. J.; Herrero, E. & Sun, S.G. *J. Electroanal. Chem*. **2013**, 688, 249-256.
9. El Sayed, M. A.; Yoo J.W. *ChemCatChem*. **2010**, 2, 268-271.
10. Lacroix, L. M.; Gatel, C.; Arenal, R.; Garcia, C. Lachaize, S.; Blon, T.; Warot-Fonrose, B.; Snoeck, E.; Chaudret, B. & Viau, G. *Angew. Chem. Int.* **2012**, 51, 4690-4694.
11. Kim, C.; Kim, S.; Yang, S.; Han, J.W. & Lee, H. *Chem. Commun.* **2012**, 48, 6396-6398.
12. Ma, M.; Zhang, Y.; Gu, N. *Colloids Surf.* **2011**, 373, 6-10.

13. Pham Minh, D.; Oudart, Y.; Baubet, B.; Verdon, C.; Thomazeau, C. *Oil & Gas Science and Technology-Rev. IFP.* **2009**, 64, 697-706.
14. Chiu, C.-Y.; Wu, H.; Yao, Z.; Zhou, F.; Zhang, H.; Ozolins, V.; Huang, Y. *J. Am. Chem. Soc*. **2013**, 135, 15489-15500.
15. Alayoglu, S.; Aliaga, C.; Sprung, C.; Somorjai, A. *Catal. Lett.* **2011**, 141, 914-924.
16. Ahmadi, T. S.; Wang, Z. L.; Green, T. C.; Henglein, A.; El-Sayed, M.A. *Science* **1996**, 272, 1924-1926.
17. Ahmadi, T. S.; Wang, Z. L; Henglein, A.; El-Sayed, M.A. *Chem. Mater.* **1996**, 8, 1161-1163.
18. Zhang, H.; Bo, X.; Guo, L. *Electrochimica Acta* **2016**, 201, 117-124.
19. Komanicky, V.; Iddir, H.; Chang, K. C.; Menzel, A.; Karapetrov, G.; Hennesey, D. C.; Zapol, P.; You, H. *Electrochimica Acta* **2010**, 55, 7934-7938.
20. Breitter, M.W. *Electrochimica Acta* **1963**, 8, 925-935.
21. Deng-Xu, C.; Ye, J.-Y.; Chen, L.; Chen, D.H.; Li, J.T.; Zhen, C.H. *Electrochimica Acta,* **2015**, 162,129-137.
22. Michel, J.A.; Morris, W. H. Lukehart, C. *J. Mater. Chem. A* **2015**, 3, 2012-2018.
23. Martínez-Rodríguez, R.A.; Vidal-Iglesias, F.J; Solla-Gullón, J.; Cabrera, C.R.; Feliu, J.M. *J. Am. Chem. Soc*. **2014**, 136, 1280-1283.
24. Martínez-Rodríguez, R.A.; Vidal-Iglesias, F.J; Solla-Gullón, J.; Cabrera, C.R.; Feliu, J.M. *ChemPhysChem.* **2014**, 15, 1997-2001.
25. Martínez-Rodríguez, R.A.; Vidal-Iglesias, F.J; Solla-Gullón, J.; Cabrera, C.R.; Feliu, J.M. *ChemElectroChem.* **2016**, 3, 1601-1608.
26. Solla-Gullon, J.; Rodes, A.; Montiel, V.; Aldaz, A.; Clavilier, J. *J. Electroanal. Chem.* **2003**, 554-55, 273-284.

27. Clavilier, J.; Armand, D.; Sun, S.G. & Petit, J. *J. Electroanal. Chem.* **1986**, 205, 267.

28. Rodes, A.; El Achi, K..; Zamackhchari, M.A. & Clavilier, J. *J. Electroanal. Chem*. **1990**, 284, 245-253.

29. Solla-Gullón, J.; Rodríguez, P.; Herrero, E.; Aldaz, A.; Feliu, J.M*. Phys. Chem. Chem. Phys.* **2008**, 10,1359-1373.

30. Markovic, N.; Hanson, M.; McDougall, G.; Yeager, E. *J. Electroanal. Chem.* **1986**, 214, 555-566.

31. García-Araez N.; Lukkien J.J.; Koper M.T.M.; Feliu J.M. J. *Electroanal. Chem.* **2006**, 588, 1-14.

32. García-Araez, N.; Climent, V.; Rodríguez, P. and Feliu, J. M. *Phys. Chem. Chem. Phys.* **2010**, 12, 12146-12152.

33. García-Araez, N.; Climent, V., Orts, J. M., Feliu, J. M., & Aldaz, A. *ChemPhysChem.* **2004**, 5, 1221–1227.

34. García-Araez, N.; Climent, V.; Rodríguez, P. and Feliu, J. M. *Electrochimica Acta* **2008**, 53, 6793–6806.

35. García-Araez, N.; Climent, V.; Rodríguez, P. and Feliu, J. M. *Langmuir* **2010**, 26, 12408-12417.

36. Feliu, J.M.; Solla-Gullón, J.; & Vidal-Iglesias, F.J.; Rodríguez, P.; Herrero, E.; Aldaz, A. (2006). Shape-Dependent Electrocatalysis: CO Monolayer Oxidation at Platinum Nanoparticles. ECS Meeting Abstracts. 501. 1541-1541.

37. Rodes, A.; Elachi, K.; Zamakhchari, M. A.; Clavilier, J. *J. Electroanal. Chem.* **1990**, 284, 245−253.

38. Clavilier, J.; Elachi, K.; Rodes, *A. Chem. Phys.* **1990**, 141, 1−14.

39. Trasatti, S., & Parsons, R. *Pure and Applied Chemistry* **1986**, 58, 437–454.

40. A. Rodes, A.; Zamakhchari, M.A.; El Achi, K.; Clavilier J., *J. Electroanal. Chem.* **1991**, 305, 115-129.

Chapter 9.

General conclusions and remarks

In this research thesis, the synthesis of shape-controlled Pt nanoparticles and their applications towards NH_3 oxidation in alkaline media have been addressed. For the first of these purposes, the effect of different acids examined in different concentrations as shape directing agents has been widely evaluated, in order to optimize the current methods in which shape-controlled nanoparticles have been prepared. Specifically, we have focused on the preparation of cubic nanoparticles, which are ideally the most active for the NH_3 oxidation.

The first part of the present Ph. D thesis (Chapters 4, 5 and 6) includes the publication of a new development of a fast, easy, room-temperature and scalable procedure for the synthesis of preferentially cubic Pt nanoparticles based on the reduction by $NaBH_4$ of a w/o microemulsion used as a shape-directing agent. **Chapter 4** evaluated the use of HCl for this purpose. The control over the percentage of HCl was the key point to obtain shape-controlled Pt nanoparticles. The optimal amount of HCl was found to be between 15 and 25%, after which the samples showed a decrease in the number of (100) wide domains as well as bone-like shapes. The electrocatalytic activity was tested towards NH_3 oxidation and the activity reported was about six times higher for the preferentially cubic Pt nanoparticles synthesized with 25 %HCl in comparison with the Pt nanoparticles synthesized with no shape-directing agent.

In **Chapter 5,** the use of H_2SO_4 as a shape-directing agent was evaluated. In this particular case, shape-controlled Pt nanoparticles obtained a particle size of 9 nm, relatively smaller to those synthesized with HCl, which had a mean particle size of 14 nm. The nanoparticles with the higher percentage of cubic structures contained approximately 50% (100) surface sites, 35% of which were wide surface domains, as determined by using the electrochemical Ge adsorption/desorption method. For this

sample, CO and NH_3 electro-oxidations were evaluated and confirmed that Pt nanoparticles prepared with 25% H_2SO_4 obtained the highest catalytic performance for these structure-sensitive reactions.

Chapter 6 summarizes the results obtained by using different acid of shape directing agents including hydrogen halides (HBr and HI), multiprotic acid (H_3PO_4) and several organic modifiers (citric acid, ascorbic acid, and oxalic acid). In addition, the effect of changing the Pt precursor from H_2PtCl_6 to K_2PtCl_4 was also evaluated with the modifiers giving the best results with the previous Pt salt (HCl and H_2SO_4). HBr, as in the case of HCl, gave preferentially cubic Pt nanoparticles as confirmed by CV and TEM analysis. Conversely, HI-modified Pt nanoparticles did not show any preferential surface structure. From the results of the evaluation of using H_3PO_4 as a surface modifier, only a minor structural modification was observed, with an increase of the percentage of (100) sites, in comparison with a polyoriented surface. Evidently, this enhancement was poorer than those obtained with H_2SO_4 as a surface modifier. In the other hand, the evaluated organic modifiers only showed a very small increase in the number of (111) sites. Finally, by testing the effect of K_2PtCl_4 as Pt precursor, similar improvements those reported with H_2PtCl_6 toward the synthesis of preferentially cubic Pt nanoparticles. In this work the nanoparticles with the highest amounts of (100) sites were tested for NH_3 electrooxidation and, as expected, its highest percentage of this type of site, the highest catalytic performance was obtained with the 15% HCl-modified Pt nanoparticles prepared with K_2PtCl_4 as Pt precursor.

The second part of this Ph. D. thesis has reports experimental results which have not been yet published including the synthesis of shape-controlled bimetallic nanoparticles and a fundamental electrochemical study using Pt single crystal electrodes. In **Chapter 7**, the synthesis of shape-controlled Pt/Rh bimetallic

nanoparticles with different ratios was successfully performed by using different acids to evaluate the surface modifier effects. In addition, the evaluation of the effect of using K_2PtCl_4 instead of H_2PtCl_6 was performed to compare the structural effects involved by changing the Pt precursor. Physical analysis, including TEM as well as the evaluation of the atomic composition by EDX, reported some shaped-controlled nanostructures with a composition close to the nominal values expected from the synthesis conditions. For the evaluation of the electrocatalytic performance, Pt_{75}/Rh_{25} and Pt_{90}/Rh_{10} showed interesting results in terms of the displacement of the onset potential to lower values for NH_3 oxidation and the highest current densities for ethanol oxidation.

Finally, **Chapter 8** shows the electrochemical behavior of the three Pt basal planes in electrolytes having the same concentrations of the acid modifiers used for the synthesis of preferentially cubic nanoparticles. The voltammetric showed to be structure sensitive. This study was extended to different shape-controlled Pt nanoparticles for the first time. As in dilute H_2SO_4, the CV's in HCl can be used as fingerprint and qualitatively about the nanoparticles surface structure. In order to understand why preferentially cubic nanoparticles are formed, a further experimental analysis is required to reach some conclusions about the mechanism on how both acids can induce modification over the surface structure of the Pt nanoparticles.

This Ph. D. research thesis is one of the first steps into the development of new methods to make nanomaterials accessible to any type of applications including the development of new technologies. For the particular case of NH_3 oxidation, the work performed in this research thesis has been successfully achieved for many applications to the development of new technology linked to this topic. One of them, has been related to the preparation of working electrodes for microbial half-cell alkaline

systems prepared in collaboration with Myreisa Morales Ph. D. and in a project related to the study of this material under the influence of non-gravity effects (See Annex I) in a prepared Direct Alkaline Ammonia Fuel Cell (DAAFC). Finally, they are currently being employed in the collaboration to develop an experimental box to be taken to the International Space Station (ISS), to study NH_3 oxidation in microgravity conditions (See Annex II). Hopefully, this research will continue in the search of new applications and the study to further develop in the field of nanotechnology.

ANNEXES

ANNEX I.

Chronoamperometric Study of Ammonia Oxidation in a Direct Ammonia Alkaline Fuel Cell under the Influence of Microgravity

Microgravity Sci. Technol. (2017) 29:253–261
DOI 10.1007/s12217-017-9543-z

ORIGINAL ARTICLE

Chronoamperometric Study of Ammonia Oxidation in a Direct Ammonia Alkaline Fuel Cell under the Influence of Microgravity

Raul Acevedo[1] · Carlos M. Poventud-Estrada[1] · Camila Morales-Navas[2] · Roberto A. Martínez-Rodríguez[2] · Edwin Ortiz-Quiles[2] · Francisco J. Vidal-Iglesias[3] · José Sollá-Gullón[3] · Eduardo Nicolau[2] · Juan M. Feliu[3] · Łuis Echegoyen[4] · Carlos R. Cabrera[2]

Received: 19 May 2016 / Accepted: 6 March 2017 / Published online: 13 April 2017

Abstract This is a study of the chronoamperometric performance of the electrochemical oxidation of ammonia in an alkaline fuel cell for space applications. Under microgravity the performance of a fuel cell is diminished by the absence of buoyancy since nitrogen gas is produced. The following catalysts were studied: platinum nanocubes of ca. 10nm, platinum nanocubes on carbon Vulcan™ and platinum on carbon nanoonion support of ca. 10nm. These nanomaterials were studied in order to search for catalysts that may reduce or counter the loss of ammonia oxidation current densities performance under microgravity conditions. Chronoamperometries at potential values ranging from 0.2 V to 1.2V vs. cathode potential (breathing Air/300ml/min/82737 Pa) in 1.0 M NH_4OH (30ml/min in anode) were done during over 30 parabolas in NASA's C9 airplane The Weightless Wonder in January 2016 from Ellington Field Houston. The current densities at 15s in the chronoamperometry experiments showed diminishing values under microgravity and in some cases improvements of up to 92%, for Pt-carbon nanoonions, and over 70% for the three catalysts versus ground at potentials ranging from 0.2 to 0.4V after 5 minutes of chronoamperometric conditions. At higher potentials, 1.0V or higher, Pt nanocubes and Pt-carbon nanoonions showed enhancements of up to 32% and 24%, respectively. At these higher potentials we will have a contribution of oxygen evolution. The changes in current behavior are attributed to the sizes of the catalyst materials and the time needed for the N_2 bubbles detachment from the Pt surface under microgravity conditions.

Keywords Ammonia oxidation · Bubble · Platinum nanoparticles · Microgravity · Carbon nanoonions

Carlos R. Cabrera
carlos.cabrera2@upr.edu

[1] Department of Physics, University of Puerto Rico, San Juan, Rio Piedras, 00931, Puerto Rico

[2] Department of Chemistry, University of Puerto Rico, San Juan, Rio Piedras, 00931, Puerto Rico

[3] Institute of Electrochemistry, University of Alicante, E-03080, Alicante, Spain

[4] Department of Chemistry, University of Texas at El Paso, El Paso, Texas, 79968-8807, USA

Introduction

Fuel cells have been previously researched for various applications: proton electrode membrane fuel cells (Radenahmad et al. 2016), microbial fuel cells (de Vet and Rutgers 2007; Kannan and Kumar 2016), and alkaline fuel cells (Bayer et al. 2016) and have been used successfully in space applications since the Apollo missions (Warshay and Prokopius 1989). Hydrogen and methanol are commonly used in fuel cells.

Ammonia for fuel cells is cheap, its output produces water and nitrogen (clean fuel) and it is manufactured and stored on an industrial scale (Radenahmad et al. 2016; Erisman et al. 2008; Afif et al. 2016). Ammonia fuel cells have been proposed in a two-step process where the ammonia first is cracked into hydrogen and then used in a fuel cell (Cheddie 2012).

However, ammonia can be used as a fuel in a direct ammonia alkaline fuel cells, without the cracking step. The

most accepted mechanism for the oxidation of ammonia was presented by Gerischer and Mauerer (1970):

$$NH_{3(aq)} \rightarrow NH_{3,ads} \quad (1)$$

$$NH_{3,ads} + OH^- \rightarrow NH_{2\ ads} + H_2O + e^- \quad (2)$$

$$NH_{2,ads} + OH^- \rightarrow NH_{ads} + H_2O + e^- \quad (3)$$

$$NH_{x,ads} + NH_{y,ads} \rightarrow N_2H_{x+y,ads} \quad (4)$$

$$N_2H_{x+y,ads} + (x+y)OH^- \rightarrow N_2 + (x+y)H_2O + (x+y)e^- \quad (5)$$

$$NH_{ads} + OH^- \rightarrow N_{ads} + H_2O + e^- \quad (6)$$

As it can be seen in the mechanism, the electrochemical oxidation of ammonia produces nitrogen gas. On the ground, nitrogen gas floats away because of the buoyancy of the gas leaving a clean platinum catalyst surface making of the platinum surface available to oxidize more ammonia. In the case of the electrochemical oxidation of ammonia under the influence of microgravity, the nitrogen gas produced near the surface of the catalyst stays in the vicinity due to the lack of buoyancy. This was demonstrated by cyclic voltammetry under microgravity conditions by Nicolau et al. (2012), showing a decrease in the ammonia oxidation peak current.

Previous experiments in microgravity have studied the formation of bubbles. Bitlloch et al. (2015) performed an analysis of bubble dispersion in turbulent jets based on data from drop tower experiments (Bitlloch et al. 2015). Sonoyama studied the formation of methane from CCl_2F_2 at a Cu modified gas diffusion electrode (Sonoyama 2007). Under the microgravity, the current efficiency for methane formation (the final product) increased. Thompson et al. studied their formation in a microgravity drop tower observing that in the absence of gravity surface tension is a driving force for the bubble detachment (Thompson et al. 1980). In addition, Kaneko et al. showed a decrease of current density with the formation of bubbles in microgravity (Kaneko et al. 1993). Herman et al. studied the effects of an electrical field on the formation of bubbles on microgravity, showing that at higher electrical fields better detachment of the bubbles is obtained (Herman et al. 2002). Carrera et al. studied the detachment of bubbles from a plate orifice and a tube orifice, showing that the plate orifice, having more area, the bubbles anchor to the surrounding surface making the detachment more difficult (Carrera et al. 2006). Buyevich and Webbon performed a theoretical study on bubble formation under microgravity finding that differences in the injector geometry could increase the bubble detachment volume due to conditions of incomplete wetting because of broadening of the bubble base (Buyevich and Webbon 1996, 1997). Balasubramaniam observed that the migration of a bubble under microgravity is due to a thermal gradient on the system (Balasubramaniam et al. 1996).

The formation of H_2 and N_2 formation of bubbles in ground forces has been studied at Pt ultramicro- and nanoelectrodes (Fernandez et al. 2014; Chen et al. 2014; Yang et al. 2015; Chen et al. 2015). They studied the formation of electrochemically generated H_2 and N_2 bubbles and subsequent detachment. The bubble detachment from the Pt electrode surface takes ca. 1-2s. Here we found that changes in ammonia oxidation currents changed after ca. 5-10 seconds under most of the Pt catalyst materials studies under microgravity.

The objective of the experiment is to compare the ammonia oxidation capabilities of three different catalysts in microgravity and on the ground (see Fig. 1). The platinum nanocubes by design have a preferential crystalline (100) sites which has shown better performance than (100) and (111) sites, oxidizing ammonia. (ref de Roberto). By using nanocubes on a carbon support (Vulcan XC-72™) we want to observe how the performance of the nanocubes change compared to the pure nanocatalyst. It is expected that dispersing the nanocubes would improve its current density. The surface area available of the pure platinum nanocubes is reduced, when platinum nanocubes in the vicinity occlude each other when they agglomerate. Also the performance of the pure platinum nanocubes and the nanocubes in Vulcan™ will be compared with platinum on carbon nanooinions. Carbon nanoonions have a higher surface area compared to Vulcan™, >984.3 m^2/g for carbon nanooinions (Echegoyen et al. 2010) vs. 262 m^2/g for carbon Vulcan™. (Sigma Aldrich)

Experimental Methods

Catalysts

Catalysts were synthesized in the laboratory. In particular, platinum nanocubes were synthesized by the water in oil emulsion method presented by Martinez-Rodriguez et al. (2014a, b) (see Fig. 2). 11 g of Brij30 and 2.1 mL of chloroplatinic acid 0.1M were added to 38.29 g of n-heptane in a container and the mixture was well mixed. Brij30 is a nonionic surfactant used to disperse the chloroplatinic acid particles by steric stabilization. This step was followed by the addition of 0.079g of sodium borohydride to reduce the dispersed platinum precursor. The reaction took place for 20 minutes. After it was finished, acetone was added to induce the precipitation of the platinum nanocubes. Once precipitated the particles were rinsed with acetone, methanol and nanopure water. Cubic particles formation was induced by adding HCl during the reduction process (Martinez-Rodriguez et al. 2014a).

The method for making the platinum supported on Vulcan™ nanoparticles is as follows: platinum nanoparticles were reduced with sodium borohydride by the method

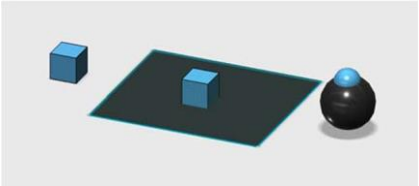

Fig. 1 Schematic representation of the three different nanomaterials used: Pt nanocubes, Pt nanocubes on Vulcan™ carbon and Pt nanoparticles on carbon nanoonions

previously explained, then added 39 mL of a solution of 5 mg/L of Vulcan™ in n-Heptane, to make a catalyst with a Pt/Vulcan™ ratio of 20:80. The solution was mixed for 30 minutes.

The platinum loading of the Pt in Vulcan™ catalysts was 20% Pt as determined by thermogravimetric analysis.

Platinum on carbon nano-onions were synthesized by the Rotating Disk Slurry Electrode (RoDSE) method presented by Santiago et al. (2012) (see Fig. 2b). Briefly, 50 mg of carbon nanoonions, produced from nanodiamond powder, were dissolved in 50 mL of 0.1 M sulphuric acid 0.1M and placed in the RoDSE electrochemical cell. A voltage of -0.2V vs. Ag/AgCl was applied to the glassy carbon rotating disk electrode while placed in the slurry solution. The rotating speed used was 900 rpm. While the potential was applied for 16 hours, 2 mL of 5 mM potassium hexachloroplatinate were added every two hours to the RoDSE electrochemical cell containing the carbon nanoonions in a slurry suspension. The produced platinum-carbon nanoonions catalyst slurry solution was vacuum filtered and dried in an oven at 60 °C for 12 hours. The platinum loading of the platinum on carbon nano-onion catalysts was 13% Pt as determined by thermogravimetric analysis.

Catalysts Ink Preparation

The following quantities were used for each catalyst ink preparation:

a. Pt nanocubes-5 mg of platinum nanocubes, 59 μL of FAA-3 liquid ionomer, 250 μL of dimethylformamide
b. Pt nanocubes-carbon Vulcan™- 25 mg, 59 μL of FAA-3 liquid ionomer, 750 μL of dimethylformamide
c. Pt carbon nanoonions-25 mg, 59 μL of FAA-3 liquid ionomer, 750 μL of dimethylformamide
d. Pt black-5 mg, 59 μL of FAA-3 liquid ionomer, 250 μL of dimethylformamide

To prepare the ink for each catalyst, 59 μL of FAA-3 liquid ionomer and 250 μL of dimethylformamide were dispensed into each vial containing the synthesized catalyst powders. The ink was homogenized in an ultrasonic bath for 2 hours. The catalyst ink was painted over the gas diffusion layer (GDL) on a hot plate at 60°C.

Membrane Electrode Assembly (MEA)

The Membrane Electrode Assembly (MEA) is the unit of the fuel cell that performs the electrochemical transformation of the fuel into electrical current. It consists of a Fumion ™FAA-3 PK-130 anion exchange membrane (Fumatech); on each side of the membrane there is a catalyst adhered to the membrane and an ELAT™LT1400W gas diffusion layer (Nuvant) over the catalyst. The microporous gas diffusion layer permits the evenly distribution of the fuel over the catalyst, the catalyst takes part into the oxidation and reduction reactions by lowering the activation energy for the reactions, and the proton conduction membrane transport the H^+ protons from the anode side to the cathode side. On the cathode side all MEAs had 1 mg/cm^2 of platinum black. The anode side carried three different catalysts: platinum nanocubes, platinum nanocubes on Vulcan™ support and platinum on carbon nanoonions support. The MEA is constructed by assembling one catalysts containing GDL against each side of the membrane. Care is taken to identify the anode side from the cathode side.

Fuel Cell

The experiment consists of a fuel cell with a 5 cm^2 active area (see Figs. 3 and 4). The fuel cell anode was fed with an ammonium hydroxide solution (1.0 M or 0.1 M) on a closed loop connected to a peristaltic pump at 30 ml/min. The cathode side was connected to a breathing air tank on the inlet and the outlet was connected to the exhaust system of the plane at 300 mL/min at 82737 Pa (Fig. 5).

Parabolic Flight

The microgravity experiments were performed aboard NASA's McDonnell Douglas C9 Skytrain II plane "The Weightless Wonder". The plane took off from Ellington Field Houston to perform a flight campaign in January 2016. The microgravity achieved by the parabolic maneuver was 0.02g for periods lasting 30 seconds.

Experiment Box

The experiment box was a modification of the box used by Nicolau et al. (2012). The box is a triple containment system made of Makrolon® designed and constructed for closed loop, self-contained experiments and it was modified to adapt an inlet hose from an external air tank and an outlet for the experiment exhaust to be connected to the

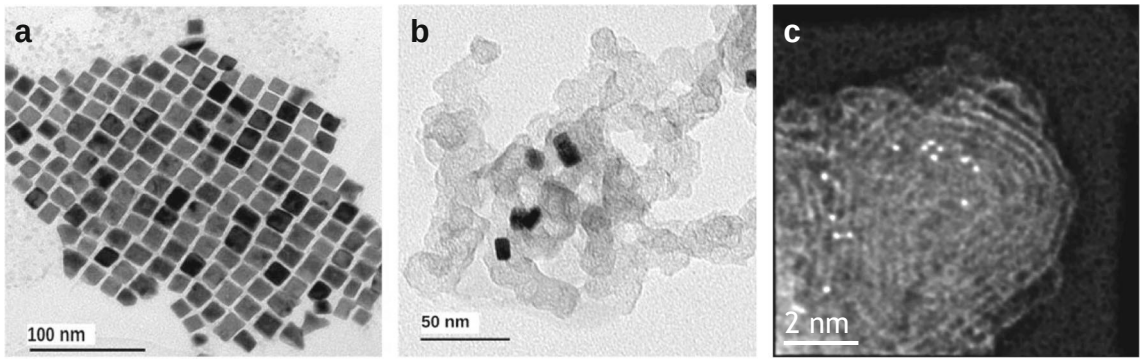

Fig. 2 Transmission electron microscopy of (**a**) Pt nanocubes, scale: 100 nm (Martinez-Rodriguez et al. 2014b), (**b**) Pt nanocubes on carbon Vulcan™, scale: 50 nm, and (**c**) Pt-carbon nanoonions, scale 2 nm, (Santiago et al. 2012)

plane exhaust system. The experiment box was bolted to the airplane floor.

Electronics Rack

The fuel cell was connected to a Biologic SP-50 potentiostat and a computer installed inside a rack system made with 80/20™ brand of structural framing system. The rack reside near the experiment box. The reference and counter electrode connections were on the cathode side of the fuel cell and the working electrode was connected to the anode.

Results and Discussion

The first experiment done with the fuel cell was to observe the current produced with respect to time at an applied potential to the anode vs. the cathode. The catalytic material used in the anode and the cathode of the fuel cell was a commercial product (1mg/cm^2 of unsupported 100% Pt Black, Sigma Aldrich). Figure 6 shows a transient representation of the current versus time for a fuel cell under an applied voltage of 0.45 V. The current was recorded for 10 parabolas during the microgravity and hypergravity period. It can be observed a decrease in current when the airplane

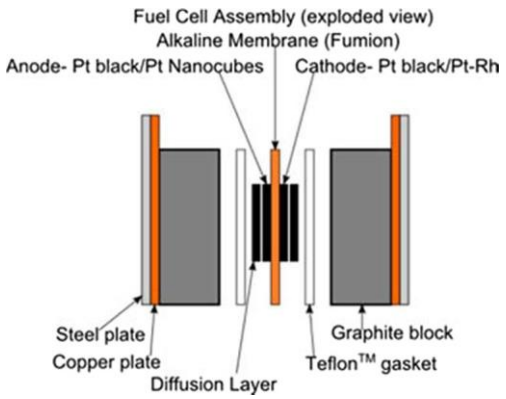

Fig. 3 Exploded side view of the direct ammonia alkaline fuel cell

change from hypergravity (410 μA at 1.7 g) to microgravity (370 μA at 0.02 g). This data validates the observations made in electrochemical half cells by Nicolau et al. (2012); there is an impairment of performance probably caused by the stagnant nitrogen gas, product of the oxidation of ammonia. On each cycle gravity changes from microgravity to normal gravity and then to hypergravity again. The current decrease phenomena are reversed when the plane returns to hypergravity, regaining the anode current production when the nitrogen gas floats away from the surface of the catalysts (Fig. 6).

Chronoamperometry with Platinum Nanocubes

The catalyst used in this experiment was pure platinum nanocubes produced in the laboratory. Platinum nanocubes are 10 nm in size and have crystalline (100) (110) and (111) sites. Figure 7s show chronoamperometric tests measuring the current produced by the fuel cell at different applied voltages (0.2 V, 0.4V, 0.6 V, 0.8V, 1.0V, and 1.2V vs. cathode). The anode had 0.1 M ammonia at 30 mL/min and on the cathode air at 300 mL/min. At 0.2 V and 0.6V, the current produced in microgravity is lower than that on ground conditions. On the other hand, the chronoamperometries at 0.4V show a very slight improvement of performance for the microgravity compared to the ground experiment up to a point where they stabilize over time giving the same performance as the ground case. This equalization of microgravity and ground performance occurs in the region of the graph where the concentration of ammonia in proximity to the electrode surface is depleted and then ammonia from the bulk solution diffuses toward the electrode. The current produced is a function of the concentration of ammonia, the concentration present is dependent on the diffusion mass transfer of ammonia from the bulk of the solution to the surface of the electrode. At 0.8V and 1.0V the performance at microgravity is better than that on the ground. Finally, at 1.2V the current performance on microgravity

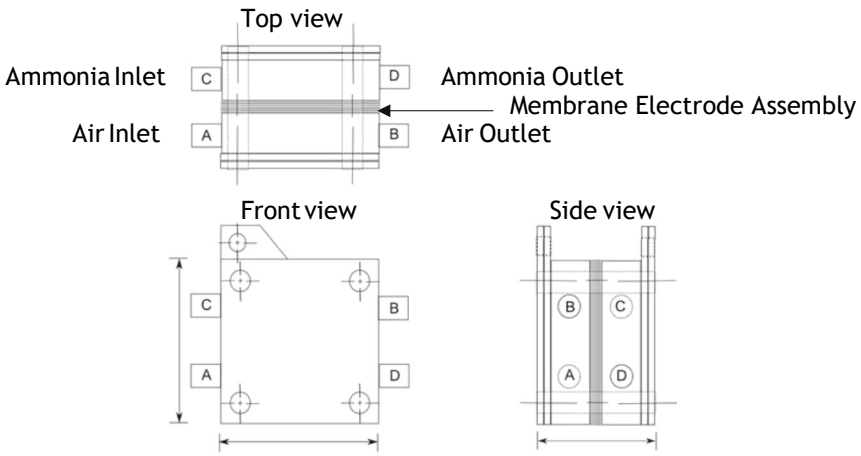

Fig. 4 Three side view of the fuel cell

is better during the period where the ammonia concentration near the electrode is not depleted, but once it enters the zone controlled by diffusion the performance decays and becomes lower than the ground counterpart. At this latter potential N_{ads}(adsorbed Nitrogen)is being formed which strongly adsorbs on platinum active sites, thus inactivating part of the platinum and reducing the catalyst activity in addition to the effect caused by the loss of buoyancy in microgravity.

Chronoamperometry with Platinum Nanocubes on Carbon Vulcan™

The catalyst material are the same platinum nanocubes used in the previous experiment dispersed on a carbon support with high surface area (Vulcan XC72™). The platinum nanocubes are 20% by weight of the catalyst. The nanocubes were deposited on the Vulcan™ by mixing the nanocubes and the Vulcan™ in acid. Figure 8 shows the chronoamperometric response of the fuel cell using platinum nanocubes supported on carbon Vulcan™ as anode at different applied potentials (0.2 V, 0.4V, 0.6 V, 0.8V, 1.0V and 1.2V). The anode is fed with 0.1 M ammonia solution at 30mL/min and the cathode with air at 300 mL/min.

At 0.2 V and 0.4V, the current produced in microgravity is significantly lower than that recorded on ground, while at 0.6 V and 0.8V, currents obtained in both conditions are very similar during the first 9 seconds of the experiments. After this time the microgravity current is slightly higher. On the contrary, for 1.0 V after this time the microgravity current becomes slightly lower than that on the ground. Finally, at 1.2V the microgravity current is lower than the current on the ground. Again, after 9 seconds is when the ammonia near the electrode is depleted and the current becomes diffusion controlled. The current produced is a function of the concentration of ammonia, the concentration present is dependent on the diffusion mass transfer of ammonia from the bulk of the solution to the surface of the electrode. As it is observed, the performance of the catalyst on microgravity improves with increasing values of applied voltage

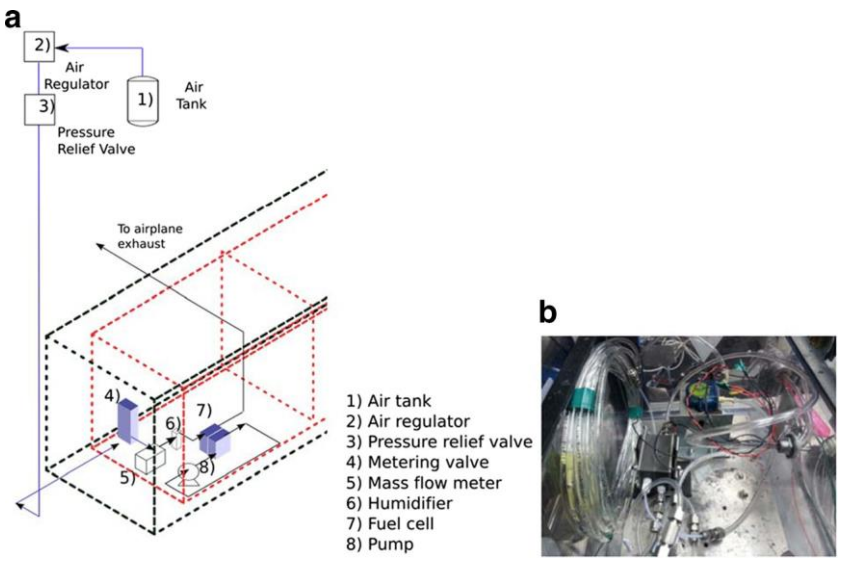

Fig. 5 Microgravity experiment set up. **a** schematic, **b** picture of the setup inside the experiment box

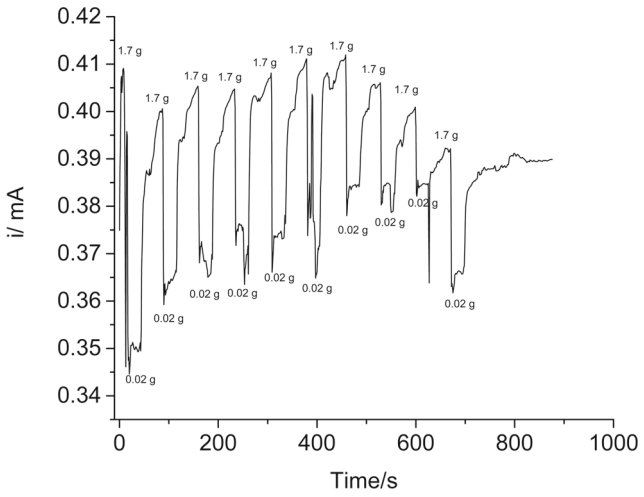

Fig. 6 Anode chronoamperometric data of an ammonia alkaline fuel cell at 0.45V vs. cathode (Breathing Air/300ml/min/82737 Pa) in 1.0M NH_4OH (30ml/min in anode) during 10 parabolas, from 0.02 g to 1.7 g. Anode (5mg of Pt black): NH_4OH 30ml/min, cathode (5mg of Pt black): Air 150 mL/min

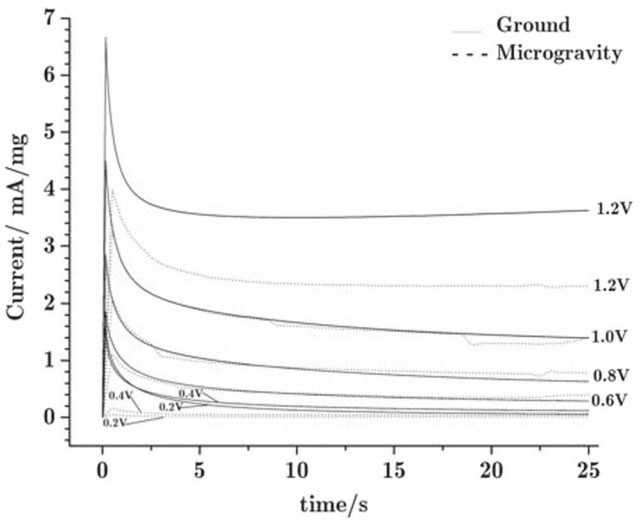

Fig. 8 Chronoamperommetry of ammonia oxidation at applied potentials of: 0.2, 0.4, 0.6, 0.8,1.0 and 1.2V vs. cathode (Breathing Air/300ml/min/82737 Pa) in 0.1M NH_4OH (30ml/min in anode). Anode-5.3mg of Pt-nanocubes in carbon Vulcan™ (ca. 20% metal loading) and cathode-5mg Pt Black

until it reaches 1.0 V, moment in which the microgravity current equates the current on ground and at even higher potentials (1.2V) then microgravity performance decreases in comparison with the ground experiments (Figs. 7 and 8).

Chronoamperometry with Platinum on Carbon Nanoonions

Platinum nanoparticles were electrodeposited on high surface area carbon nanoonions. Figure 9 show the chronoamperometric tests using platinum nanoparticles on carbon nanoonions as anode. The solution composition and flows as well as the applied potentials were the same as those measured for the other catalysts.

In this case, for the applied voltages of 0.2V, 0.6V and 0.8V the performance of the catalysts was reduced in microgravity conditions. On the other hand, at 0.4V, 1.0V and 1.2V the performance in microgravity decreased until after 5 to 6 seconds the current became diffusion controlled and the microgravity performance was better. The current produced is a function of the concentration of ammonia, the concentration present is dependent on the diffusion mass transfer of ammonia from the bulk of the solution to the surface of the electrode.

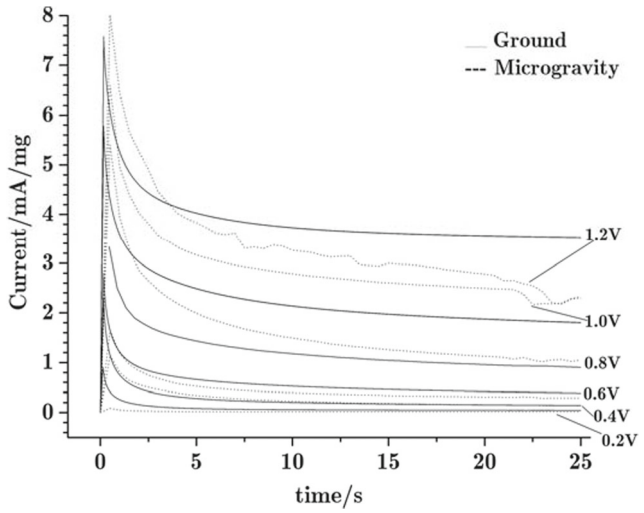

Fig. 7 Chronoamperommetry of ammonia oxidation at applied potentials of: 0.2, 0.4,0.6, 0.8,1.0 and 1.2V vs. cathode (breathing air/300ml/min/82737 Pa) in 0.1M NH_4OH (30ml/min in anode). Anode-5.2mg of Pt-nanocubes and cathode-5mg Pt Black

Comparative Performance of the Catalysts

Finally, in order to determine if there was a shift in the potential of the cathode electrode that was used as a counter/reference electrode, currents at 15s from the chronoamperometry were taken for each potential. A plot of currents at 15s vs. the applied potential is shown in Fig. 10. Of all three catalysts, the platinum on carbon nanoo- nions showed the best performance increase in microgravity versus ground at 0.4V (99%). The high surface area and spherical morphology of the carbon nanoonions may be taking part on improving the release of the stagnant nitrogen gas that interferes with the oxidation of the ammonia. The higher surface area of the carbon nanoonions (>984.3 m^2/g vs. 262 m^2/g for carbon Vulcan ™) provides more nucleation sites where the nitrogen gas can grow and be released (Echegoyen et al. 2010). The improved current in

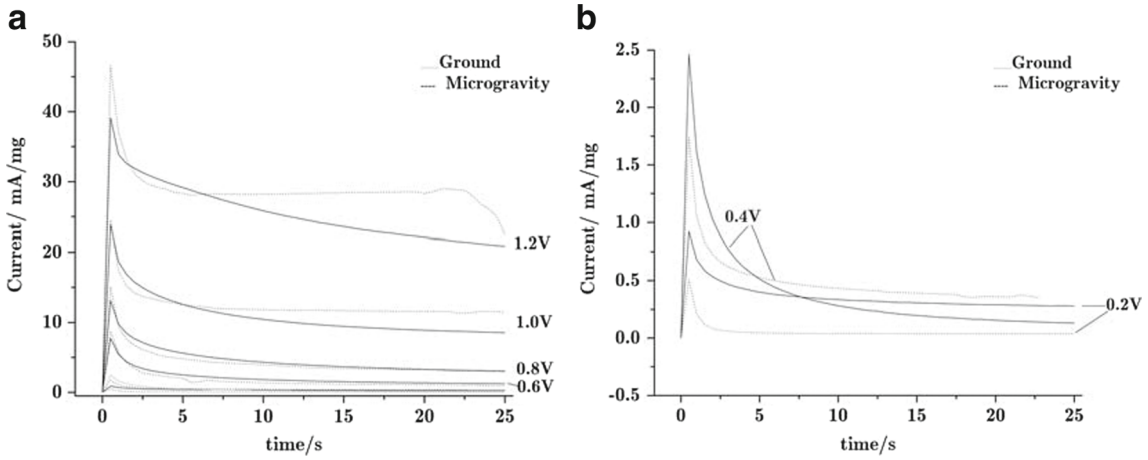

Fig. 9 a Chronoamperommetry of ammonia oxidation at applied potentials of: 0.2, 0.4, 0.6, 0.8, 1.0 and 1.2V vs. cathode (breathing Air/300ml/min/82737 Pa) in 1.0M NH4OH (30ml/min in anode). Anode- 3.2mg of Pt in carbon nanoonions (ca. 13% loading) and Cathode-5mg Pt. **b** expanded view of 0.2 V and 0.4 V

the platinum carbon nanoonions catalyst can be related to a better release of the nitrogen bubbles that hinder ammonia oxidation. The curved surface of the 5 nm nanoonion particles works in an analogous way to the tube orifice in Carrera et al. (2006) paper, in the sense that curvature offers less surrounding surface where the bubble can anchor (see Table 1).

Bubble Formation

The mechanism of bubble formation at ground has been studied at Pt ultramicroelectrodes and nanoelectrodes showing the formation of electrochemically generated H_2 and N_2 bubbles and subsequent detachment (Fernandez et al. 2014; Chen et al. 2014; Yang et al. 2015; Chen et al. 2015) The bubble detachment from the Pt electrode surface takes ca. 1-2s. In our case, we find that the detachment of N_2 from the platinum nanoparticles at microgravity conditions may be occurring at ca. 5-10 seconds in the time scale. This may be explained by the protective shielding the N_2 bubble may have on the Pt surface to avoid its prompt passivation that occurs in ground conditions. In general, under microgravity the lack of buoyancy in this nanomaterials have a positive effect on its catalytic performance at time longer that 5-10 seconds. This happens mainly at potentials higher than 0.8V vs. cathode. At such voltages it could be occurring an effect of electrowetting, the reduction of the surface tension and contact angle in the bubble caused by an electric field leading to bubble detachment from the electrode, it has been demonstrated experimentally the transport of air bubble in microchannels using this phenomenon (Zhao and Cho 2007).

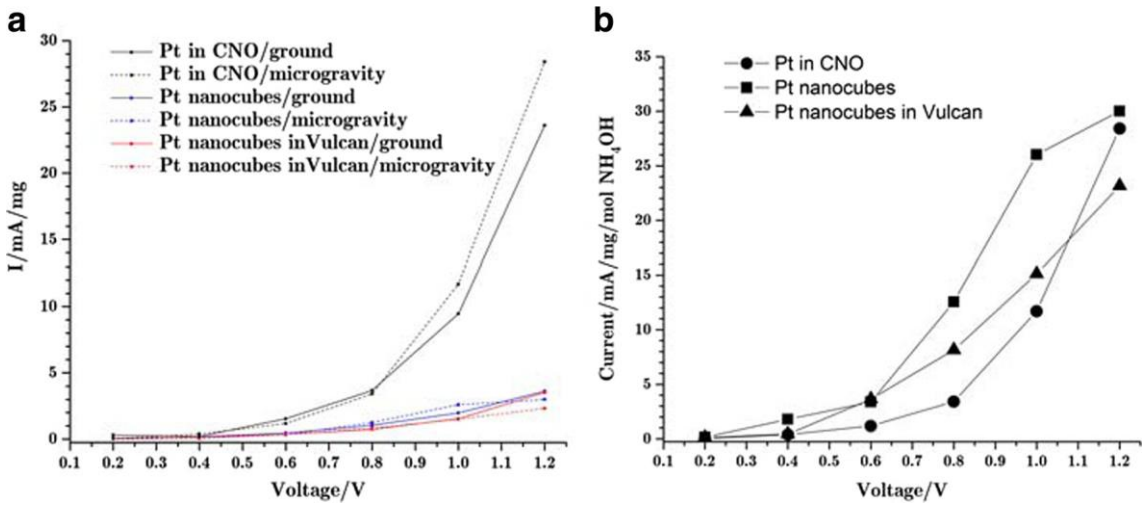

Fig. 10 (**a**) Current (normalized by Pt mass) values at 15 seconds obtained from the chronoamperometries performed at different potentials (from 0.2V to 1.2 V) shown in Figs. 5, 6, and 7 for Pt nanocubes, Pt nanocubes in Vulcan™ and Pt in carbon nanoonions and (**b**) Comparison of the currents normalized by Pt mass and molarity of NH_4OH for the three catalysts

Table 1 Comparative performance of catalyst in microgravity versus ground (positive values are an increase of performance) at 15s of the chronoamperometric data taken at 0.45V

Applied voltage vs. cathode (breathing air/300ml/min/82737 Pa) at in 0.1M NH_4OH (30ml/min in anode)	Pt nanocubes (100% metal loading)	Pt-nanocubes Carbon Vulcan ™ (20% metal loading)	Pt-nano-onions (13% metal loading)
0.2 V	−73%	−86%	−88%
0.4 V	5%	−71%	99%
0.6 V	−27%	3%	−23%
0.8 V	21%	9%	−7%
1.0 V	32%	−1%	24%
1.2 V	−17%	−34%	20%

The flight maneuver used was FL230-Fl310 so the experiment would observe a Op between 43368.0 Pa and 55158.1 Pa, top to bottom of the parabola (the outside pressure being 40954.9 Pa and 28751.1 Pa). The cabin pressure does not excerpt direct influence in the fuel cell because the fuel cell was sealed in a double containment system. The vent system was sized, that in the event of a vent station being wide open, the flow rate was less than the make-up rate of the cabin pressurization system. Therefore, the vent does not affect significantly the cabin altitude.

The C9 plane's overboard vent system was connected to the outlet of the fuel cell cathode (air) side. The vent system could have created a pressure differential from the anode side to the cathode side. Considering that the trajectory of the plane is a parabola the pressure at the start of the parabola and at the end of the parabola would be quite similar, a difference would be noticed at the peak of the parabolic trajectory (ca. 12.5 s). No periodic or reversible effect was observed in the chronoamperometries, suggesting that the effect of the vent on the fuel cell current performance is negligible.

Conclusions

This research has shown the difference between the performance of the same catalysts in an ammonia fuel cell under microgravity and ground experimental conditions in terms of normalized current densities. In the case of a fuel cell with platinum black as catalyst on the anode there is a reduction in the produced mass-normalized current densities of around 7.5% between the hypergravity and microgravity experimental episodes. This decrease was shown to be reversed when gravity effects were once again applied to the fuel cell, confirming the direct influence from microgravity on the electrochemical oxidation of ammonia.

For the platinum nanocubes the decrease in current in microgravity was also shown, except for the applied voltages of 0.4V (5%), 0.8 V (21%) and 1.0V (32%), for which the current produced in microgravity was higher than on the ground. Nanocubes are 10 nm crystalline Pt (100) planes, being this orientation the most active for the ammonia oxidation.

For the platinum nanocubes supported on carbon Vulcan™, higher current densities were observed at 0.6V (3% current increase vs. ground) and 0.8V (9% current increase vs ground) in microgravity conditions when the ammonia electrooxidation was taking place at the diffusion controlled zone.

Finally, the platinum on carbon nanoonions support showed higher Pt mass-normalized current densities at 0.4V (99% current increase vs. ground), 1.0V (24% current increase vs. ground) and 1.2V (22% current increase vs. ground) in microgravity conditions.

Acknowledgements This work was financially supported by the NASA-MIRO Center for Advanced Nanoscale Materials at the University of Puerto Rico-R´ıo Piedras Campus Grant number NNX10AQ17A and NASA-EPSCoR grant number NNX14AN18A, Puerto Rico NASA Space Grant Consortium: NASA cooperative agreement NNX10AM80H, NASA Flight Opportunities Program Announcement of Flight Opportunities (AFO) NOCT110 call #5 and Ministerio de Econom´ıa y Competitividad (projects CTQ2013-44083-P and CTQ2013-48280-C3-3-R). Also I want to say thanks to Robert Roe, Dominic Del Rosso and Terry Lee from the NASA Flight Opportunities Program, their support was immensely important to the success of this project.

References

Afif, A., Radenahmad, N., Cheok, Q., Shams, S., Kim, J.H., Azad, A.K.: Ammonia-fed fuel cells: a comprehensive review. Renew. Sust. Energ. Rev. **60**, 822–835 (2016). doi:10.1016/j.rser.2016.01.120

Balasubramaniam, R., Lacy, C.E., Woniak, G., Subramanian, R.S.: Thermocapillary migration of bubbles and drops at moderate values of the Marangoni number in reduced gravity. Phys. Fluids **8**(4), 872–880 (1996). doi:10.1063/1.868868

Bayer, T., Cunning, B.V., Selyanchyn, R., Daio, T., Nishihara, M., Fujikawa, S., Sasaki, K., Lyth, S.M.: Alkaline anion exchange membranes based on KOH-treated multilayer graphene oxide. J.

Membr. Sci. **508**, 51–61 (2016). doi:10.1016/j.memsci.2016.02.017

Bitlloch, P., Ruiz, X., Ramirez-Piscina, L., Casademunt, J.: Turbulent bubble jets in microgravity. Spatial dispersion and velocity fluctuations. Microgravity Sci. Technol. **27**(3), 207–220 (2015). doi:10.1007/s12217-015-9436-y

Buyevich, Y.A., Webbon, B.W.: Bubble formation at a submerged office in reduced gravity. Chem. Eng. Sci. **51**(21), 4843–4857 (1996). doi:10.1016/0009-2509(96)00323-5

Buyevich, Y.A., Webbon, B.W.: The isolated bubble regime in pool nucleate boiling. Int. J. Heat Mass Transfer **40**(2), 365–377 (1997). doi:10.1016/0017-9310(96)00097-x

Carrera, J., Parthasarathy, R.N., Gollahalli, S.R.: Bubble formation from a free-standing tube in microgravity. Chem. Eng. Sci. **61**(21), 7007–7018 (2006). doi:10.1016/j.ces.2006.07.021

Cheddie, D.: Ammonia as a hydrogen source for fuel cells: a review. In: Minic, D. (ed.) Hydrogen Energy - Challenges and Perspectives. InTech (2012)

Chen, Q., Luo, L., Faraji, H., Feldberg, S.W., White, H.S.: Electrochemical measurements of single h-2 nanobubble nucleation and stability at pt nanoelectrodes. J. Phys. Chem. Lett. **5**(20), 3539–3544 (2014). doi:10.1021/jz501898r

Chen, Q.J., Wiedenroth, H.S., German, S.R., White, H.S.: Electrochemical nucleation of stable n-2 nanobubbles at pt nanoelectrodes. J. Am. Chem. Soc. **137**(37), 12064–12069 (2015). doi:10.1021/jacs.5b07147

de Vet, S.J., Rutgers, R.: From waste to energy: First experimental Bacterial Fuel Cells onboard the International Space Station. Microgravity Sci. Technol. **19**(5-6), 225–229 (2007)

Echegoyen, L., Ortiz, A., Chaur, M.N., Palkar, A.J.: Carbon Nano Onions. In: Akasaka, T., Wudl, F., Nagase, S. (eds.) Chemistry of Nanocarbons. Wiley, Chichester (2010). doi:10.1002/9780470660188.ch19

Erisman, J.W., Sutton, M.A., Galloway, J., Klimont, Z., Winiwarter, W.: How a century of ammonia synthesis changed the world. Nat. Geosci. **1**(10), 636–639 (2008). doi:10.1038/ngeo325

Fernandez, D., Maurer, P., Martine, M., Coey, J.M.D., Moebius, M.E.: Bubble formation at a Gas-Evolving microelectrode. Langmuir **30**(43), 13065–13074 (2014). doi:10.1021/la500234r

Gerischer, H., Mauerer, A.: Untersuchungen Zur Anodischen Oxidation von Ammoniak an Platin-Elektroden. J. Electroanal. Chem. **25**(3), 421–433 (1970)

Herman, C., Iacona, E., Foldes, I.B., Suner, G., Milburn, C.: Experimental visualization of bubble formation from an orifice in microgravity in the presence of electric fields. Exp. Fluids **32**(3), 396–412 (2002). doi:10.1007/s003480100366

Kaneko, H., Tanaka, K., Iwasaki, A., Abe, Y., Negishi, A., Kamimoto, M.: Water electrolysis under microgravity condition by parabolic flight. Electrochim. Acta **38**(5), 729–733 (1993). doi:10.1016/0013-4686(93)80245-u

Kannan, M.V., Kumar, G.G.: Current status, key challenges and its solutions in the design and development of graphene based ORR catalysts for the microbial fuel cell applications. Biosens. Bioelectron. **77**, 1208–1220 (2016). doi:10.1016/j.bios.2015.10.018

Martinez-Rodriguez, R.A., Vidal-Iglesias, F.J., Solla-Gullon, J., Cabrera, C.R., Feliu, J.M.: Synthesis and Electrocatalytic Properties of h2SO4-induced (100) Pt Nanoparticles Prepared in Water-in-Oil Microemulsion. Chem. Phys. Chem. **15**(10), 1997–2001 (2014a). doi:10.1002/cphc.201400056

Martinez-Rodriguez, R.A., Vidal-Iglesias, F.J., Solla-Gullon, J., Cabrera, C.R., Feliu, J.M.: Synthesis of Pt Nanoparticles in Water-in-Oil Microemulsion: Effect of HCl on Their Surface Structure. J. Am. Chem. Soc. **136**(4), 1280–1283 (2014b). doi:10.1021/ja411939d

Nicolau, E., Poventud-Estrada, C.M., Arroyo, L., Fonseca, J., Flynn, M., Cabrera, C.R.: Microgravity effects on the electrochemical oxidation of ammonia: a parabolic flight experiment. Electrochim. Acta **75**, 88–93 (2012). doi:10.1016/j.electacta.2012.04.079

Radenahmad, N., Afif, A., Petra, P.I., Rahman, S.M.H., Eriksson, S.-G., Azad, A.K.: Proton-conducting electrolytes for direct methanol and direct urea fuel cells - a state-of-the-art review. Renew. Sust. Energ. Rev. **57**, 1347–1358 (2016). doi:10.1016/j.rser.2015.12.103

Santiago, D., Rodriguez-Calero, G.G., Palkar, A., Barraza-Jimenez, D., Galvan, D.H., Casillas, G., Mayoral, A., Jose-Yacaman, M., Echegoyen, L., Cabrera, C.R.: Platinum electrodeposition on unsupported carbon Nano-Onions. Langmuir **28**(49), 17202–17210 (2012). doi:10.1021/la3031396

Sonoyama, N.: Effect of micro gravity on the product selectivity of dichlorodifluoromethane electrolysis at metal supported gas diffusion electrodes. Microgravity Sci Technol. **19**(1), 22–24 (2007). doi:10.1007/bf02870985

Thompson, R.L., DeWitt, K.J., Labus, T.L.: Marangoni bubble motion phenomenon in zero gravity. Chem. Eng. Commun. **5**(5-6), 299–314 (1980). doi:10.1080/00986448008935971

Warshay, M., Prokopius, P.R.: The fuel cell in space: yesterday, today and tomorrow Retrieved from http://ntrs.nasa.gov/search.jsp?R=19900002488 (1989)

Yang, X., Karnbach, F., Uhlemann, M., Odenbach, S., Eckert, K.: Dynamics of single hydrogen bubbles at a platinum microelectrode. Langmuir **31**(29), 8184–8193 (2015). doi:10.1021/acs.langmuir.5b01825

Zhao, Y., Cho, S.K.: Micro air bubble manipulation by electrowetting on dielectric (EWOD): transporting, splitting, merging and eliminating of bubbles. Lab Chip. **7**(2), 273–280 (2007). doi:10.1039/B616845K

ANNEX II.

Research report for the preparation of the experimental procedure that will be performed in the International Space Station (ISS)

ANNEX II

RESEARCH REPORT FOR THE PREPARATION OF THE EXPERIMENTAL PROCEDURE THAT WILL BE PERFORMED IN THE INTERNATIONAL SPACE STATION (ISS)

The following report focuses on the preparation of the experimental procedure to study ammonia oxidation in microgravity conditions in the International Space Station (ISS) continuing the research published in Annex I, where this special condition could only be maintained form 20-25 s.

1.1. Sample selection

The chosen samples were preferentially cubic Pt nanoparticles prepared both as Vulcan supported in a mass ratio of Pt_{20}/V_{80}, and as non-supported. To work with both samples having similar area per nanoparticle suspension volume unit, an electrochemical analysis was performed to calculate the active surface area per microliter (µl) of the sample. The voltammetric profile of both Pt nanoparticles is shown in figure 1.

The nanoparticles where prepared using the methodology previously explained in Chapter 3 and 4 using as Pt precursor H_2PtCl_6 as Pt precursor and 20% HCl as shape directing agent. The nanoparticles were prepared in the same batch and those supported on Vulcan were taken from the reactor used in the synthesis before adding NaOH, which cause phase separation. Then, the required amount of carbon Vulcan was added and sonicated as indicated in section 3.1.1.

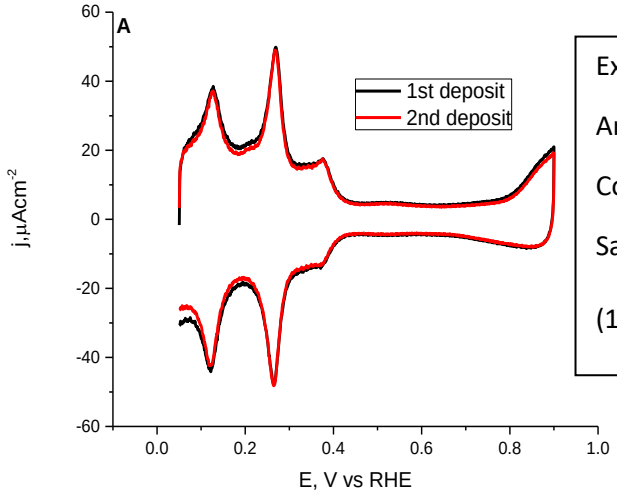

Experiments with 4 μL pure Pt nanoparticles

Area: 0.64 cm^2

Concentration: ~0.16 cm^2/ μL

Sample preparation:

(1 ml sample + 4 ml H_2O) **~0.03 cm^2/ μL**

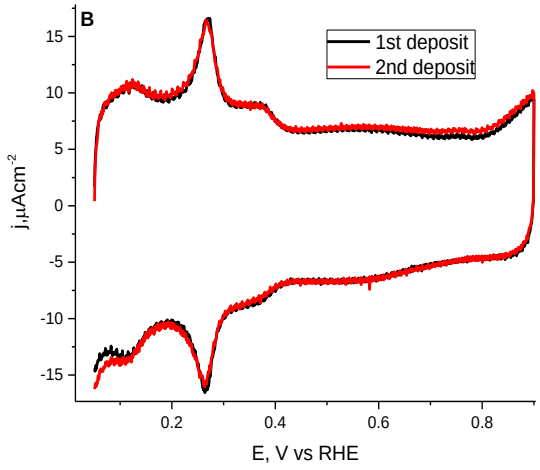

Experiments with 4 μL Pt/V 20 wt %

Area: 0.123 cm^2

Sample preparation

~0.03 cm^2/ μL

Figure 1. Voltammetric profiles of preferentially Pt nanocubes, (A) non-supported and (B) Vulcan supported Pt_{20}/V_{80} nanocubes. Working solution: 0.5 M H_2SO_4. Scan rate: 50 $mV \cdot s^{-1}$.

As seen in figure 1, the non-supported Pt nanoparticles have more area per volume unit, so they were diluted in order to obtain a similar value to that obtained for the Pt/V nanocubes. The active surface areas obtained were 0.032 and 0.031 cm^2/μL

for the non-supported and the supported Pt nanocubes, respectively. Reproducibility was analyzed by comparing two different deposits of the same sample. The catalyst ink was prepared with ultra-pure water as solvent. By adequately drying, the sample it remains on the support without any problem, thus, the use of Nafion was not necessary for sample attachment. The two inks prepared are shown in figure 2.

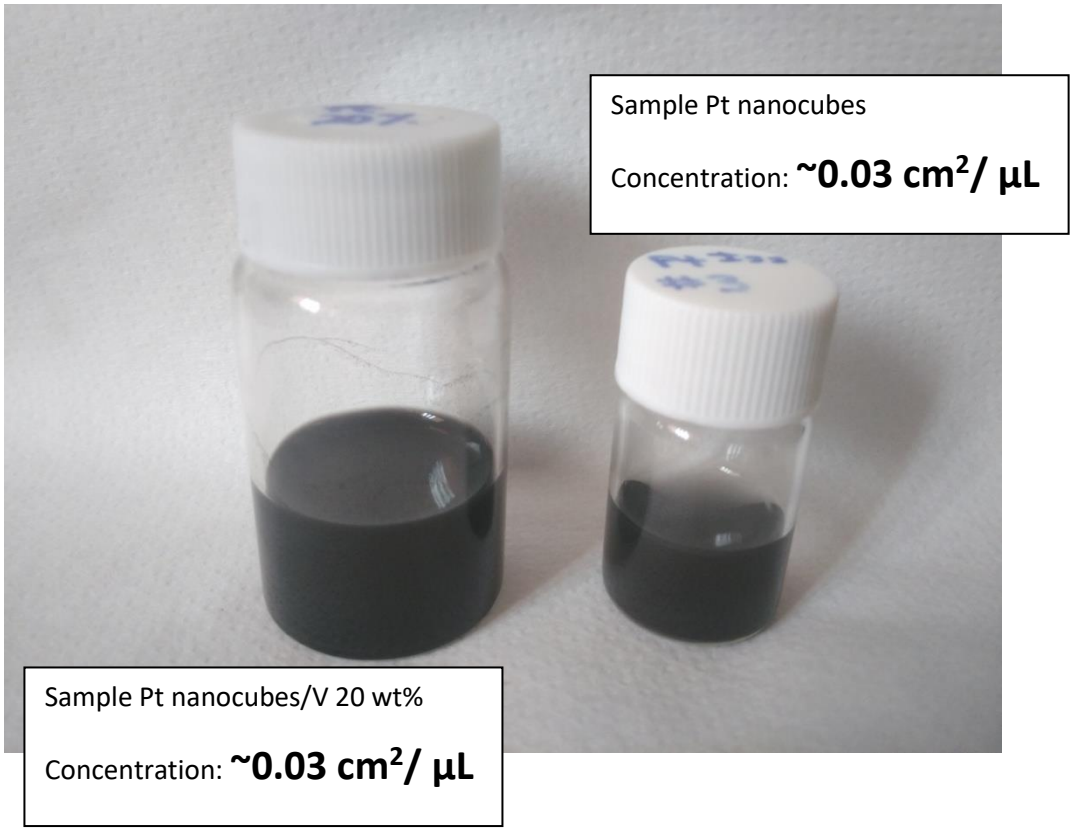

Figure 2. Image of the Catalyst ink

1.1.2. TEM analysis

Transmission electron microscopy (TEM) experiments were performed in order to obtain information about the shape (figure 3 and figure 4A), size distribution (figure 4B) and degree of dispersion of the samples. These analyses were performed with a JEOL, JEM-2010 working at 200 kV and with a JEOL, JEM-1400 working at 120kV. In

order to prepare the carbon-supported samples for TEM measurements a small amount of the powder catalyst was ultrasonically dispersed in isopropanol for 30 s. The original colloidal mother suspension (before cleaning) and the water suspension containing the non-supported Pt nanoparticles, were also analyzed. In all cases, the samples for TEM measurements were prepared by placing a drop of the corresponding solution onto a Formvar-covered copper grid and evaporating the drop-in air at room temperature. In order to obtain the size distribution, more than 200 particles from different parts of the grid were used to estimate the average size.

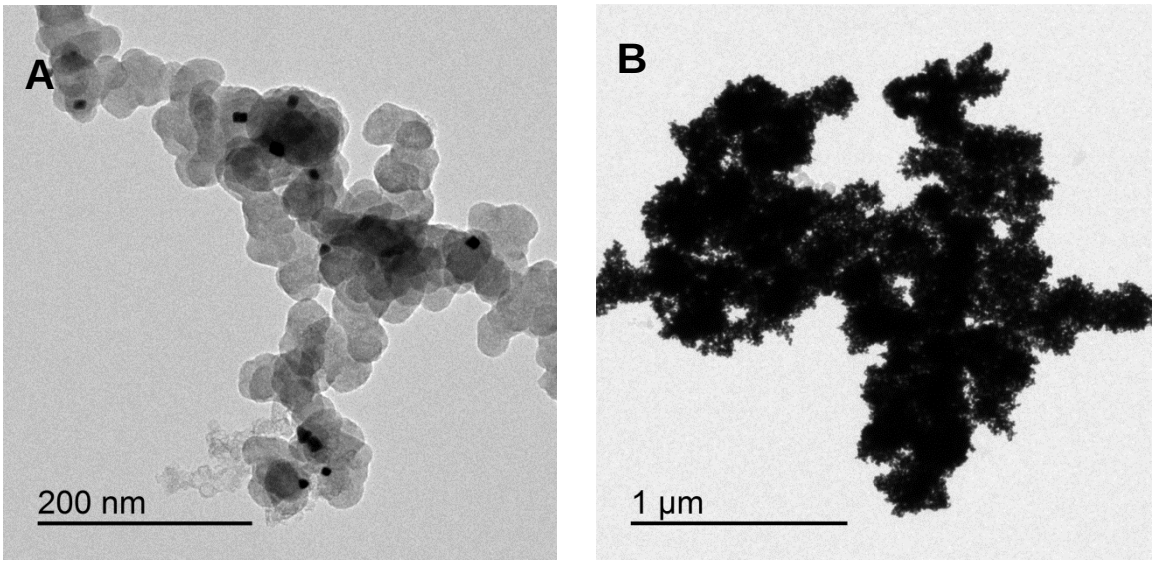

Figure 3. TEM images of (A) Sample 20 wt% Pt nanocubes / Vulcan XC-72R and (B) non-supported Pt nanocubes after cleaning.

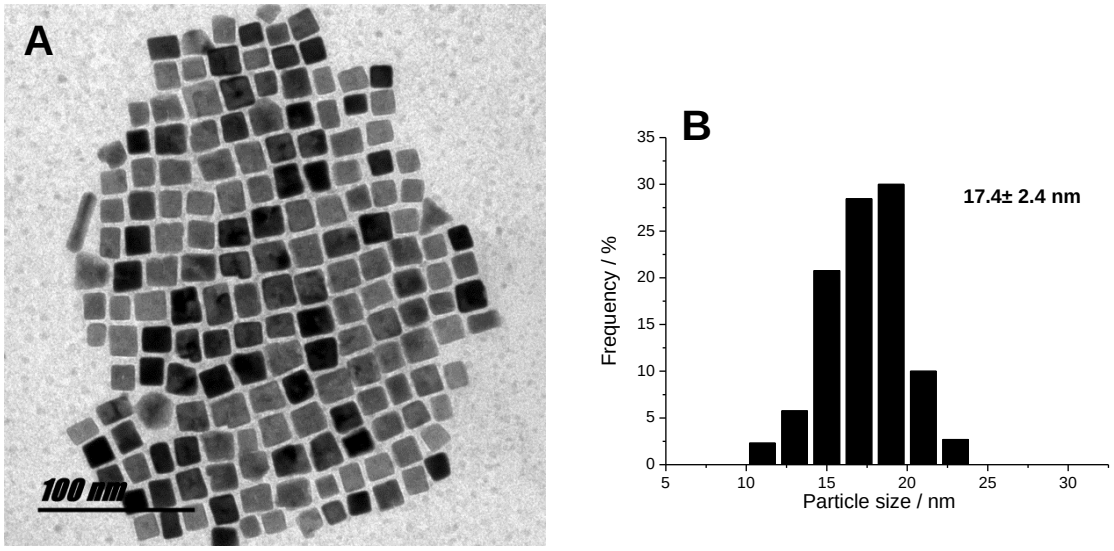

Figure 4. (A) TEM image of the non-supported Pt nanocubes sample taken directly from the microemulsion and (B) its corresponding size histogram.

1.1.3. Thermogravimetric analysis (TGA)

The Pt loading was experimentally evaluated by using thermogravimetric analyses (TGA) using a Mettler-Toledo TGA/SDTA851 thermobalance (figure 5). Experiments were run with a temperature ramp of 10 ºC·min^{-1} from 25 to 850 ºC and carried out in an oxidative atmosphere (N_2/O_2 = 4/1).

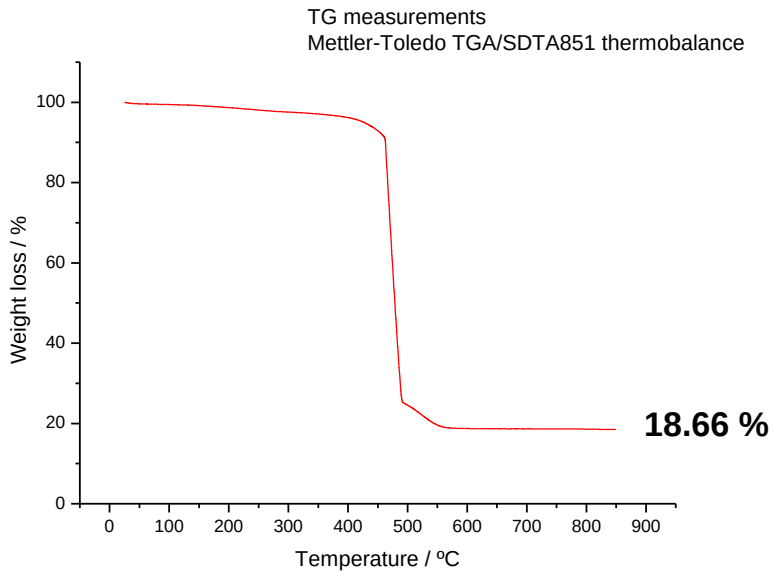

Figure 5. TGA of the sample prepared with 20 wt % Pt nanocubes / Vulcan XC-72R.

1.2. Ammonia oxidation with the prepared samples

Dropsens supplied electrodes (Figure 6A) were used in order to have similar conditions to the multiple arrangement of the electrodes to be used for the experiments in the ISS. As observed in figure 6A, the screen-printed electrode has a carbon working and counter electrodes, and a pseudo Ag reference electrode. The only difference is the larger size of the working electrode area for which a deposit of about 6µL of the ink was used to evaluate the electrochemical behavior. Previous to each deposit, the screen-printed electrodes were clean with ultra-pure water and finally dried with Argon (Ar) as shown in figure 6B.

Once the drop of the ink was deposited, the electrode was dried under an Ar (g) atmosphere until the drop dried. Then, the electrode was cleaned with ultra-pure water and dried again under an Ar atmosphere. Then a drop of about 100 µL of the working solution was deposited onto the electrode as shown in figure 6A. For each electrochemical measurement a new deposit of the catalyst ink was deposited in a new electrode due to the considerable decrease of the catalytic performance.

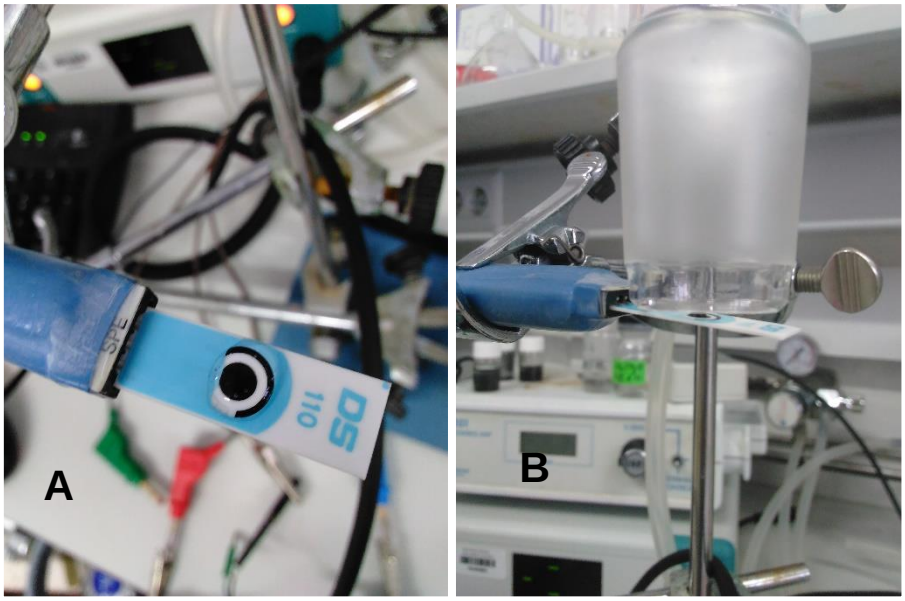

Figure 6. Images of (A) the drying process used for the ink deposit into the single unit Dropsens micro-electrodes and (B) the microelectrode with the working solution and ready for the electrochemical evaluation.

The first measurement was performed in order to select the working solution to be used for the ISS experiments. The observed catalytic activity and stability were

analyzed for this purpose into three different working solutions (figure 7) containing NH_3 including:

- Commercial Solution of NH_3 1 M from Sigma-Aldrich Bio Ultra.
- Solution prepared with 0.2 M NaOH + 0.05 M $(NH_4)_2SO_4$ (pH =13).
- Commercial NH_3 1 M + NaOH with pH = 13.

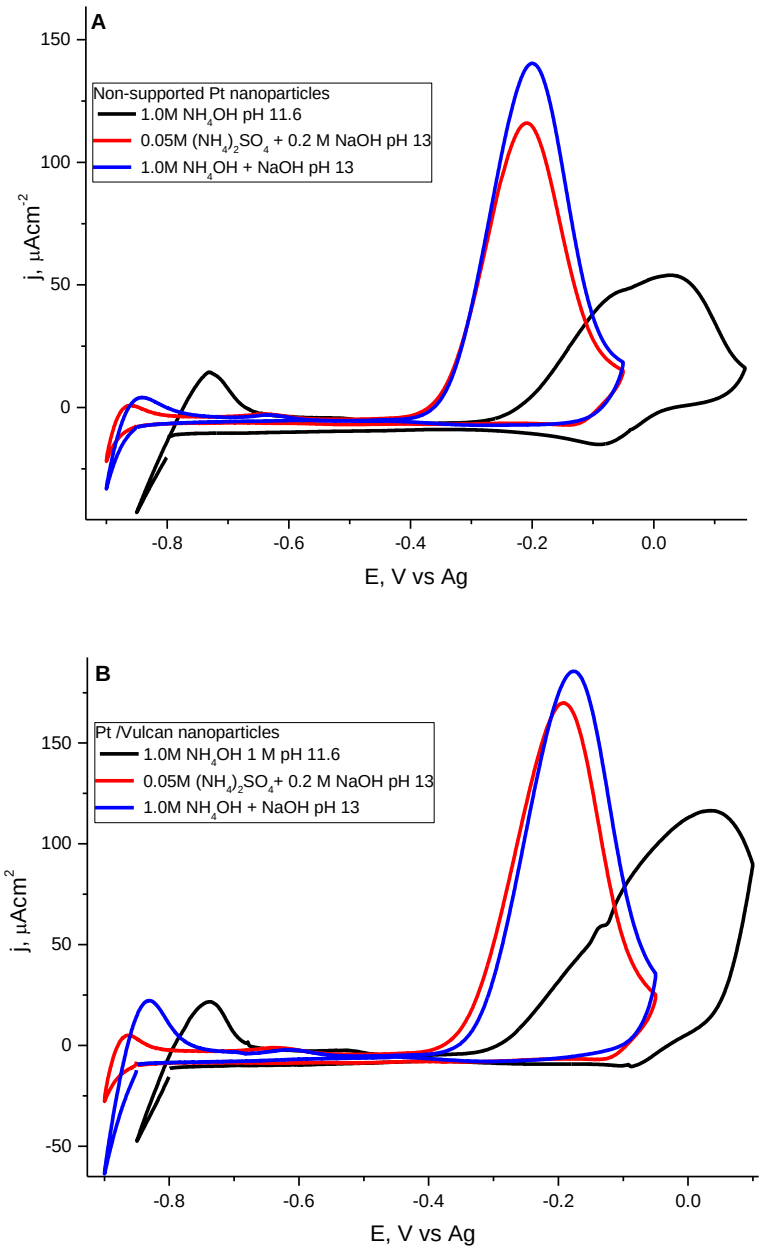

Figure 7. Voltammetric profile of the NH_3 oxidation of the (A) Non-supported Pt and (B) Pt / V nanoparticles into three different working solutions. Scan rate: 10 mVs^{-1}.

In the electrochemical analysis of the catalytic performance, both samples got the lowest activity in the working solution prepared with 1.0 M NH_4OH pH 11.6, bringing also an undesired resistive behavior. This result may be attributed to the low pH value, which could slightly displace the equilibrium of NH_3 to NH_4^+ and probably to the absence of species that could keep the pH value fixed close to the electrode surface. Figure 8 shows the change of the voltammetric profile in this solution of the Pt nanoparticles from the first to the second scan.

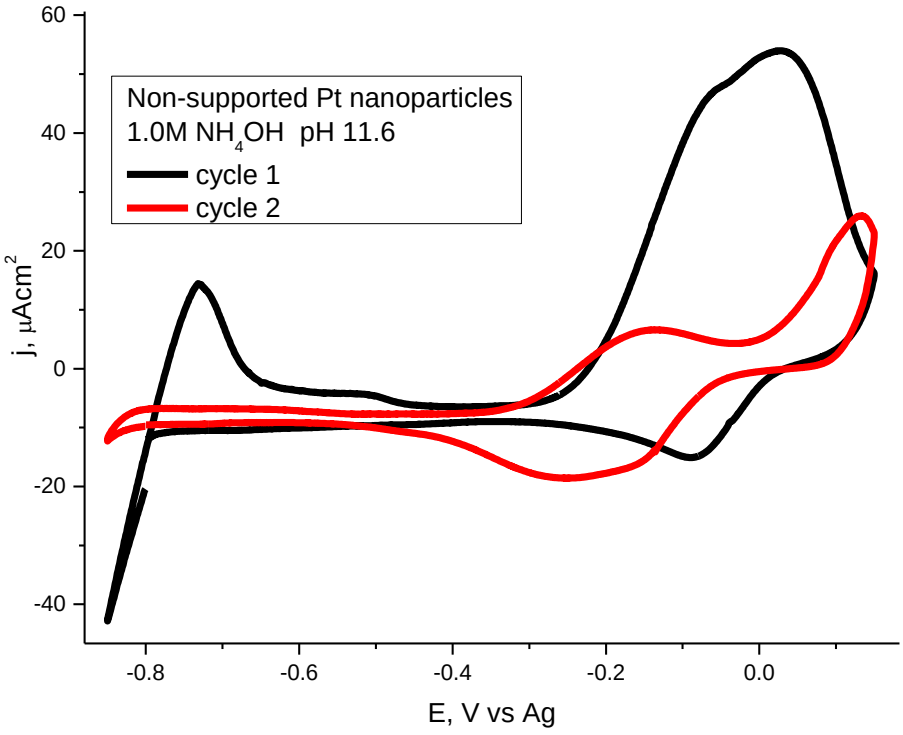

Figure 8. Voltammetric profile of the NH_3 oxidation in Pt nanocubes. Scan rate: 10 mVs^{-1}.

To compare the other two working solution, an experimental analysis of the oxidation decay curve of the NH_3 oxidation was performed. The aim of this part of the work is to choose the best solution in order to obtain the highest current intensities as well as the best poison tolerance. In figure 9 the voltammetric profile of the first and the third scans for the non-supported Pt nanocubes, is reported. As it is observed, the current density obtained for the working solution prepared with approximately 10 times more NH_3, is relatively higher but not significant in terms of the differences in concentration of both working solutions.

In addition, the current intensity decay of the NH_3 oxidation for the most concentrated ammonia solution showed to be larger when comparing the first and the third scan currents. This comparison helps to conclude that the most adequate working solution for the experimental analysis is the solution prepared with 0.05 M $(NH_4)_2SO_4$ + 0.2M NaOH due to the best results obtained.

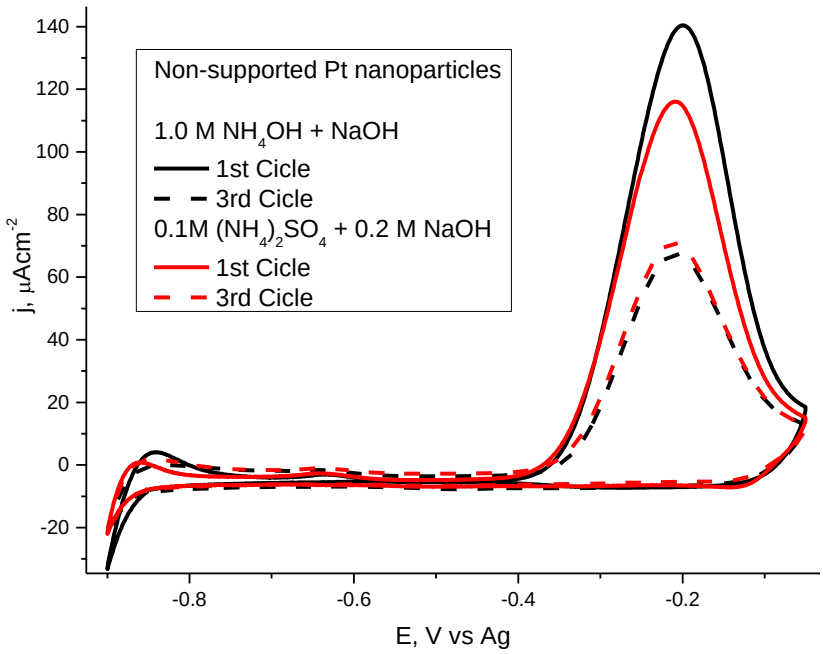

Figure 9. Voltammetric profile of the first and the third scan for NH_3 oxidation on preferential Pt nanocubes under two different working solutions at pH 13. Scan rate: 10 m Vs^{-1}.

Once the working solution was chosen, another electrochemical study was performed in order to determine the level of contamination of the nanoparticles towards NH_3 oxidation. The electrochemical study consisted in analyzing consecutive voltammograms made in the chosen NH_3 solution. For this study the upper potential limit of the CV was kept at a relatively low potential (-0.3 V vs. Ag) in which it is possible to observe the oxidation of NH_3 but without reaching the peak and thus, minimize the formation of adsorbed monatomic nitrogen (N_{ads}), which acts as a poison of the electrode surface. Figure 10 shows the four cycles evaluated for the NH_3 oxidation in which it is evident the current reduction.

Once the 4 cycles were completed, the electrode was washed with ultrapure water, dried with Ar and then, a second drop of working solution was added to the same electrode in order to continue studying the NH_3 oxidation. It is important to emphasize that the main purpose of this study was to discard the possibility that current drops were caused by the decrease of the NH_3 concentration of ammonia in the drop due to its high volatility. In the voltammetric profile showed (Figure 10), oxidation started where the cycle # 4 of the analysis with the first drop finished. This leads to the conclusion that in both samples the Pt is poisoned in such a way that it loses its catalytic activity for NH_3 oxidation in this type of system. With this analysis it was also concluded that the screen-printed electrode should be only used for a single electrochemical measurement.

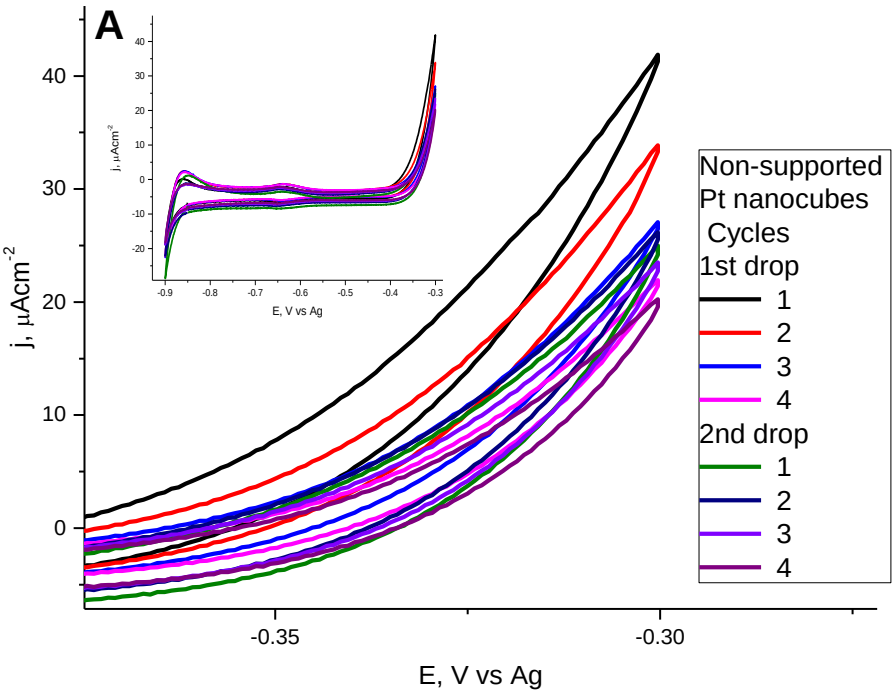

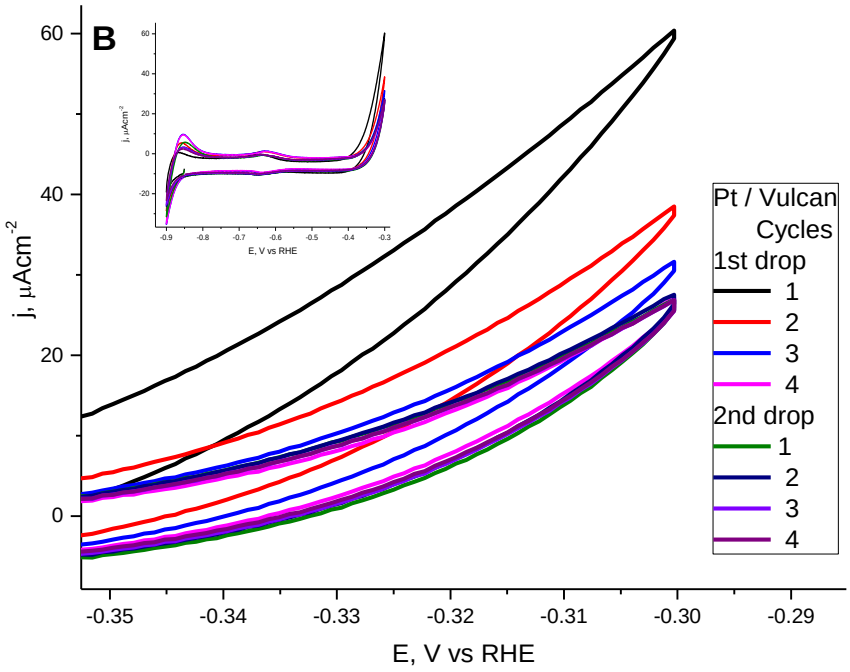

Figure 10. Voltammetric profiles of the first 4 cycles for the NH_3 oxidation in 0.05 M $(NH_4)_2SO_4$ + 0.2 M NaOH up to -0.3 V vs Ag for (A) non-supported Pt and (B) Pt/V nanocubes. Scan rate. 10 mVs^{-1}.

To compare the quality of the electrodes to be used in the system to be sent to the ISS, a similar test to those performed with the single Dropsens electrodes were used in a multiple Dropsens screen-printed electrodes (figure 11). These electrodes have a smaller area compared to those described above, so the addition of catalyst ink to the working electrode was reduced from 6 to 2 µL per electrode. The drying process and the rest of the parameters were the same. For this type of component the CV were recorded in air.

Figure 11. Dropsens multiple (x8) screen-printed carbon electrode.

In this study, about 100 µl of working solution was added to each of the electrodes for the corresponding measurements. Figure 12 shows the result of the experimental reproducibility for both non-supported Pt and Pt/V nanoparticles. Based on this study, it is remarkable to emphasize a series of precautions that must be taken into account to improve the quality of the experiment, including the cleaning of the electrodes, the previous sonication of the samples before being deposited into the electrodes, the time and the flow of the gas that will be used to dry the sample and finally the cleaning and drying process after the nanoparticles being deposited.

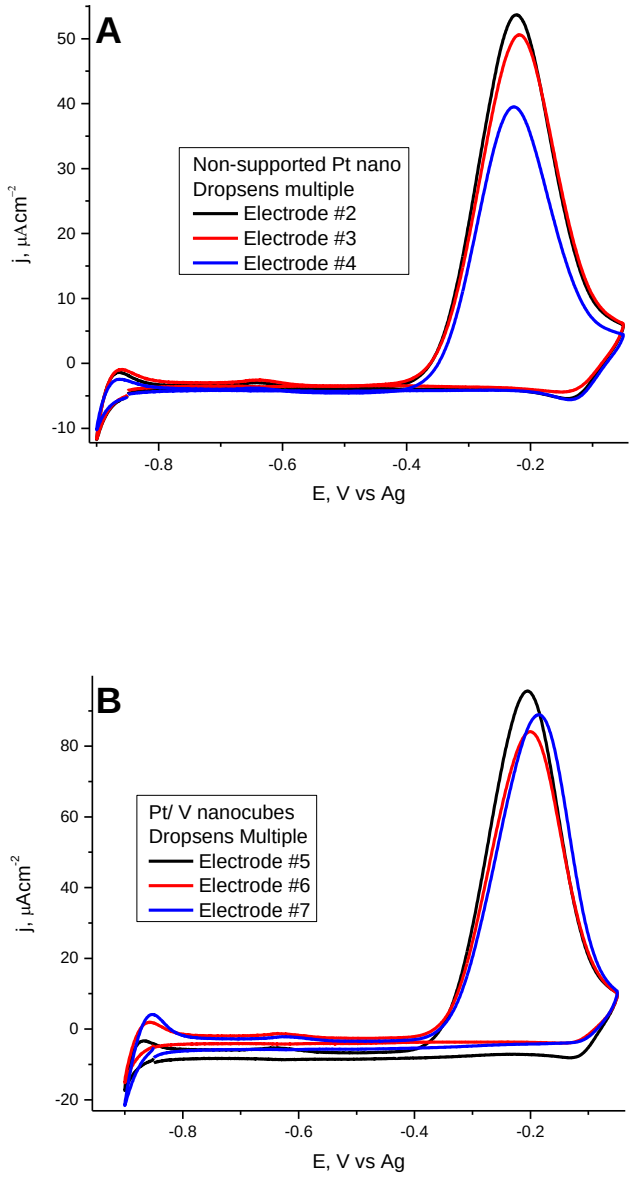

Figure 12. Voltammetric profiles of the NH_3 oxidation in 0.05 M $(NH_4)_2SO_4$ + 0.2 M NaOH for (A) non-supported Pt and (B) Pt/V nanocubes. Scan rate: 10 $mV \cdot s^{-1}$.

1.3. Electrochemical study of the system prepared for the ISS experiments

ISS experiments are planned to be carried out in a flow cell supplied by Dropsens. Before any measurement, the cubic nanoparticles were deposited, after their sonication, on the WE areas of the multiple screen-printed electrode. While the catalyst ink was deposited, all the electrodes were protected with an Ar flow. Once all the samples were dried, the electrodes were cleaned again with ultra-pure water which was subsequently removes with Ar. The system was prepared by adjusting the two "Allen" screws which are observed in figure 13 close to the inlet and the outlet tubing used to pump the working solution through the experiment. The flow of the working solution to the system was controlled with a peristaltic pump. It is important to mention that the system was not filled evenly with the flow rate initially suggested (0.45 ml/min) which was that of the pump that will be used to carry out the experiments in the ISS. For that reason, a visual analysis was made to remove the remaining air bubbles located on the electrodes. These bubbles were easily removed by increasing the flow rate of the variable flow peristaltic pump with which we worked in this study. The working solution was recirculated through the system in order to reproduce similar conditions those that will be used in the ISS.

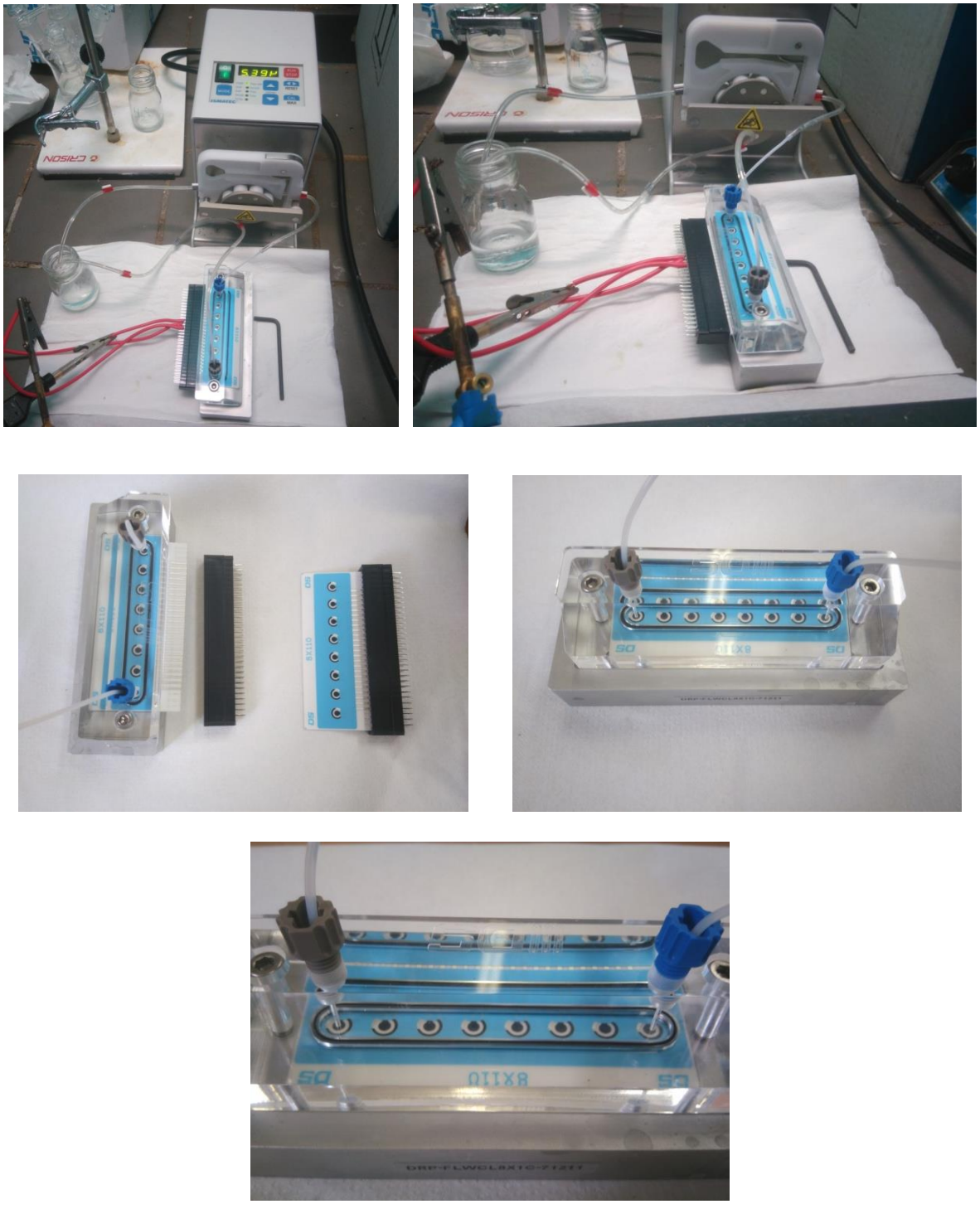

Figure 13. Pictures of the Dropsens multiple electrode system with the variable flow peristaltic pump 0.45 ml/min.

The next experiment was performed to determine the effect of the dissolved oxygen (O_2) in the working solution. To perform the electrochemical analysis, a deposit of non-supported Pt (electrodes 2,3 and 4) and Pt / V (electrodes 5,6 and 7) were performed. It is important to mention that electrodes 1 and 8 were not used due to the possible constant interaction with the inlet and the outlet of the working solution that could affect the electrochemical measurement because those are located exactly on top of both electrodes. Figure 14 shows the data corresponding to three different deposits. The next 3 curves in both figures correspond to a new multiple electrode with similar deposits (due to the reason that each experiment requires a new deposit), but after Ar bubbling into the working solution for almost 30 minutes.

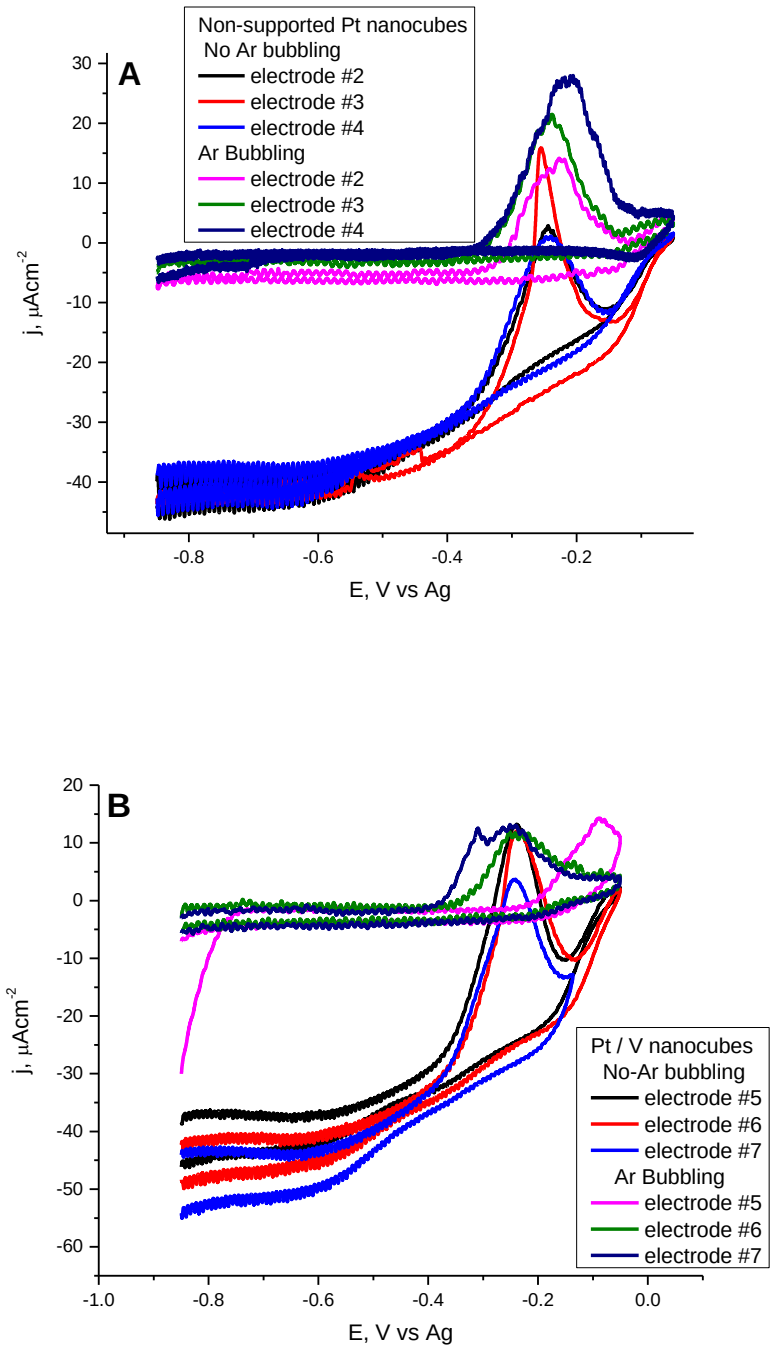

Figure 14. Voltammetric profiles for the NH_3 oxidation into the system that will be used in the ISS for (A) non-supported Pt and (B) Pt/V nanoparticles using 0.05 M $(NH_4)_2SO_4$ + 0.2 M NaOH. Scan rate: 10 mVs^{-1}.

As it can be observed, the presence of oxygen into the working solution produces a very important change in the voltammetric profile. Its presence has dramatic consequences over the CV and results are not reproducible with the three different deposits. To circumvent this problem, Ar was bubbled into the working solution. However, we also observed that for the tests in which Ar was bubbled, the oxidation current was also lower than expected. This may due to the NH_3 loss as a consequence the constant Ar bubbling.

In order to solve these problems, some alternatives were proposed including the previous Ar bubbling of the working solution before the cell encapsulation prior to be sent to the ISS, assuming that during the time from when the system is closed no oxygen will enter to the system. Anyways Ar bubbling through the ISS experiments would not be possible for obvious reasons.

The last electrochemical study was carried out to analyze the effect of the peristaltic pump continued to oxygen supply to the electrode surface by stopping it during the whole cyclic voltammetry experiment. This parameter was controlled to compare the electrochemical behavior in both previously deoxygenated and not deoxygenated working solutions.

An important fact is that deoxygenated solutions, were prepared by Ar bubbling the 0.2 M NaOH solution previous to the addition of $(NH_4)_2SO_4$ salt in order to avoid the NH_3 losses. After the bubbled process was performed, which took about for about 10-15 minutes, $(NH_4)_2SO_4$ salt was added and an Ar atmosphere was kept, so that O_2 could not enter mimicking the ISS conditions, in which the NH_3 deposit would be sealed. Figures 15A and 16A show the electrochemical behavior of the non-supported Pt nanoparticles and Pt / V in the presence of the constant flow produced by the the

peristaltic pump (0.45 mL/min) and deoxygenated working solution. As can be seen, in both cases the oxidation current shows positive values and the currents of the three different deposits are quite similar, so we can conclude that the level of reproducibility between electrodes is good.

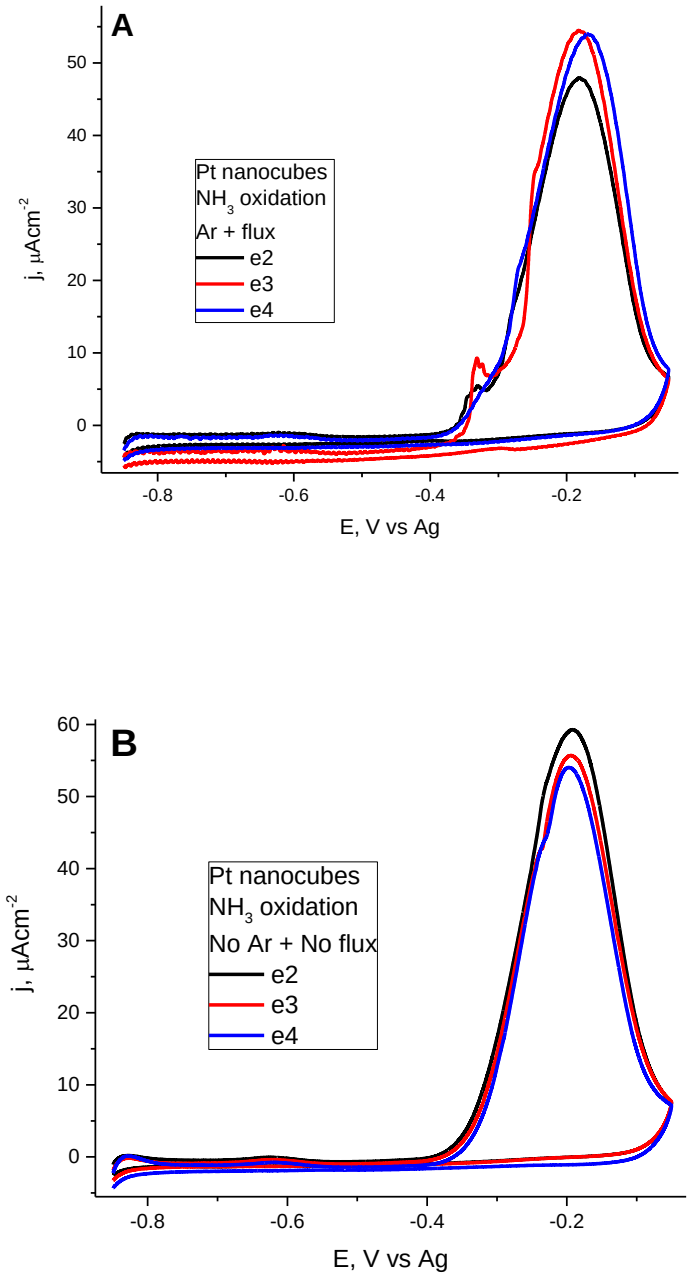

Figure 15. Voltammetric profiles of the non-supported Pt nanoparticles with (A) deoxygenated working solution with Ar and constant flow, and (B) with non-deoxygenated working solution without the pump flow. Working solution 0.05 M $(NH_4)_2SO_4$ + 0.2 M NaOH. Scan rate: 10 mVs^{-1}.

Figures 15 (B) and 16 (B) showed the catalytic performance of the three different deposits in the presence of the oxygenated working solution and the absence of flow due to the stop of the peristaltic pump through the CV. From the results it was concluded that the oxygen and if the working solution is not previously deoxygenated there will be a competition between NH_3 and O_2. However, if the solution is not deoxygenated but there is no flow of the working solution, the catalysts can oxidize the NH_3 and a profile similar to those presented can be obtained, as the O_2 is consumed at the beginning of the CV no affecting the NH_3 oxidation process.

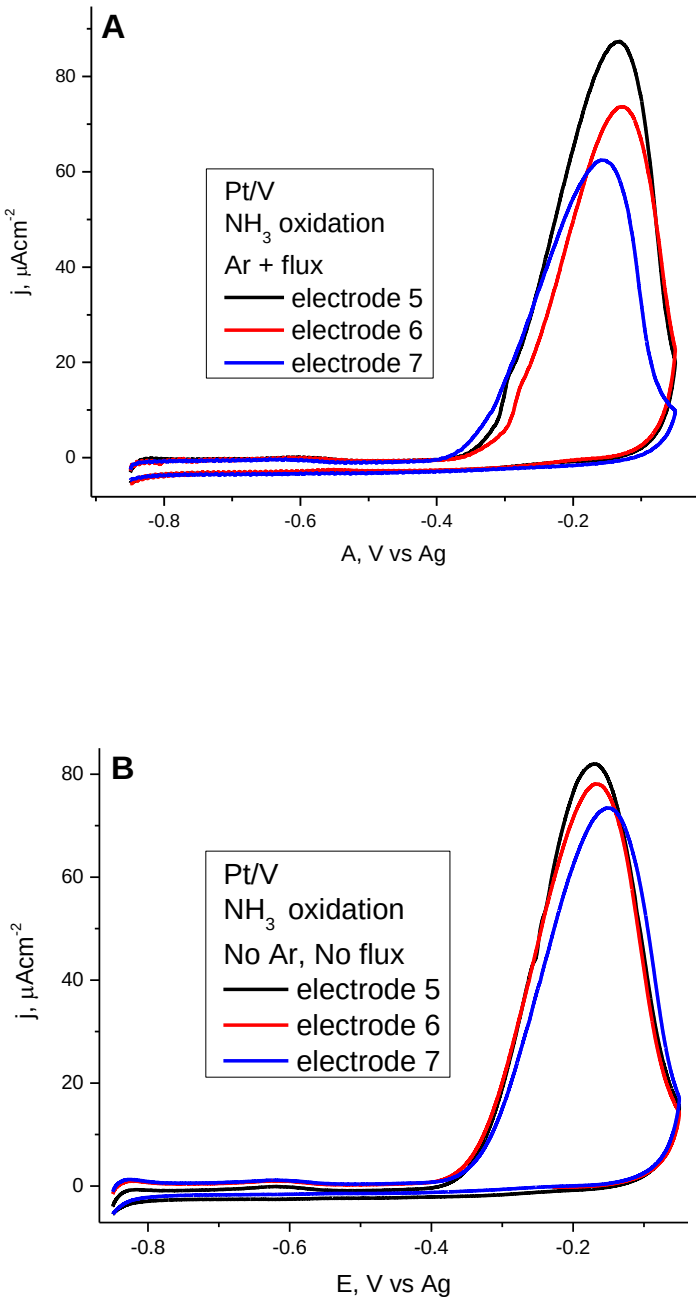

Figure 16. Voltammetric profiles of the pure Pt/V nanoparticles with (A) deoxygenated working solution with Ar and constant flow, and (B) without these parameters. Working solution 0.05 M $(NH_4)_2SO_4$ + 0.2 M NaOH. Scan rate 10 mVs^{-1}.

1.4. Conclusions

This section summarizes the most important findings that should be considered for the preparation of the final experiment to be carried out in the ISS.

• The catalyst ink solution must be deposited in the electrodes position from 2 to 7 (avoid electrodes 1 and 8)

• Due to the low flow rate provided by of the pump to be used at the ISS and which it may be convenient to pre-fill all the lines with ultrapure water. This could help to avoid the presence of bubbles into the line and may avoid the Pt poisoning if NH_3 were used.

• Samples must be well sonicated before making the deposit so that same deposits give the same areas. It is very significant that catalyst deposits have the same active area to be able to compare the results.

• In previous experiments (not shown) high currents caused the formation of N_2 bubbles into the electrodes. This must be avoided because with the flow rate provided by the peristaltic pump to be used in the ISS these bubbles cannot be removed and consequently, they can block the electrode surface.

• A lot of care has to be taken when drying the samples. The Ar flow must be low. At high flow rates, the samples would not deposit uniformly on the entire surface and finally could be agglomerated onto the edges of the working electrode.

• It is recommended to use the working solution 0.05 M of $(NH_4)_2SO_4$ + 0.2 M NaOH with a pH = 13 due to the reproducibility of the results. In addition, the formation of N_2 bubbles by using this working solution was negligible. In the

case of using the other NH_3 commercial solution, it is recommended to add a supporting electrolyte that adjusts the pH to 13.

• For the experimental procedure it should be considered that if there is solution flowing during the measurements, it has to be deoxygenated to avoid the O_2 reduction reaction. In addition, it is not possible to deoxygenate the solution while taking measurements, it will be necessary to stop peristaltic pump to keep stationary the working solution to record the electrochemical measurements and when the experiment finish, use the peristaltic pump to move the used working solution to remove the bubbles produced by the oxidation process.

ANNEX III.

Supporting Information

Synthesis of Pt nanoparticles in water-in-oil microemulsion: on the effect of HCl on their surface structure

ANNEX III SUPPORTING INFORMATION

Synthesis of Pt nanoparticles in water-in-oil microemulsion: on the effect of HCl on their surface structure

Experimental Section

Synthesis of Pt nanoparticles

Pt nanoparticles (Pt NPs) were synthesized by reducing H_2PtCl_6 with sodium borohydride ($NaBH_4$) using a water-in-oil (w/o) microemulsion of water (3%)/polyethylene glycol dodecyl ether (BRIJ®30) (16.5%)/n-heptane (80.5%) in a similar methodology to that previously reported.[1] The values in brackets represent the volume percentage of each compound. The concentration of the H_2PtCl_6 solutions was always 0.1 M although, to evaluate the effect of the presence of HCl, these were prepared using aqueous solutions containing a certain percentage of HCl. These percentages were varied from 37% (commercial solution, PA quality) to 0% (pure water) HCl. The Pt chemical reduction was performed by directly adding $NaBH_4$ to the water-in-oil microemulsion solution. The concentration of the added $NaBH_4$ was 1 M ($NaBH_4$/Pt molar ratio of 10). After complete reduction, which takes place in few minutes, acetone was added to the solution to cause phase separation. Afterwards, these Pt NPs were cleaned with successive acetone, acetone-water mixtures and water washes to finally achieve a water suspension with clean nanoparticles. This procedure allows cleaning the nanoparticles avoiding

electrochemical adsorption of oxygen and thus preserving the initial surface structure of the nanoparticles. Finally, the nanoparticles were stored in ultra-pure water as a suspension.

Characterization of Pt nanoparticles by TEM

Transmission electron microscopy (TEM) experiments were carried out to estimate the shape and size distribution of each type of sample. These experiments were performed with a JEOL, JEM-2010, working at 200 kV. The samples for TEM analyses were obtained by placing a drop of each colloidal suspension of dispersed Pt NPs onto a Formvar-covered copper grid and evaporating it in air at room temperature. For each sample, more than 100 particles from different parts of the grid were used to estimate the average size.

Figure S1 shows some representative TEM images for nanoparticles prepared with increasing amounts of HCl in the aqueous phase of the water-in-oil microemulsion.

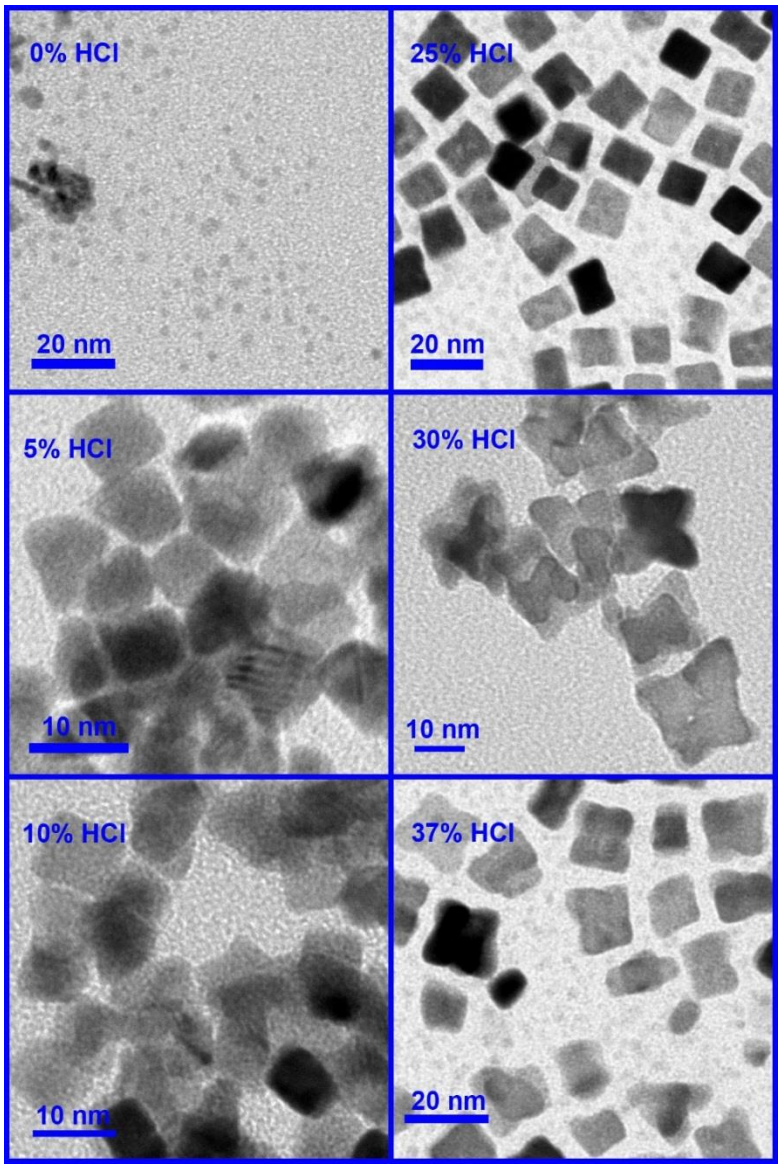

Figure S1. TEM image of platinum nanoparticles prepared in water-in-oil microemulsion in the presence of different HCl%.

Due to the presence of HCl in the water phase, the Formvar-covered Cu grids were slightly damaged, and some small spherical dots were visible in the TEM images. The effect is clearly visible for the sample of 37% and 25% HCl. In order to avoid this problem, the samples were also observed after their chemical cleaning, that is, once the Pt NPs

were dispersed in water. However, when cleaned and stored in water, nanoparticles are not so well dispersed and therefore, TEM images show the nanoparticles more aggregated, see for instance 5%, 10% and 30% HCl in figure S1. In addition, in order to verify the nature of the small spherical dots, EDX analysis of the regions containing the dots was carried out. Figure S2 shows the results obtained. It is worth noting the absence of platinum signals thus indicating that these dots are not due to the presence of small Pt NPs.

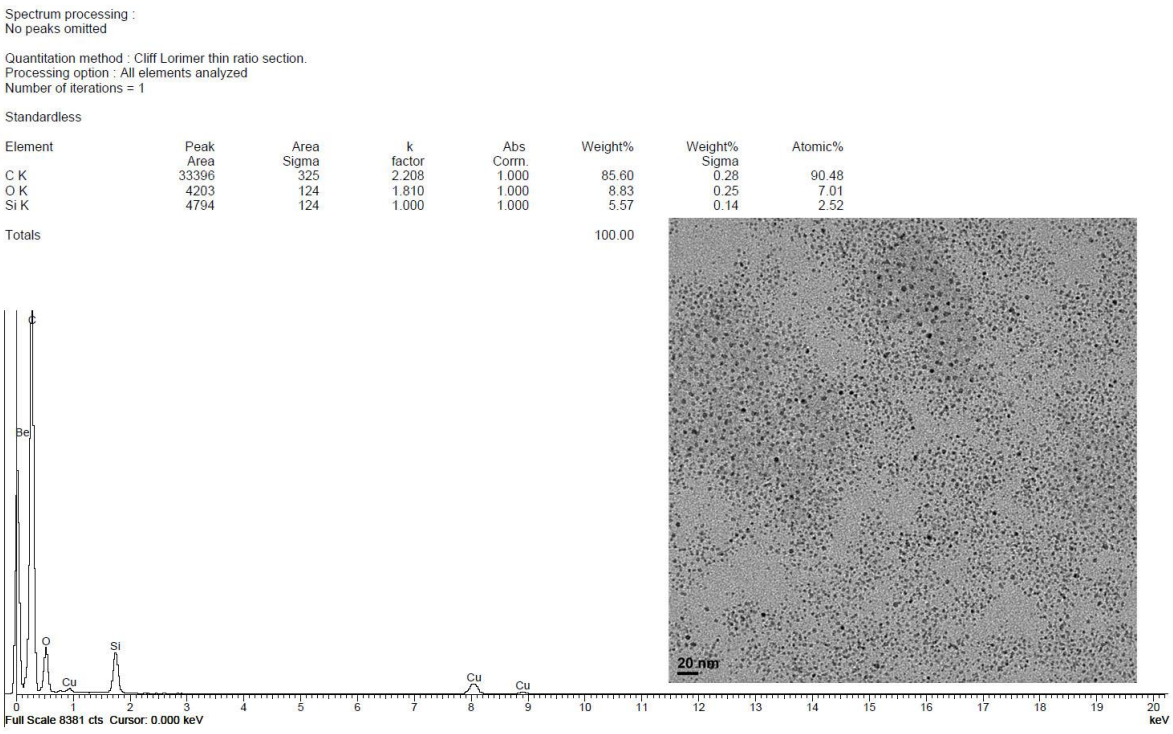

Figure S2. XRD analysis and TEM image of a Formvar-covered copper grid on which a drop of a colloidal suspension of dispersed Pt NPs prepared in the presence of 25% HCl was deposited.

ELECTROACTIVE SURFACE AREA NORMALIZATION

In order to measure the electrochemically active surface area, the voltammetric profiles shown in figure 1 of the manuscript were employed (0.5 M H_2SO_4 solution at room temperature). Electrolyte solutions were prepared from Milli-Q® water and Merck “p.a.” sulphuric acid every day an experiment was carried out. A three-electrode electrochemical cell was used. The electrode potential was controlled using a VMP3 multichannel potentiostat (BioLogic) with a *NStat* configuration (1 counter electrode, 1 reference electrode and 8 working electrodes working simultaneously). The counter electrode was a platinum wire. Potentials were measured against a reversible hydrogen electrode (RHE) connected to the cell through a Luggin capillary. Before each experiment, the gold collector electrode used to deposit the Pt NPs over was mechanically polished with alumina and rinsed with ultra-pure water to eliminate NPs from previous experiments. The active surface area of the Pt NPs was determined by the charge involved in the so-called hydrogen UPD region (between 0.06 V and 0.6 V) after the subtraction of the double layer charging contribution and assuming the calibration ratio (UPD charge)/(Pt surface area) as 0.23 $mC \cdot cm^{-2}$.[2]

DETERMINATION OF (100) ORDERED DOMAINS

The determination of the % of (100) surface domains was performed as described in previous contributions[3,4]. The adsorption of germanium was performed in a 10^{-2} M GeO_2 + 1M NaOH solution. The electrode, with a droplet of the previous solution, was transferred to an electrochemical cell containing 0.5 M H_2SO_4 and immersed at 0.1 V vs

RHE. From the area of the peak in the positive sweep scan, the charge related to the Ge desorption (q_{Ge}) can be calculated (fig. S3).

$$2.55768 \cdot 10^{-6} \frac{A \cdot V}{cm^2} \cdot \frac{1}{0.05 \frac{V}{s}} = \frac{2.55768 \cdot 10^{-6}}{0.05} \frac{C \cdot V}{s \cdot cm^2} \cdot \frac{s}{V} = 51.15 \frac{\mu C}{cm^2}$$

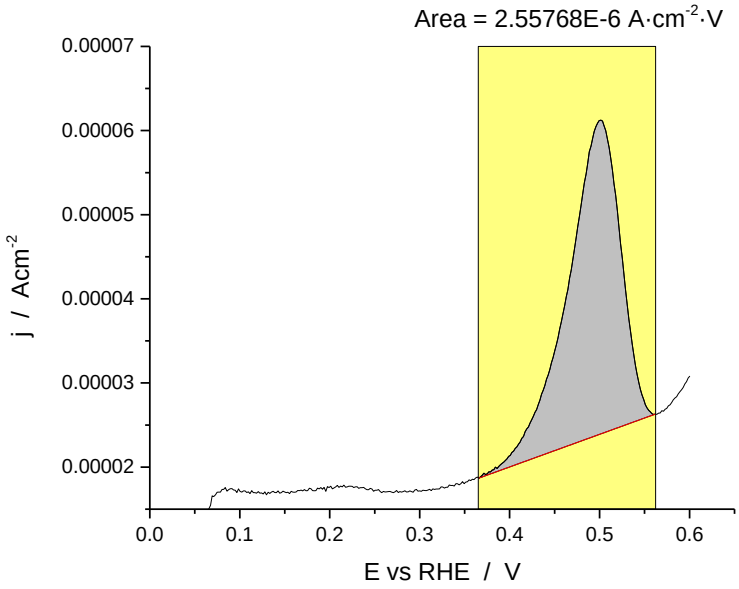

Figure S3. Positive sweep scan for germanium desorption on Pt nanoparticles prepared in the presence of a 25 %HCl. Test solution: 0.5 M H_2SO_4. Sweep rate: 50 mVs^{-1}.

From this charge value and using the following equation extracted from literature[3]

$$q_{Ge} = 0.56 q^{t}_{(100)}$$

the charge of the (100) terraces ($q^{t}_{(100)}$) can be obtained. After that and from the value of 209 μCcm^{-2} for a Pt(100)[4] (100% (100) sites), the percentage of (100) terrace sites can be obtained as follows.

$$q^{t}_{(100)} = \frac{51.15}{0.56}\frac{\mu C}{cm^2} = 91.34\,\frac{\mu C}{cm^2}$$

$$\frac{q^{t}_{(100),Pt^{15\,\%HCl}_{nano}}}{q^{t}_{(100),Pt(100)}} = \frac{91.34}{209} \rightarrow 43.7\%$$

EFFECT OF CHLORINE AND pH ON THE SHAPE OF THE PLATINUM NANOPARTICLES

Figure S4 shows the characteristic voltammetric profiles obtained for nanoparticles prepared with 15% NaCl and 15% $HClO_4$ in the aqueous phase of the water-in-oil microemulsion. The voltammograms are obtained in similar conditions than those used in figure 1 of the manuscript.

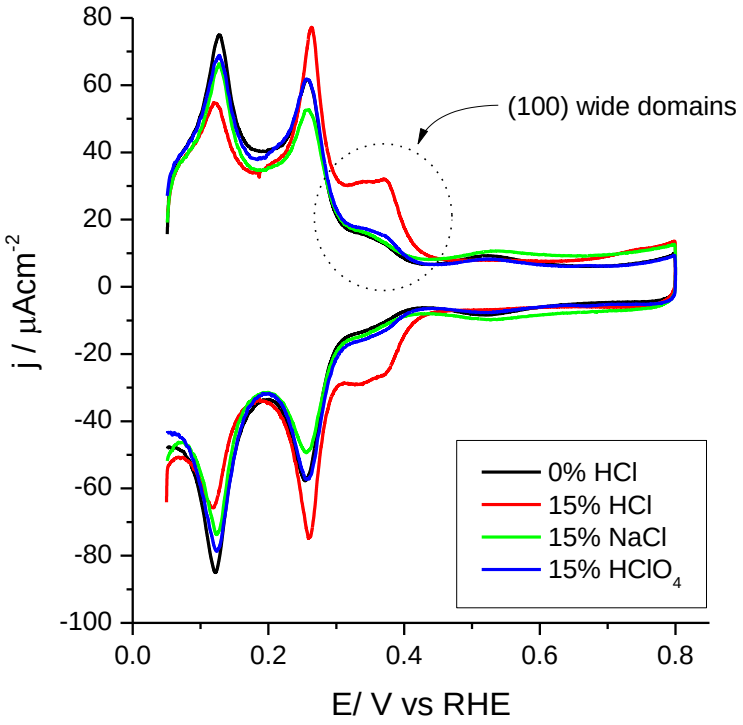

Figure S4. Voltammetric profiles of the Pt nanoparticles synthesized in the presence of different additives in the aqueous phase of the microemulsion. The dotted open circle highlights the contribution ascribed to the presence of (100) wide domains. Test solution: 0.5 M H_2SO_4. Scan rate: 50mVs^{-1}.

For the sake of comparison, the voltammetric profiles of 0% and 15% HCl are also plotted. As it can be seen, neither the presence of NaCl nor of $HClO_4$ seem to induce any clear preferential (100) orientation. The contributions given in the voltammograms ascribed to the presence of (100) wide domains are encircled in figure S4.

The amount of (100) sites was also quantitatively measured by Ge irreversible adsorption, and the values are summarized in Table S1, confirming the almost negligible effect of both NaCl and $HClO_4$.

Table S1. Amounts of (100) sites measured by Ge irreversible adsorption for different additives in the aqueous phase of water-in-oil microemulsion.

Additive	**% (100) Pt sites**
None (0% HCl)	14
15% HCl	40
15% NaCl	13
15% $HClO_4$	15

AMMONIA OXIDATION ON PLATINUM SINGLE CRYSTALS

Ammonia oxidation has been extensively studied for single crystal surfaces. [5-7] Nevertheless, the typical ammonia concentrations were much lower than those usually employed when studying nanoparticles[8,9] for which higher concentrations are used to avoid mass transport limitations. Therefore, in order to properly compare nanoparticles and single crystals, ammonia oxidation experiments were also performed with single crystals at higher ammonia concentration. Figure S5 shows the voltammetric behavior of

Pt (2n-1,1,1) single crystals in a 0.1 M NH_3 solution. Pt (2n-1,1,1) surfaces are composed of (100) terraces (n atoms width) and (111) steps. For example, a Pt (711) has 4 atom width terraces ((7+1)/2=4) separated by monoatomic (111) steps. As in the case of the oxidation at 10^{-3} M NH_3 solutions, electrocatalytic activity increases with the amount of (100) sites (width of the terrace).[5,6]

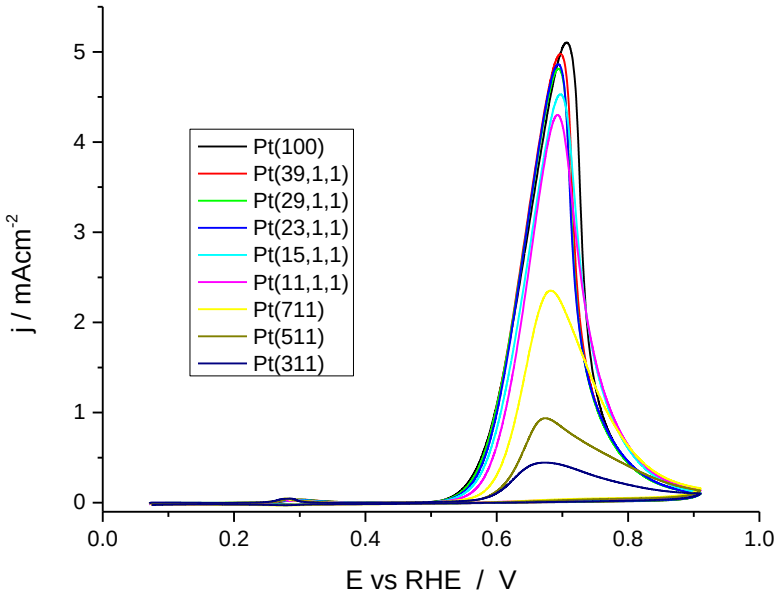

Figure S5. Voltammetric profile for ammonia oxidation with several Pt(2n-1,1,1) surfaces and Pt (100). Test solution: 0.2 M NaOH + 0.1 M NH_3. Scan rate: $10mV \cdot s^{-1}$.

References

1. Solla-Gullón, J.; Vidal-Iglesias, F. J.; López-Cudero, A.; Garnier, E.; Feliu, J. M.; Aldaz, A. *Phys. Chem. Chem. Phys.,* **2008**, *10*, 3689.

2. Chen, Q. S.; Solla-Gullon, J.; Sun, S. G.; Feliu, J. M. *Electrochim. Acta,* **2010**, *55*, 7982.

4. Solla-Gullón, J.; Rodríguez, P.; Herrero, E.; Aldaz, A.; Feliu, J. M. *Phys. Chem. Chem. Phys.,* **2008**, *10*, 1359.

5. Rodríguez, P.; Herrero, E.; Solla-Gullón, J.; Vidal-Iglesias, E. J.; Aldaz, A.; Feliu, J. M. *Electrochim. Acta,* **2005**, *50*, 3111.

6. Vidal-Iglesias, F. J.; Garcia-Araez, N.; Montiel, V.; Feliu, J. M.; Aldaz, A. *Electrochem. Commun.,* **2003**, *5*, 22.

7. Vidal-Iglesias, F. J.; Solla-Gullón, J.; Montiel, V.; Feliu, J. M.; Aldaz, A. *J. Phys. Chem. B,* **2005**, *109*, 12914.

8. Rosca, V.; Duca, M.; de Groot, M. T.; Koper, M. T. M. *Chem. Rev.,* **2009**, *109*, 2209.

9. Vidal-Iglesias, F. J.; Solla-Gullón, J.; Rodríguez, P.; Herrero, E.; Montiel, V.; Feliu, J. M.; Aldaz, A. *Electrochem. Commun.,* **2004**, *6*, 1080.

10. Vidal-Iglesias, F. J.; Solla-Gullón, J.; Montiel, V.; Feliu, J. M.; Aldaz, A. *J. Power Sources,* **2007**, *171*, 448.